

AD/A-001 750

HYDRODYNAMICS OF A BODY OF REVOLUTION  
WITH FAIRWATER AND RUDDERS AT A CON-  
STANT ANGLE OF ATTACK

Joseph Luckard, Jr.

Massachusetts Institute of Technology

Prepared for:

Office of Naval Research

March 1974

DISTRIBUTED BY:

**NTIS**

National Technical Information Service  
U. S. DEPARTMENT OF COMMERCE

UNCLASSIFIED

SECURITY CLASSIFICATION OF THIS PAGE (When Data Entered)

REPORT DOCUMENTATION PAGE		READ INSTRUCTIONS BEFORE COMPLETING FORM
1. REPORT NUMBER	2. GOVT ACCESSION NO.	3. RECIPIENT'S CATALOG NUMBER <b>AD/A-00/750</b>
4. TITLE (and Subtitle) <b>HYDRODYNAMICS OF A BODY OF REVOLUTION WITH FAIRWATER AND RUDDERS AT A CONSTANT ANGLE OF ATTACK</b>		5. TYPE OF REPORT & PERIOD COVERED <b>Final Report Oct. 71- March 74</b>
		6. PERFORMING ORG. REPORT NUMBER
7. AUTHOR(s)  <b>Joseph Luckard Jr.</b>		8. CONTRACT OR GRANT NUMBER(s)  <b>N00014-67-A-0204-0058</b>
9. PERFORMING ORGANIZATION NAME AND ADDRESS <b>Massachusetts Institute Of Technology Department of Ocean Engineering Cambridge, Mass. 02139</b>		10. PROGRAM ELEMENT, PROJECT, TASK AREA & WORK UNIT NUMBERS
11. CONTROLLING OFFICE NAME AND ADDRESS		12. REPORT DATE <b>March 1974</b>
		13. NUMBER OF PAGES
14. MONITORING AGENCY NAME & ADDRESS (if different from Controlling Office)		18. SECURITY CLASS. (of this report)  <b>UNCLASSIFIED</b>
		18a. DECLASSIFICATION/DOWNGRADING SCHEDULE
16. DISTRIBUTION STATEMENT (of this Report)  This document has been approved for public release and sale; Its distribution is unlimited.		
17. DISTRIBUTION STATEMENT (of the abstract entered in Block 20, if different from Report)		
18. SUPPLEMENTARY NOTES		
19. KEY WORDS (Continue on reverse side if necessary and identify by block number)  <b>HYDRODYNAMICS SUBMARINE CONTROL LIFTING SURFACE SLENDER BODY</b>		
<div style="display: flex; justify-content: space-between;"> <div> <p>Reproduced by <b>NATIONAL TECHNICAL INFORMATION SERVICE</b> US Department of Commerce Springfield, VA. 22151</p> </div> </div>		
20. ABSTRACT (Continue on reverse side if necessary and identify by block number) An investigation is made of the hydrodynamic forces and moments on a submerged body of revolution, resulting from the addition of an assym- metric fairwater and hull-control surfaces, and the results of their interaction. Experimental, flow visualization, numerical, and analytical approaches are described. The work described herein is also presented in the author's MIT Engineer thesis "Hydrodynamic Forces and Moments on a Submerged Body of Revolution Resulting from a Fairwater and Contro		

DD FORM 1473  
1 JAN 73

EDITION OF 1 NOV 65 IS OBSOLETE

UNCLASSIFIED

SECURITY CLASSIFICATION OF THIS PAGE (When Data Entered)

351120

ia

MASSACHUSETTS INSTITUTE OF TECHNOLOGY

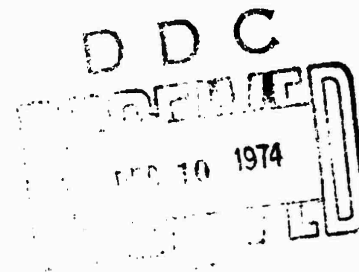
Department of Ocean Engineering

Report 74-8

HYDRODYNAMICS OF A BODY  
OF REVOLUTION WITH FAIRWATER  
AND RUDDERS AT A CONSTANT  
ANGLE OF ATTACK

Joseph Luckard Jr.  
March 1974

Approved for public release;  
distribution unlimited



This research was carried out under the Naval Ship Systems Command General Hydromechanics Research Program Sub-project SR 009 01 01, administered by the Naval Ship Research and Development Center. Prepared under O. N. R. contract N00014-67-A-0204-0058. M. I. T. DSR 73836



Hydrodynamics of a  
Body of Revolution with Fairwater  
and Rudders at a constant  
angle of attack

ABSTRACT

An investigation is made of the hydrodynamic forces and moments on a submerged body of revolution, resulting from the addition of an asymmetric fairwater and hull-control surfaces, and the results of their interaction. Experimental, flow visualization, numerical, and analytical approaches are described. The work described herein is also presented in the author's MIT Engineer thesis "Hydrodynamic Forces and Moments on a Submerged Body of Revolution Resulting from a Fairwater and Control Surfaces".



ACKNOWLEDGEMENT

The author would like to express his appreciation for assistance, support, and advice throughout this project to Dr. Damon E. Cummings, project supervisor, whose proposal initiated this project, sponsored by the General Hydrodynamics Research Program of NSRDC; and to Dr. J. N. Newman, whose participation helped to broaden my background in hydrodynamics.

Thanks are also extended to Dean Lewis, Engineer in charge of the Hydrodynamics Laboratory (water tunnel), for his time, effort and interest expended during the experimental portion of this project; and to Alice Pobuda for her perseverance in the expert typing of this thesis.

Finally, I would like to extend my appreciation to my wife Kathi, not only for the proofreading of this thesis, but also for her understanding throughout the last two and one half years, so that this culmination could be achieved.

TABLE OF CONTENTS

<u>TITLE</u>	<u>PAGE</u>
ABSTRACT	11
ACKNOWLEDGEMENT	111
TABLE OF CONTENTS	iv
LIST OF FIGURES	v
I. INTRODUCTION	1
II. BACKGROUND	4
III. METHODOLOGY	12
IV. SUBMERSIBLE MODEL EXPERIMENTAL RESULTS	24
V. FAIRWATER MODEL EXPERIMENTAL RESULTS	73
VI. THEORETICAL BASIS FOR NUMERICAL MODEL	98
VII. COMPARISON OF EXPERIMENTAL SUBMERSIBLE RESULTS	114
VIII. CONCLUSION	134
LIST OF REFERENCES	136
APPENDIX A. THE M.I.T. VARIABLE PRESSURE WATER TUNNEL	138
APPENDIX B. DYNAMOMETER PROGRAM USED FOR EXPERIMENTAL MODEL TEST	144
APPENDIX C. NUMERICAL PROGRAM TO GENERATE OFFSETS FOR CONSTRUCTION OF FOIL SHAPES	155
APPENDIX D. NUMERICAL MODEL OF A SUBMERSIBLE BODY OF REVOLUTION WITH LIFTING SURFACE APPENDAGES	159

LIST OF FIGURES

<u>FIGURE</u>		<u>PAGE</u>
1	Variable Pressure Water Tunnel Control and test section	17
2	Dynamometer Coordinate System at center of model axis, center of tunnel	17
3	Fairwater Coordinate System	18
4	Model orientation	19
5	Model dimensions (inches)	20
6	Submersible Model	21
7	Fairwater Model	22
8	Cam pattern for rudders of submersible model	23
9-14	Submersible Model - Heave Force (FYO)	28-33
15-21	Submersible Model - Pitch Moment (MZ)	36-42
22	Submersible Model - Sway Force (FZ) - Shaft Effect	47
23	Interpretation of hydrodynamic effects for graphic results	48
24-28	Submersible Model - Sway Force (FZ)	49-53
29-32	Submersible Model with flow visualization (Tufted)	54-57
33-37	Submersible Model - Roll Moment (MX)	61-65
38-42	Submersible Model - Yaw Moment (MYO)	68-72
43	Hydrodynamic Characteristics of Fairwater Model	77
44-49	Fairwater Model - Net Roll Moment - Flat Tip	78-83

50-51	Fairwater Model - Net Roll Moment - Tapered Tip	84-85
52-57	Fairwater Model - Lift Force (FZO) - Flat Tip	86-91
58-59	Fairwater Model - Lift Force (FZO) - Tapered Tip	92-93
60-62	Fairwater Model - Drag Force (FXO) - Flat Tip	94-96
63	Fairwater Model - Drag Force (FXO) - Tapered Tip	97
64	Vortex Lattice	104
65-68	Submersible Model - Lateral (Sway) Force Coefficient (Y')	115-118
69-71	Submersible Model - Yawing Moment Coefficient (N')	119-121
72	Axi-symmetric body	125
73	Lift Coefficient of Axi-symmetric body	126
74-76	Submersible Model - Lift Force (FZO)	127-129
A-1	M.I.T. Variable Pressure Water Tunnel	143
B-1	Sample Data Sheet	150

## I. INTRODUCTION

In March 1971, a technical proposal was submitted by the Department of Naval Architecture and Marine Engineering, now the Department of Ocean Engineering, Massachusetts Institute of Technology, to the General Hydrodynamics Research Program of the Naval Ship Research and Development Center to investigate hull-control surface interactions on submerged bodies, to include the effects imposed on the body by the fairwater and rudders (1). This proposal was divided into two problem areas: the constant yaw angle case, and the unsteady (time dependent) state case. This thesis will cover investigation performed in the first problem area of the project, that of the steady angle of attack in the horizontal plane. Particular items of interest are:

A. The geometry of the trailing vortex sheet shed from the fairwater when operating at an angle of attack. Where is the sheet with respect to the hull, and control surfaces downstream, such as the rudder? What velocities are induced on the hull and rudder by the trailing vortex sheet, and what forces and moments result from this interaction?

B. The lift generated on the fairwater due to side (sway) velocity when operating at an angle of attack. Besides the external trailing vortex sheet described above in A, an image system of trailing vorticity is required within the hull

surface to satisfy the boundary condition of zero velocity normal to the hull surface, and Kelvin's theorem of conservation of circulation. A net circulation around the hull of a submersible, aft of the fairwater, is implied by this reasoning. The combination of this net circulation and sway velocity leads to a net lift on the hull. This resultant lift resolves itself into a heave force and pitch moment excitation, which must either be compensated for by the vehicle control system, or result in an unanticipated coupling between yaw, heave and pitch motions of the vehicle. Nonsymmetric design of most submersibles, caused by the single fairwater, also combines with this resultant side force (lift component) into a roll moment on the vehicle.

Quantitative assessment of these forces and moments were investigated by experimental, analytical and numerical procedures. Experimental results were necessary to determine actual forces and moments experienced on a submerged body, to visually observe resulting hydrodynamic effects, and to be used as a basis of comparison for numerical results. To satisfy the primary objective of the project, a general and useable motion control prediction model, both analytical and numerical modeling were used.

Experimental results are presented for a fairwater model and a submersible model of different configurations.

Theoretical results, based on another part of this GHR project in which Newman and Rodriguez investigated a linearized low-aspect ratio slender body theory, are compared with the applicable experimental results of this project.

Some numerical results are presented also, but are not final. Continuing modifications are being made to the computer program for the most realistic results, before a final project report is submitted to the Navy in early fall 1973.

Dr. Damon E. Cummings was the project supervisor and Dr. J. N. Newman was a participating faculty member throughout this investigation.

## II. BACKGROUND

The design of submersible vehicles has changed drastically since the first successful American military submarine was built in the 19th century by the Holland Torpedo Boat Company. This first vessel, the HOLLAND, had many basic design features which eventually were reinstated into present day research and military submersible designs, especially since the development and design of the ALBACORE in 1950. This latter vessel was designed purposely to maximize submerged features at the expense of surface capabilities, emphasizing high submerged speed and maneuverability.

Particular hydrodynamic points of interest of HOLLAND to this investigation are:

1. A body of revolution hull form;
2. Little superstructure and no fairwater (sail), to minimize submerged resistance;
3. Stern planes and rudder surface located at the vertical centerline; and
4. Forward hydroplanes not employed.

The only features in military submarine and some research submersible design which have not returned to the HOLLAND configuration are the retention of the fairwater (sail) and forward hydroplanes, which are presently located on the fairwater (sail planes) for both military and hydrodynamic per-



formance purposes. Some research and test submersible vehicles have returned to the basic HOLLAND design in all aspects in an attempt to achieve an optimum submersible design.

Drag force components on a submersible resulting from appendages such as control surfaces, fairwater, shafts, and struts are of extreme importance when obtaining propulsion requirements for a particular vessel, but are of relatively minor importance when investigating stability and control. Much effort has been placed in this area for the last two decades to obtain an efficient design. This aspect will not be pursued in this report.

Present day submersible design has put an extraordinary requirement on stability and control. Although the military and research submersibles have vastly different performance capabilities, particularly the speed spectrums, the requirements of precise control and retention of stability remain. In particular, this is true for motions in the vertical plane, where a submersible must have the ability to operate, at slow or high speeds, within a relatively narrow vertical range. Full employment of a vessel's depth capabilities is desirable, but accidental penetration of depths beyond its maximum operating depth might lead to disaster. Nor is accidental broaching of the surface of the water a desirable maneuver in both the military and the research submersibles. Although

the horizontal plane is usually not as narrow ranged as the vertical, horizontal motions are important, especially in restricted waterways.

In the vertical (and horizontal) plane there are basically four performance criteria: (2)

1. Ability to maintain constant depth (course) with minimum plane movement and minimum depth (course) error;
2. Ability to enter into a maneuver as rapidly as possible;
3. Ability to exit from a maneuver as rapidly as possible;
4. Ability to return to equilibrium as quickly as possible when the controls are returned to zero.

An additional performance criterion only in the horizontal plane is the ability to execute a steady-turning maneuver with minimum tactical diameter, advance, transfer, loss of speed, and with minimum cross-coupled motions such as roll.

Most recent submarines have been equipped with fairwater (sail) planes, rather than bow planes, to reduce noise, alleviate the requirement for retraction, and to gain larger span dimensions within the submarine block dimensions. It has been shown on operational submarines that the drag of the fairwater planes compares favorably with previously used bow planes, even though fairwater planes have about 75% more

relative area. This same comparison shows 85% more relative vertical force, although only 20% more moment for fairwater planes than bow planes, because of the reduction in length of the moment arm (2).

For high speed maneuvering, forward hydroplanes are redundant. Depth changes can more readily be obtained by adjusting the angle on the stern planes, rather than applying a force close to the center of gravity. At low speeds, forward hydroplanes do make depth control somewhat easier.

Forward hydroplanes are desirable to help compensate for the nonsymmetrical hull form in the vertical plane, resulting from the fairwater, and to create a hydrodynamic vertical force and hydrodynamic moment in the vertical plane.

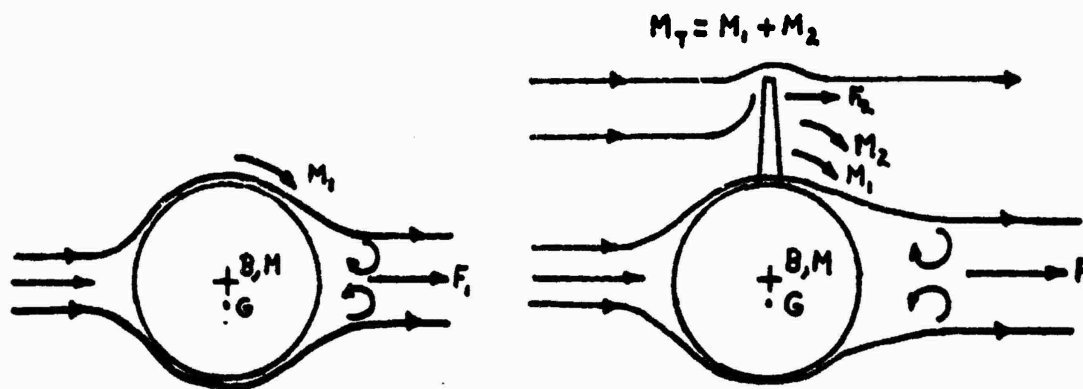
The hydrodynamic effects caused by asymmetry occur even when the hull body axis is parallel to the inflow velocity due to drag on the fairwater. In order to compensate for this effect and maintain constant depth, a hull angle of attack and a stern plane angle must be present, and are referred to as neutral angles of a particular vessel. These angles depend on the size of the fairwater and inflow velocity vector. If inflow velocity is assumed to be maintained horizontal, these angles introduce a pitch angle on the vessel equal to the hull angle of attack. This pitch angle in turn introduces a speed-dependent longitudinal metacentric moment, which is

the reason why the hull angle of attack and stern plane angle are speed-dependent. A critical range occurs at very slow speeds, in which the required angles for constant depth are too great to be accomplished by the stern planes only. Forward planes become a necessity at this time to reduce the magnitude of the requirements on the stern planes.

In the horizontal plane, the performance criterion that a vessel have the ability to execute a steady-turning maneuver with minimum tactical diameter, advance, transfer, loss of speed, and, in particular, minimum crosscoupled motions is of extreme importance and will require the major portion of this investigation for a valid understanding.

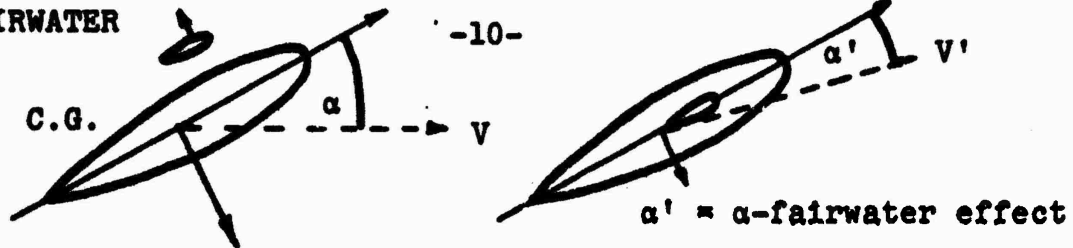
Of particular interest are the effects that a fairwater has on the above performance criterion concerning the steady-turning maneuver. The fairwater causes an increase in roll angle during a turn. One reason for this effect lies in the positions of the center of gravity (G), and center of buoyancy (B) of the vessel with respect to the axis of revolution of the hull body. When a submersible with a body of revolution, whose metacenter (M) is at the axis of symmetry because of wrap-around ballast tanks, is submerged completely, the waterplane area disappears. When this occurs, the location of the center of buoyancy (B) shifts from a position below the center of gravity (G) to one above. The location of the center of gravity (G), which has always been located below

the metacenter for the surfaced situation, is lowered even more by the added ballast. This low center of gravity, although increasing the roll stability of the vessel, introduces an asymmetry when the body of revolution is acted upon by hydrodynamic forces, in particular during a steady-turning maneuver. This occurs whether a fairwater is present or not, although it is more pronounced with a fairwater.



Fairwaters are located forward of the center of gravity; therefore, the hydrodynamic effects resulting in the horizontal plane during a steady turn are both stabilizing and destabilizing. Since the fairwater is essentially a lifting surface, it develops an effective lift force which is directed towards the turning circle center. This force, when combined with the vessel's velocity vector components, tends to decrease the angle of attack, which would be a stabilizing effect.

## FAIRWATER



Yet, when this force is combined with the distance forward of the center of gravity, the resulting moment is destabilizing. It tends to increase the yaw moment on the vessel in the horizontal plane, thus effectively reducing the turning diameter, which is desirable. However, in the roll-heave plane, the point of action of the lift force on the fairwater induces a roll moment on the vessel that is undesirable. The total roll moment experienced by the submersible is not entirely due to the fairwater. Part of this roll moment results from the hydrodynamic side force acting on the body of revolution above the center of gravity (G), which is below the body axis, for stability reasons. Table 5 of reference 2 reports of a model tested with a fairwater at a speed of 20 knots, rudder angle of 35 degrees and in a steady turn, which resulted in an angle of heel of 11.3 degrees. When this same model was tested without the fairwater, the angle of heel was reduced, but still present at 2.5 degrees. It was also shown during these tests that removal of the fairwater increased the turning diameter by about 25 per cent.

Although this investigation is pursuing the hydrodynamic effects at constant angles of attack, a brief statement on

the transient phenomenon of "snap-roll" is of interest. Snap-roll describes what occurs shortly after the initiation of a turn, corresponds to the amplitude of the first half cycle of roll and is believed to be an overshoot phenomenon. After the snap-roll occurs, the roll angle decreases to the steady-roll value. Values for snap-roll in the model tests described in the last paragraph were 39 degrees for the model with fairwater, and 12.5 degrees when the fairwater was removed. As before, the effect of the location of the center of gravity below the axis of symmetry is evident (2).

Since snap-roll is so immediate and of such a large magnitude on high-speed submersibles, control response time and knowledge of a submersible's particular characteristics are of extreme importance. When the snap-roll occurs, in combination with a rudder angle on for the turn, a cross-coupling results in an effective diving attitude for the vessel. Although this effect can be alleviated by judicious handling of available control surfaces, a problem of overshoot can arise. As previously mentioned, snap-roll only lasts for a relatively short period of a turn, after which the steady-turn phase is incurred. As a result, the effective diving attitude decreases. If the correction imposed for snap-roll is not reduced accordingly, the vessel's attitude will be one of decreasing depth, with an extreme result of broaching.

### III. METHODOLOGY

The purposes of the experiments reported on in this project were to investigate the hydrodynamic forces and moments that act on a submerged body in a steady flow both on a symmetrical slender body and on one to which appendages were added.

Possible methods were also investigated to redistribute the forces and moments to alleviate undesirable hydrodynamic effects caused by asymmetry, which is present in most submersible designs.

#### Measurement of Hydrodynamic Effects

Tests were conducted in the Variable Pressure Water Tunnel (see Appendix A) located in the Hydrodynamics Laboratory at M.I.T., see Figure 1. Measurement of the forces and moments on a particular model is accomplished through the application of a dynamometer which has six degrees of freedom, see Figures 2 and 3. These six degrees of freedom can be measured with respect to any point along the height of the test area. A computer program is used to deduce the three forces and three moments on the model being evaluated (see Appendix B). For the model tests covered in this project, coordinate systems were located at the center of the test area, along the axis of revolution of the submersible model,



see Figure 2, and at the tunnel wall, base of the fairwater model, see Figure 3.

Hydrodynamic Notation of Dynamometer Coordinate System

(With respect to model, about end of shaft)

- FX - Surge - applied force on longitudinal axis
- FY - Heave - applied force on vertical axis
- FZ - Sway - applied force on transverse axis
- MX - Roll - moment applied about the longitudinal axis
- MY - Yaw - moment applied about the vertical axis
- MZ - Pitch - moment applied about the transverse axis

Note: FXO, MXO, FZO, MZO, FYO, MYO are simultaneously-computed hydrodynamic effects from "general" dynamometer program for evaluation of model test in which results are desired with respect to water tunnel flow (free stream flow).

Experimental Models

Two different models were designed and built to measure the hydrodynamic forces and moments on a submerged body after symmetry to tunnel water flow is lost by the addition of appendages (fairwaters, control surfaces) and increased angle of attack (angular difference between free stream flow and body of appendage line of symmetry).

The two models include:

A) A streamlined body of revolution (tear-drop shape), with detachable fairwater sail and stern section, see Figures 4a, 5a and 6, to investigate the interaction effects of hydrodynamic forces and moments between a submersible hull, fairwater and control surfaces at various angles of attack and velocities (model hull and fairwater were constructed out of lucite; stern section and control surfaces were constructed out of brass).

The hull was constructed with a length (L) of 24.5 inches, a maximum diameter (D) of 3.5 inches occurring at a distance of 9.8 inches from the bow, resulting in a L/D ratio of 7.0. This slenderness and a fine stern should prevent most separation, and also enhance the applicability of slender body theory. The support shaft was located at a distance, from the bow, of 40 per cent of the model length; and

B) A fairwater with detachable and independent control surfaces, see Figures 4b, 5b, 6 and 7.

Construction of Fairwater and Control Surfaces

In conjunction with both model experiments, foil shapes were required for fairwater and control surfaces. The lucite fairwater (submersible model) and planes (fairwater model) were produced on a manual milling machine, from offsets developed from a computer program for this particular project (see Appendix C). This computer program is in a general form to meet any particular designs of thickness, chord length, taper, setback and foil design (NACA\_\_\_). This program calculates steps of thickness along the length of chord and span to be milled. These depths of cut are determined by foil geometry, end mill size and step size between milling runs. After milling of the step functions, the foil is finished by hand.

The stern control surfaces (submersible model) were produced on the Guggler Profile machine, located in the Gas Turbine laboratory shop of Building 31 (Sloan Laboratories). This machine requires a 4:1, plus 1/2 inch, scale model of surface to be developed, and is limited in the width of model fed between cam follower surface. Extra 1/2 inch is added on to compensate for abrupt changes in model shape (trailing edge).

Since the rudders used for the submersible were of foil shape, with no taper or setback, a simplified model (cam) was

made of an NACA foil shape, see Figure 8. Extended lengths of the foil shape can be produced and divided into various lengths of span. Cam followers are adjustable, so foil chord and thickness dimensions can be varied within limits, while using the same model (cam).



Figure 1 Variable Pressure Water Tunnel control and test section.

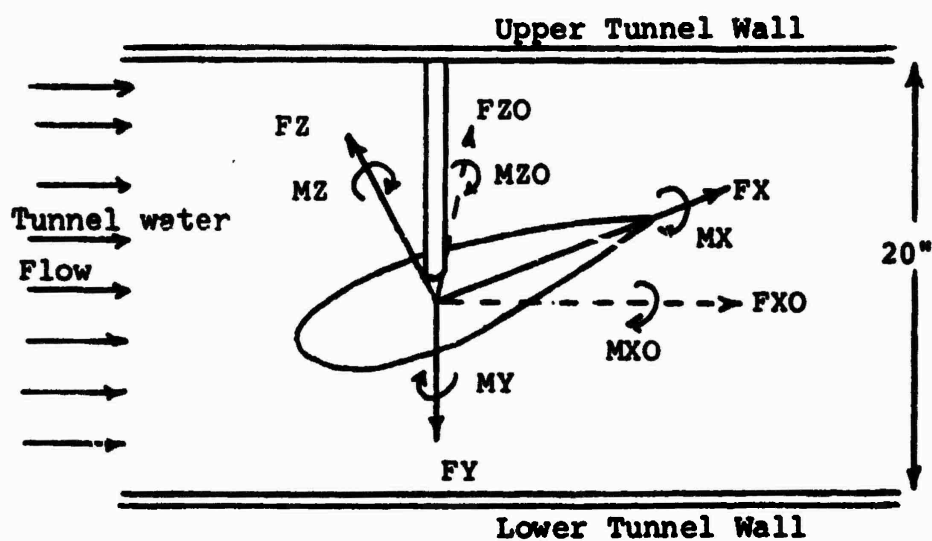
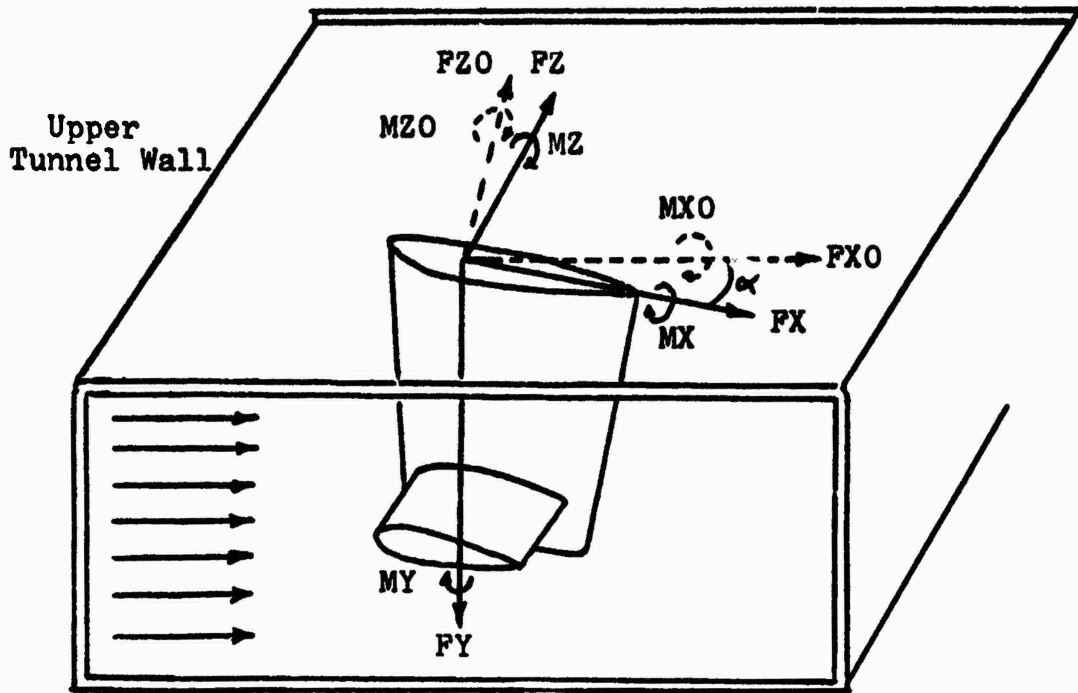
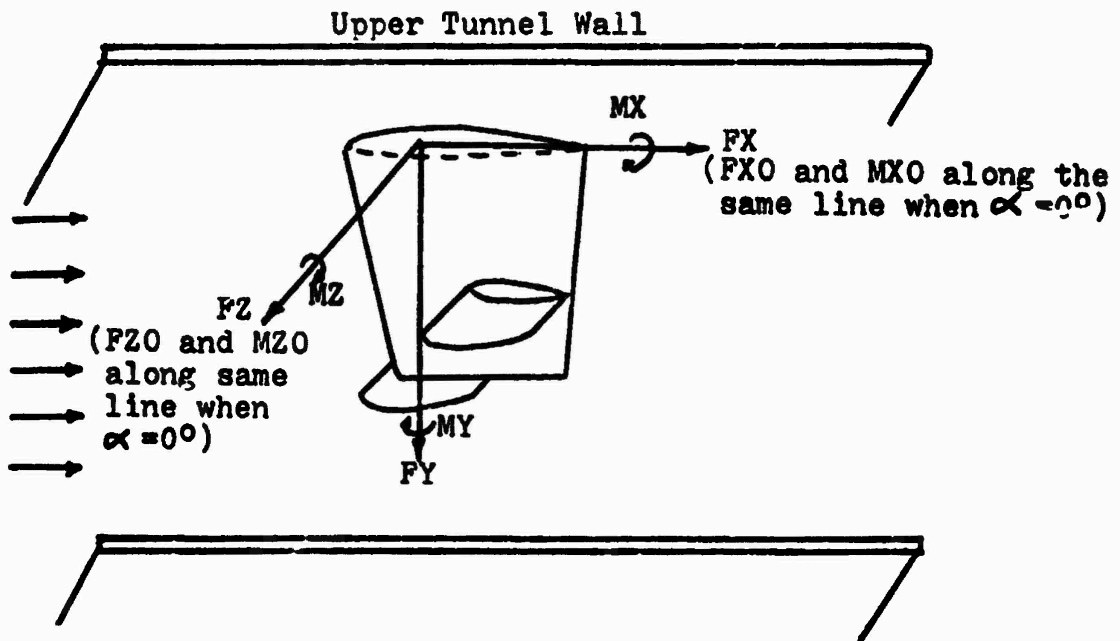


Figure 2 Dynamometer Coordinate System at center of model axis, center of tunnel.

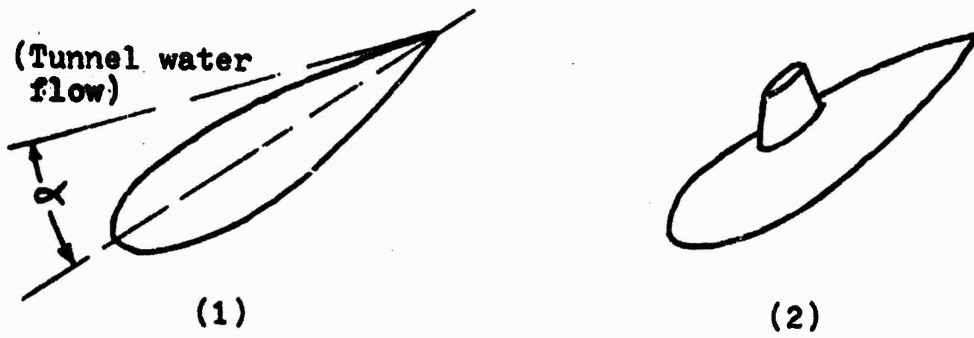


a. Dynamometer Coordinate System at base of model, against upper tunnel wall, at an angle of attack ( $\alpha$ ).



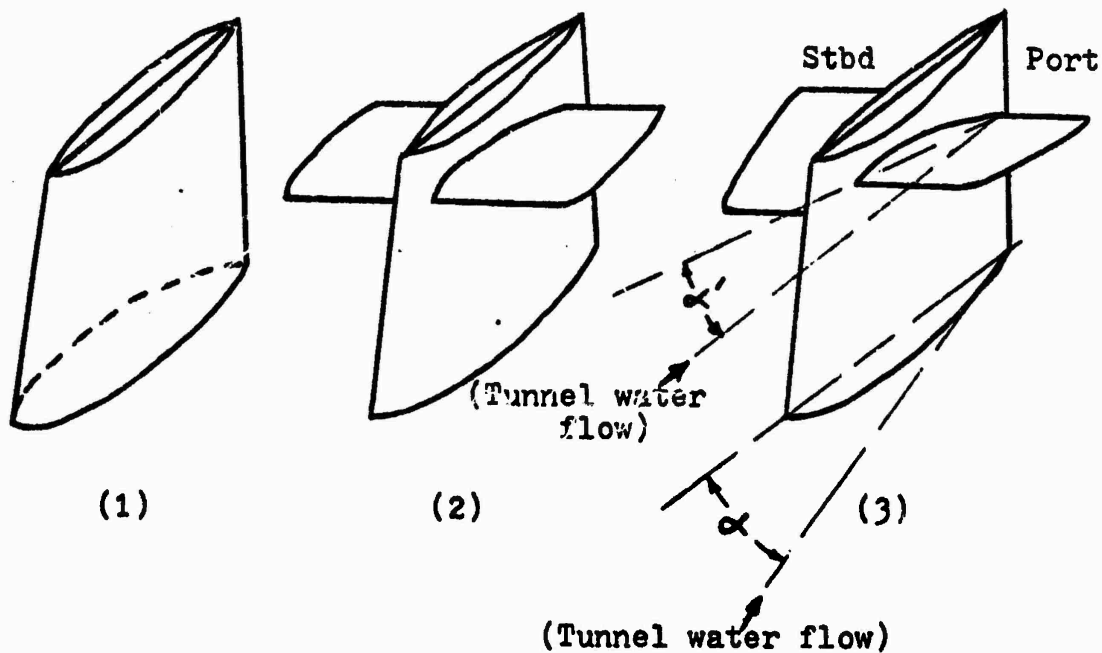
b. Dynamometer Coordinate System at base of model, against upper tunnel wall, parallel to tunnel flow.

Figure 3 Fairwater Coordinate System



a. Streamlined body of revolution (tear-drop shape)

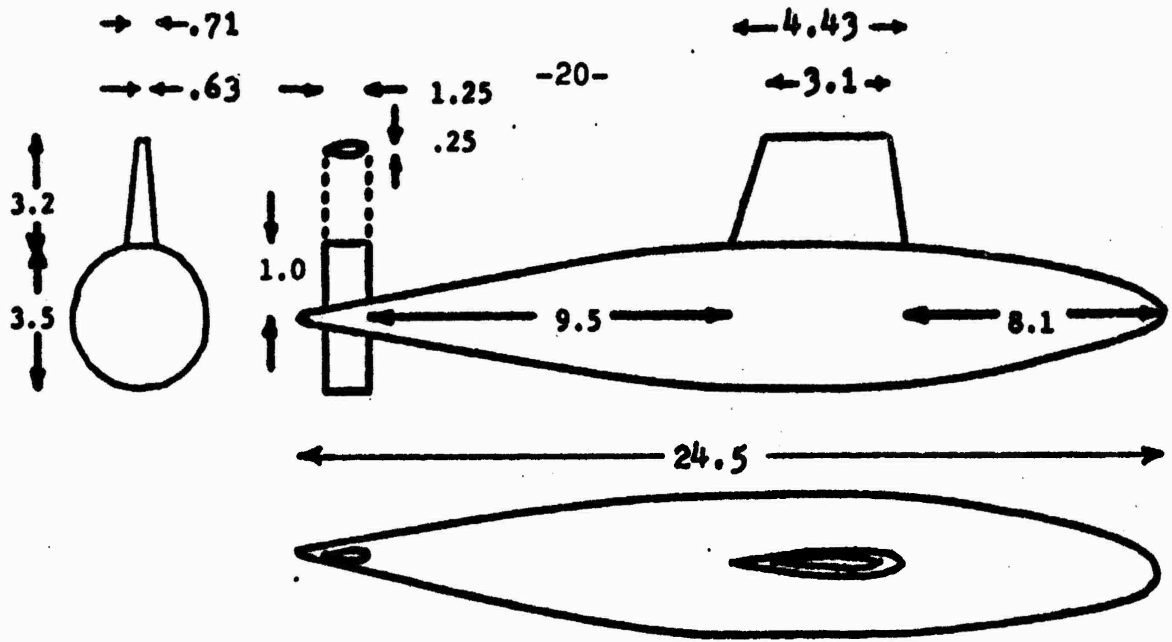
- (1) without fairwater
- (2) with fairwater



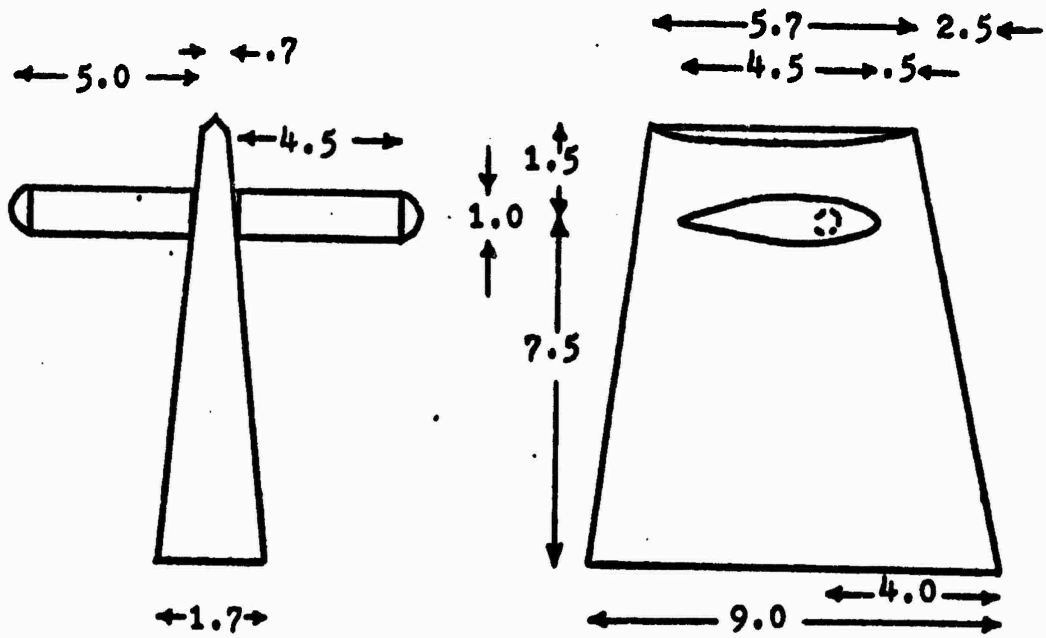
b. Fairwater design

- (1) without control surfaces
- (2) with control surfaces, at same angle of attack ( $\alpha'$ )
- (3) with independent control surfaces, port side positive, and starboard (stbd) side negative angle of attack ( $\alpha'$ ).

Figure 4 Model orientation.



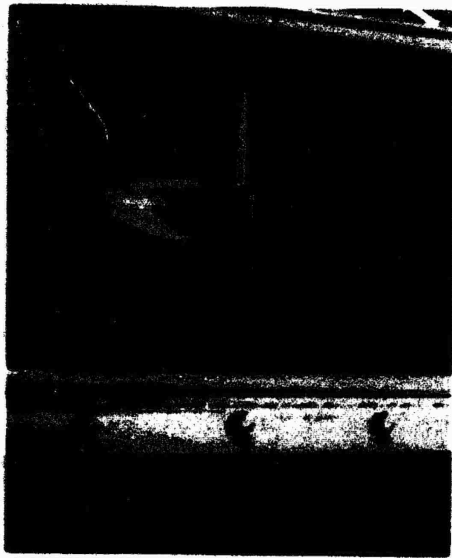
a. Submersible with fairwater



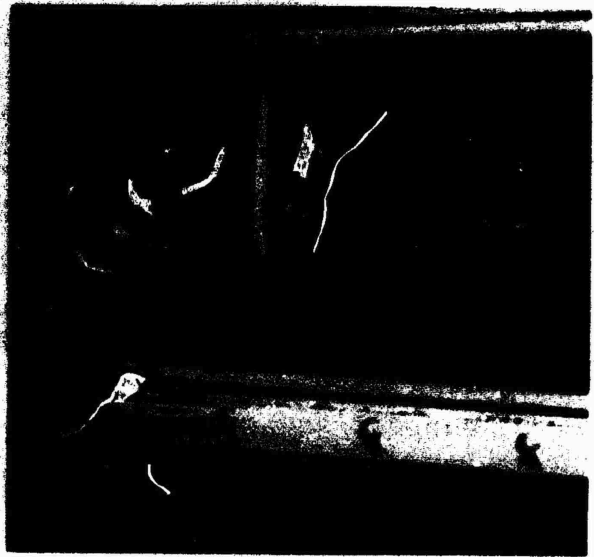
b. Fairwater with control surfaces

Figure 5 Model dimensions (inches)

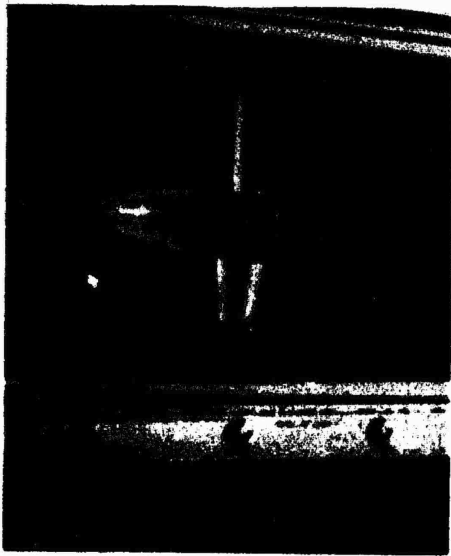




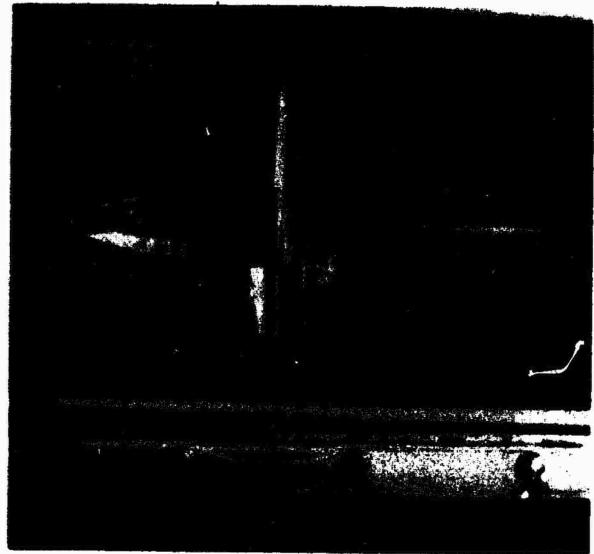
a. Oblique view without fairwater (Clean Hull).



b. Side view without fairwater (Clean Hull).

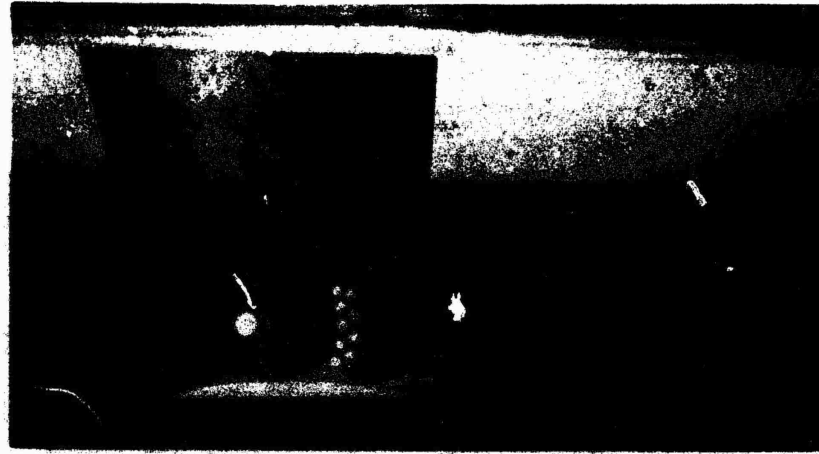


c. Oblique view with fairwater.



d. Side view with fairwater.

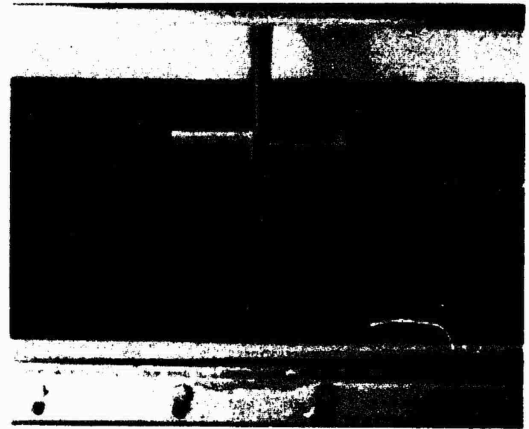
Figure 6 Submersible model



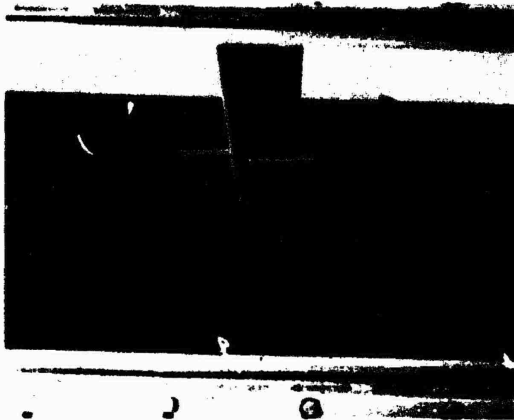
a. Side view of fairwater, without control surfaces. (Note support and guide locations used with control surfaces)



b. Oblique view, with control surfaces at  $\alpha' = 0^\circ$ .



c. Front view, with control surfaces at  $\alpha' = \pm 20^\circ$ .

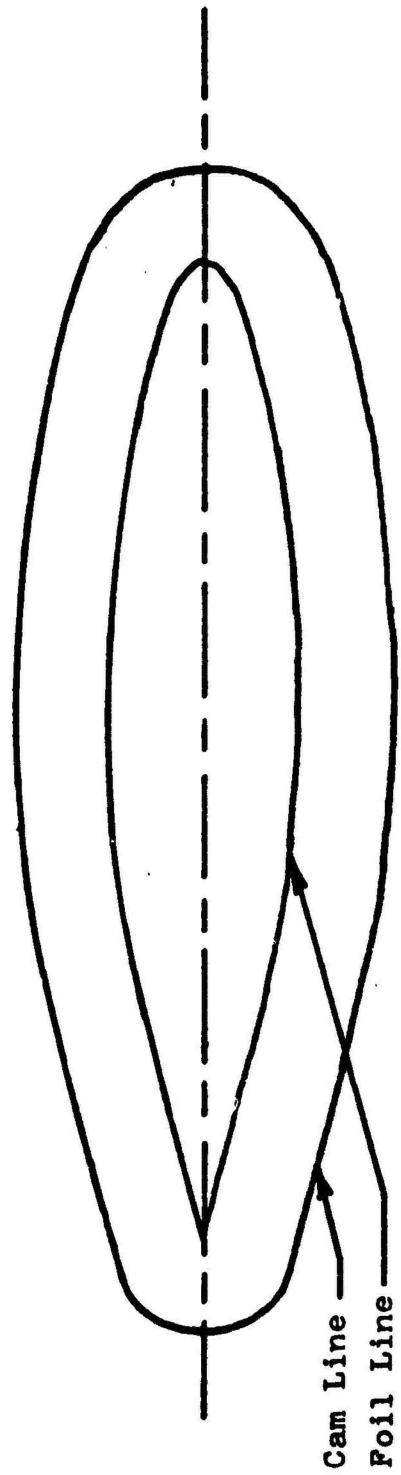


d. Oblique front view, with control surfaces at  $\alpha' = \pm 20^\circ$ .



e. Oblique rear view, with control surfaces at  $\alpha' = \pm 20^\circ$ .

Figure 7 Fairwater model



Cam pattern for rudders of submersible model

NACA 66-010

Chord = 1.25 inches

Thickness = .25 inches

Figure 8

#### IV. SUBMERSIBLE MODEL EXPERIMENTAL RESULTS

To experimentally investigate the hydrodynamic forces and moments on a submerged body of revolution, and how these effects are altered by the addition of appendages, the following different model configurations were tested:

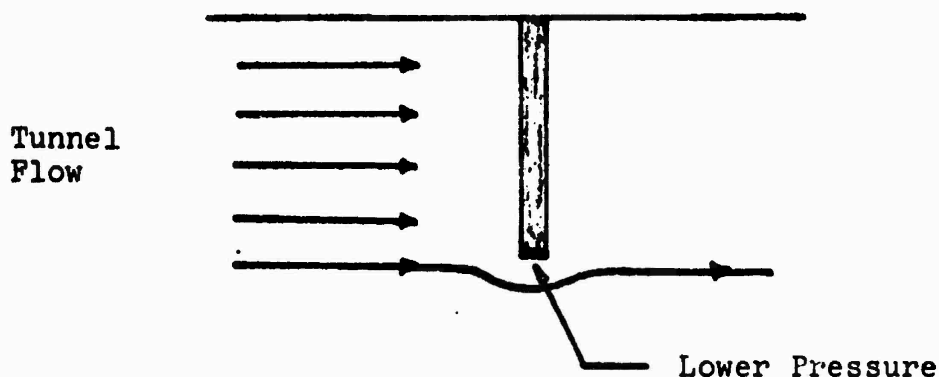
1. clean hull (no appendages)
2. with fairwater
3. with fairwater and upper rudder
4. with fairwater, upper rudder and lower rudder.

Flow velocities of 10, 15 and 20 feet per second were used, and angles of attack in the yaw-sway plane were varied between  $\pm 25$  degrees for tests evaluated at 10 feet per second, and  $\pm 15$  degrees for tests evaluated at 15 and 20 feet per second.

Caution must be used when interpreting the experimental results obtained during this investigation. All photographs and graphical displays of the results are shown according to the coordinate system previously described. Therefore, it must be kept in mind at all times that the model and results are inverted, since the model is mounted upside down on the top of the tunnel.

The support shaft used during the submersible model testing was evaluated by testing a bare shaft to determine

the forces and moments it would experience in the water tunnel. These effects were then deducted from the model test, to obtain results representing only the model. The interactions caused by the shaft on the hull and control surfaces were not investigated, but must be considered when interpreting the experimental results. Also, the lower pressure at the exposed end of the base shaft, caused by the flow pattern past the shaft, was not considered.



### Heave Force (FY0)

#### 1. Shaft Effect

Although the heave force on a bare support shaft, vertical and perpendicular to the flow, should have a constant value with respect to angle of yaw, the results obtained fluctuated and decreased for negative angles, see Figure 9. This is most likely a result of measuring accuracy of the dynamometer load cells used. An approximation was made to obtain a constant value of heave to be deducted from each model results, to alleviate the shaft effect. These values

were:

- 1) 1 lb, for a velocity of 15 ft/sec
- 2) 1.7 lb, for a velocity of 20 ft/sec

## 2. Model Results

When configuration 1 (clean hull) is tested, an initial negative heave force is registered at zero angle of yaw. According to the coordinate system used, this would appear as a downward force if the model were right side up. As the model is adjusted for both positive and negative angles of yaw, a symmetrical, increasingly more positive result occurs, see Figures 10 and 11. There should not be any heave force on this symmetrical model configuration, but the results could possibly be caused by the model not being perfectly aligned in the tunnel test area, or support shaft interaction with the flow around the body.

Configuration 2 (with fairwater) induces a drastic change in the pattern of the heave force imposed on the model. The results follow that of configuration 1 up to  $\pm 5$  degrees yaw. After  $\pm 5$  degrees, the slope decreases rapidly, reversing and producing a heave force at  $\pm 10$  to  $\pm 15$  degrees yaw comparable to that experienced at zero angle of yaw, see Figures 10 and 11. Thus it would appear that the addition of the fairwater and its resulting trailing wake induces a circulation and velocity on the hull body which generates a

decreasing slope of heave force per degree yaw in the coordinate system used. This is comparable to an increasingly large force downward, if the model were in an upright position.

The sensitivity of the results can be seen from Figure 12, in which results of tests 3 and 5, conducted on different days, were compared to see if they were compatible. The magnitude of test 5 varied, but the curve followed the same characteristic pattern as test 3. This difference in magnitude could result from a small difference in model alignment in the water tunnel or variation in the calibration of the dynamometer system on different days.

When configuration 3 (fairwater and upper rudder) and configuration 4 (fairwater plus both rudders) were tested, there appeared to be no effective change from the result of configuration 2, see Figures 13 and 14. The circulation and trailing wake off the rudders did not have any afterbody on which to induce a heave force component.

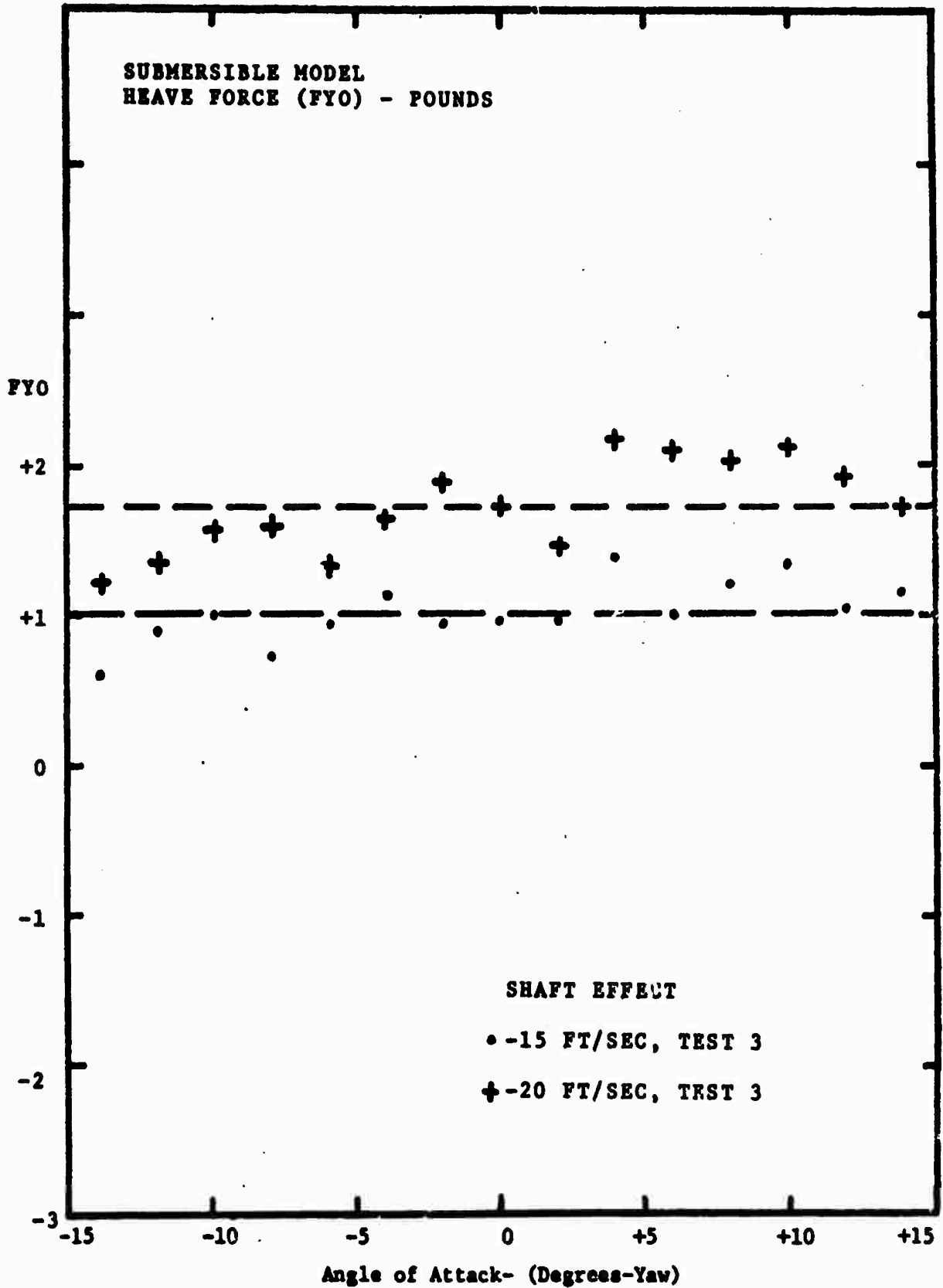


Figure 9



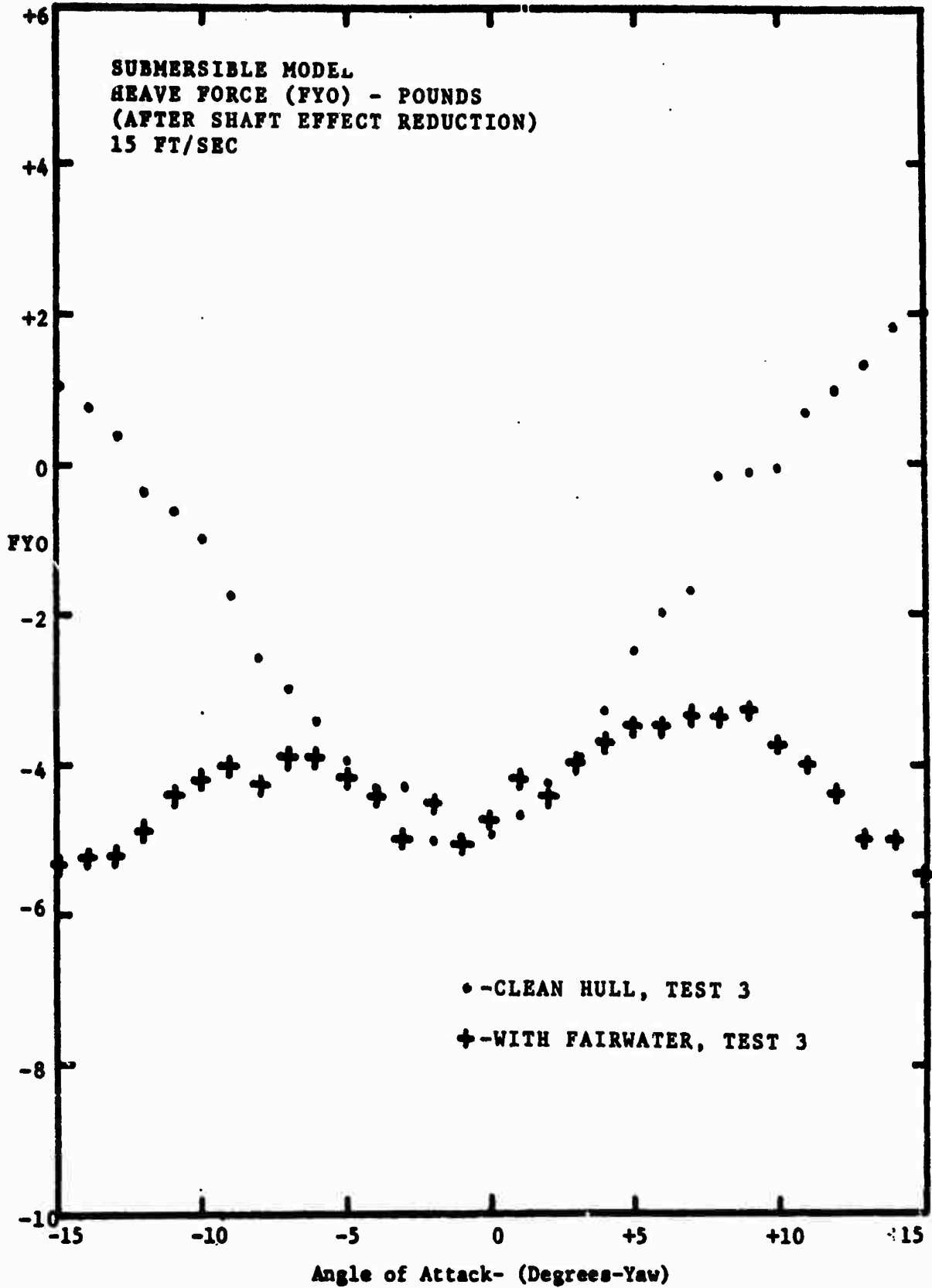


Figure 10

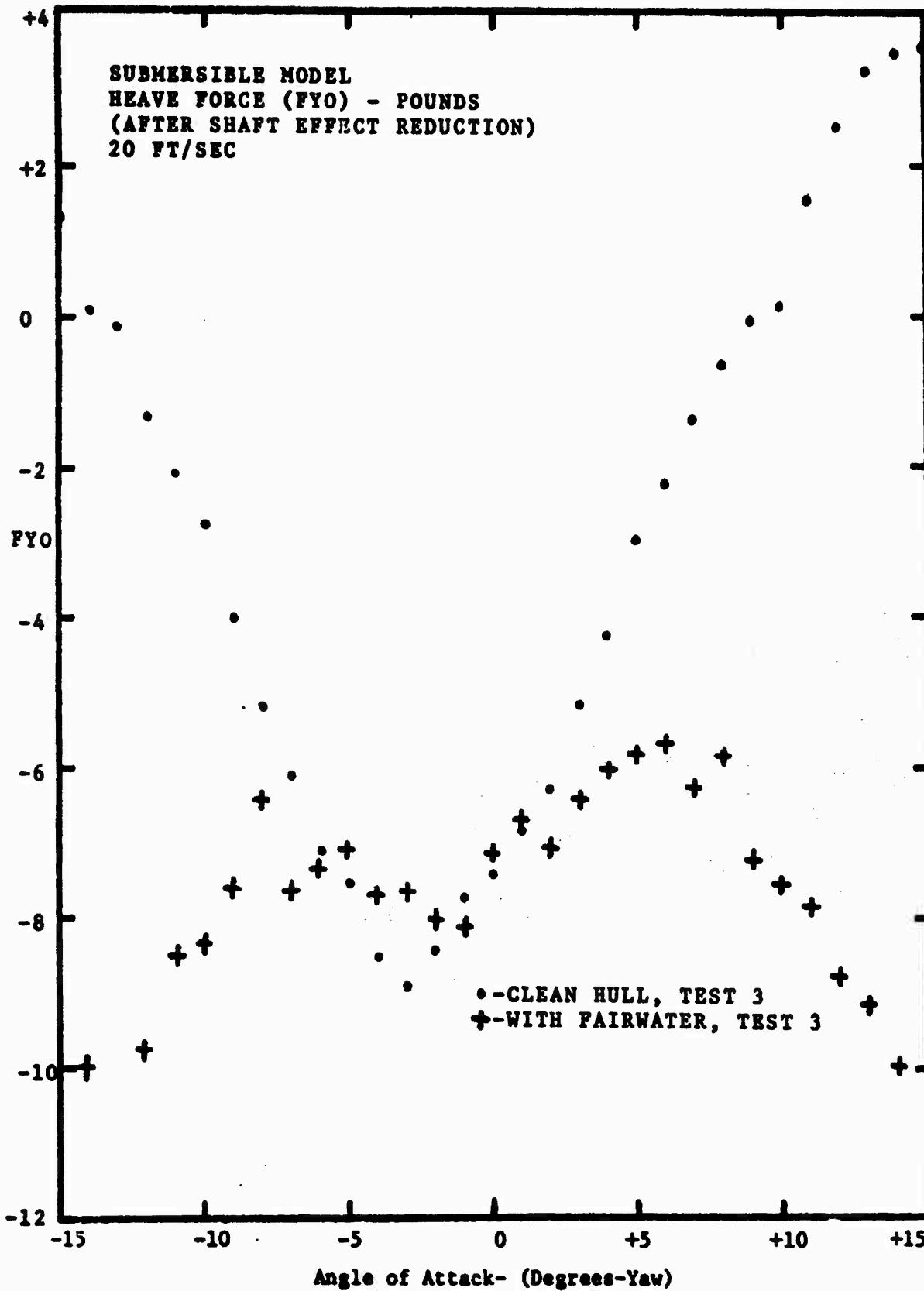
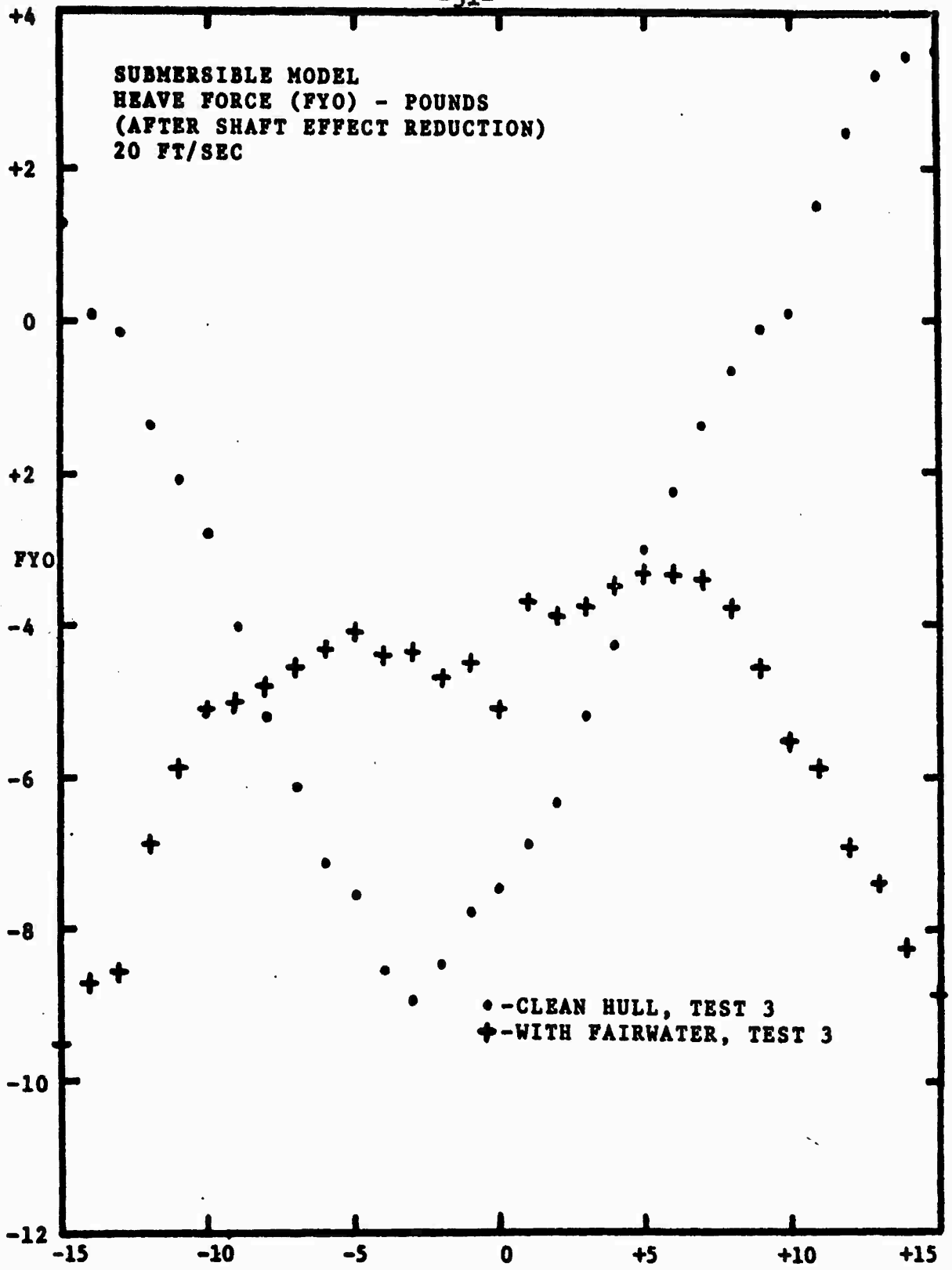


Figure 11



Angle of Attack- (Degrees-Yaw)

Figure 12

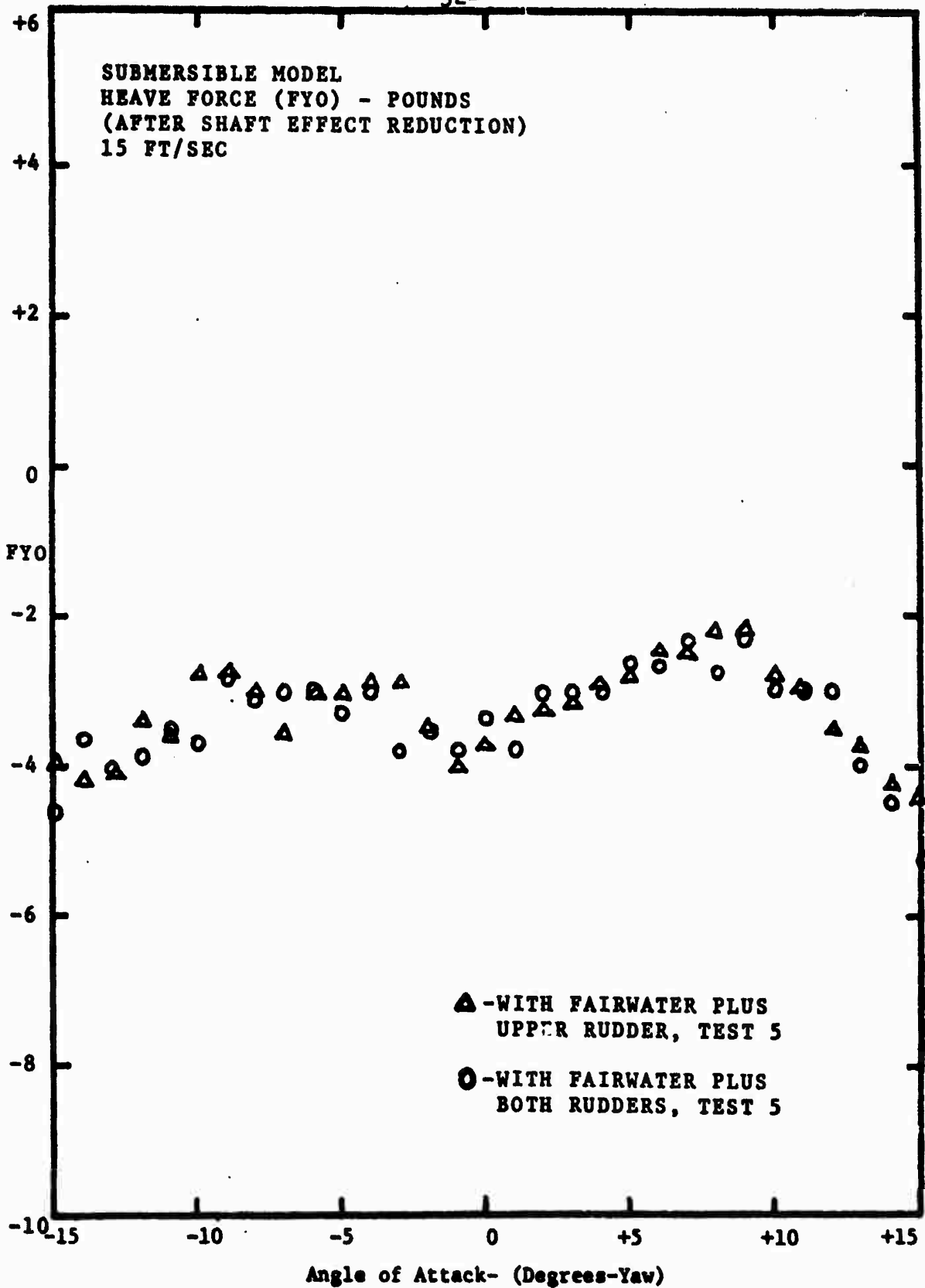


Figure 13

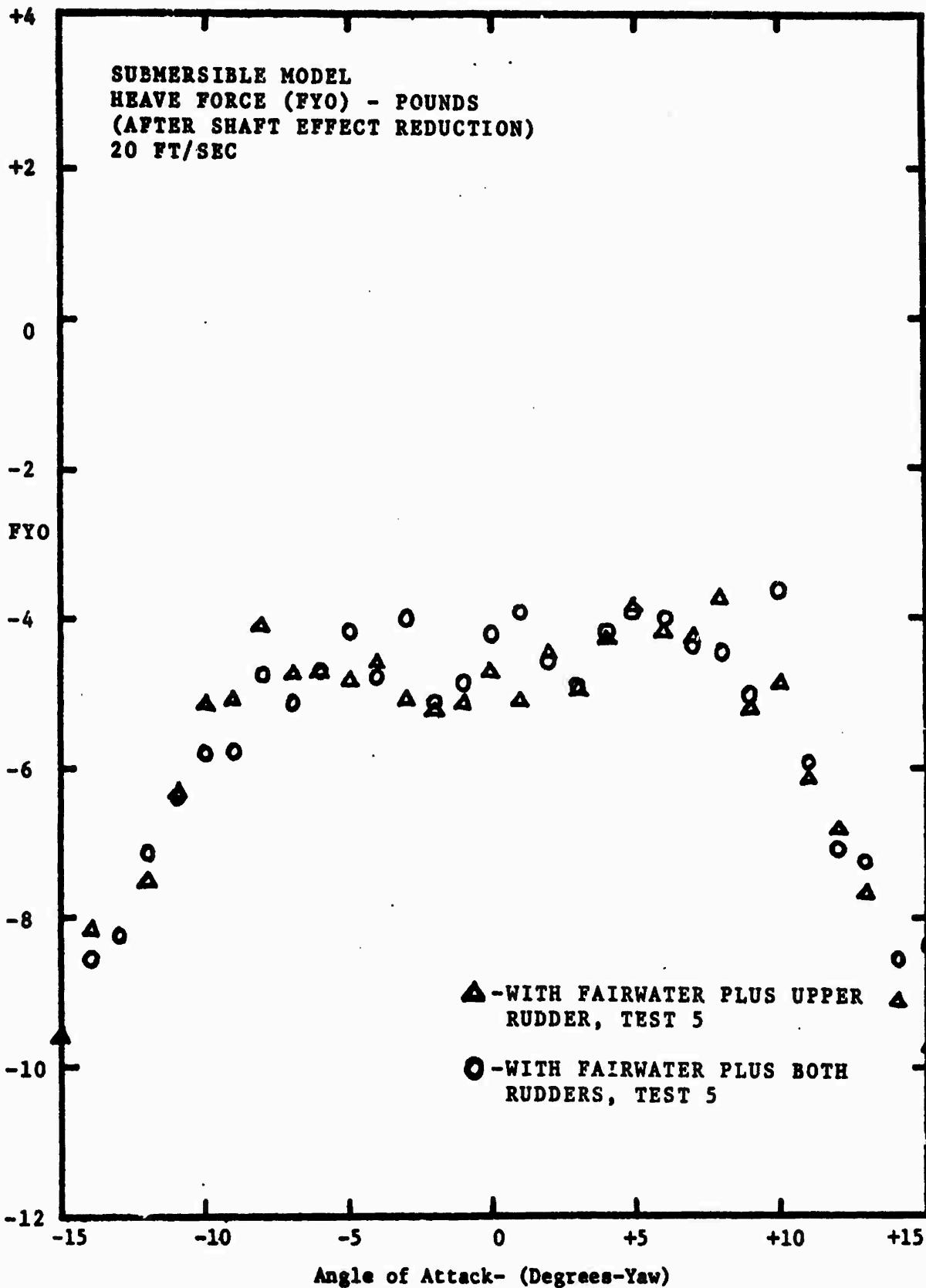


Figure 14

## Pitch Moment (MZ)

### 1. Shaft Effect

Since the pitch moment on the base shaft should decrease with increasing angle of yaw ( $\alpha$ ), the reduction factor ( $\cos \alpha$ ) can be assumed to be unity for the range of deflection at which the shaft was evaluated (zero to  $\pm 15$  degrees). Therefore, the reduction for the shaft effect is assumed to be constant, and a mean value of the experimental results, at different velocities, can be deducted from the model test to arrive at values of pitch moment, for the different model configurations, which approach that of a non-supported model. The resulting mean values were:

- 1) 40 in-lb, for a velocity of 15 ft/sec, and
- 2) 71 in-lb, for a velocity of 20 ft/sec, see Figure 15.

### 2. Model Results

Pitch moment on the various model configurations followed the same pattern of results obtained for heave force. Configuration 1 (clean hull) produced a negative moment at zero angle of yaw and a steadily increasing moment, with a decreasing slope, as yaw angle is increased, see Figures 16 and 17. The negative moment at zero angle of yaw could be caused by model alignment, or shaft interactions. The flow past the shaft causes a high pressure area at the forward stagnation point and a low pressure area on the aft portion

of the circumference. Fairwater drag would also produce a similar effect, but the magnitude of the negative moment was equivalent to that obtained for configuration 1 (clean hull).

Configuration 2 (with fairwater) produced an increasing moment, which followed the results of configuration 1 between about  $\pm 5$  to  $\pm 10$  degrees, after which the pitch moment decreased, as fast as it had increased, see Figures 16 and 17. This result would be comparable to a submersible, in an upright position, experiencing an initial bow up pitch moment at zero angle of yaw. This is due to shaft-hull interaction, a minor model misalignment in the vertical plane, or possibly miscalibration of equipment. This is followed, with increasing angle of attack, by a bow down pitch moment, caused by a lift force on the hull aft of the fairwater. This is finally succeeded by a bow up pitch moment, resulting from the drag component of the fairwater, and the circulation and induced velocity from the fairwater on the aft section of the hull body.

As in the heave force results, pitch moment did not seem to be affected by the addition of the upper rudder (configuration 3), see Figures 18, 19 and 20, or when tested with both rudders attached (configuration 4), see Figures 19 and 21. Their induced velocities have very little effect on the hull, which precedes them in the fluid flow, and their wakes have no afterbody to affect either.

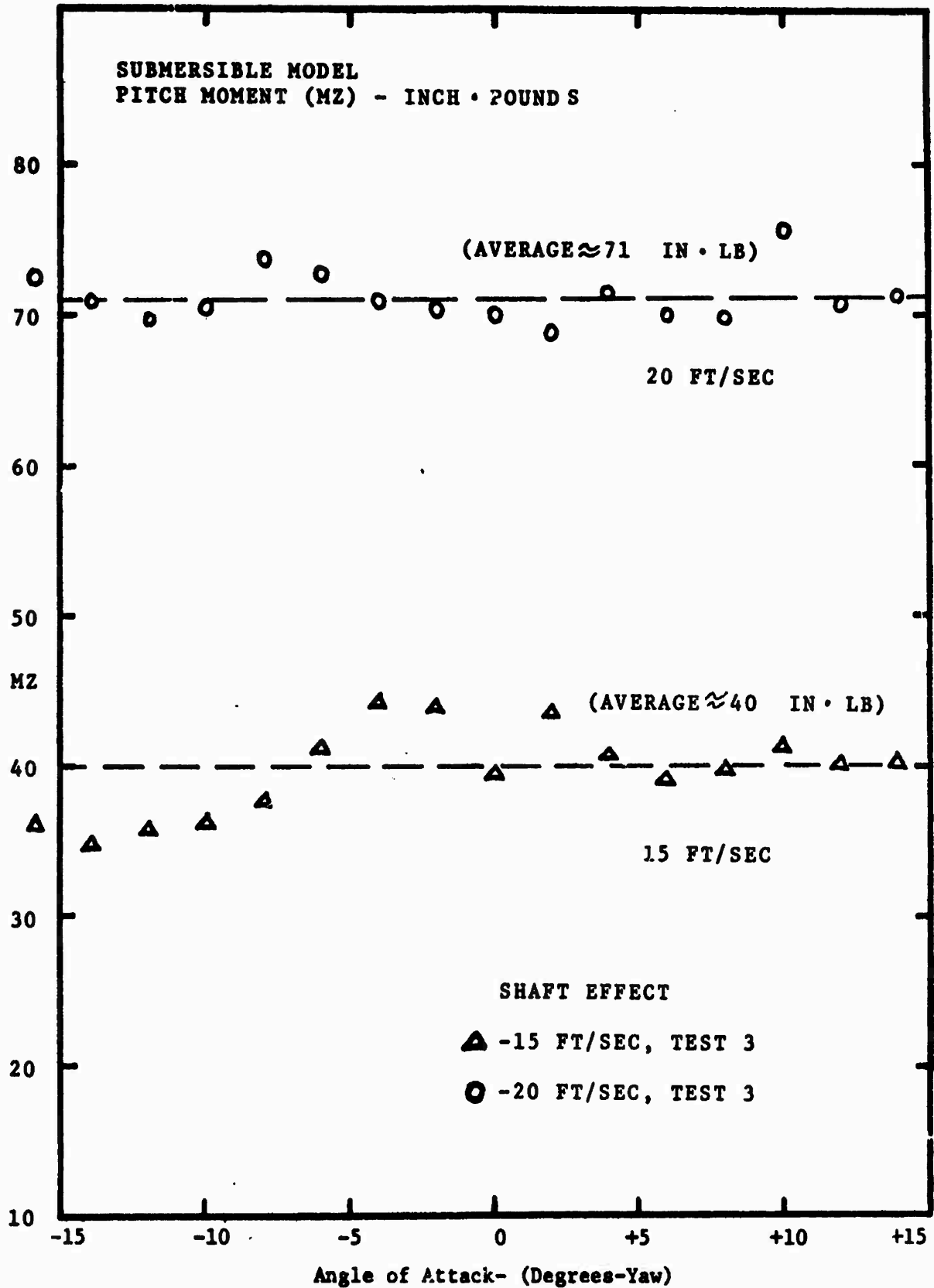


Figure 15



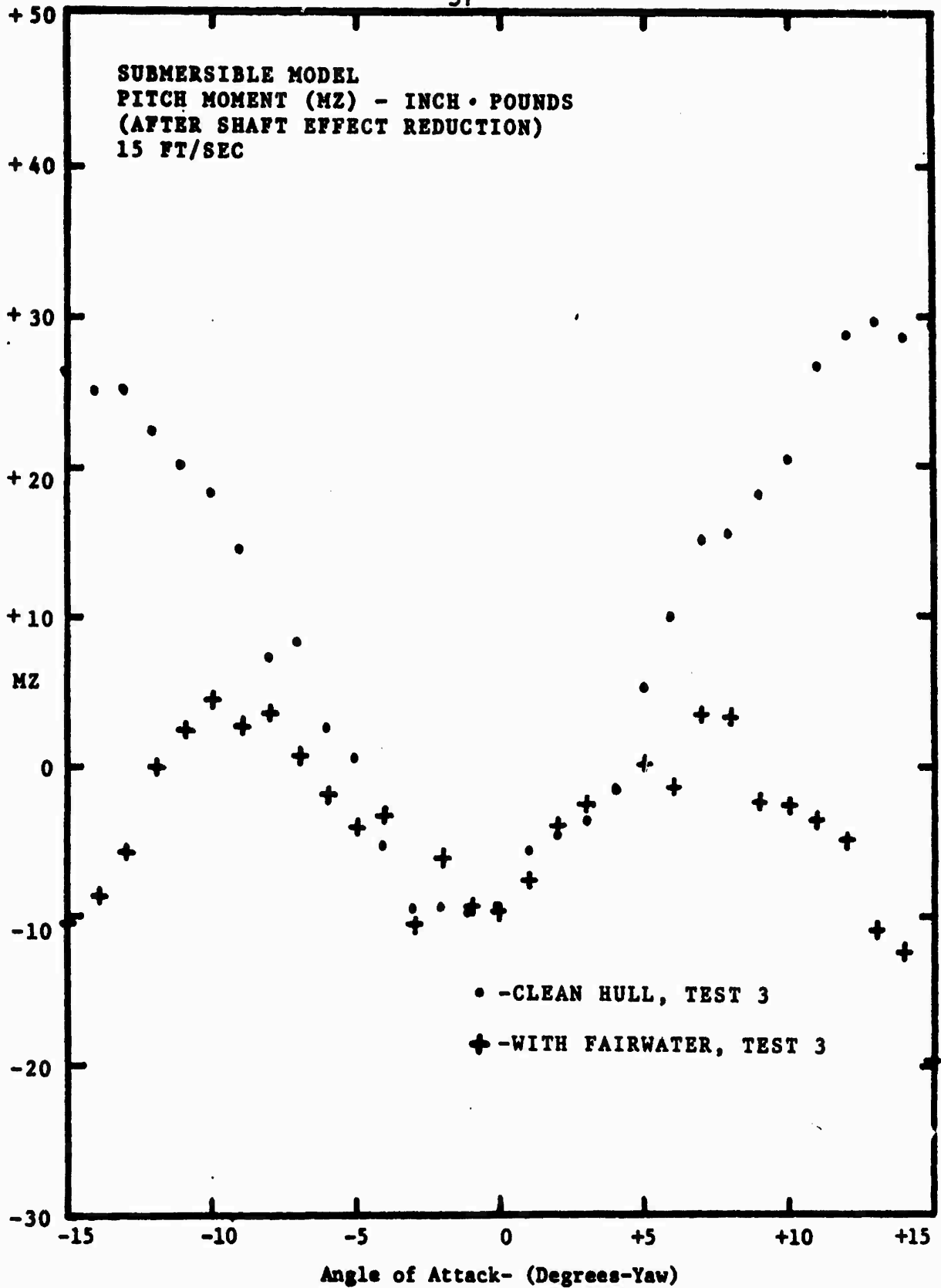


Figure 16

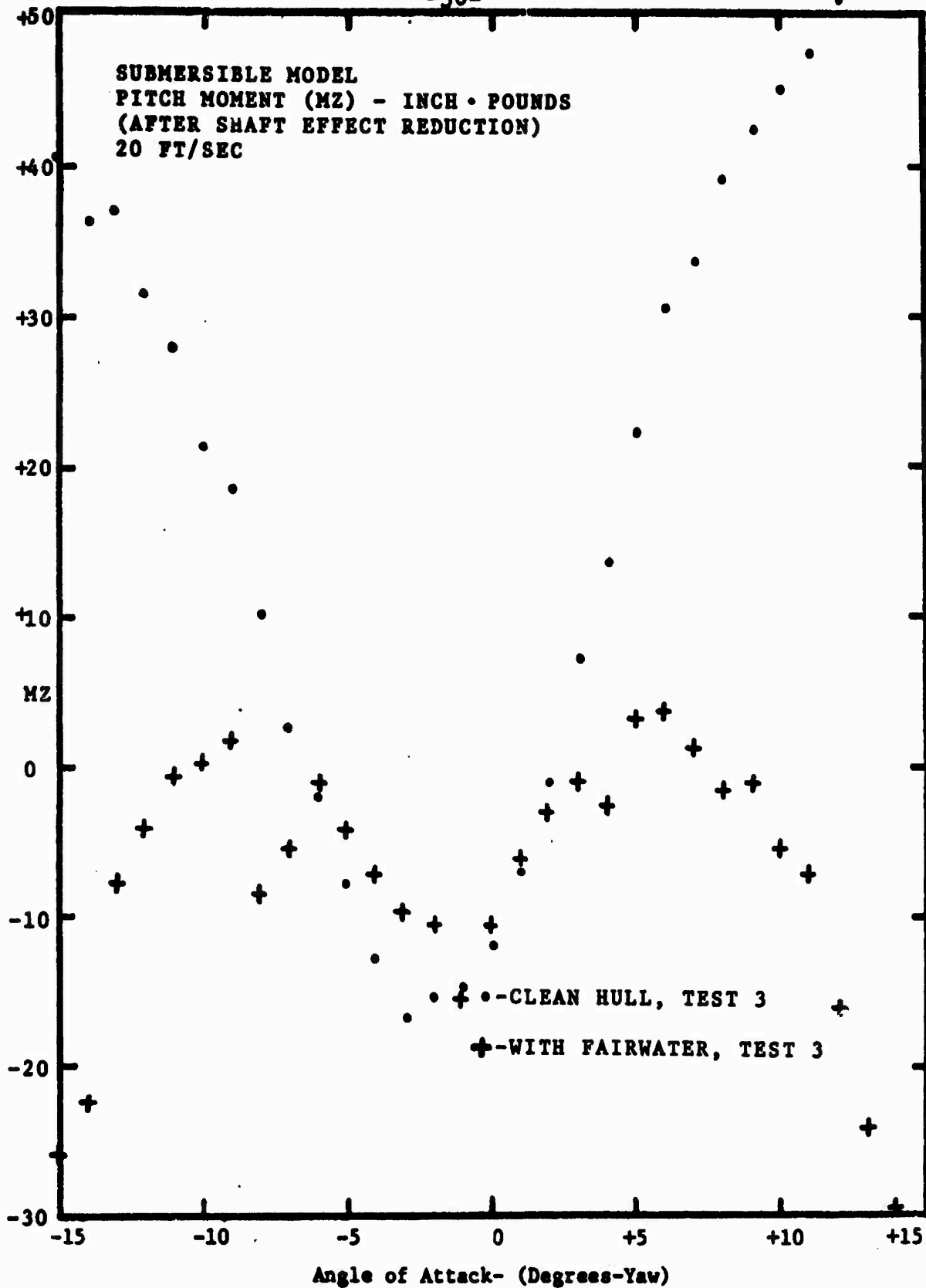


Figure 17

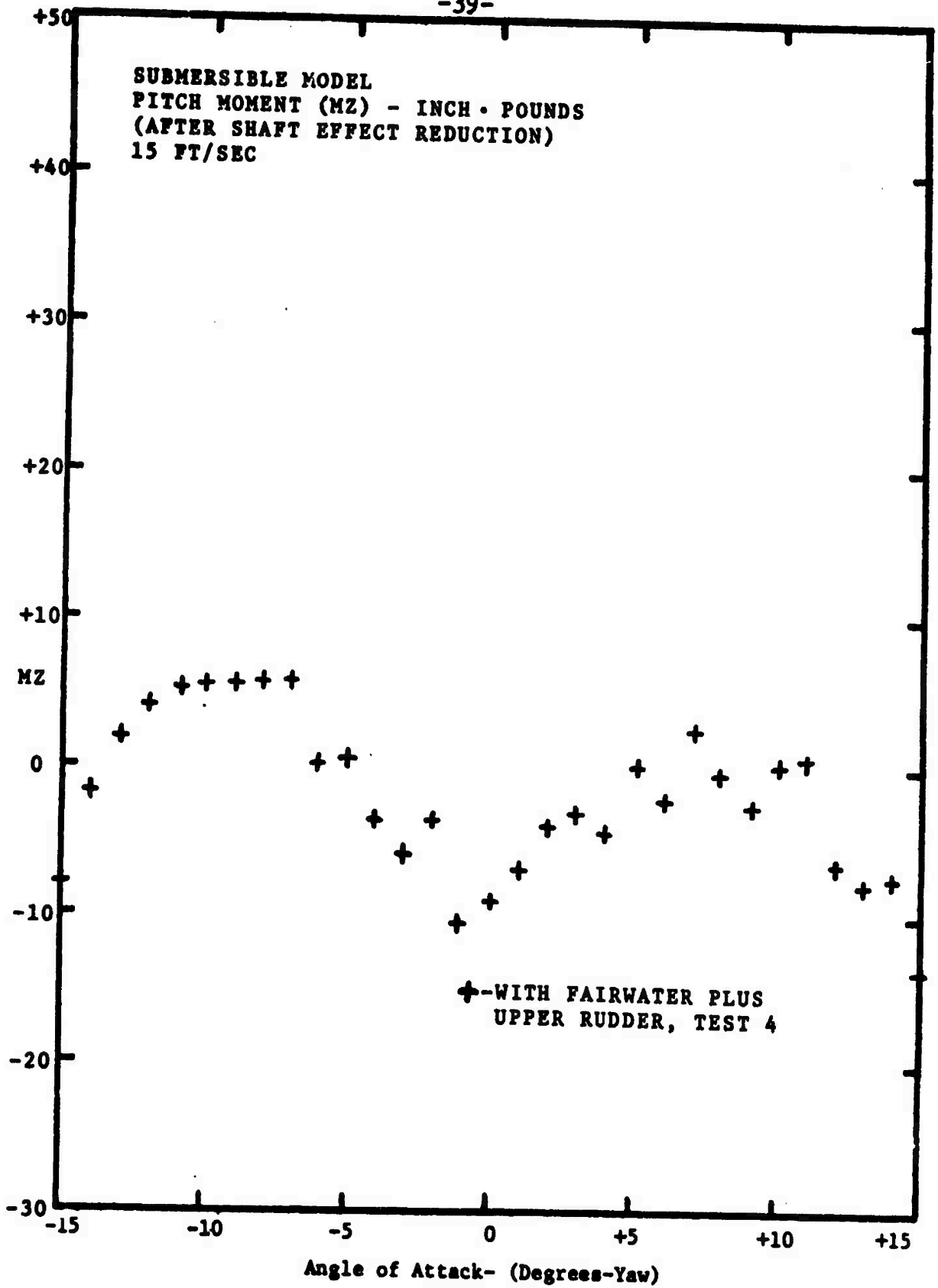


Figure 18

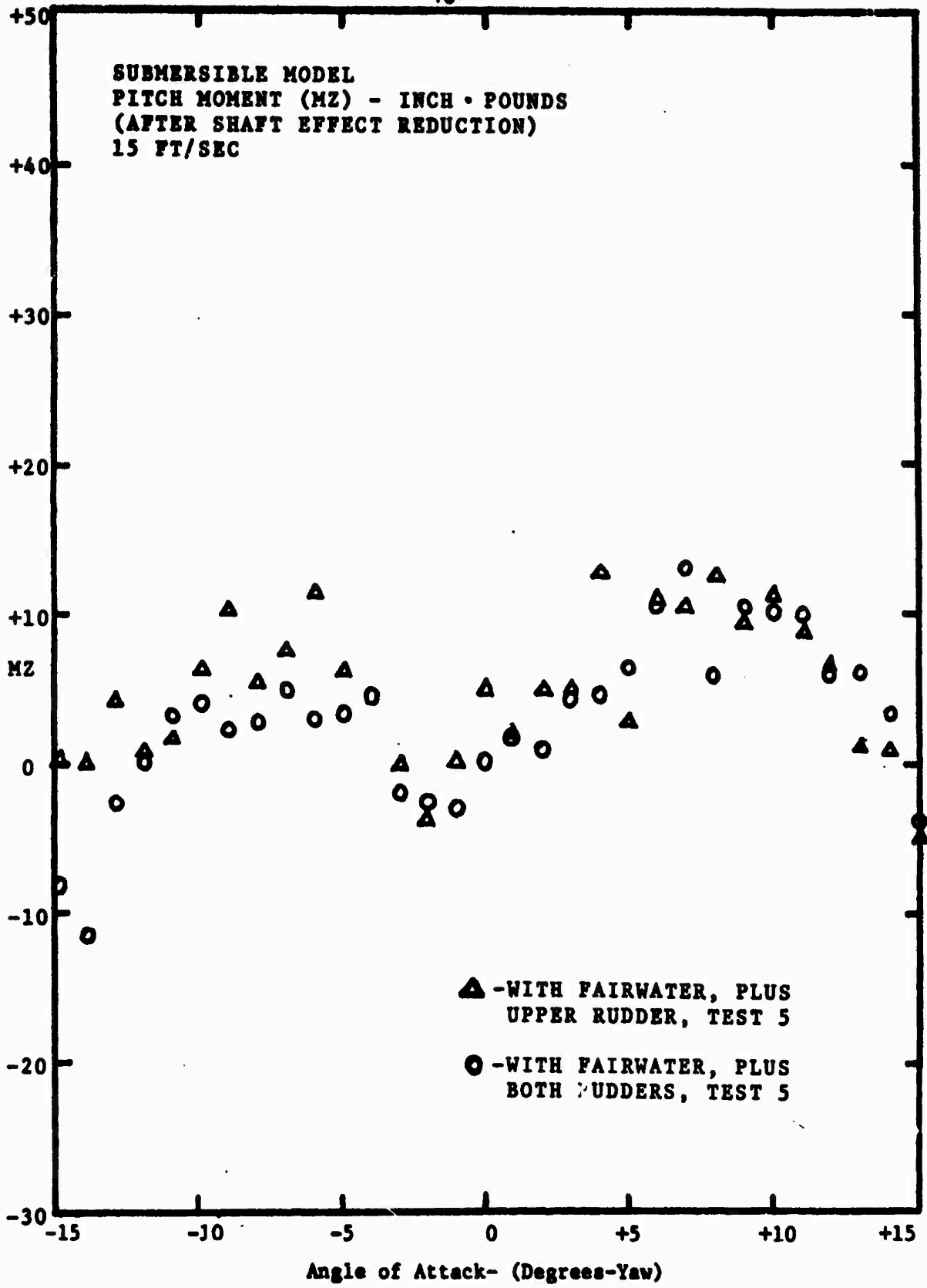


Figure 19

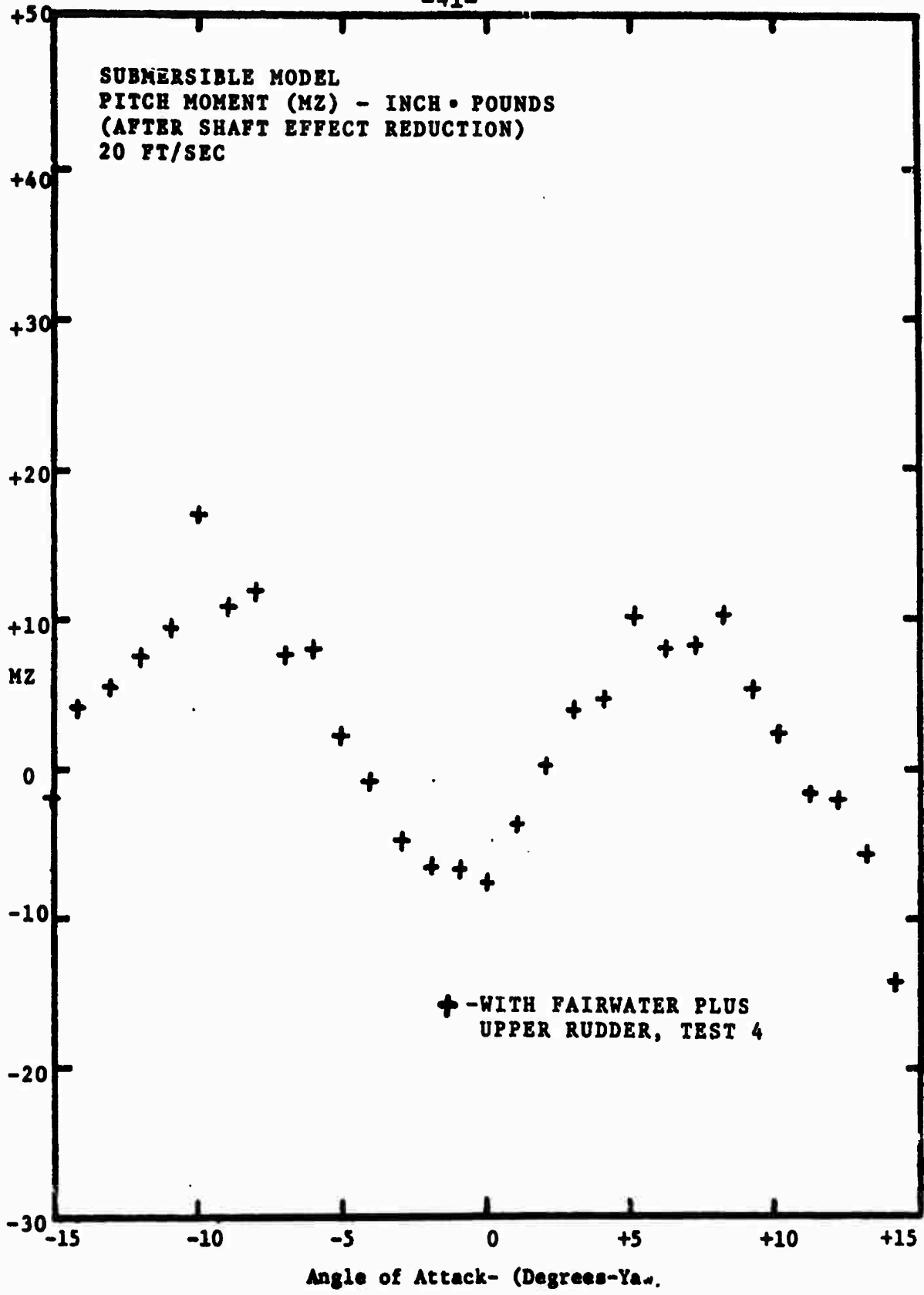


Figure 20

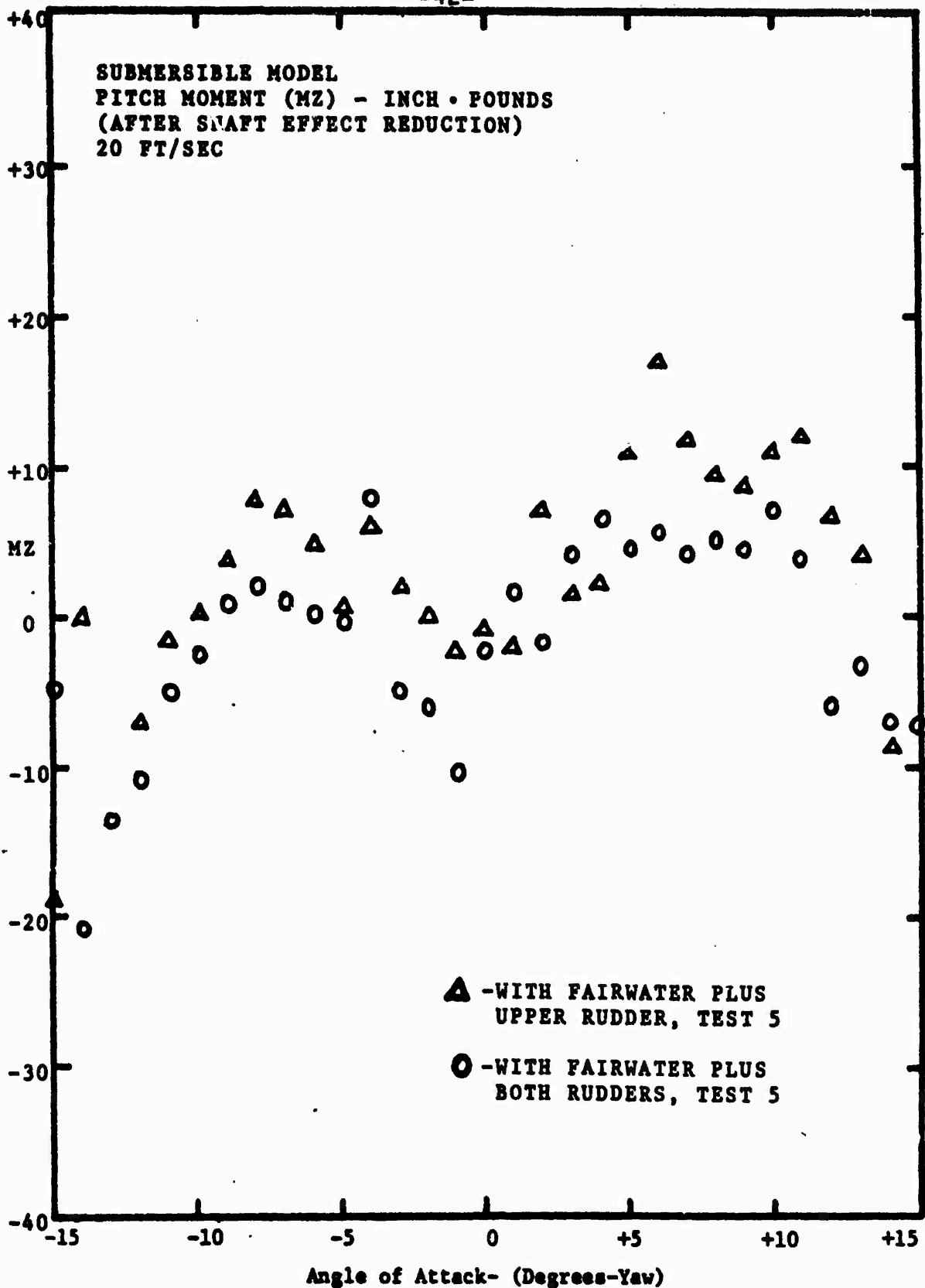


Figure 21

## SIDE FORCE (FZ)

### 1. Shaft Effect

The side force on the bare shaft, although relatively small, was a linear function, and increased with angle of yaw and flow velocity, see Figure 22. The slopes of the lines obtained experimentally were:

A.  $1.5 \text{ lb}/10 \text{ degrees} = .15 \text{ lb/degree}$ , for 15 ft/sec,

B.  $2.4 \text{ lb}/10 \text{ degrees} = .24 \text{ lb/degree}$ , for 20 ft/sec.

An approximation of  $.05 \text{ lb/degree}$  was made for the slope expected for a velocity of 10 ft/sec.

### 2. Model Results

Every model configuration tested resulted in a side force that increased linearly with angle of yaw and flow velocity. The total side force on a configuration was due to appropriate contributions of side force on the symmetric body of revolution, the fairwater and the rudders, see Figure 23. The side force on the body of revolution results from viscous effects, changes in the crossflow pattern along the length of the model, separation of the flow past the body, and interaction with the fairwater. The fairwater and rudders are essentially lifting surfaces that generate a side force component when placed at an angle of incidence to the flow.

The resulting slopes for the configurations tested were:

<u>Configuration</u>	<u>Velocity (ft/sec)</u>	<u>Slope (lb/degree)</u>	<u>Reference Figure Number</u>
1	15	.50	24
1	20	1.05	25
2	15	1.70	24
2	20	3.20	25
3	15	1.90	27
3	20	3.30	28
4	10	.94	26
4	15	2.00	27
4	20	3.40	28

Although the addition of the fairwater (configuration 2) resulted in a step increase of the side force from that of the clean hull (configuration 1), the addition of the upper rudder (configuration 3) and the lower rudder (configuration 4) resulted in relatively no increase of the side force on the body. The reason for the latter result was found by investigation of the flow past the body. A flow visualization method was used in which the hull body, fairwater and



rudders were tufted, in order to observe and photograph the flow at various angles of yaw, see Figures 29, 30, 31 and 32. The flow past the forward portion of the model showed the increasing crossflow component resulting from increasing angle of yaw as seen by the angle of deflection of the tufts from the body axis. Yet, the flow past the aft portion of the model appears as that observed for a reduced angle of yaw. The difference between these two sections is the location of the fairwater. The change in the flow pattern, resulting from the fairwater shedded wake and its induced velocity, reduces the effective angle of yaw on the upper rudder. The upper rudder is defined as that which is on the same side of the submersible as the fairwater.

The lower rudder, on the opposite side from the fairwater, experiences a similar effect due to the presence of the support shaft, but the magnitude is not as great. The flow visualization test was performed at three water tunnel velocities - 10 ft/sec, 15 ft/sec, and 20 ft/sec - and until separation on the fairwater and both rudders occurred. The flow patterns and initiation of separation on the lifting surfaces did not depend on flow velocity, but only on angle of yaw. The initiation of separation occurred at different angles of yaw for each of the three lifting surfaces. Separation on the fairwater was observed at an angle of yaw equal to 16.5 degrees. At this angle, neither of the rudder surfaces showed any

signs of separation. Separation on the lower rudder appeared when the body of the model was placed at 20 degrees yaw angle. The upper rudder still showed no signs of separation. The angle of yaw was increased until separation was observed at a model yaw angle of 29 degrees, see Figure 32c. Figure 32d was included to show the flow pattern along the model at a negative angle of yaw (15 degrees).

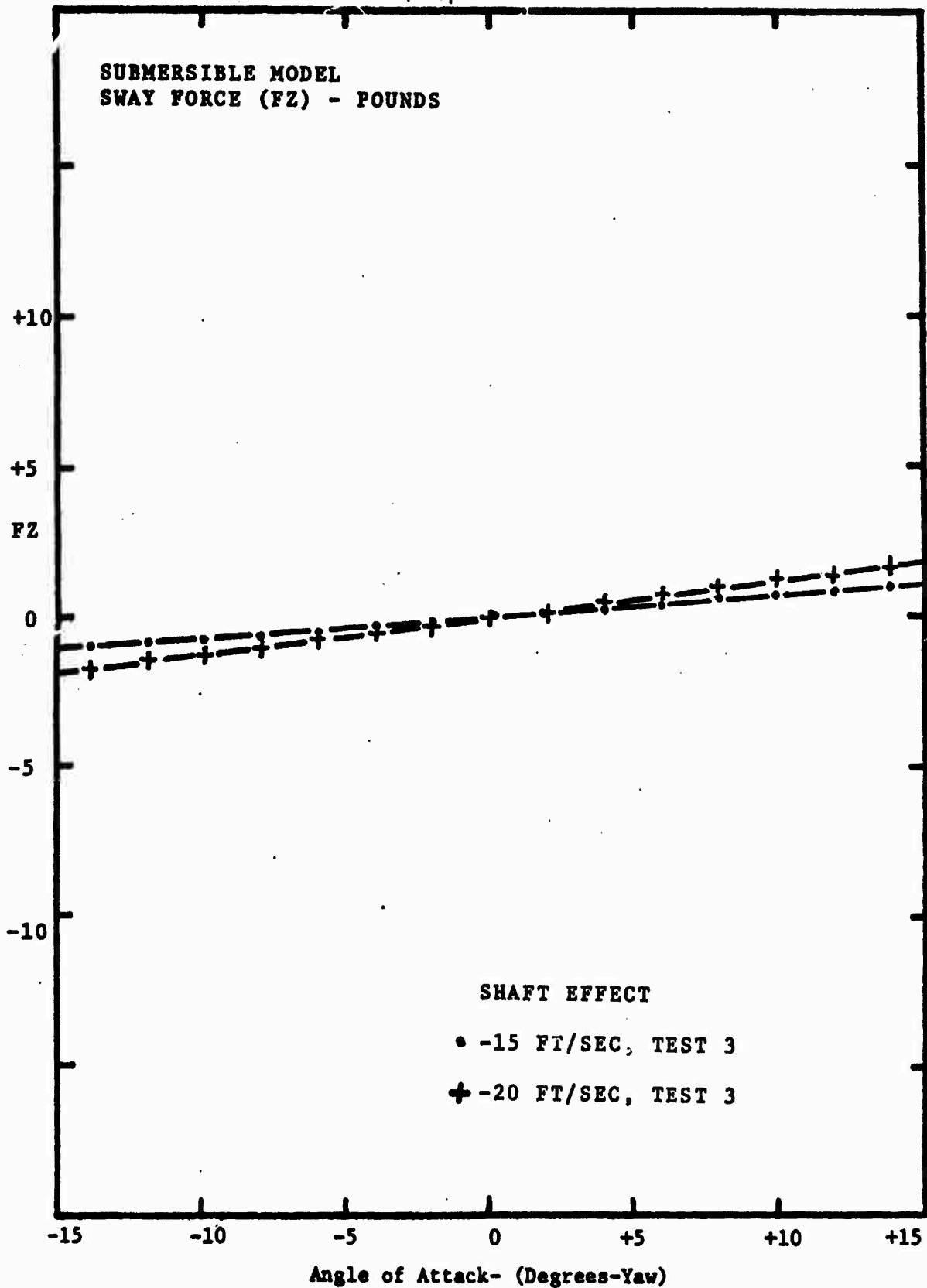
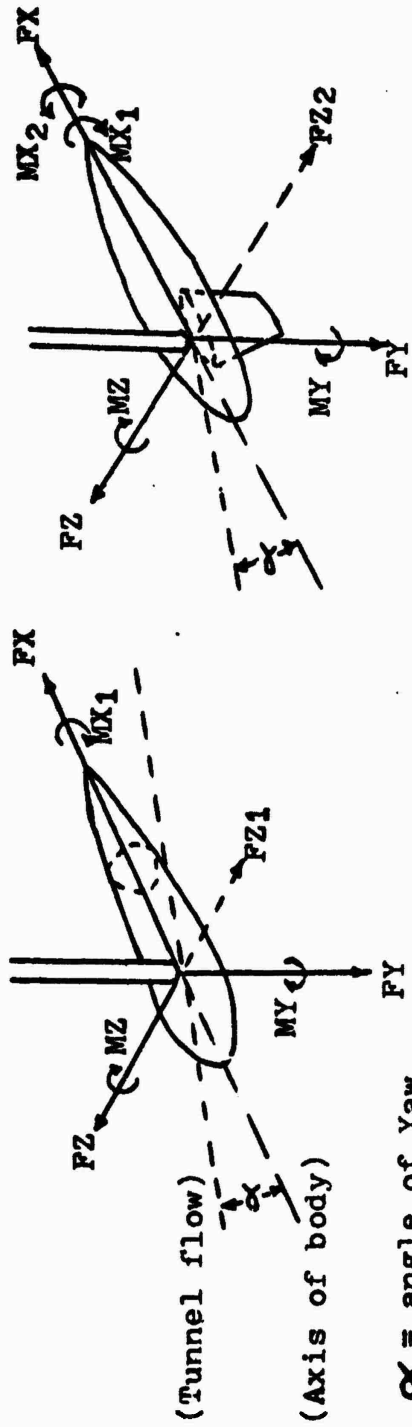


Figure 22



- a. Without fairwater
  - b. With fairwater
- a.  $MX_1$  = Roll moment about body axis, resulting from non-symmetry of streamlined body, (the supporting shaft)
- $FZ_1$  = Side force on the body, due to form drag at angles of Yaw
- b.  $MX_2$  = Roll moment about body axis, resulting from non-symmetry of added fairwater, (Net roll moment on model,  $MX = \Sigma MX_i$ ; in above case,  $MX = MX_2 - MX_1$ )
- $FZ_2$  = Side force resulting from the addition of the fairwater to the body, (Net side force,  $FZ = \Sigma FZ_i$ ; in above case,  $FZ = FZ_1 + FZ_2$ )

Figure 23 Interpretation of hydrodynamic effects for graphic results

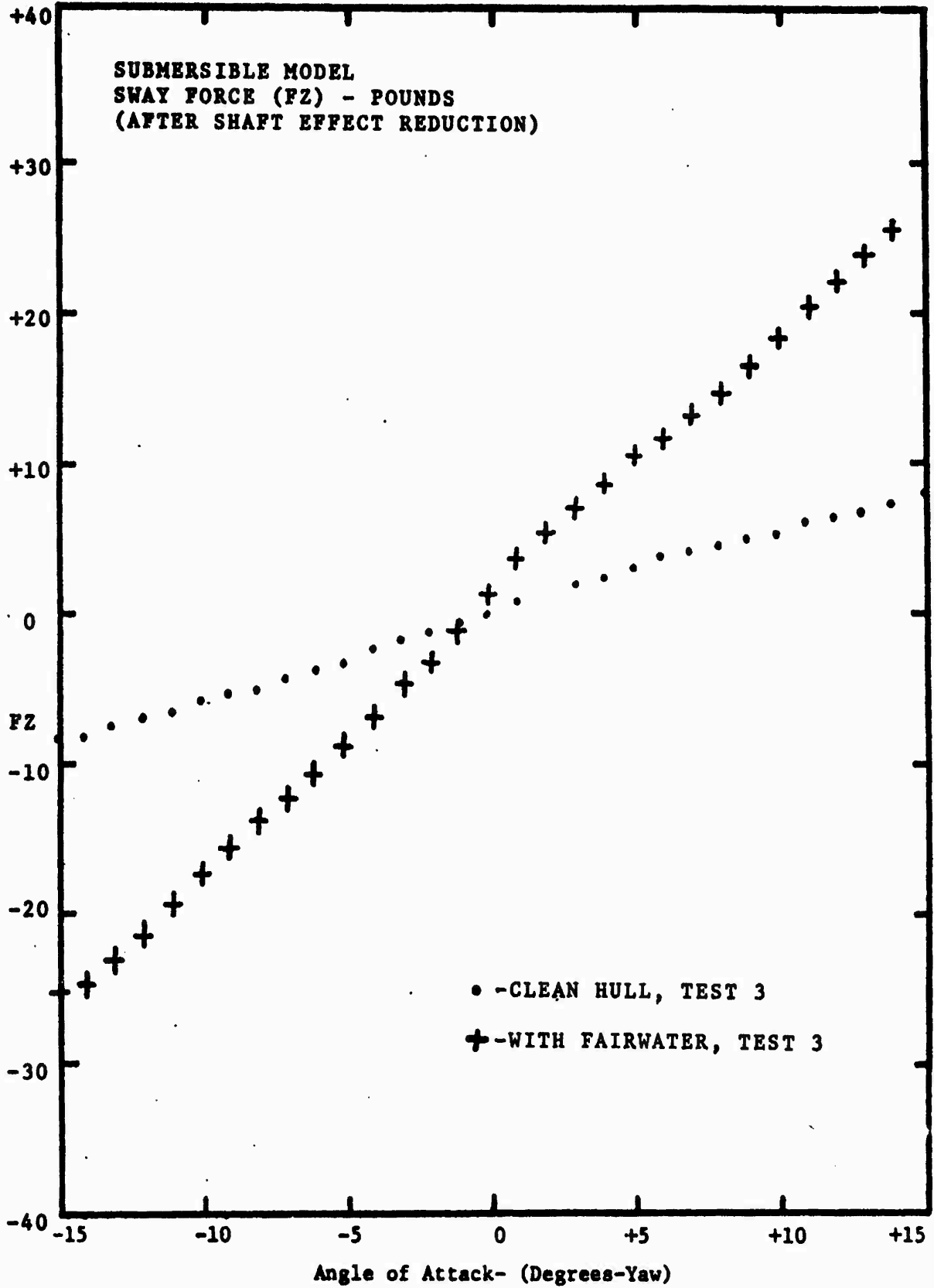


Figure 24

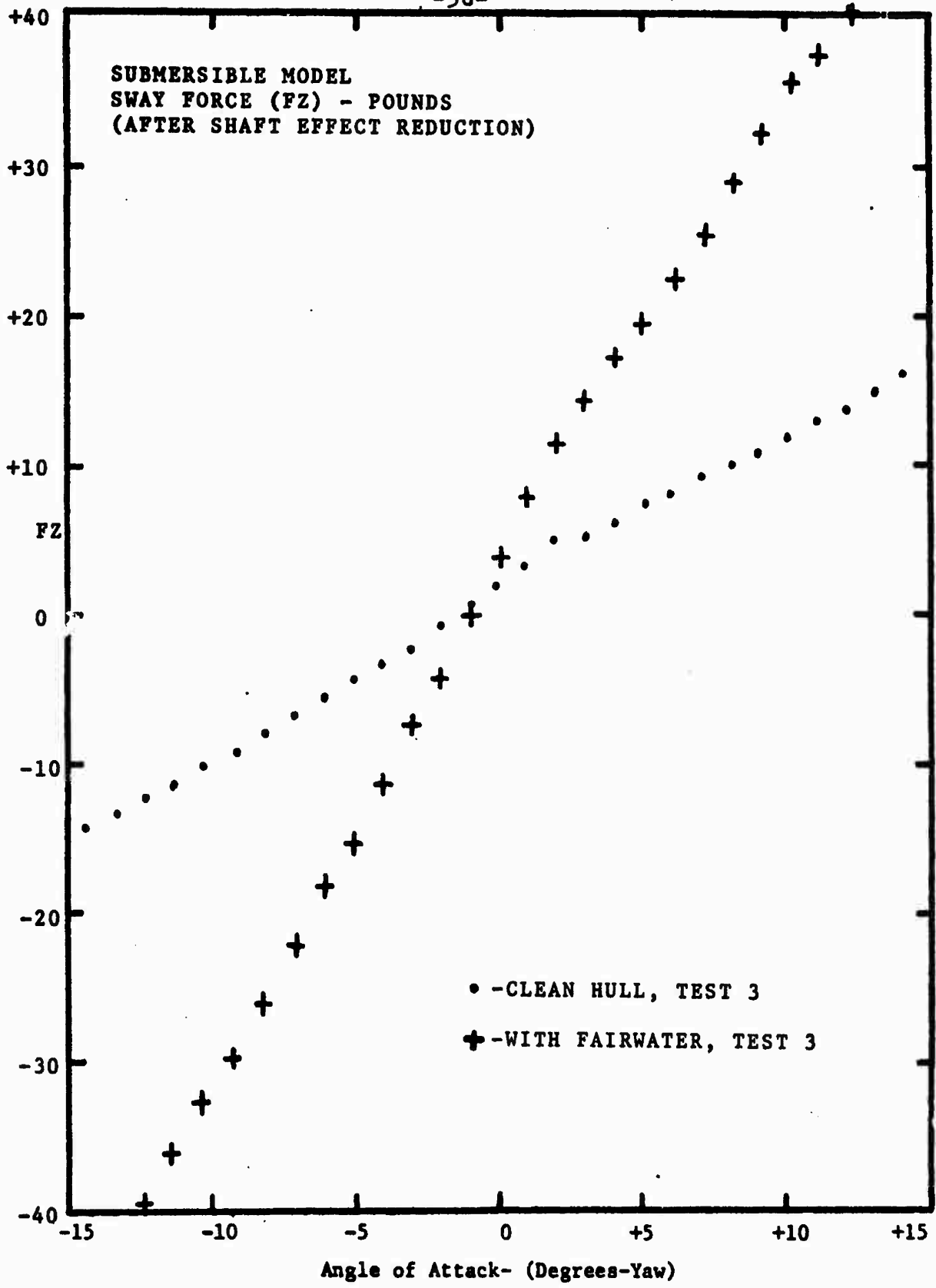


Figure 25

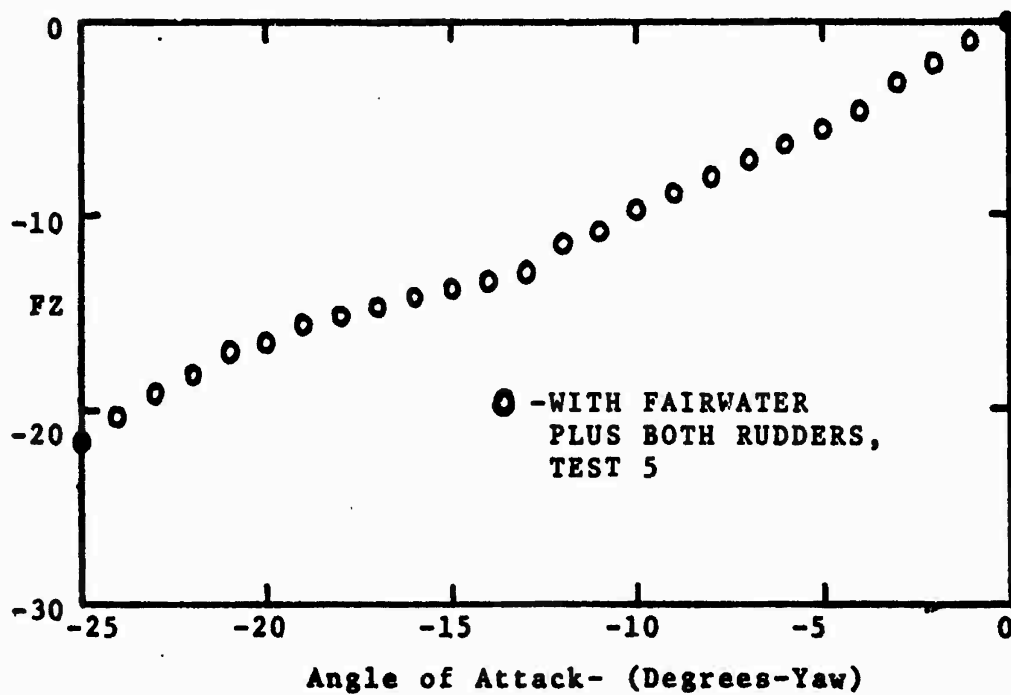
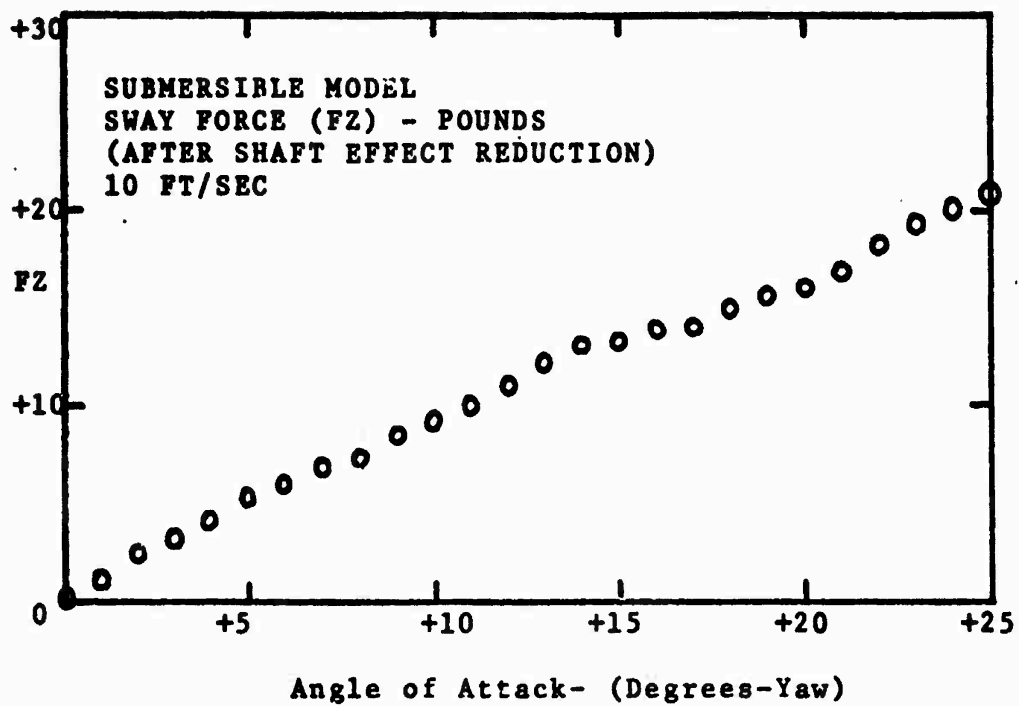


Figure 26

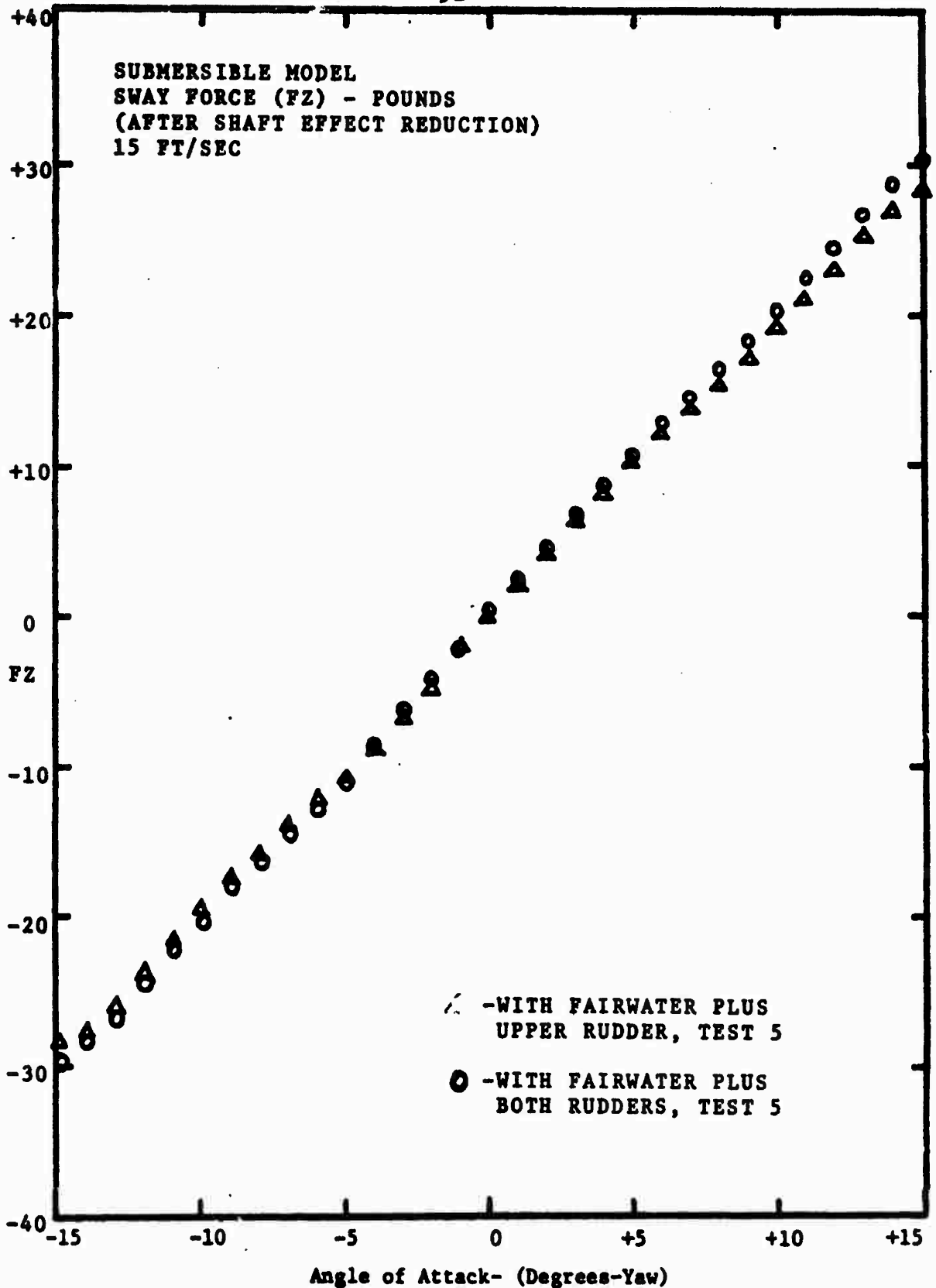


Figure 27



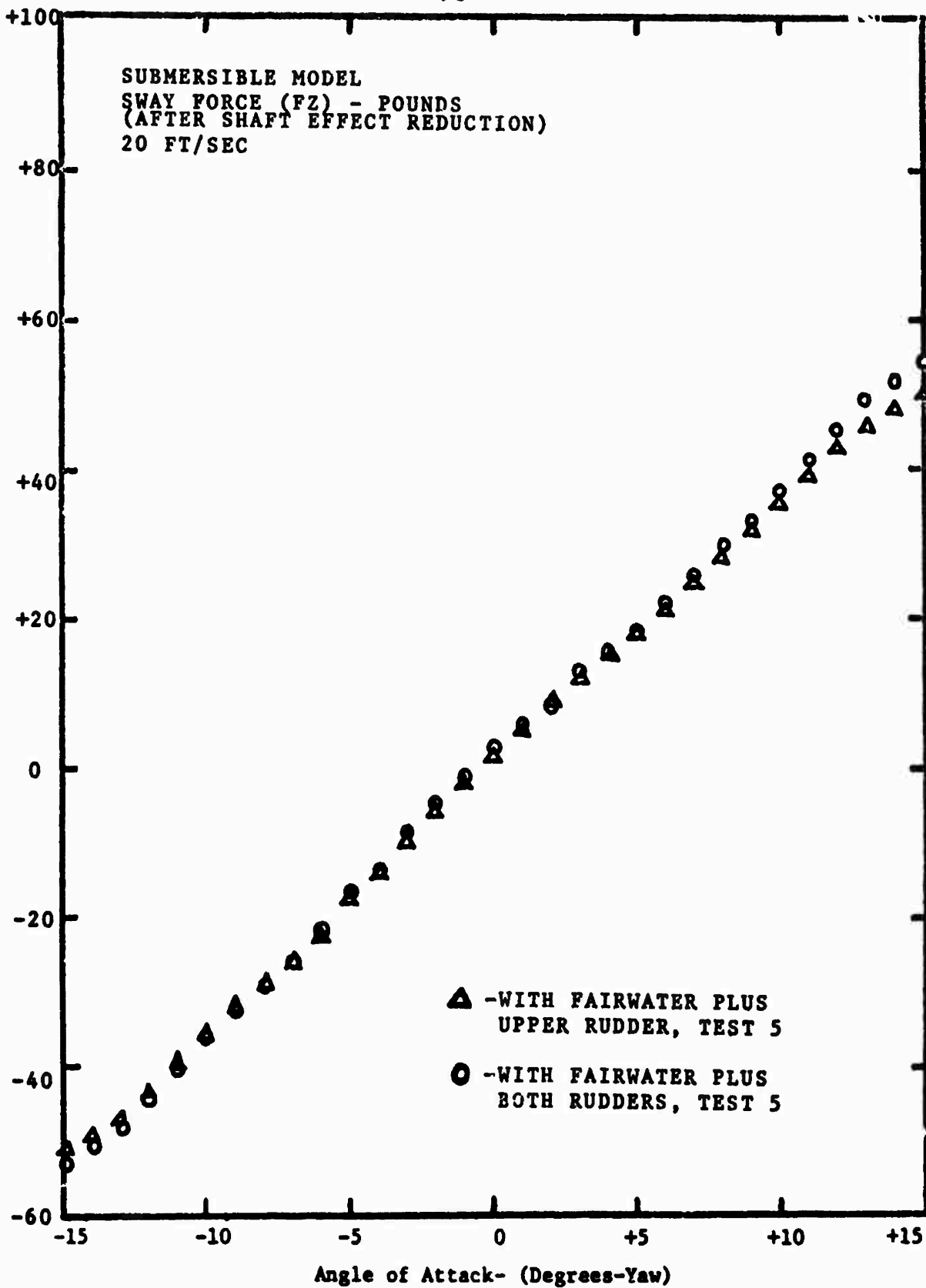


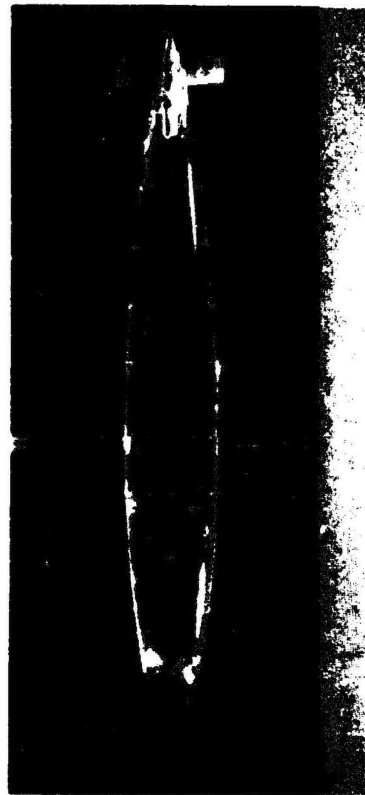
Figure 28



a. When submersible is parallel to water tunnel flow,  $\alpha = 0$  degrees



b. When submersible is parallel to water tunnel flow,  $\alpha = 0$  degrees



c. When  $\alpha = 5$  degrees



d. When  $\alpha = 5$  degrees

(Note:  $\alpha =$  Yaw angle)

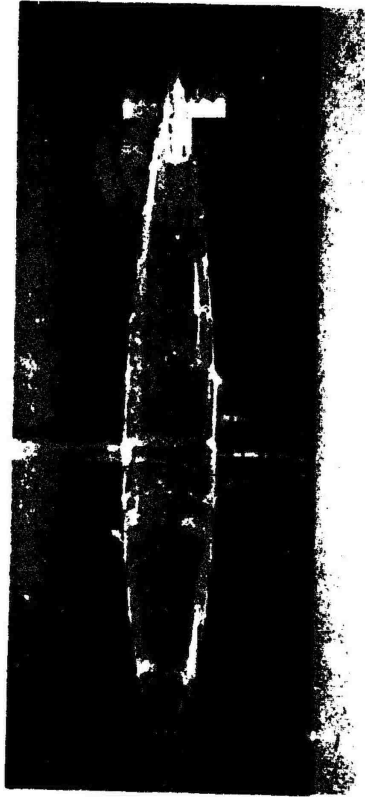
Figure Submersible model with flow visualization (Tufted)



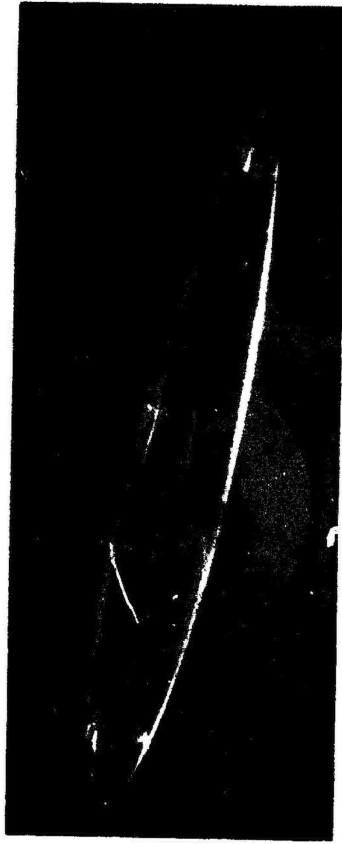
a. When  $\alpha = 10$  degrees



b. When  $\alpha = 10$  degrees

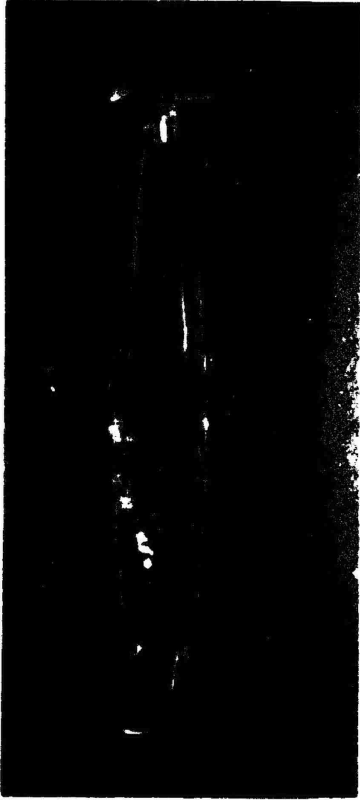


c. When  $\alpha = 15$  degrees



d. When  $\alpha = 15$  degrees

Figure Submersible model with flow visualization (Tufted)



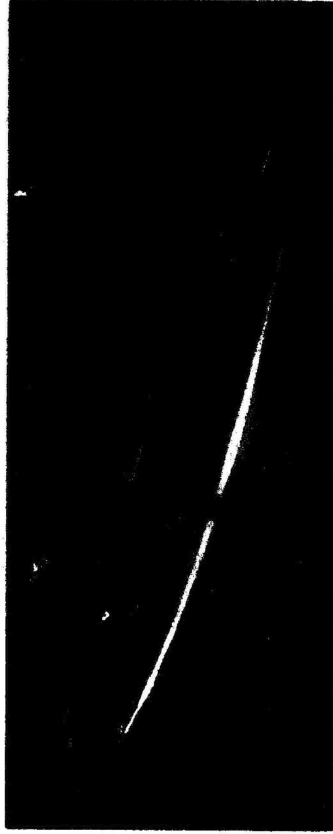
a. Separation on fairwater, but not on either of the rudders, when  $\alpha = 16.5$  degrees.



b. Separation on fairwater, but not on either of the rudders, when  $\alpha = 16.5$  degrees.



c. Separation on fairwater and one rudder, other rudder still effective, when  $\alpha = 20$  degrees.



d. Separation on fairwater and one rudder, other rudder still effective, when  $\alpha = 20$  degrees.

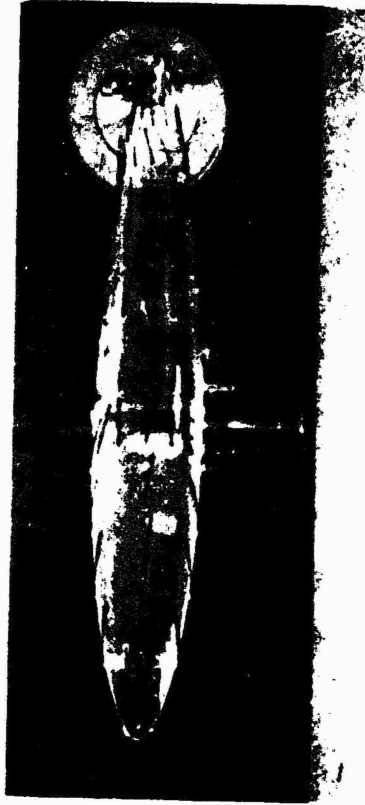
Figure Submersible model with flow visualization (Tufted)



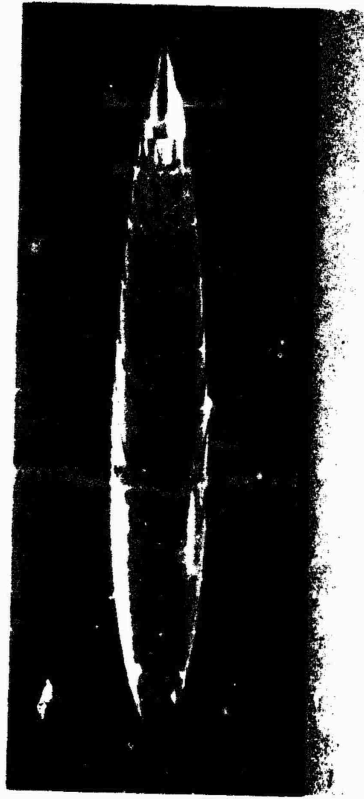
a. Separation on fairwater and one rudder, other rudder still effective, when  $\alpha = 25$  degrees.



b. Separation on fairwater and one rudder, other rudder still effective, when  $\alpha = 25$  degrees.



c. Separation on all three lifting surfaces is experienced (see backflow), when  $\alpha = 29$  degrees.



d. Flow when  $\alpha = -15$  degrees; tangle on one rudder resulted from a previous test run.

Figure Submersible model with flow visualization (Tufted)

## ROLL MOMENT (MX)

The roll moment on a submerged body of revolution at an angle of yaw, with and without appendages, is a direct result of the side forces (FZ) previously reported and the relative location of their concentrations with respect to a reference point. For an actual submersible, the reference point would be the center of gravity, which would be below the body axis of symmetry. The reference point for the model tested was at the origin of the coordinate system, which is on the body axis of symmetry.

### 1. Shaft Effect

The roll moment obtained on the base shaft decreased with an increasing angle of yaw and increasing flow velocity in a linear fashion, see Figure 33. When a linear result was approximated, the slopes of the lines formed were:

- A. Slope =  $-7 \text{ in. lb}/10 \text{ degrees} = -.7 \text{ in. lb/degree}$ ,  
for a velocity of 15 ft/sec.
- B. Slope =  $-13.5 \text{ in. lb}/10 \text{ degrees} = -1.35 \text{ in. lb/degrees}$ ,  
for a velocity of 20 ft/sec.

### 2. Model Results

Model configuration 1 (clean hull) is symmetrical in all respects, unlike an actual submersible of comparable configuration, whose center of gravity is below the body axis, for

roll stability. This caused an experimental result of zero roll moment for the clean hull at all angles of yaw and all velocities evaluated, see Figures 34 and 35. In actuality, a roll moment would occur on a submersible, due to the asymmetry described above. This fact is reflected in the results of all subsequent configurations, in the form of a difference in total magnitude of roll moment.

With the addition of the fairwater (configuration 2), an increasing roll moment is encountered with both increasing flow velocity and increasing angle of yaw, see Figures 34 and 35. The increase was approximately linear with the following slopes:

- A. Slope = 28 in. lb/10 degrees = 2.8 in. lb/degree,  
for a velocity of 15 ft/sec.
- B. Slope = 54 in. lb/10 degrees = 5.4 in. lb/degree,  
for a velocity of 20 ft/sec.

A decrease in the magnitude of the roll moment and a reversal of slope was noticeable when the model was placed in a yaw angle of about 15 degrees. This was caused by the separation on the fairwater, and the resulting loss of side force (lift component).

Configuration 3 (with fairwater and upper rudder) produced very little change in the roll moment on the model, see Figures 36 and 37. This is a result of a decrease in the effective angle of yaw on the rudder by the perturbations in

the flow due to the fairwater and its shedded wake, see Figures 29, 30, 31 and 32 for flow visualization. A decrease in moment, caused by separation on the fairwater, was experienced again at about 15 degrees yaw angle.

Configuration 4 (with fairwater and both rudders) decreased the magnitude of the roll moment, but only slightly, see Figures 36 and 37. A greater reduction in roll moment should have been obtained for the lifting surface added, but as in configuration 3, the effective angle of yaw on the lifting surface (rudder) in question was reduced. In this case, the support shaft sheds a wake, which interacts with the in-flow velocity on the lower rudder. A similar loss of lift on the fairwater, as in configurations 2 and 3, was obtained for configuration 4.



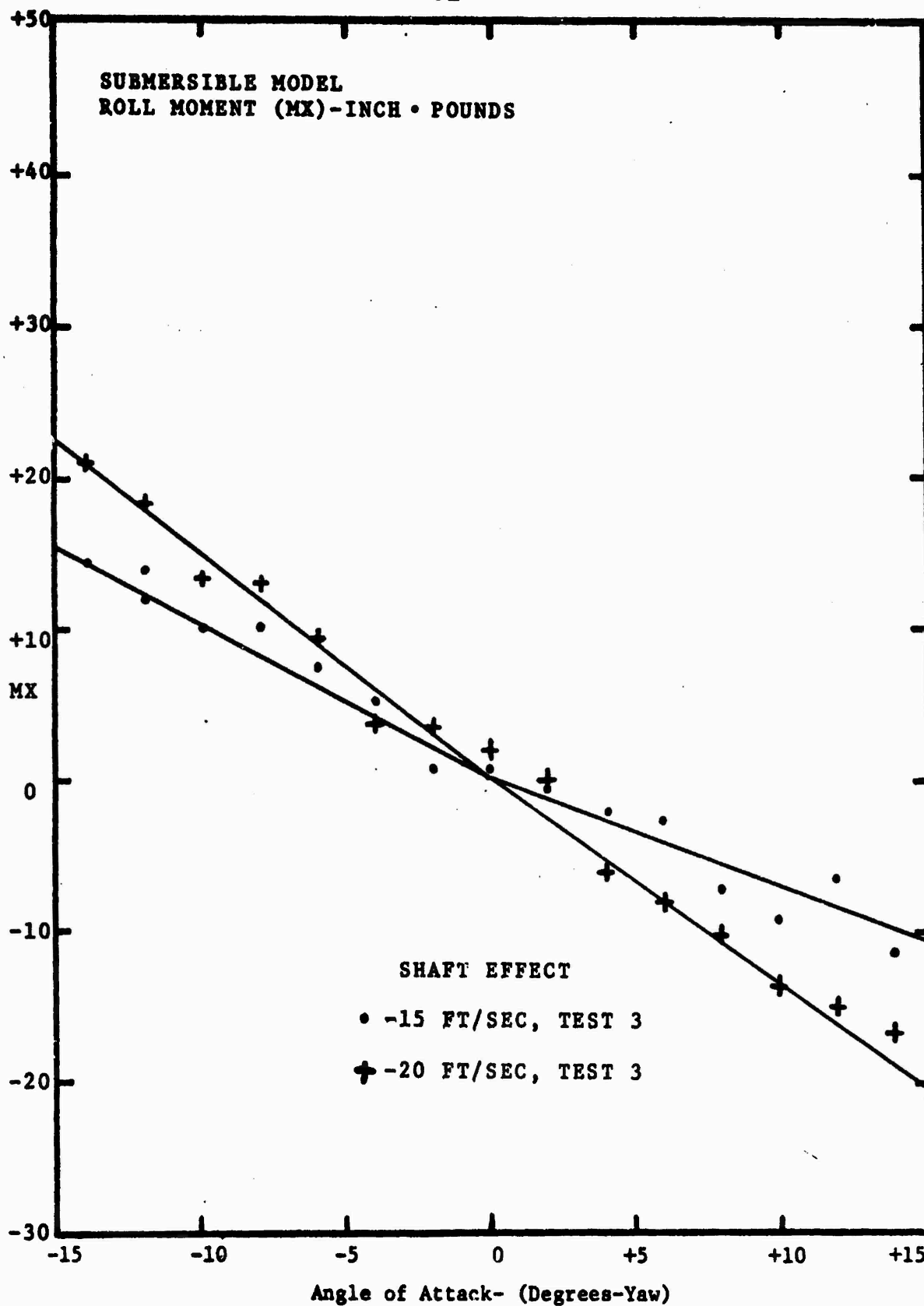


Figure 33

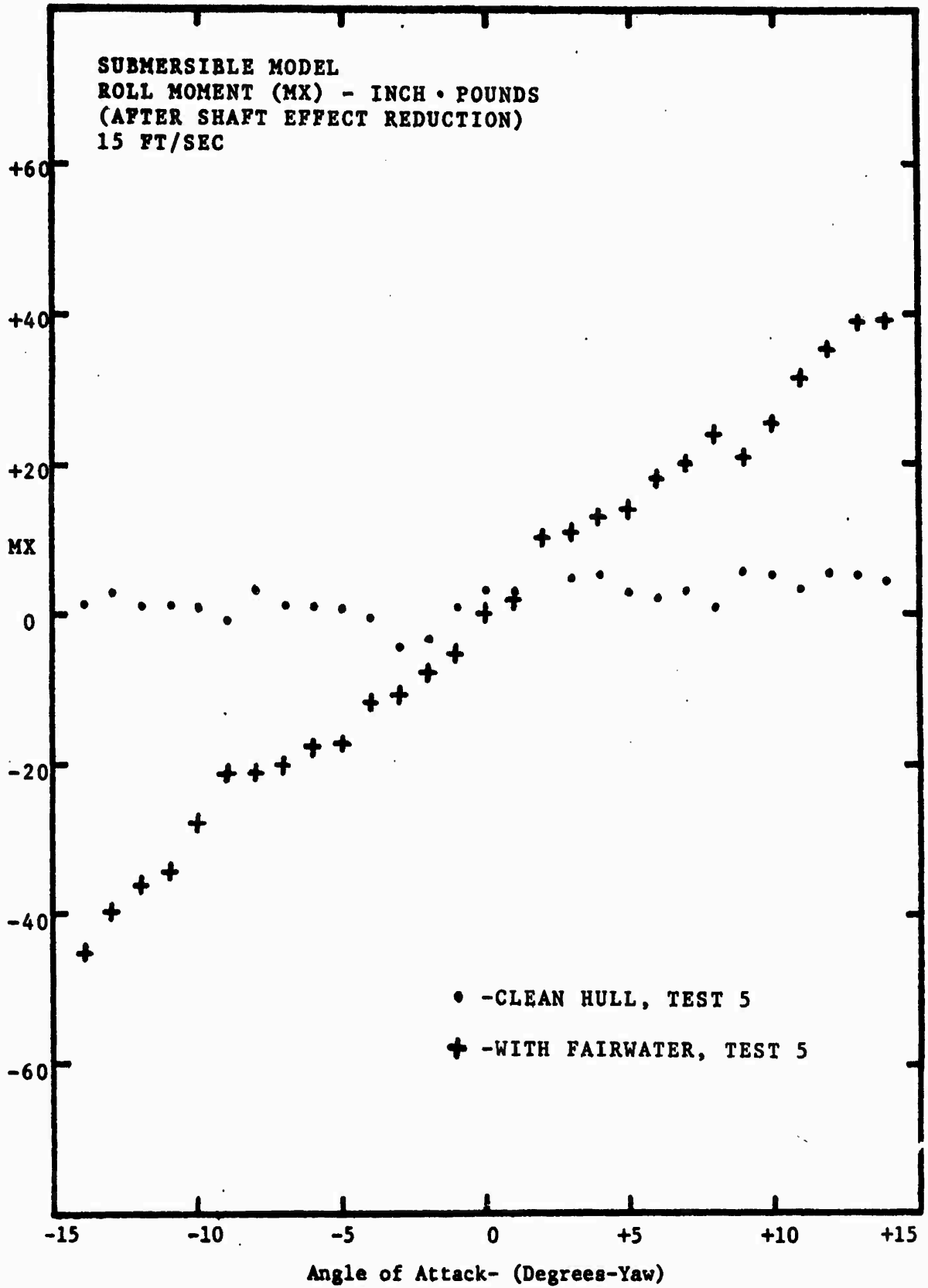


Figure 34

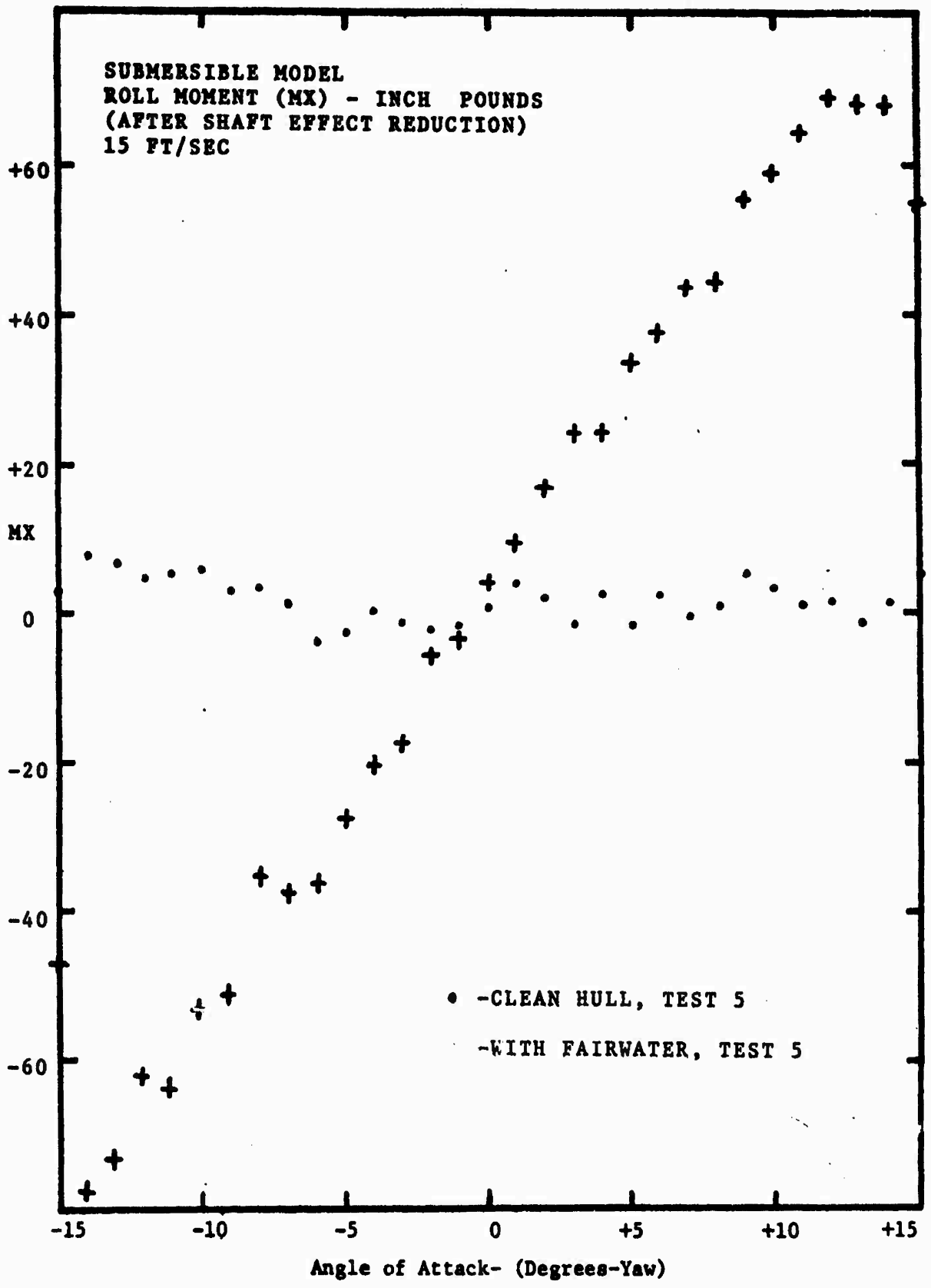


Figure 35

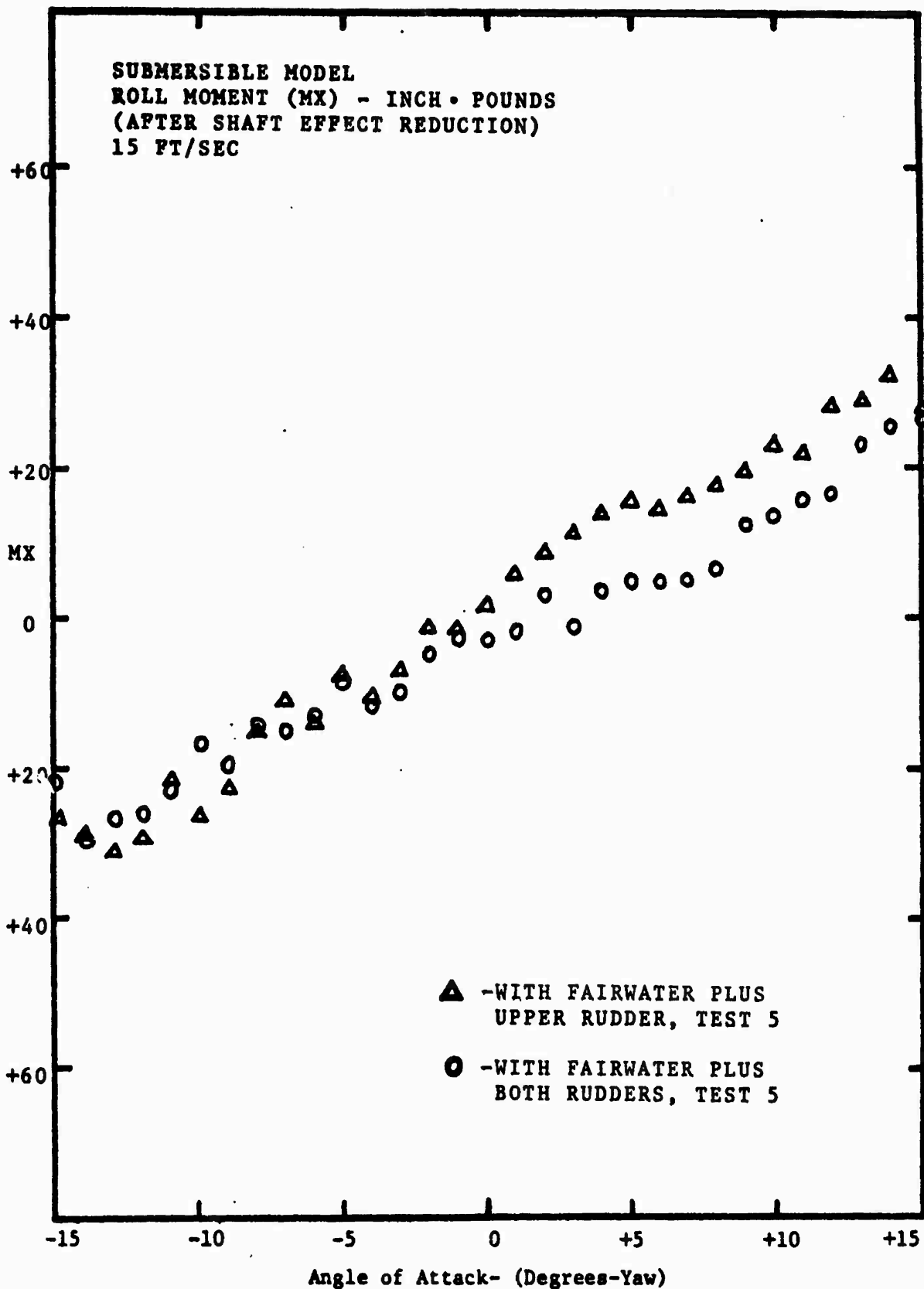


Figure 36

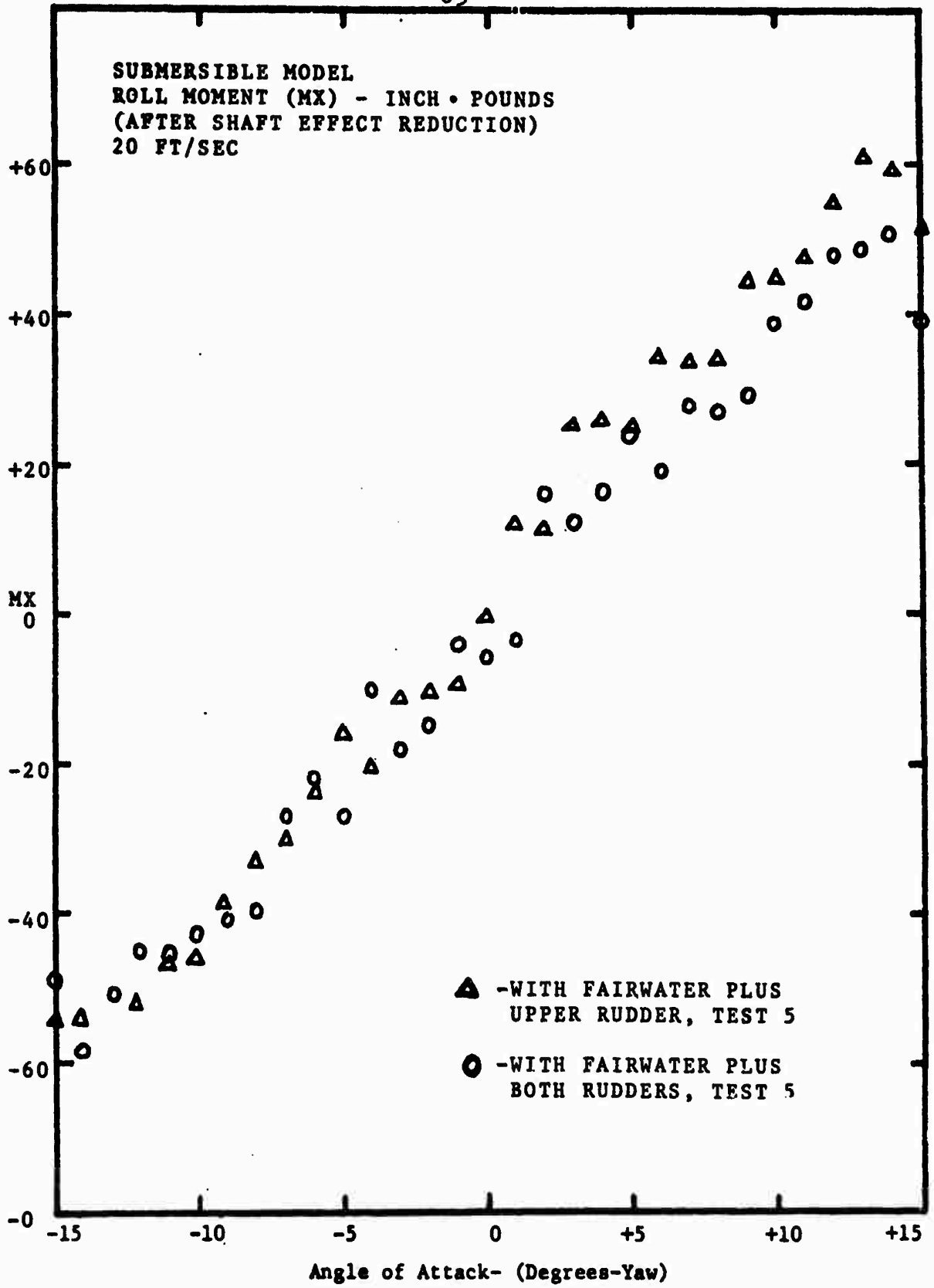


Figure 37

## YAW MOMENT (MYO)

### 1. Shaft Effect

No shaft effect was, or should be, obtained for yaw moment, as this moment is measured about the shaft axis of symmetry.

### 2. Model Results

Configuration 1 (clean hull) produced a linear result that increased with increasing angle of yaw and flow velocity, see Figure 38. Yaw moment components resulted from form drag and changes in the cross flow pattern along the length of the model. The resulting slopes for the two velocities evaluated were:

- A. Slope = 43 in. lb/10 degrees = 4.3 in. lb/degree,  
for 15 ft/sec,
- B. Slope = 80 in. lb/10 degrees = 8.0 in. lb/degree,  
for 20 ft/sec.

When the fairwater (configuration 2) was added, there appears to be no effect until a yaw angle of 4 degrees is reached. Then, the yaw moment increases at a greater rate until the fairwater incurs separation (about 15 degrees yaw angle) and the yaw moment decreases until it reaches the magnitude obtained for the clean hull at that angle of yaw, see Figure 39.

When configuration 3 (with fairwater and upper rudder)

was tested, the magnitude of the yaw moment was decreased slightly due to the opposing yaw moment component from the upper rudder, see Figure 40. The yaw component from the rudder would have been larger if the fairwater had not caused any interaction, as previously described, to reduce the side force on the rudder. This configuration follows the same pattern as configuration 2; it incurs a rapid change in slope when the fairwater separates, but at a lower magnitude.

Configuration 4 (with fairwater and both rudders) produced a very powerful effect on reduction of yaw moment, see Figure 41. The side force developed by the addition of the lower rudder, combined with its moment arm, produces a yaw component that eventually supercedes that caused by the fairwater and forward portion of the body of revolution. When this model configuration was tested at an extreme yaw angle of 25 degrees, in both directions, and a flow velocity of 10 ft/sec, the resulting yaw moment was zero. The result for positive angles of yaw can be seen in Figure 42. Negative angles of yaw produced symmetrical results.

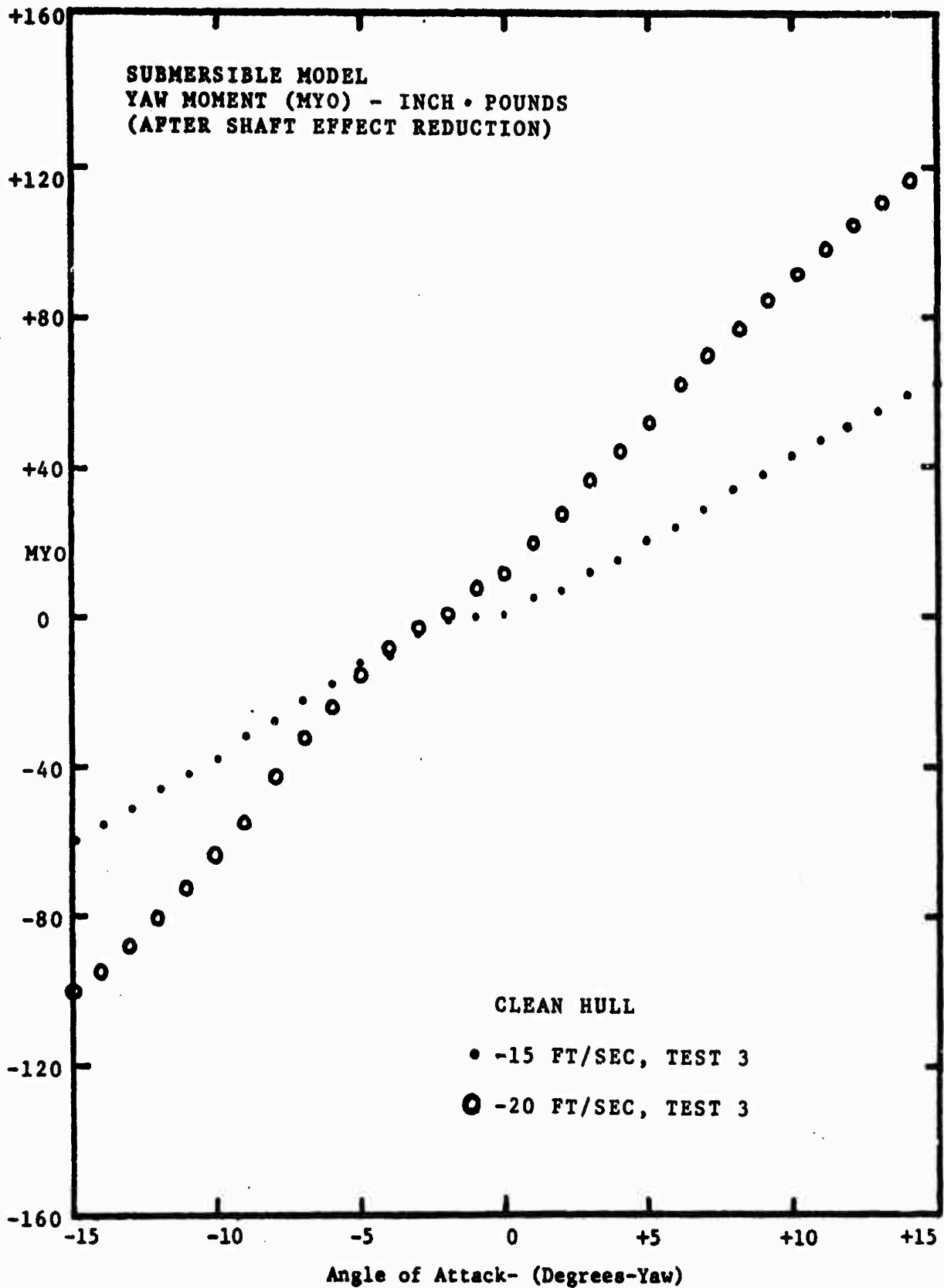


Figure 38



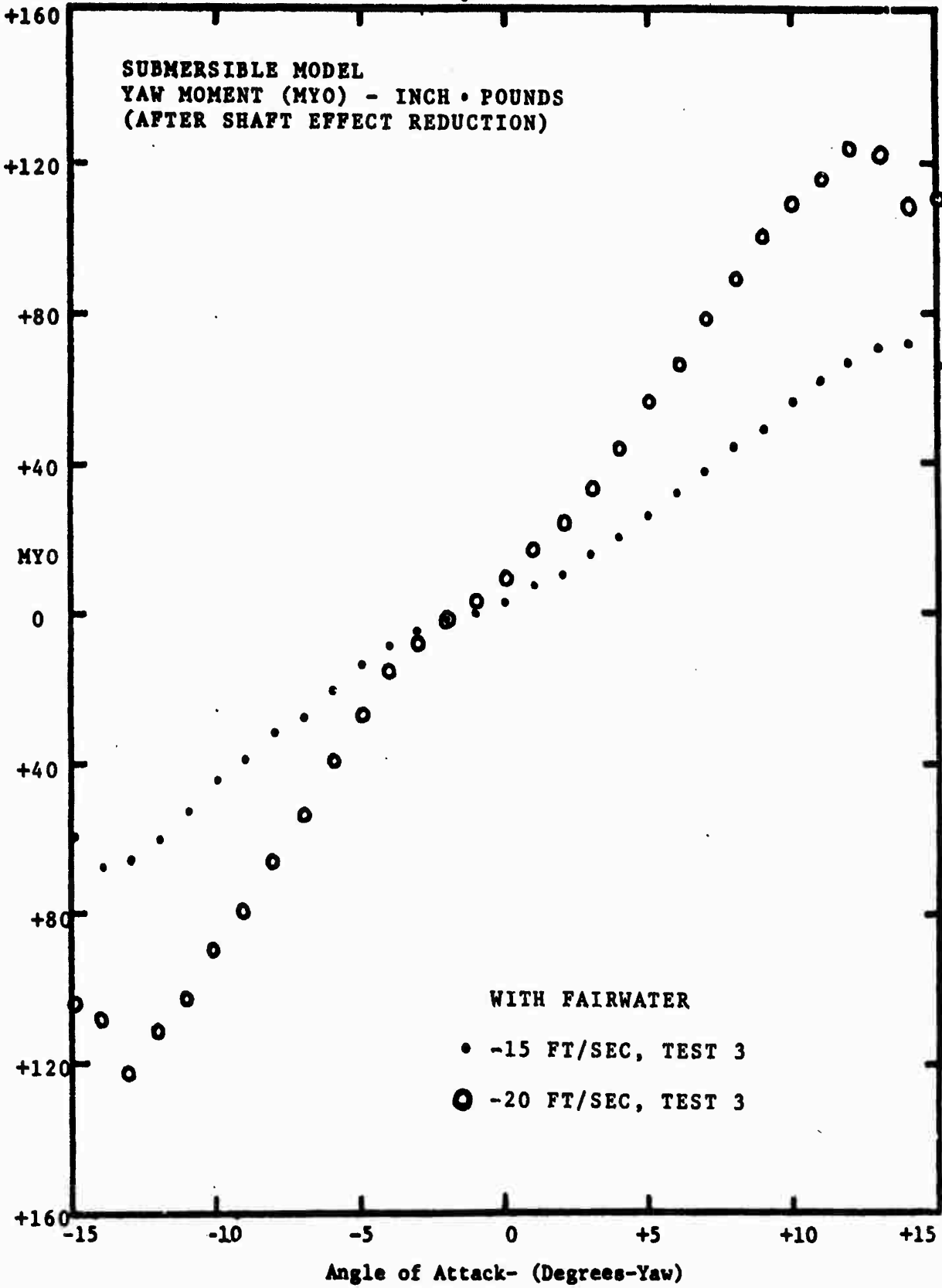


Figure 39

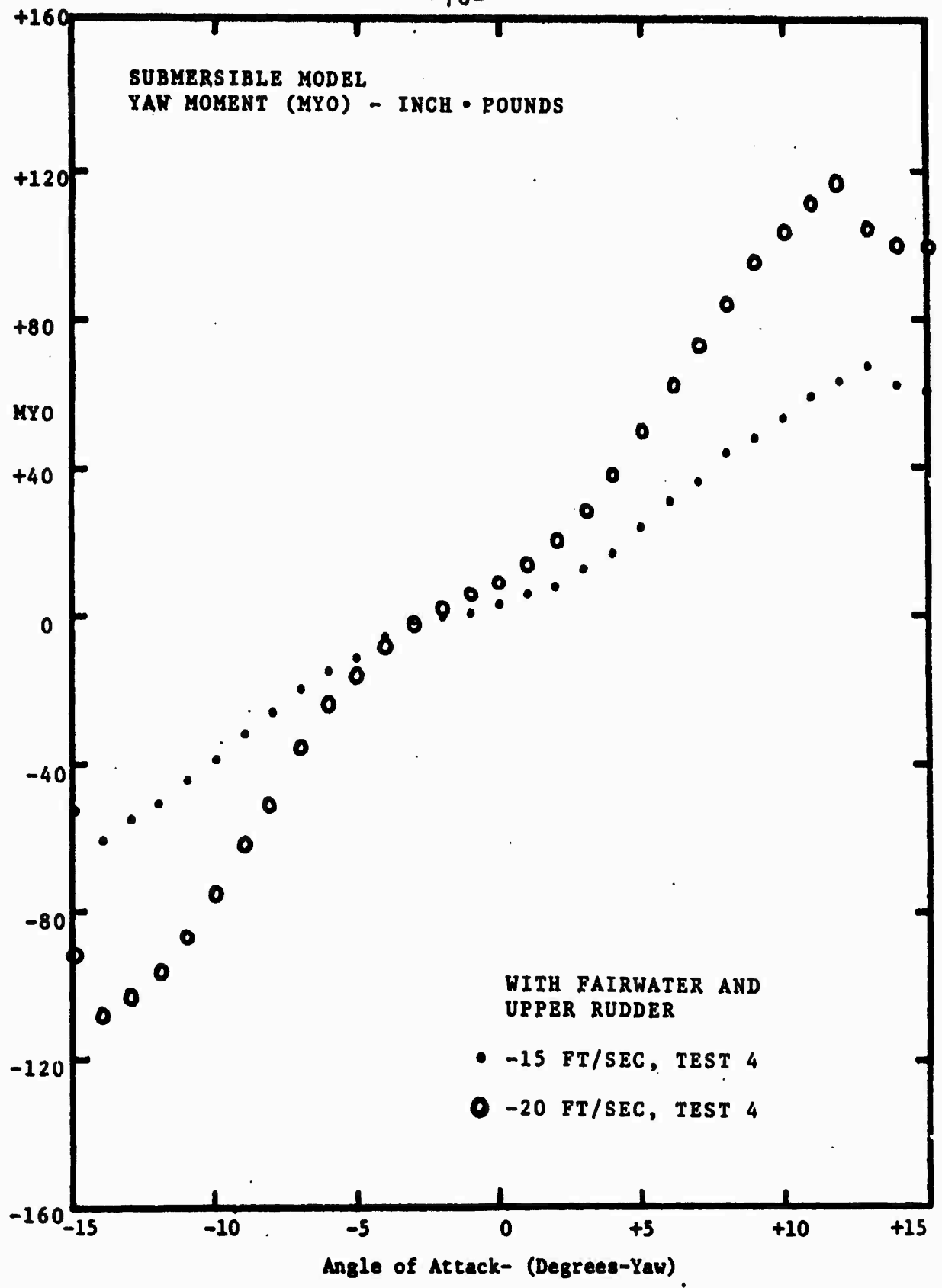


Figure 40

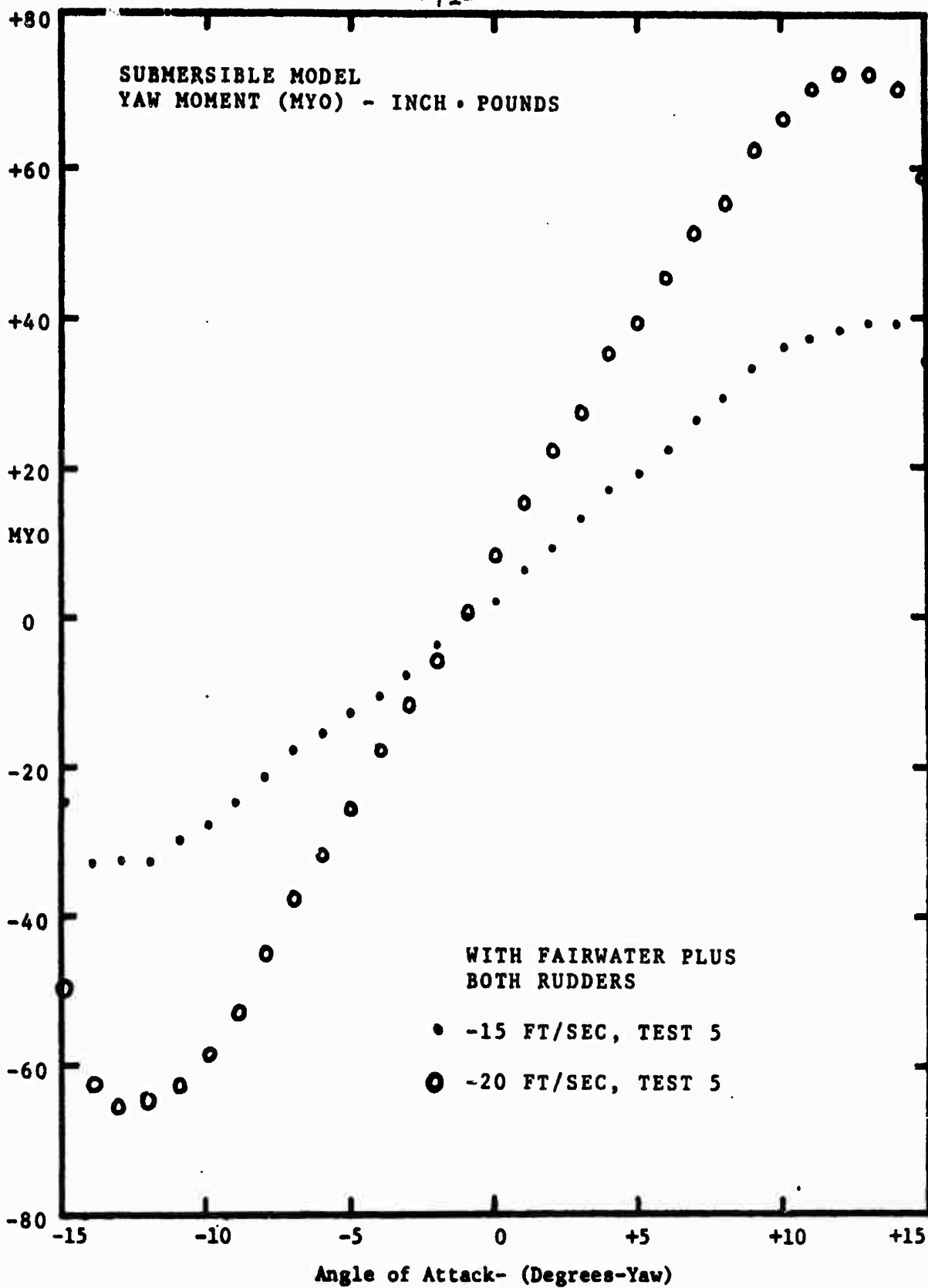


Figure 41

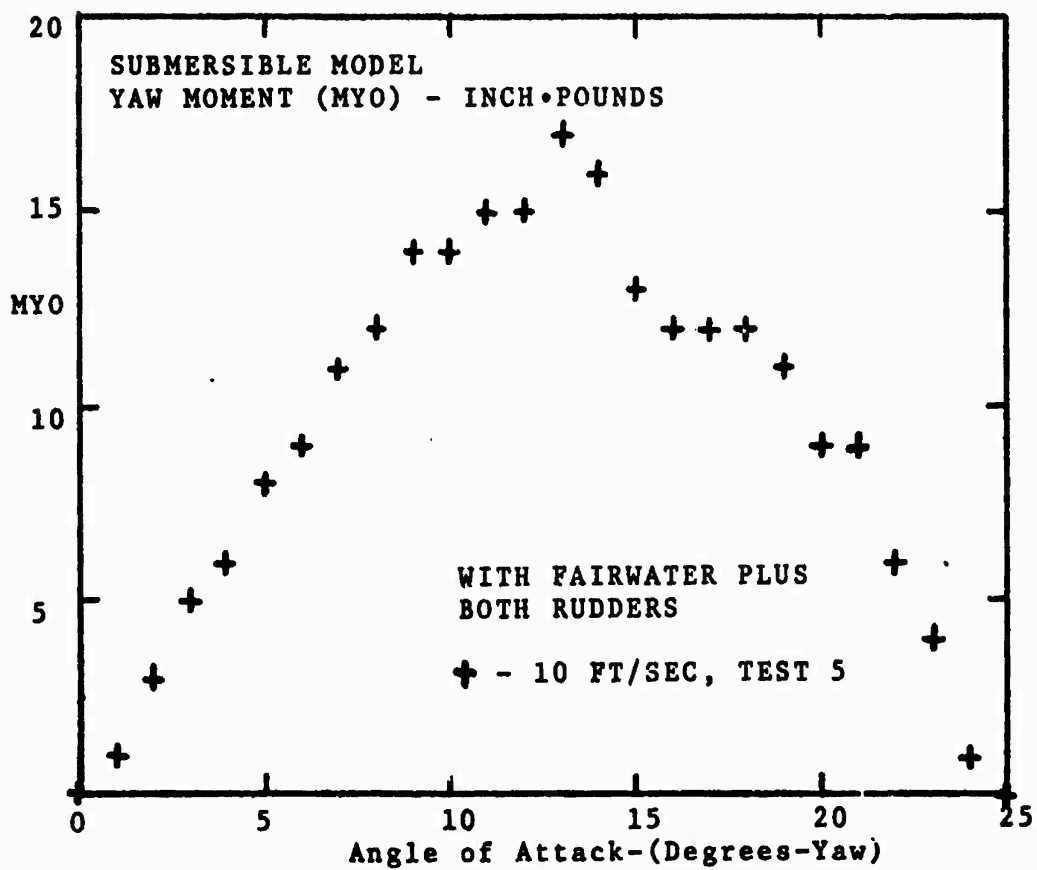


Figure 42

## V. FAIRWATER MODEL EXPERIMENTAL RESULTS

The second set of experiments conducted in the M.I.T. Variable Pressure Water Tunnel consisted of testing the fairwater model, without control surfaces and then with control surfaces attached. The control surfaces were attached to the fairwater by means of a shaft through both the control surfaces and the fairwater. The shaft was used for transferring hydrodynamic forces and moments on the control surfaces to the fairwater, in effect, to the body of the submersible. To control and maintain particular angles of attack of the control surfaces, a guide pin was installed on each of the two separate control surfaces, between the location of the shaft and trailing edge. Guide holes were placed on each side of the fairwater for angles of attack to be evaluated, see Figure 7a. The particular angles of attack of the control surfaces ( $\alpha'$ ) tested were:  $0^\circ$ ,  $\pm 5^\circ$ ,  $\pm 10^\circ$ ,  $\pm 15^\circ$ , and  $\pm 20^\circ$ .

Six different tests (configurations) were conducted on the above model, and consisted of:

- Test 1 - fairwater clean, no control surfaces, see Figure 7a;
- Test 2 - fairwater, with control surfaces at  $\alpha' = 0^\circ$ , see figure 7b;
- Test 3 - fairwater, with control surfaces at opposite angles of attack,  $\alpha' = \pm 5^\circ$ ;

Test 4 - fairwater, with control surfaces at opposite angles of attack,  $\alpha' = \pm 10^\circ$ ;

Test 5 - fairwater, with control surfaces at opposite angles of attack,  $\alpha' = \pm 15^\circ$ ;

Test 6 - fairwater, with control surfaces at opposite angles of attack,  $\alpha' = \pm 20^\circ$ , see Figures 7c - e.

Each test considered fairwater angles of attack ( $\alpha$ ) from  $0^\circ$  through stall on both sides of the fairwater, to cover the full spectrum of possible configurations, see Figure 43.

The purpose of these tests was to determine the hydrodynamic effect of using fairwater control surfaces independent of each other to generate side forces and moments to help alleviate the roll-moment (MZ) and side forces (FZ) caused by angle of attack ( $\alpha$ ) in yaw of the fairwater, which is the same as that of the submersible. These control surfaces are located as close as possible to the fairwater tip, contrary to usual practice on current submersible design.

These tests were developed into more meaningful results by transforming the side forces (FZ) and roll moments (MZ) of the fairwater to the center of an imaginary submersible, to evaluate only the effects of a fairwater and control surfaces on a submersible.

An imaginary submersible moment arm, in the vertical plane, was obtained by scaling the fairwater model with that of an actual submersible. The resulting roll moment:

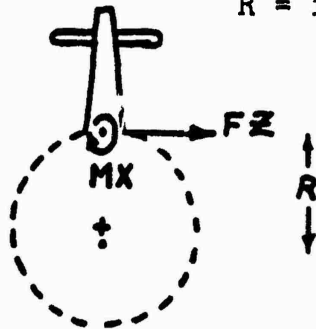
Net Roll Moment =  $MX + (FZ) \cdot (R)$ ,

where:

$MX$  = roll moment at fairwater base

$FZ$  = side force at fairwater base

$R$  = imaginary submersible moment arm = 6.3".



The results were: for an increasing angle of attack ( $\alpha'$ ) of the control surfaces, the effective angle of attack ( $\alpha$ ) of the fairwater (submersible) in yaw is reduced. For a maximum angle of attack ( $\alpha'$ ) of  $\pm 20^\circ$ , the reduction is approximately  $4.5^\circ$  for the first series of model test, see Figures 44 - 49.

This first series of tests of the fairwater used control surfaces with non-tapered tips. A second series of tests was performed with tapered end tips added, to alleviate some of the possible drag of the flat-ended configuration of the control surfaces. The results of this second series of tests showed an increase in desired effect, or a decrease in effective angle of attack of the fairwater from the first series of tests. This difference in the second test was approximately  $2^\circ$  beyond the first, see Figures 50 and 51.

Compatible results for lift ( $FZ_0$  - component perpendicular to tunnel flow) and drag ( $FX_0$  - component parallel to

tunnel flow) on the fairwater model for the flat tip and tapered tip fairwater control surfaces are given in Figures 52 - 59, and Figures 60 - 63 respectively.



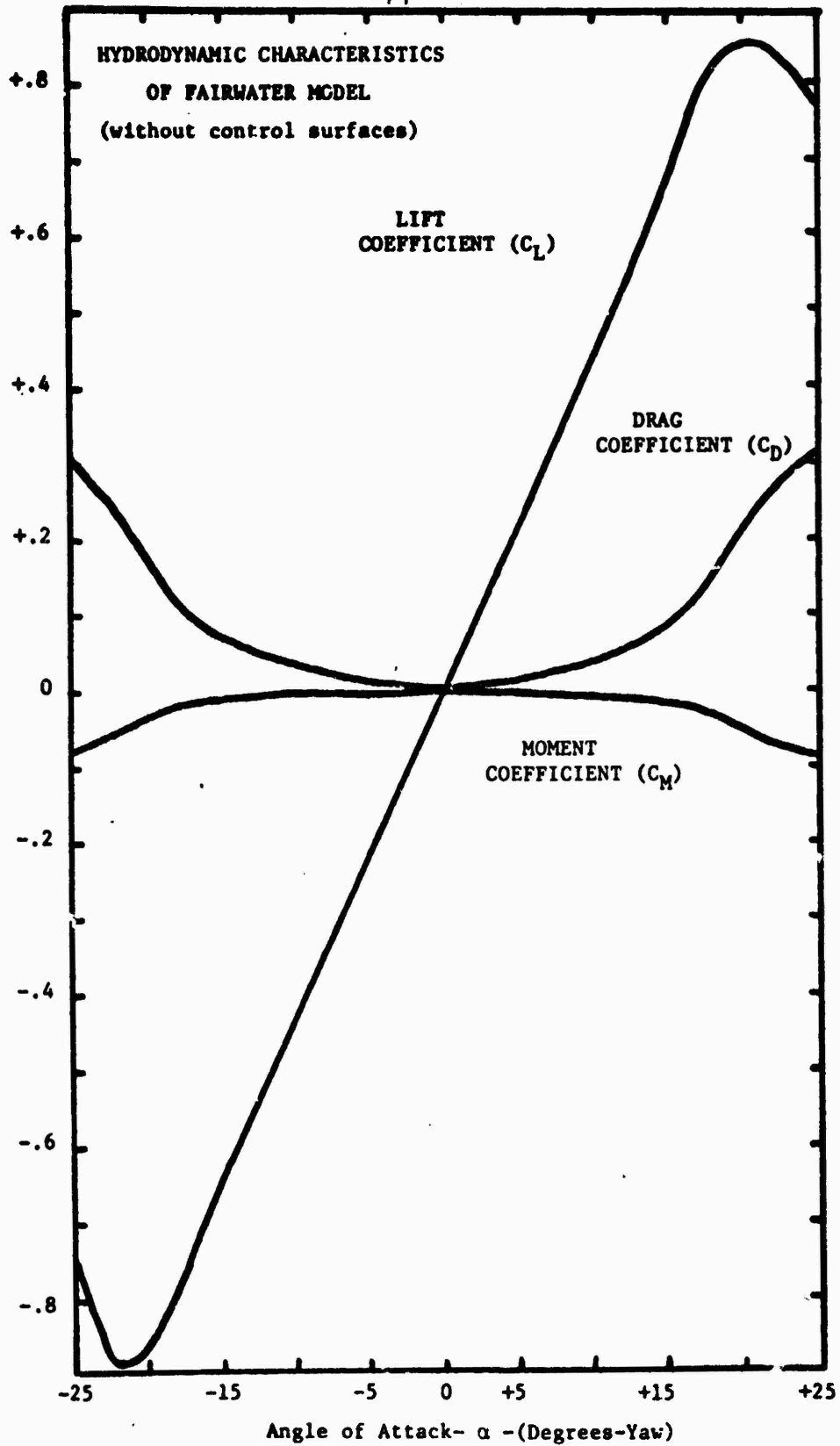


Figure 43

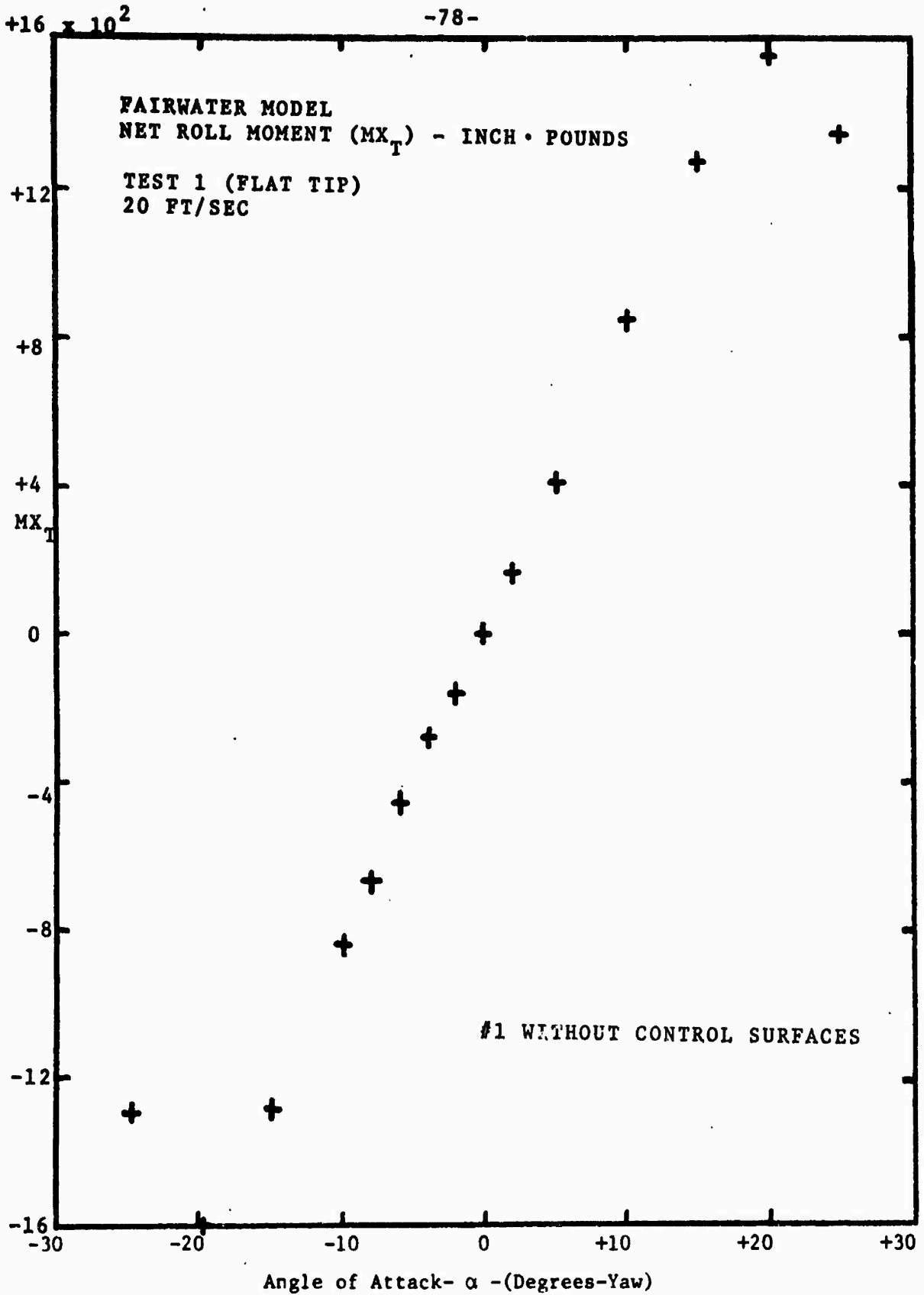


Figure 44

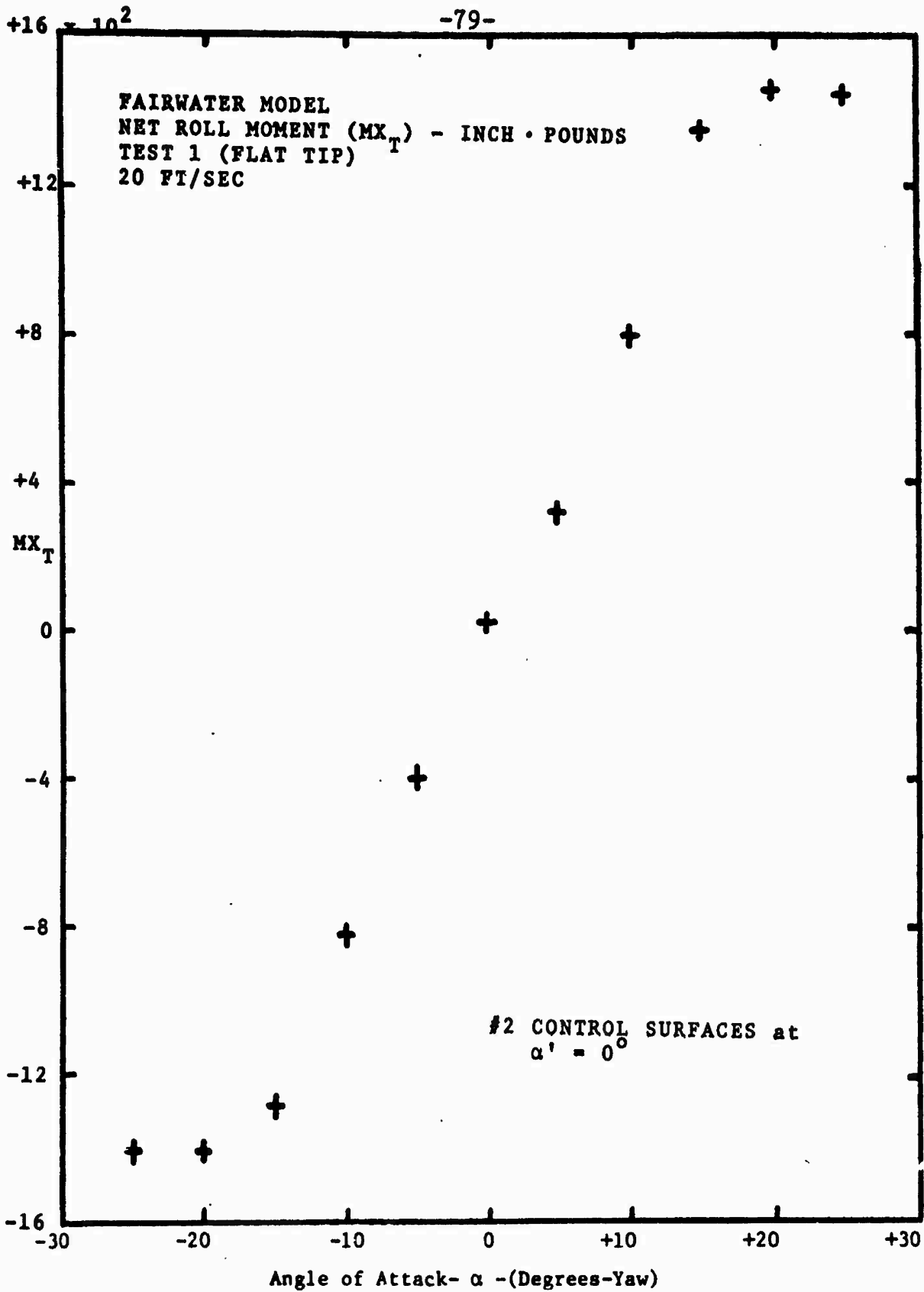


Figure 45

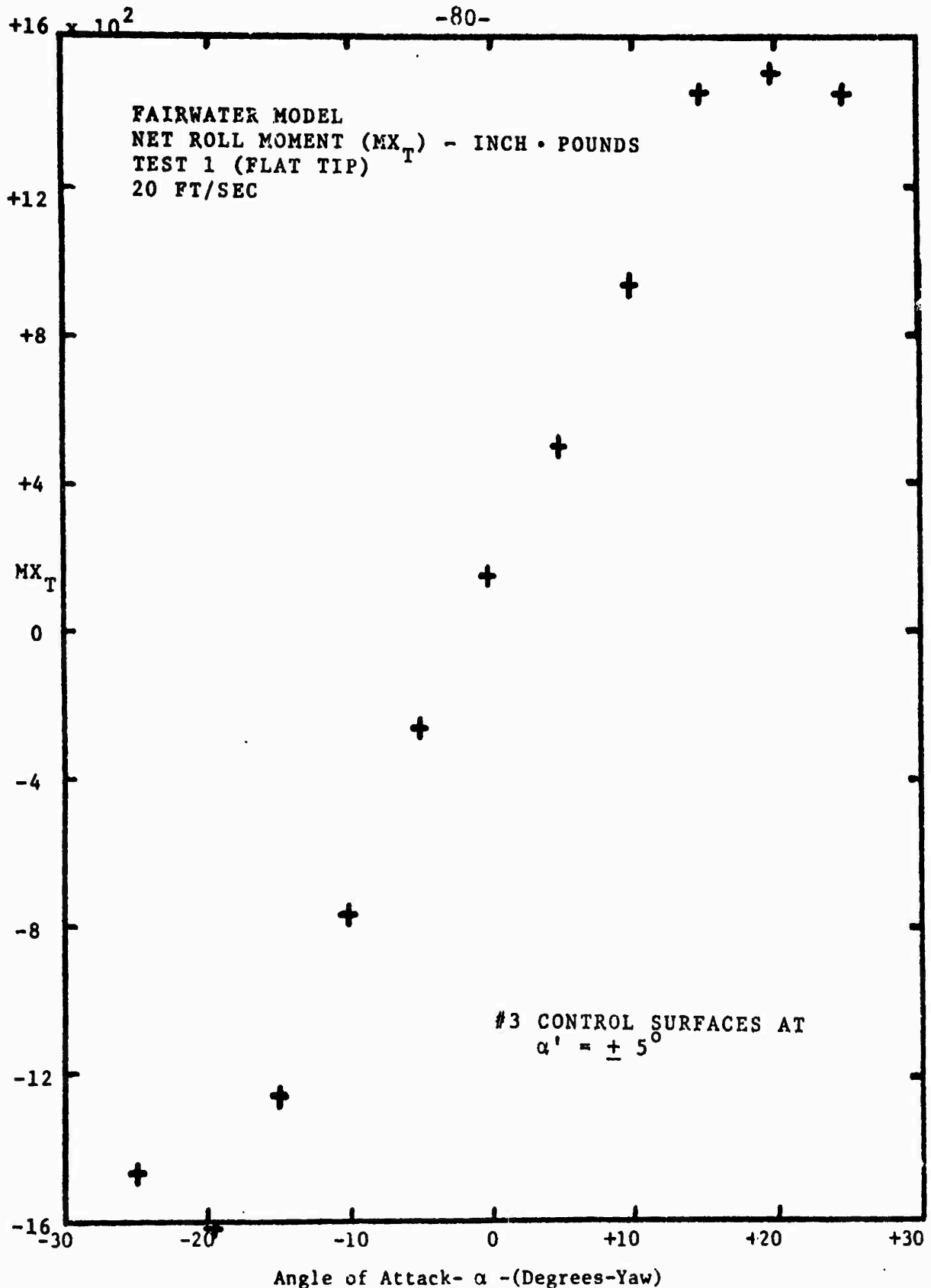
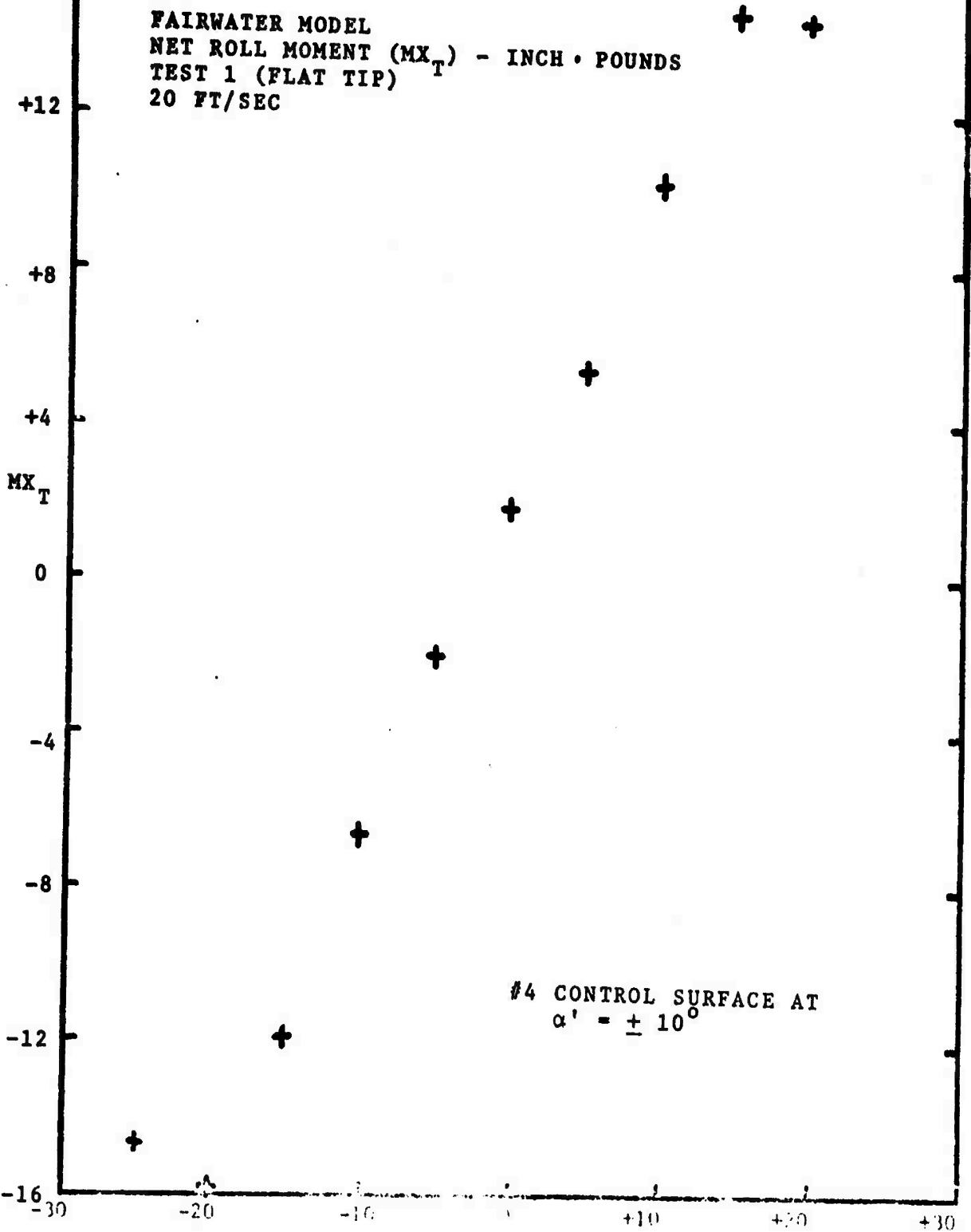


Figure 46

+16 x 10<sup>2</sup>

-81-



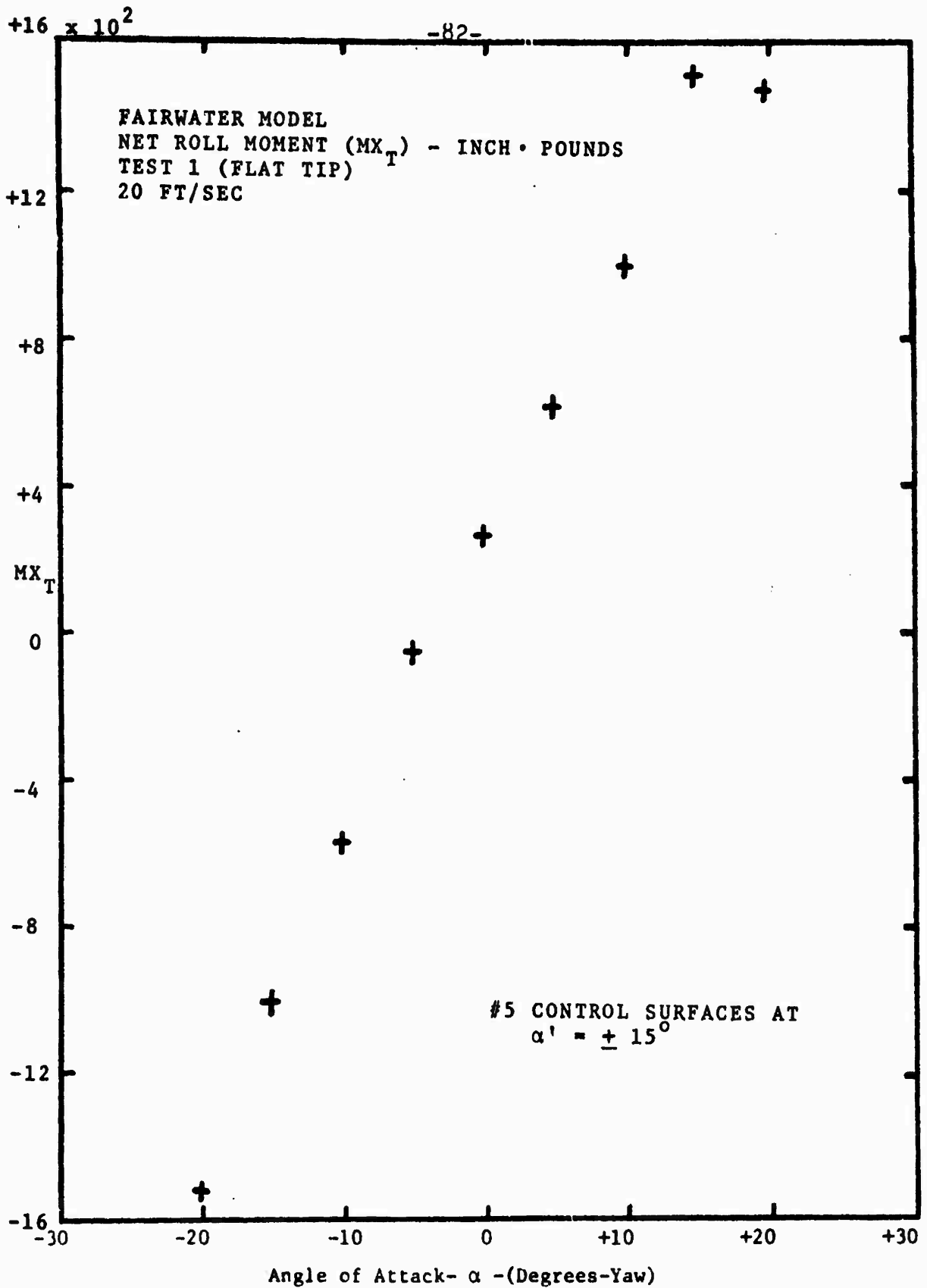


Figure 48

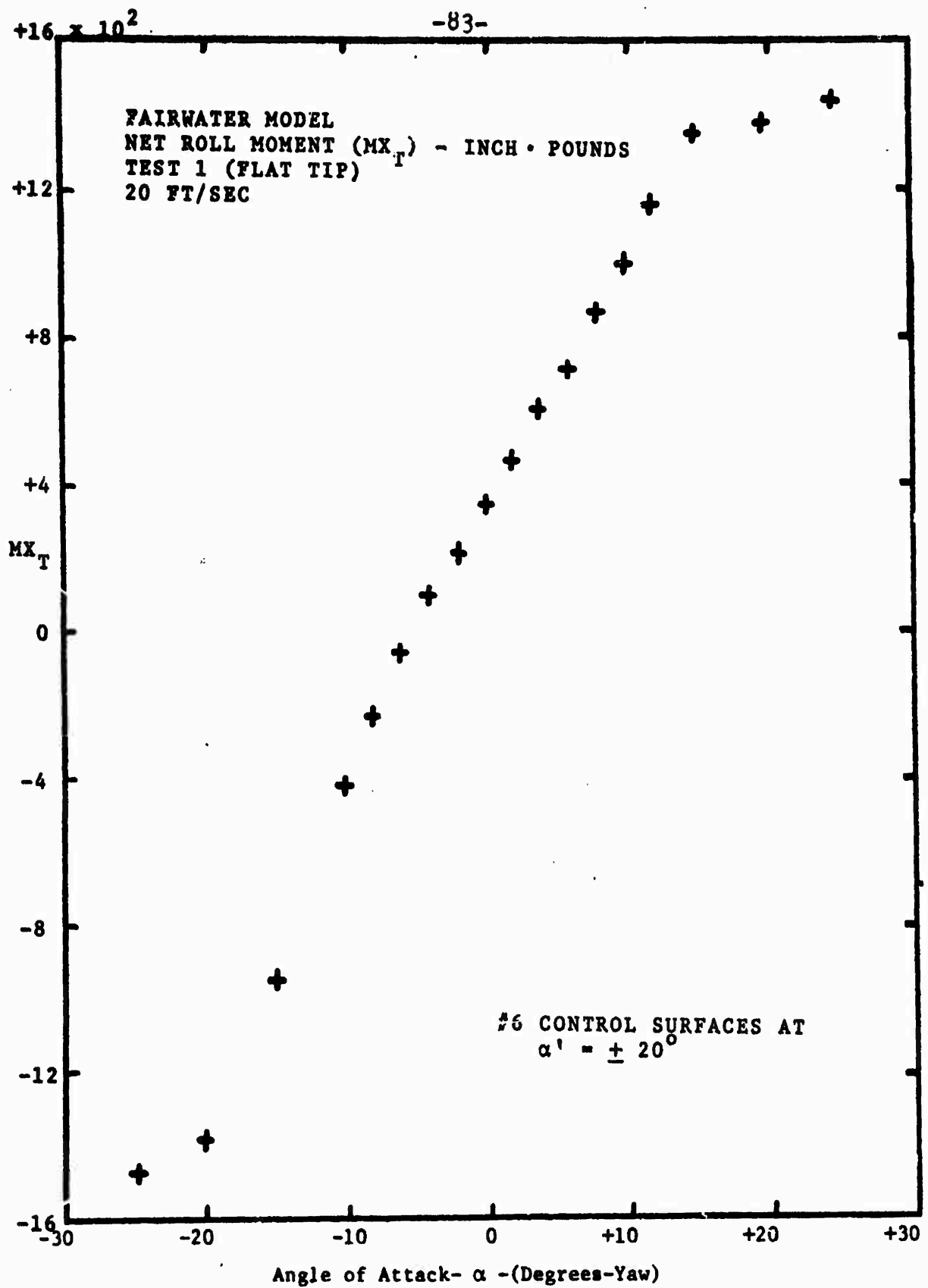


Figure 49

+16 x 10<sup>2</sup>

-84-

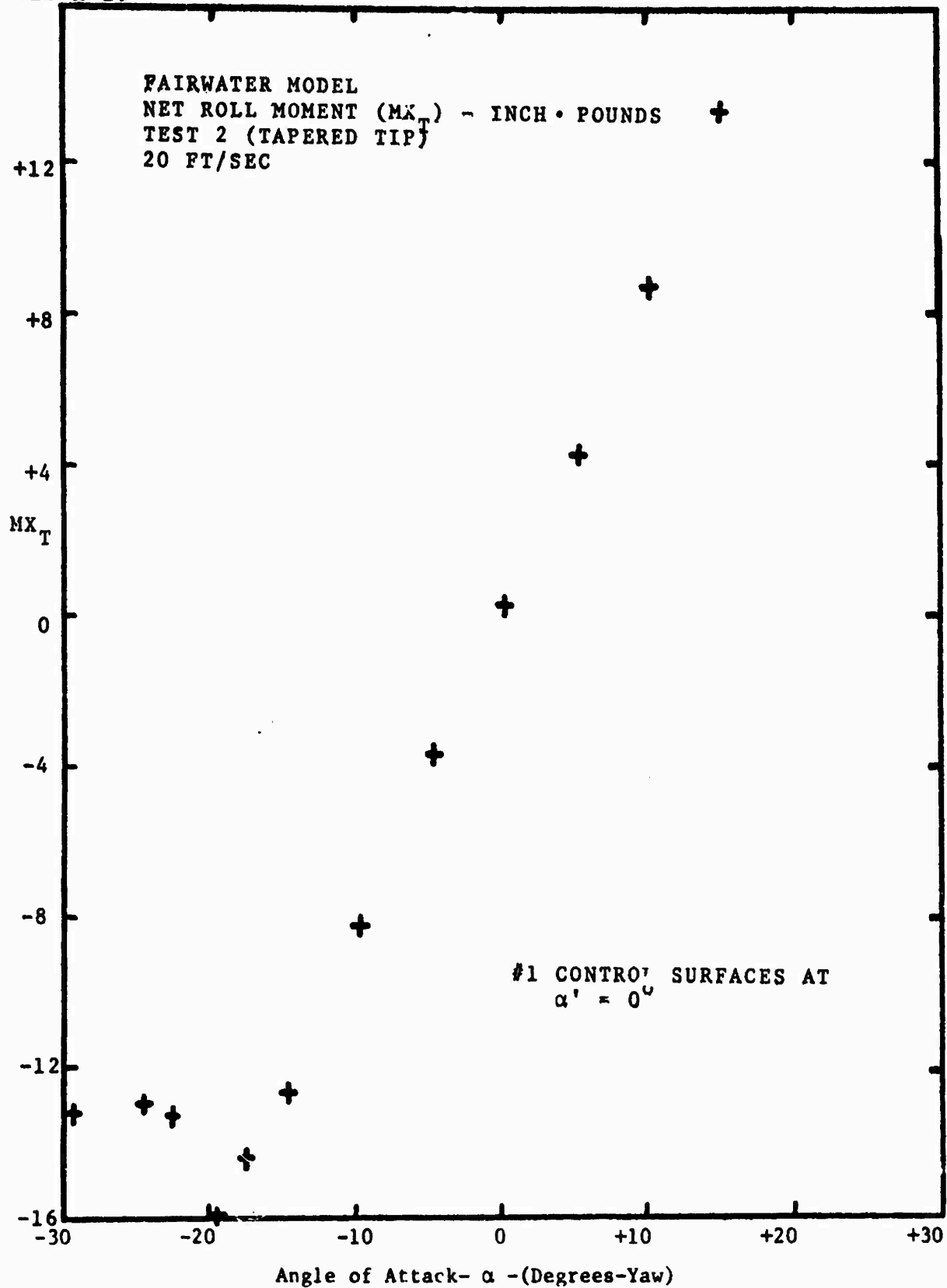


Figure 50



+16 x 10<sup>2</sup>

-85-

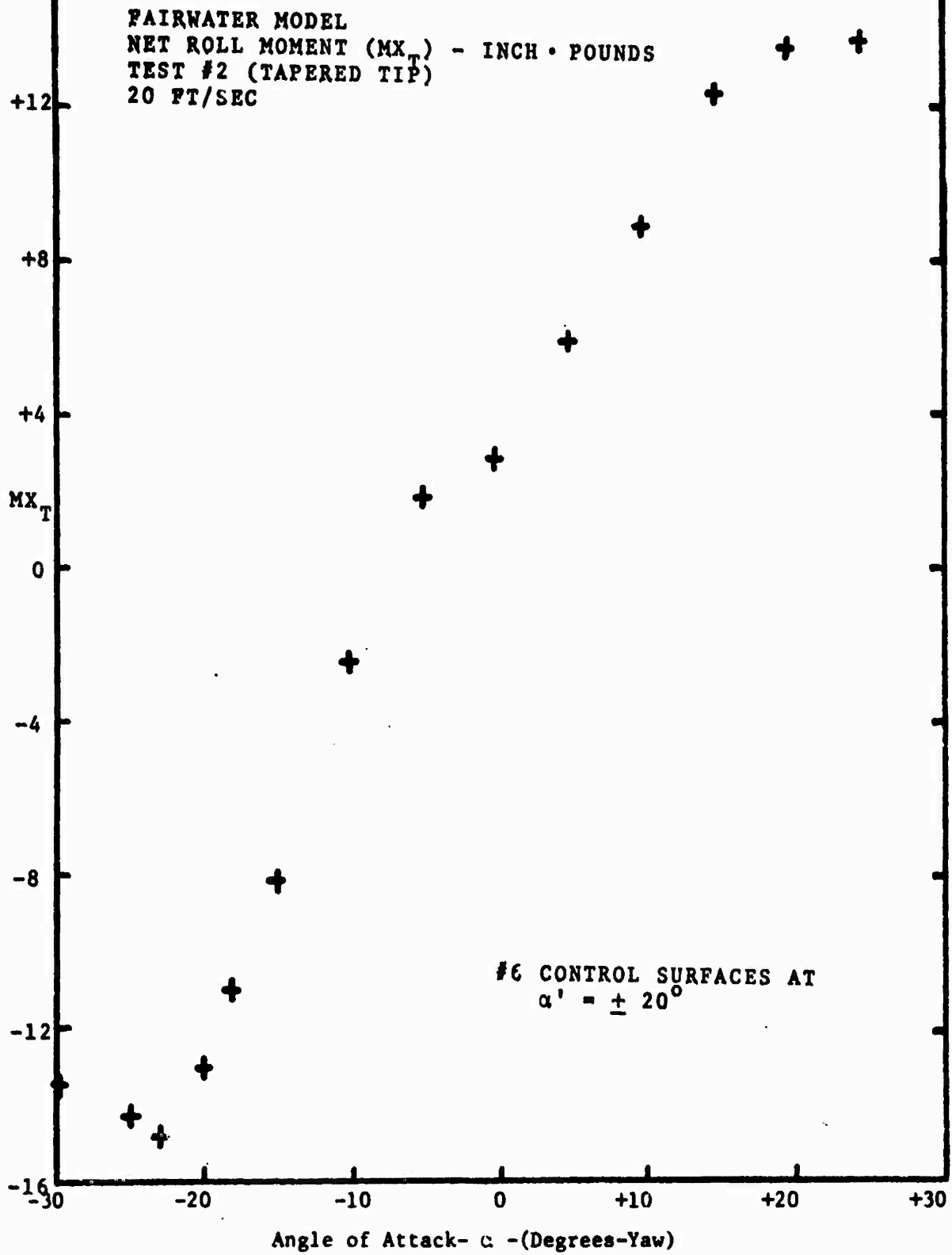


Figure 51

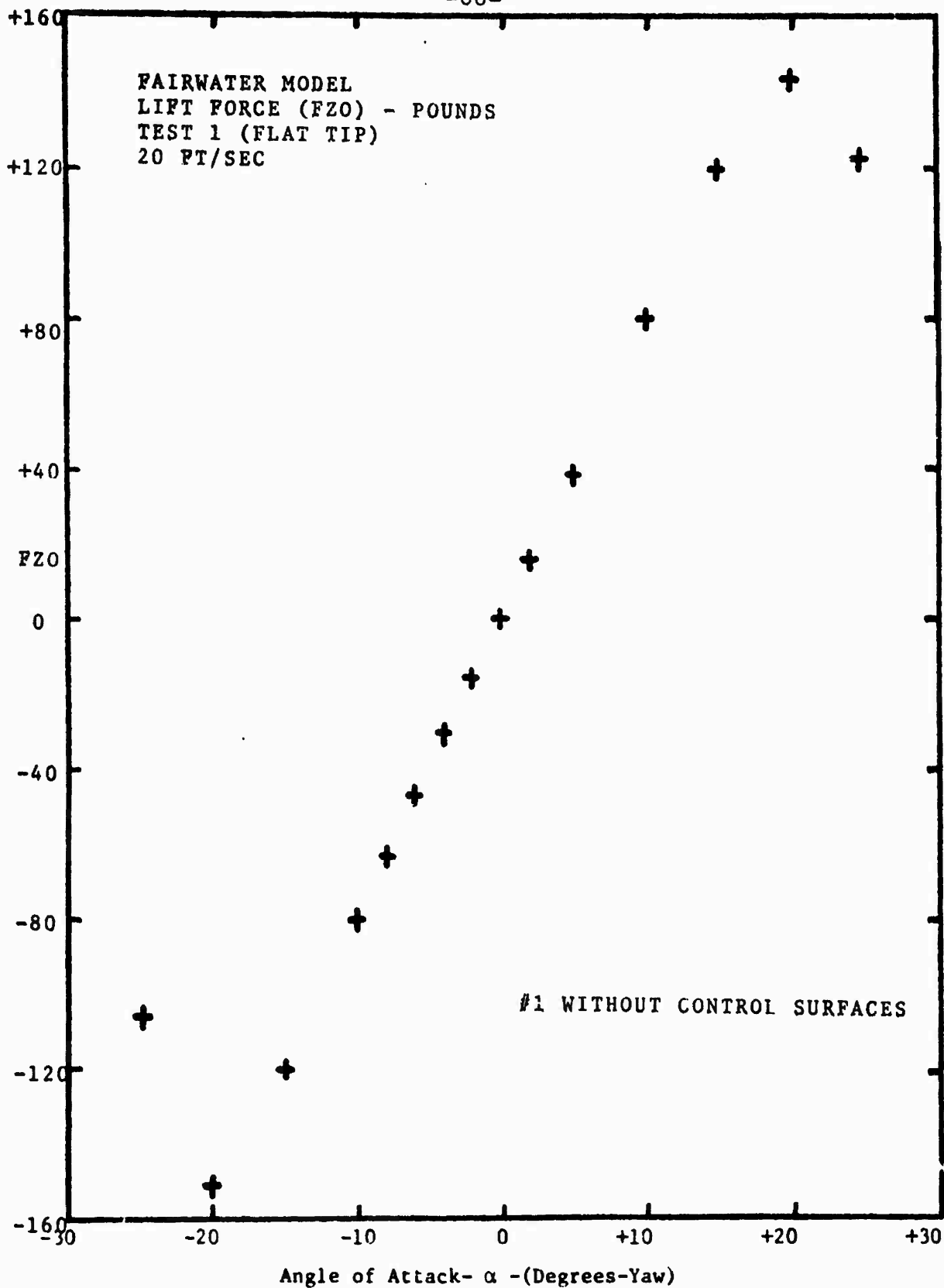


Figure 52

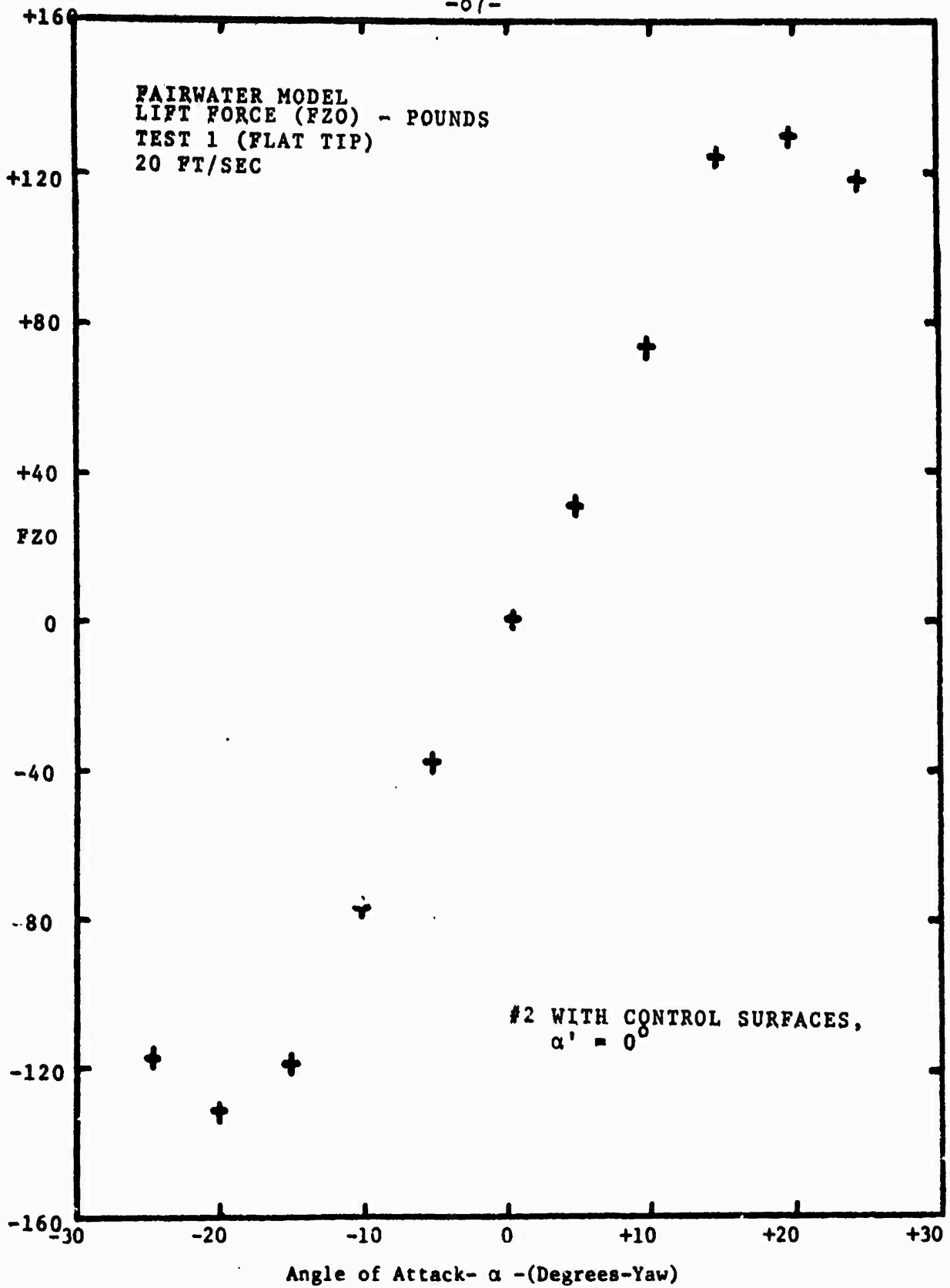


Figure 53

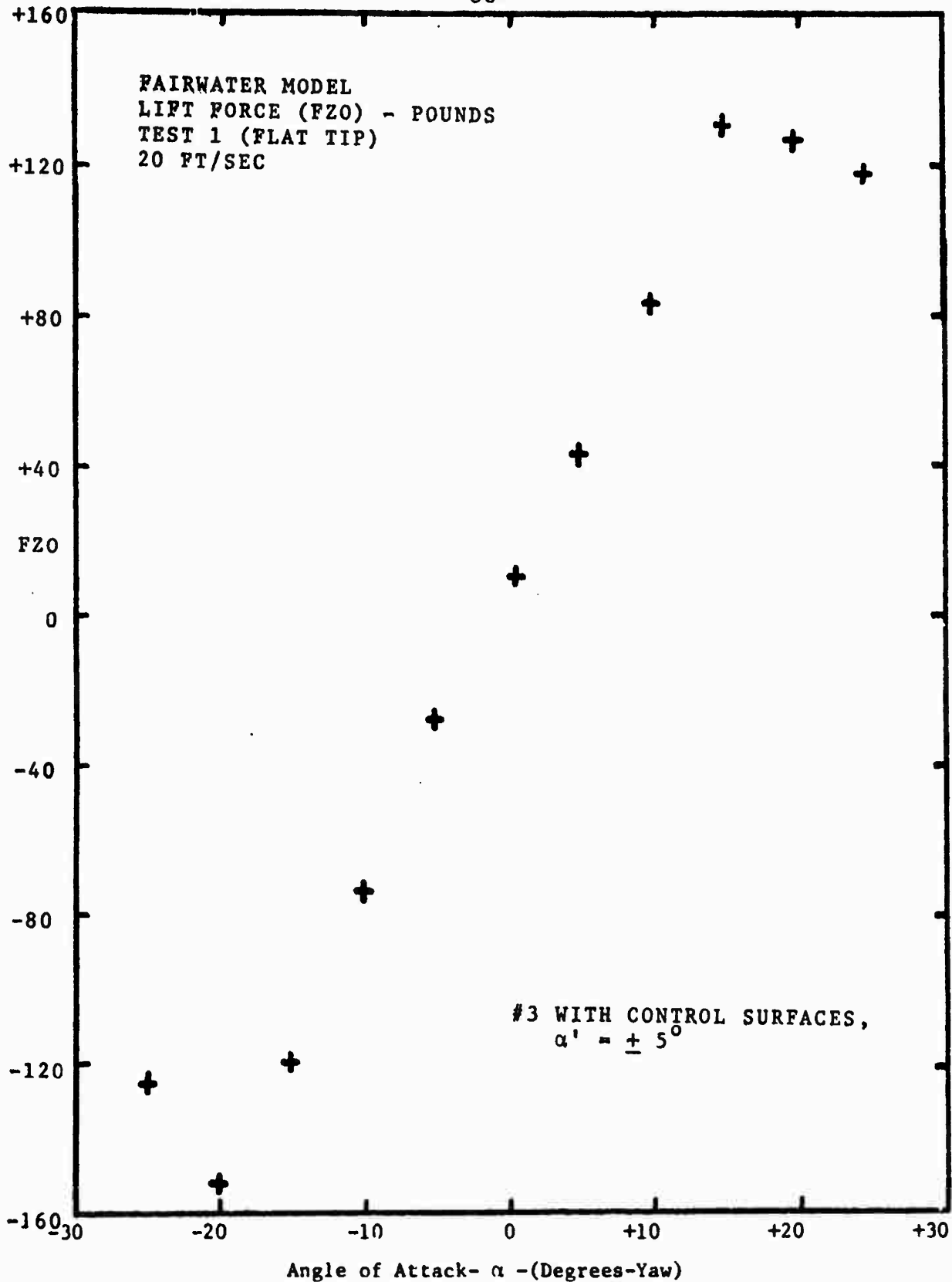


Figure 54

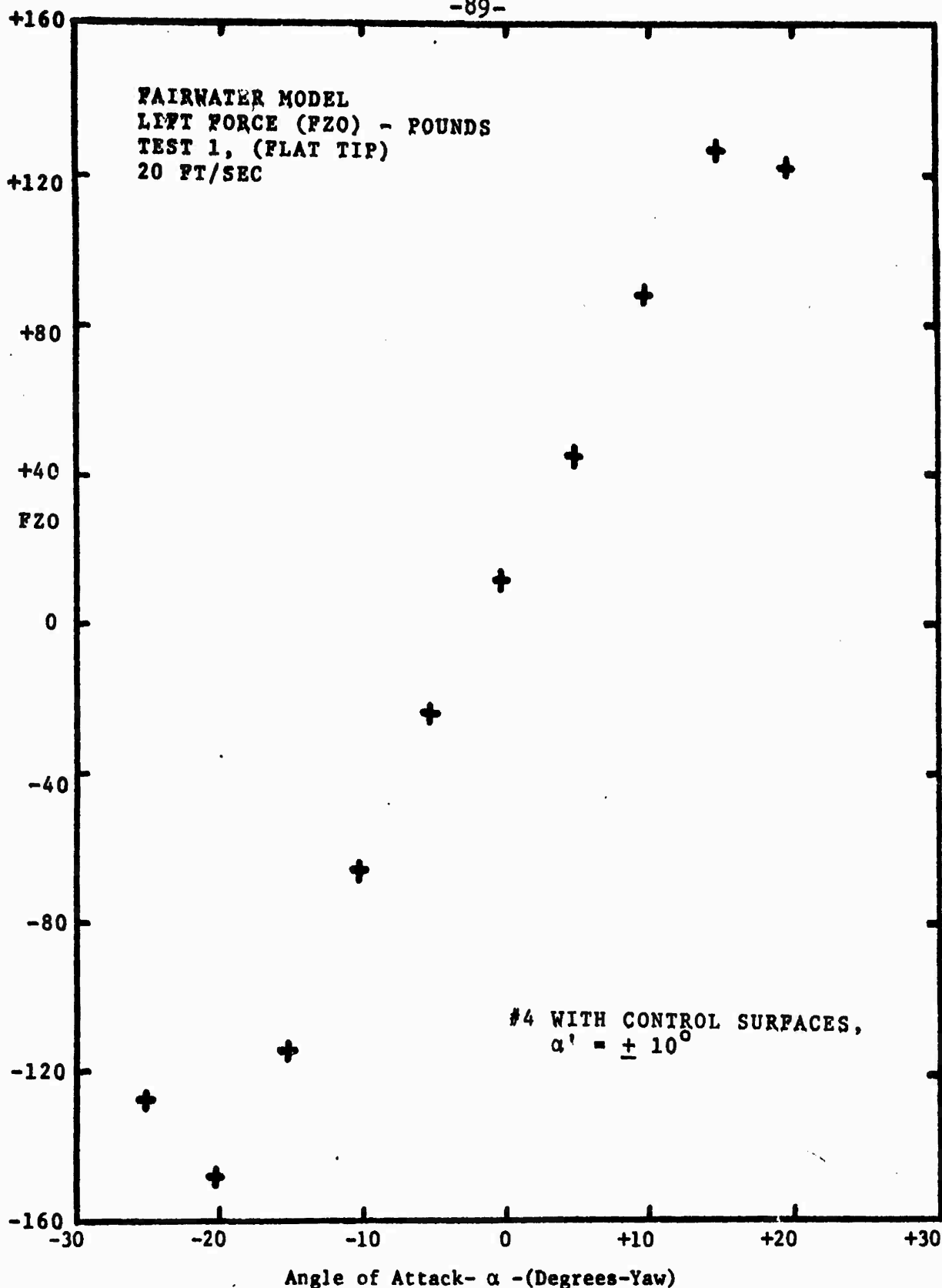


Figure 55

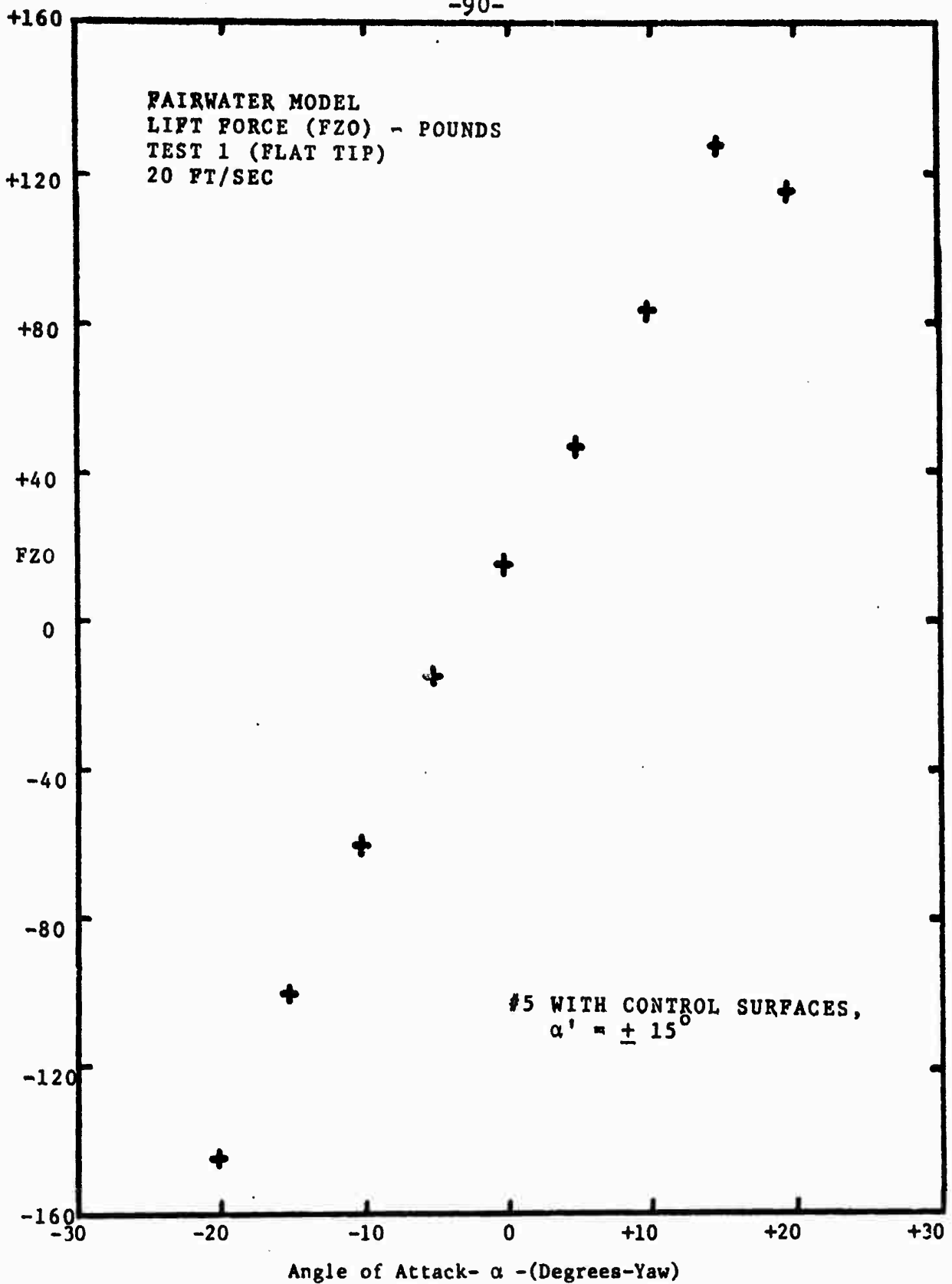


Figure 56

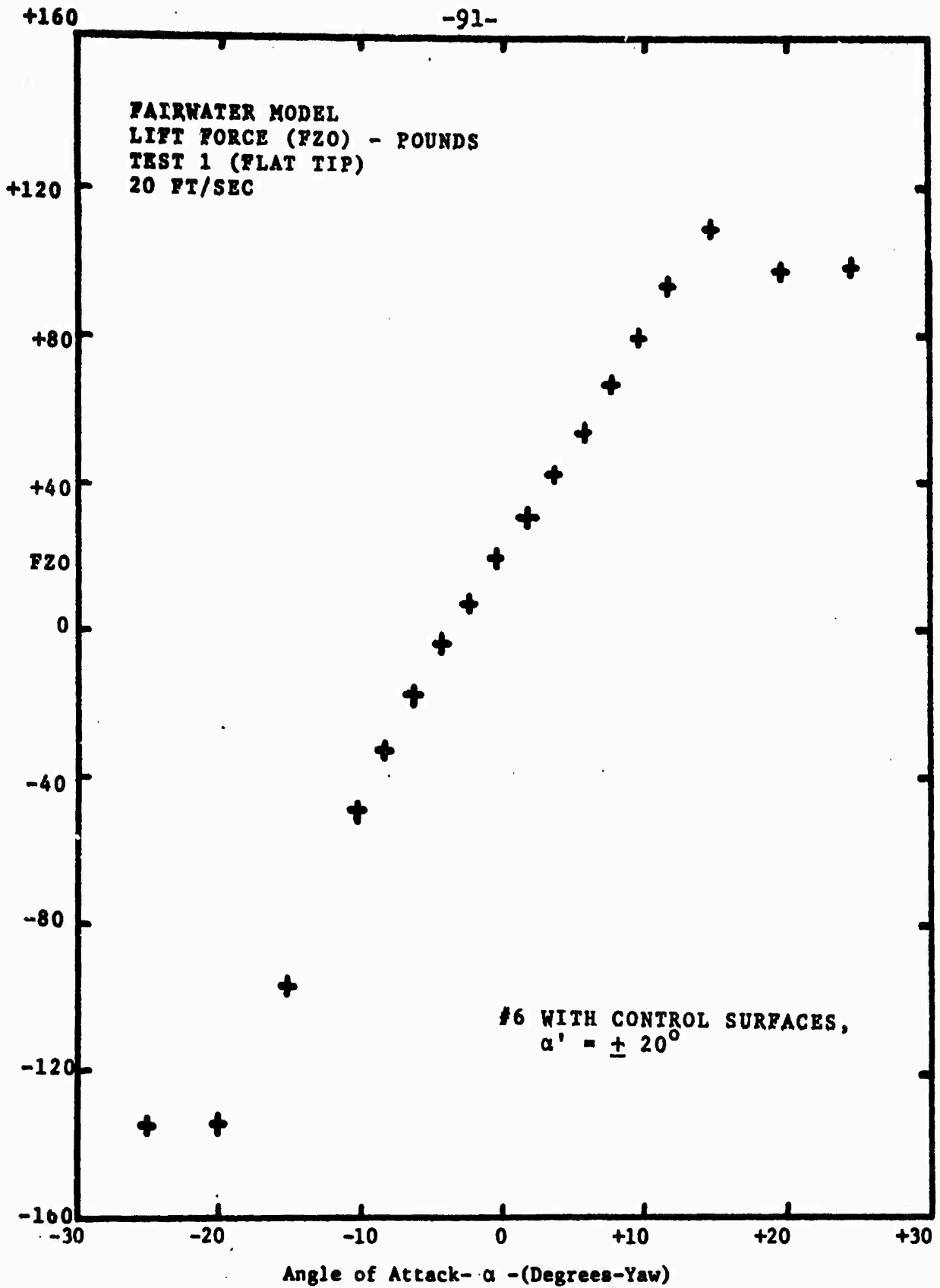


Figure 57

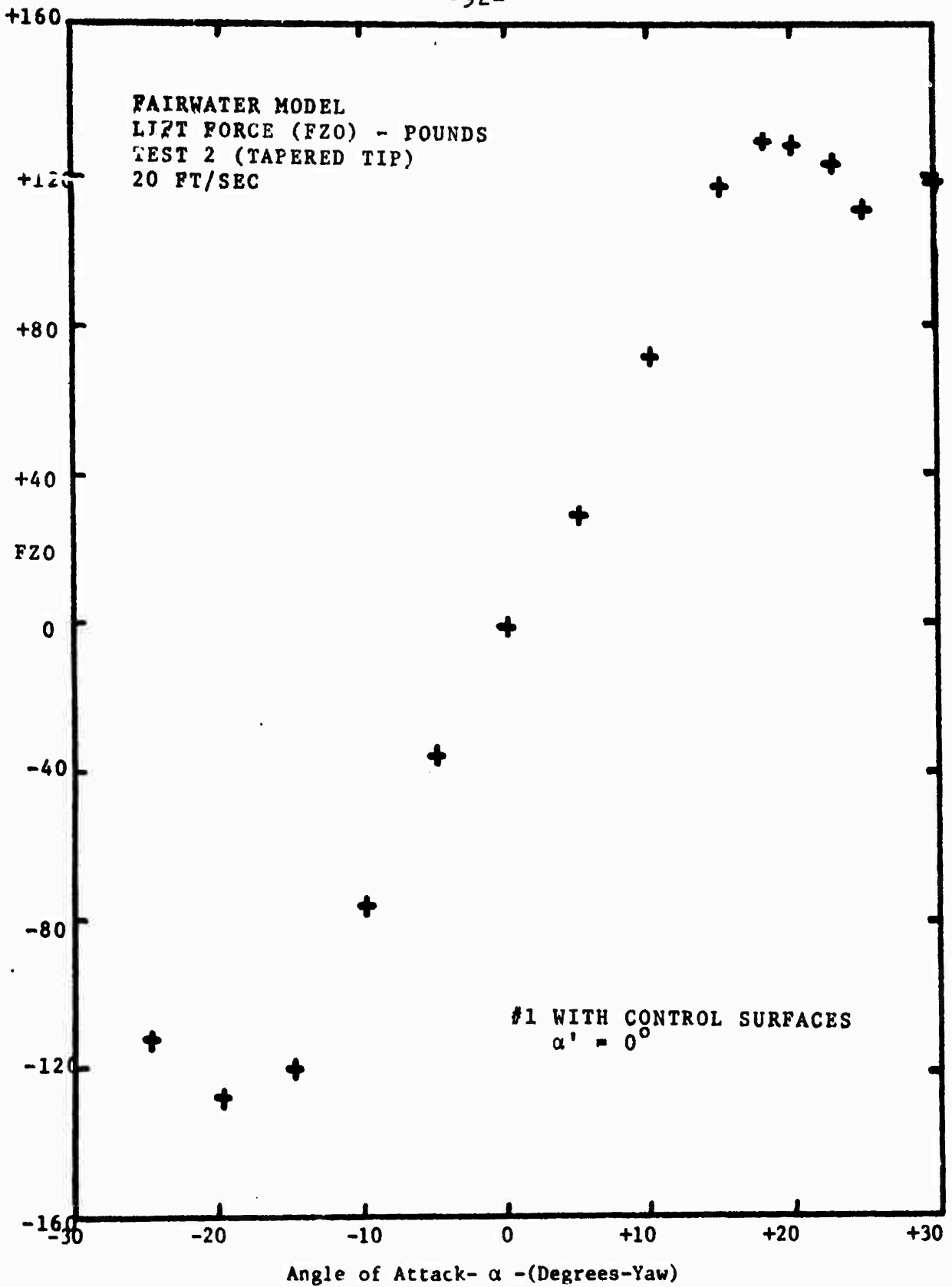


Figure 58



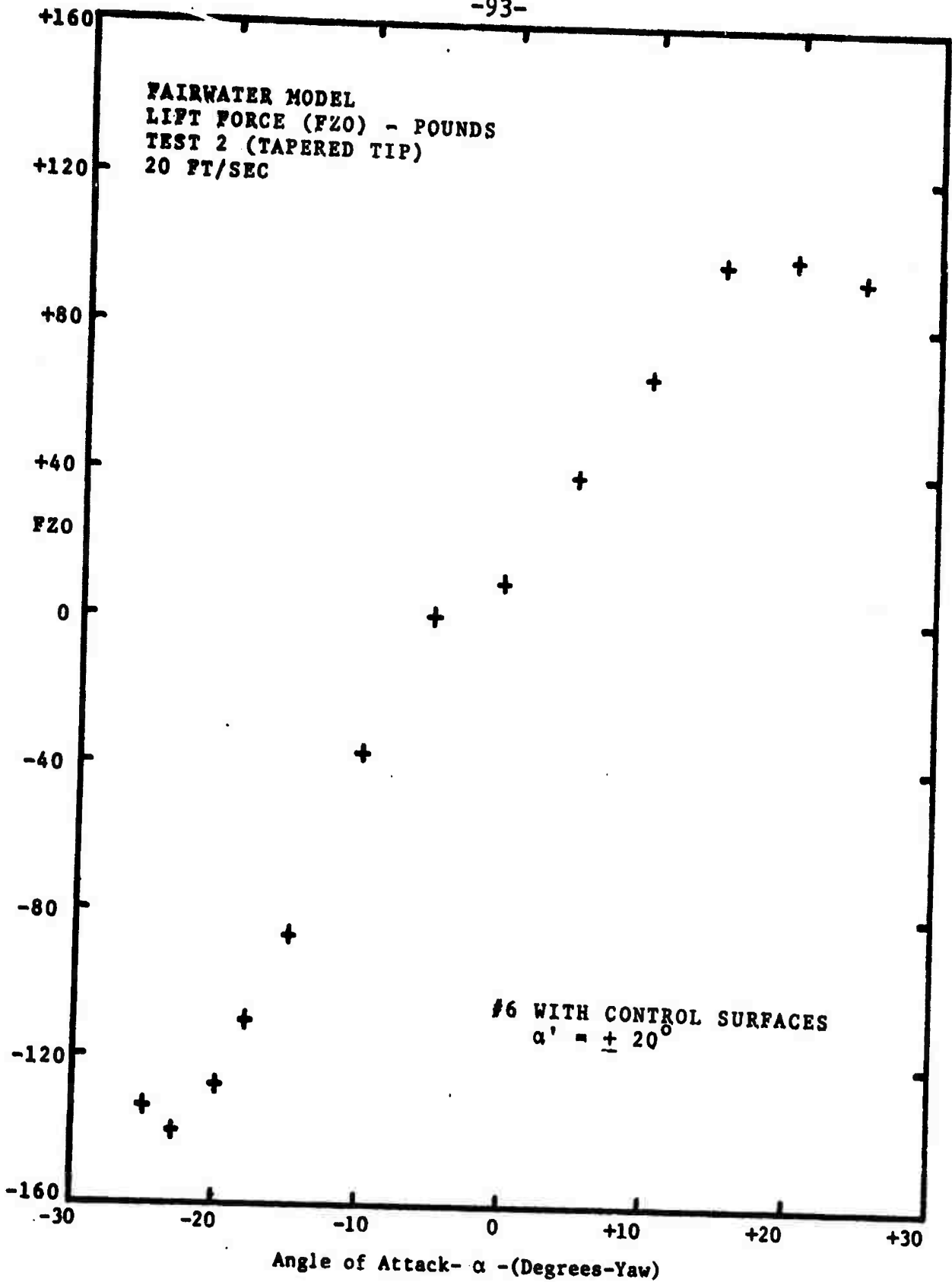


Figure 59

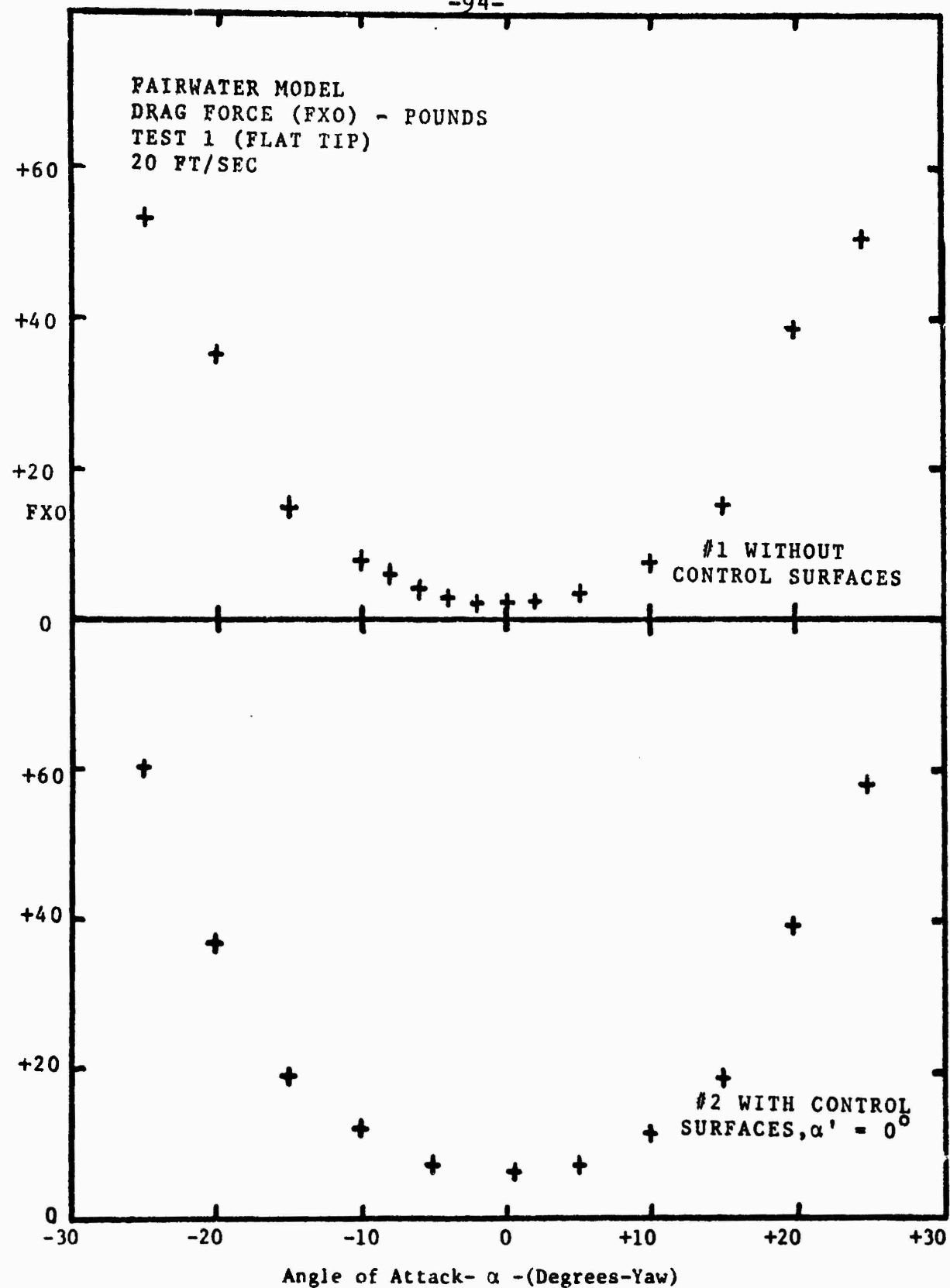


Figure 60

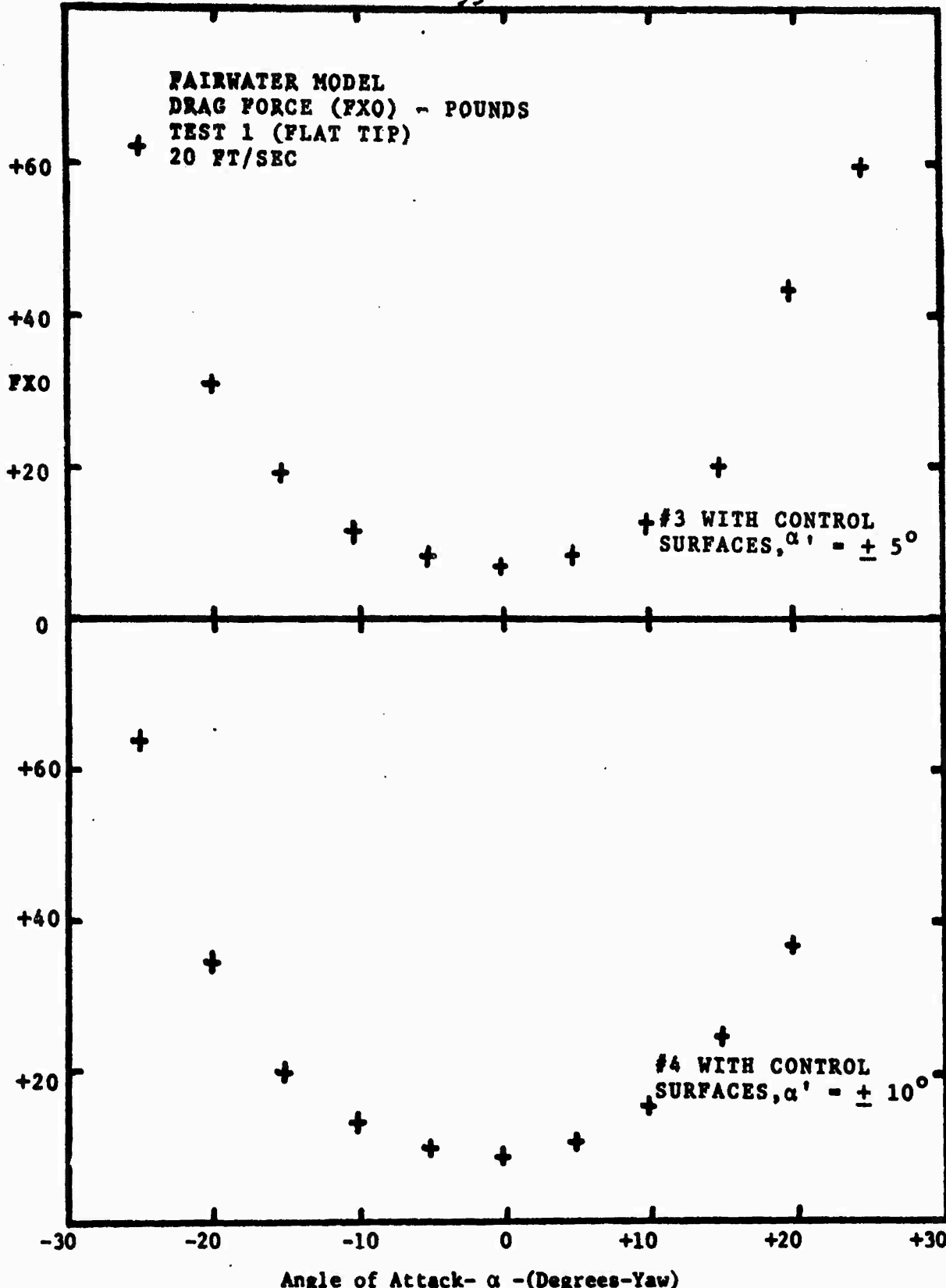


Figure 61

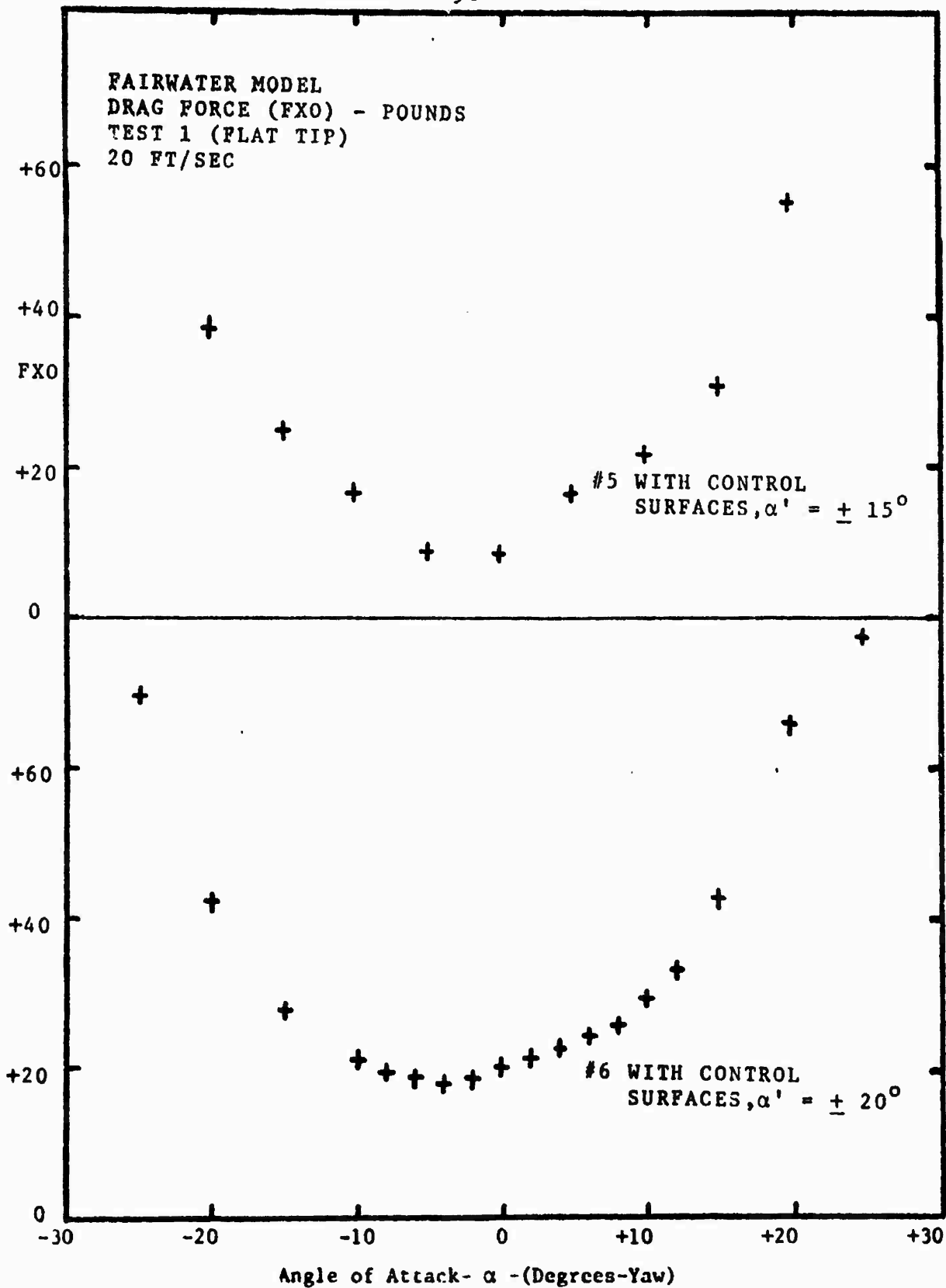


Figure 62

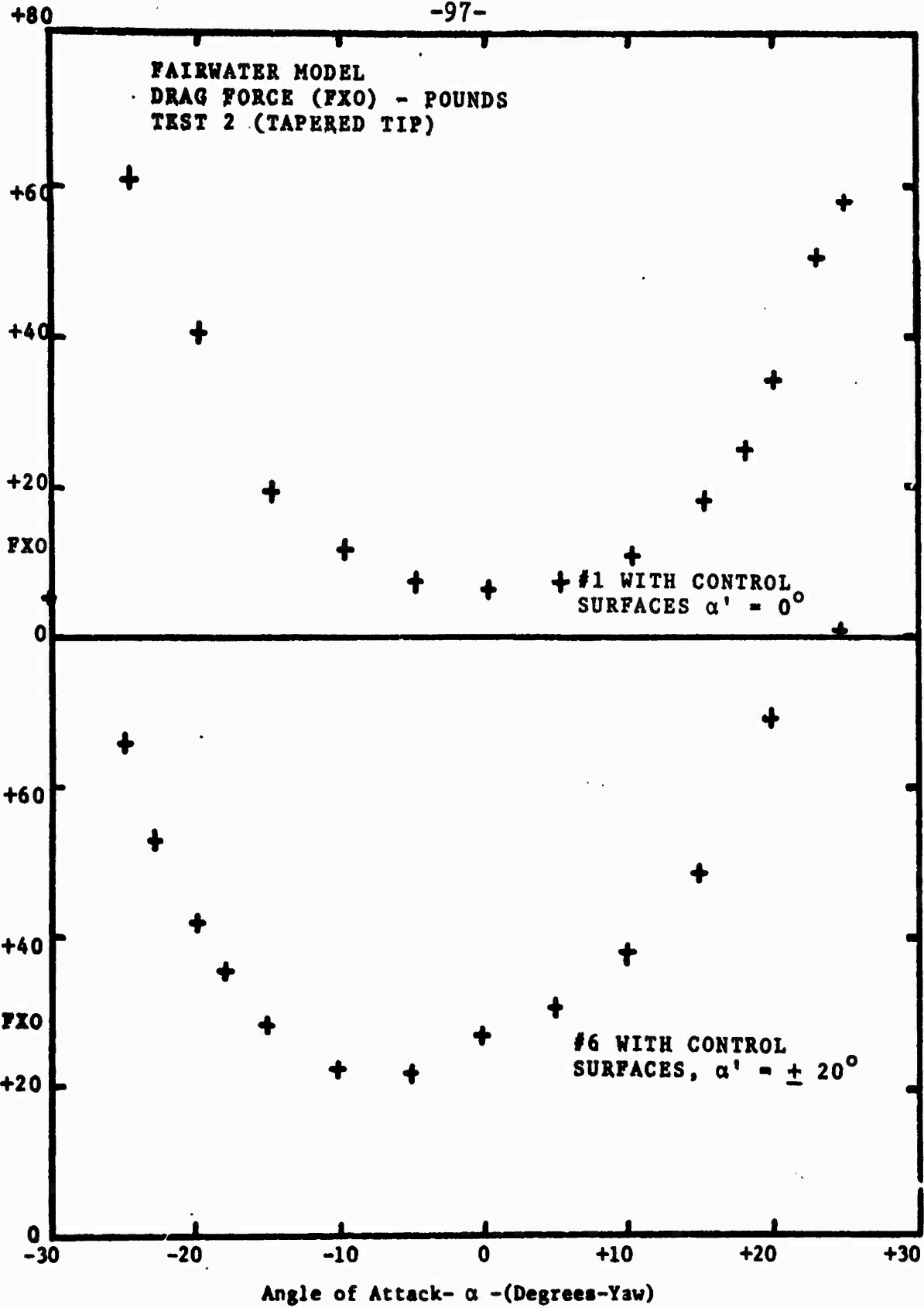
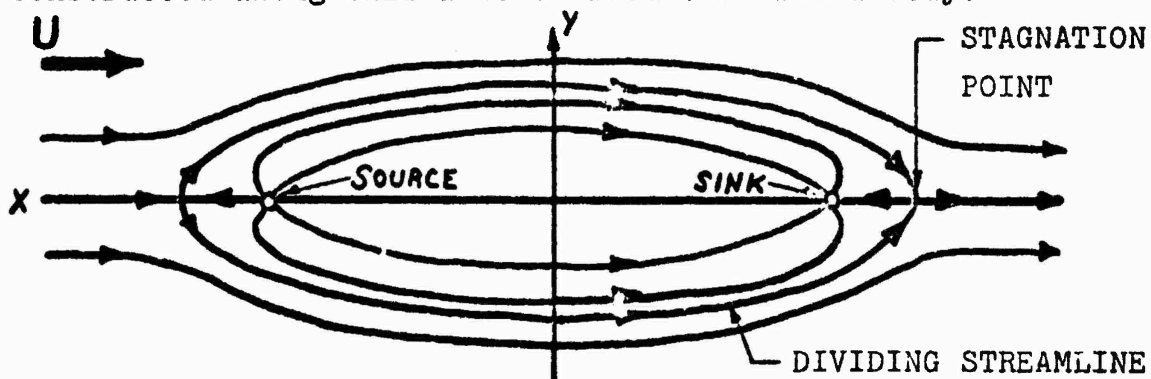


Figure 63

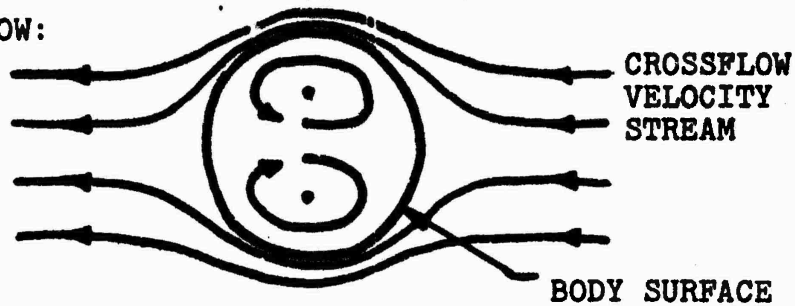
## VI. THEORETICAL BASIS FOR NUMERICAL MODEL

In developing a numerical method for predicting the flow characteristics, and eventually the forces and moments, on a submerged body of revolution, it was necessary to use potential flow as the basic theory. Therefore, simplifying assumptions of an ideal fluid were initially required of the flow: inviscid, incompressible, homogeneous, and irrotational. The submerged body, in this case a slender body of revolution, is approximately represented by the combination of two different appropriate distributions. To model the flow along the longitudinal body axis, a distribution of sources and sinks was constructed along this axis to form the closed body.



In order to satisfy the crossflow along the body, resulting from an angle of incidence between the body axis and free stream, a distribution of doublets was similarly placed along the body axis.

IDEAL FLUID FLOW:

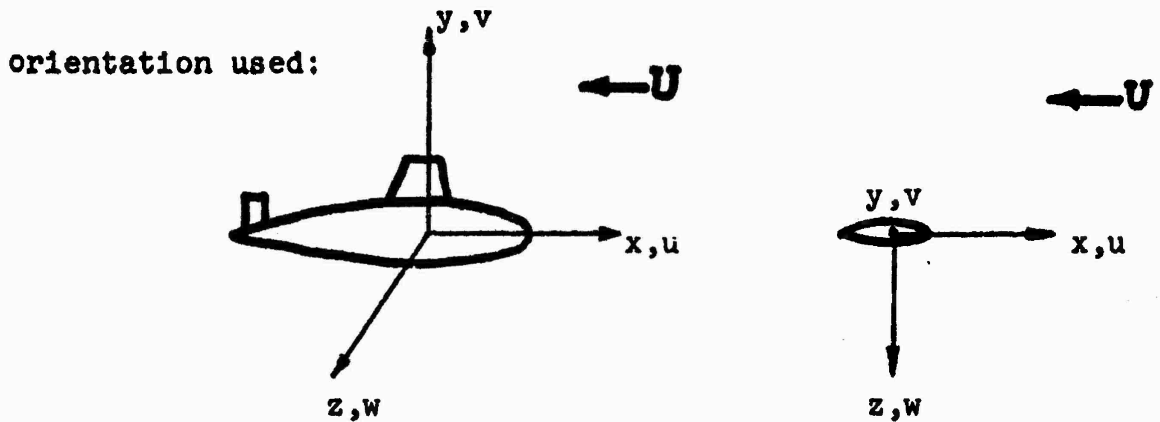


The basis of the approach used for lifting surface calculations was the linearized two-dimensional hydrofoil theory for a thin foil and the law of Biot-Savart, which is a governing relationship for an induced velocity in space by a three dimensional vortex.

Using the linearized two-dimensional hydrofoil theory for a thin foil with the required assumptions of no separation, and the Kutta condition imposed on the trailing edge, the lift force and moment resulting from the hydrodynamic pressure can be obtained. This result, Kutta-Joukowski theorem, states that for a two-dimensional body, moving with constant velocity in an unbounded inviscid fluid, the hydrodynamic pressure force (lift) is directed normal to the velocity vector and is equal to the product of the fluid density, velocity, and the circulation around the body.

$$L = \rho U \Gamma = \text{lift/unit length of span}$$

Circulation ( $\Gamma$ ) is defined as the integrated tangential velocity around the closed contour, in this case a lifting surface, in a fluid. With the standard hydrodynamic reference



Circulation,  $\Gamma = \oint u dx$ , where

$u$  = horizontal perturbation velocity component

$U$  = free stream velocity component

The hydrodynamic moment about the y-axis is represented by the pressure integral:

$$M = \rho U \int u dx$$

The coordinate system used during the experimental portion of this project required the above system to be rotated 180 degrees in the horizontal plane, to be compatible with the water tunnel construction and dynamometer program.

In order to satisfy the presence and the effects of lifting surface appendages (fairwater and rudders) and the discontinuity in pressure, pressure loading across these surfaces was modeled by a distribution of vorticity. The axis for each distribution of vorticity is on the center plane of the



representative lifting surface and normal to the incoming flow, and this vorticity is referred to as a bound vorticity distribution. To fulfill continuity of vorticity, an additional distribution of vorticity, whose axis is on the representative lifting surface and parallel to the incoming flow, was required. This latter distribution is referred to as trailing vortices, or more commonly, trailers. Trailing vortices extend to infinity in the wake formed behind each respective lifting surface, while the effects of the bound vortices are only experienced on the lifting surface itself.

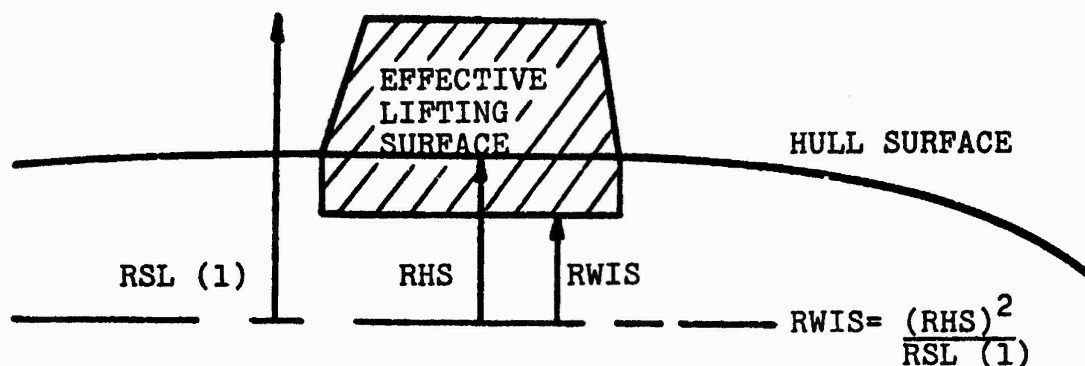
The thickness of the lifting surfaces described above could be represented by a distribution of sources and sinks of appropriate strength, but were defined as being of zero thickness.

#### Effective Span of Lifting Surfaces

Since the lifting surfaces are each connected to the hull, essentially a curved ground board, an effective span length must be calculated for a valid modeling. This was accomplished using a relationship from Milne-Thomson (3), in which a distance from the body axis to the new effective base is generated. This distance is equal to the ratio of the actual hull radius, at the mid-point of the actual base of lifting surface, squared, divided by the maximum radial distance from

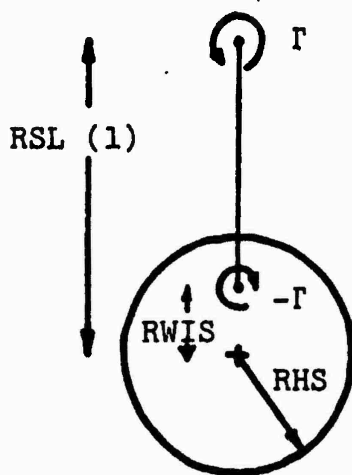
the body axis to the lifting surface tip.

FAIRWATER EXAMPLE:



Effective Span of Fairwater = SPNS =  $RSL(1) - RWIS$

The image system is based on the theory that when a pair of two dimensional vortices of equal and opposite strength are located on the same radial line, there is no normal induced velocity on a circle of radius RHS, if RSL is equal to the radius of the outer vortex, and RWIS the radius of the image vortex.



By using this image system for the fairwater and rudder(s), the solid boundary condition of the hull is satisfied.

The technique used, distribution of vorticity, is similar to a method developed by Falkner for lift distribution of wings (4, 5, 6, 7, 8). A continuous distribution of bound and trailing vortices is replaced by a discrete element approximation, in which a lattice of horse-shoe shaped discrete vortex lines are used. The lifting surface is divided into a series of finite rectangular elements in which the lift is considered to be constant within each element, and each element is a horse-shoe of the total lattice, see Figure 64. As the number of elements chordwise and spanwise is increased, the approximation to the actual surface is refined. The trailing vortex sheet formed is assumed, as a first approximation, to remain a flat sheet to infinity downstream while the sheet angle to the vehicle longitudinal axis is adjustable. A selected minimum number of control points are then systematically located chordwise and spanwise midway between vortices on each lifting surface. At the control points, the induced velocity by each horse-shoe lattice element is determined by integration using the Biot-Savart law:

$$\bar{w} = \frac{\Gamma}{4\pi} \int \frac{d\bar{l} \times \bar{S}}{S^3}$$

(u,v,w)

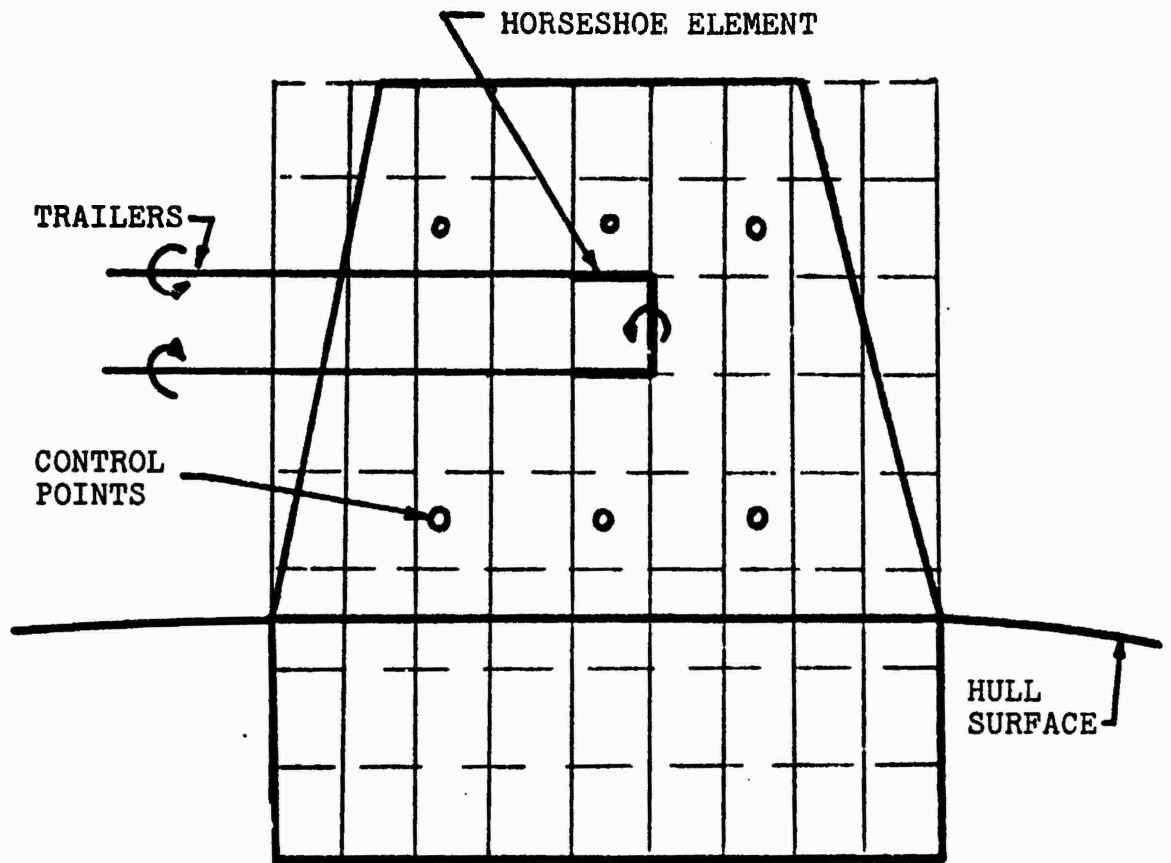


Figure 64 Vortex Lattice

where  $\Gamma$  = vortex strength

$\bar{S}$  = vector distance from vortex element to control point

$\bar{dl}$  = vector element of distance along the vortex

$\bar{w}$  = vector-induced velocity of an element.

The bound vortex strength of each element is first numerically solved using 2 modes of distribution spanwise and 2 modes chordwise; one of a flat plate and the other for camber over the various chord lengths along the length of the effective span.

To insure zero slope, but not necessarily zero value of the circulation at the actual hull surface, an approximated series form for the bound circulation was taken from Kerwin and Leopold (9). This series:

$$\text{nondimensional circulation} = G(q) = (1 - q^2)^{\frac{1}{2}} \sum_{j=1}^J a_j q^{(2j-2)}$$

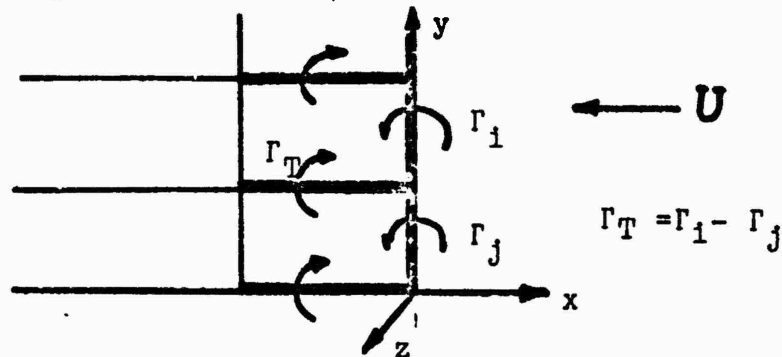
$$\text{where } q = \frac{r - r_h}{1 - r_h}$$

$r$  = radius of image vortex (RWIS, RWIR)

$r_h$  = radius of hull (RHS, RHR)

$a_j$  = unknown coefficient to  
be determined from  
modal distributions

Since the strength of a trailing vortex of an element is equal to the difference in bound circulation between adjacent bound vortices, as a vortex may not end in a fluid, the vortex strengths are readily calculated also.



Using the law of Biot-Savart, and the bound vortex strengths just calculated, the induced velocities of each element on each of the control points of the lifting surface are calculated. Then, the same method is repeated for the induced velocities resulting from the trailing vortices.

The number of control points used should be a minimum, yet retain accuracy, to reduce the size of the resulting matrix of induced velocities that is eventually developed for each lifting surface, to reduce computation time. Although accuracy should be improved by a greater number of control points and smaller horse-shoe element size, a point of diminishing return will eventually occur, and care must be

taken not to allow the matrix, a set of simultaneous linear equations, to become too nearly singular to be solved numerically.

Since the bound and trailing vortices do not yield the total induced velocity on the lifting surface, the trailing wake of the surface in question, the hull, and other adjacent lifting surface wakes must also be considered and their effects combined.

The induced velocity on the control points from the wake of the surfaces is determined by the Biot-Savart law with respect to the control points. The induced velocity on the lifting surfaces from the hull results from the singularities used in developing the hull model and the potential flow around it. The sources and sinks do not cause any induced velocities, but the crossflow compensating doublet distribution along the body axis does contribute induced velocity normal to the lifting surfaces. These velocities are developed from the doublets distributed at the corresponding locations of the lifting surfaces with respect to the body axis. Their effects on the previously-designated control points are deduced by an equation which is a function of the crossflow velocity, and the ratio of body radius and perpendicular control point distance from body axis at corresponding points on the body axis. This relationship:

$$WDS = W(x) \frac{R^2}{YCP^2}$$

where:

WDS = induced velocity of doublet

R = body radius at XCP (long. location of control point)

YCP = vertical location of control point

W(x) = crossflow velocity

is the component normal to the lifting surface of the velocity due to a doublet in a uniform crossflow, and is found by differentiating the potential of the doublet (10).

The wake of each lifting surface connected to the body also produces induced velocities on all other lifting surfaces and the hull. The magnitude and relative importance of each induced velocity is based on the relative distance and location of the wakes with respect to the other surfaces, and is determined by the Biot-Savart law. In the numerical procedure developed for this project, (see Appendix D), the effect of the rudder wake on the fairwater is assumed to be negligible, because of its relative location, and was not considered.

The combined induced velocities at each control point of a particular lifting surface result in a set of simultaneous linear equations, a matrix of induced velocities, which relate:



- (1) the modal vortex strength of the lattice elements to the lifting surface shape;
- (2) wake effects;
- (3) applicable effects of other lifting surfaces (wake, surface); and,
- (4) the induced velocity of the hull doublet distribution, based on inflow velocity and yaw angle.

The different mode strengths for each lifting surface are then generated for subsequent development of force and moment calculation.

The hydrodynamic forces and moments on the hull result from induced velocity contributions of each lifting surface wake, the crossflow velocity, source and sink distribution, and doublet distribution.

As before, the induced velocity imposed by each wake on the hull is found by the Biot-Savart law, at each station along the body axis. This externally-induced velocity is combined with the crossflow, or sway, velocity to give a total externally-induced velocity at each station on the centerline.

The induced forces and moments at each station are derived using the above externally-induced velocities as a major governing parameter. Using a relationship from McCreight (11, 12) based on Lagally's theorem, the resulting force on a source distribution of constant strength per unit length along the body axis, when subjected to the above

externally-induced velocity, is equal to:

$$U_{\rho} \sum_{1}^{NSTA} S'(M)W(M)$$

where:

U = free stream velocity

$\rho$  = density of fluid

S'(M) = slope of hull surface at input point M;

M = station number

W(M) = externally induced velocity

NSTA = number of stations

The slope of the hull surface (S'), being a measure of the change in area per unit length, is also the source strength at the station in question. The moment due to the source distribution is found from the numerically-integrated product of the force at a station and distance from axial reference point.

Since the doublet distribution does not contribute a force when an induced velocity is imposed, we are only interested in its moment contributions. Using a method introduced

by von Karman (1930) for crossflow past airships and the assumptions:

- 1) uniform crossflow in the transverse plane; and,
- 2) body and flow radius do not change drastically along the body axis;

the crossflow effect can be represented by the flow past a circular cylinder in which the doublet strength is equal to:

$$\bar{\gamma}(x) = -\frac{1}{2} r^2(x)W(x)$$

where:

$r(x)$  = body radius at cross-section

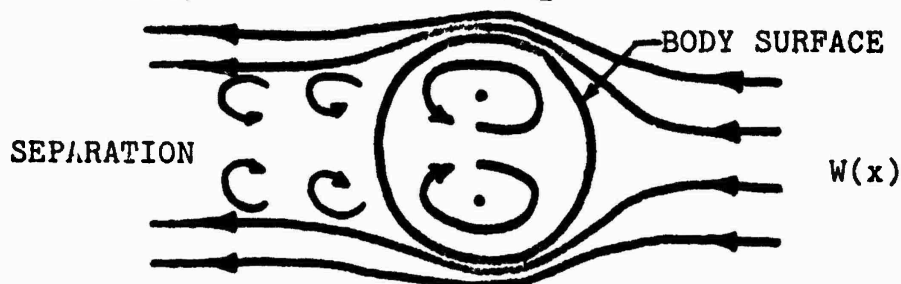
$W(x)$  = externally induced velocity (crossflow)

Since the doublets with a vertical axis are in a horizontal uniform velocity stream  $U$ , the moment is equal to  $-4\pi\rho\bar{\gamma}(x)$ . When this moment is integrated over the length of the body axis the resulting integral is formed:

$$M = 2 \pi\rho U \int_x r^2(x)W(x)dx$$

This is numerically approached by calculating the surface area at each station and knowing the crossflow velocity  $W(x)$  at each station.

Since the above two models, of sources and doublets, do not account for viscous effects - separation of flow around the body and crossflow drag -



consideration and provisions must be made to compensate for this failure, as the effects are significant with respect to some of the hydrodynamic forces and resulting moments acting on a submerged body in the steady state case. A first approximation is made by adjusting with a linear distribution factor (FAC) along the portion of the body length aft of the coordinate system reference point. This adjustment is accomplished by a factor which increases the force and moment effect of the sinks, and decreases the moment due to the doublet distribution aft.

The forces on the lifting surfaces are found by numerically integrating the four spanwise modal circulation effects to obtain the circulation along the effective span, and, in accordance with the Kutta-Joukowski theorem, determine the lift (side force) caused by the fairwater and rudder(s) separately.

The moments resulting from these lifting surfaces are

determined from the numerically integrated product of the spanwise modal circulation effects and the appropriate chordwise moment arm, based on the center of pressures for the flat plate and camber modes along the chord.

The total force and moment experienced on the submerged body is obtained from the vector summation of each individual component calculated.

Total Side Force = Rudder(s) Side Force + Fairwater Side Force + Source Side Force

Total Moment = Rudder(s) Moment + Fairwater Moment + Source Moment + Doublet Moment

An attempt to model heave force and pitch moment is made by taking the induced circulation around the hull caused by the strength of the trailer-forming wake off the external portion of the actual fairwater span. The Kutta-Joukowski theorem again is used to determine the heave force and pitch moment.

## VII. COMPARISON OF EXPERIMENTAL SUBMERSIBLE RESULTS

### A. NSRDC Model Test

A model test was conducted at the Naval Ship Research and Development Center (NSRDC) to investigate the forces and moments on a submerged body of revolution for various rudder aspect ratios. The final results of this investigation have not been completed, and only preliminary results of the clean hull configuration were comparable with these experimental results. Lateral force coefficients and yawing moment coefficients were calculated and plotted for all submersible model configurations for comparison when the final NSRDC results are available, see Figures 65 - 71. The clean hull results obtained for this experiment were about 40 per cent higher for lateral coefficients, but showed only minor differences for yawing moment coefficients.

+40 x 10<sup>-3</sup>

-115-

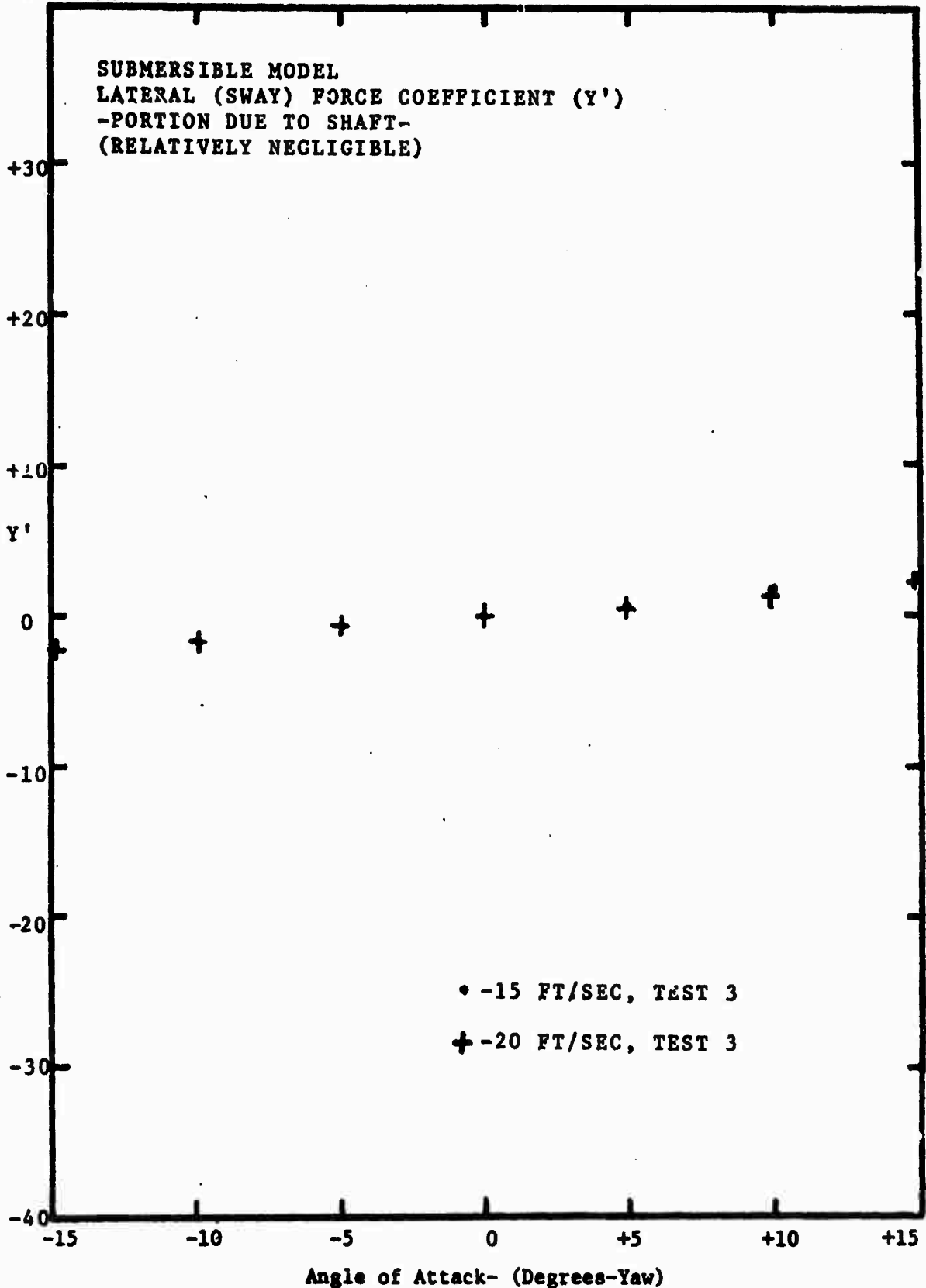


Figure 65

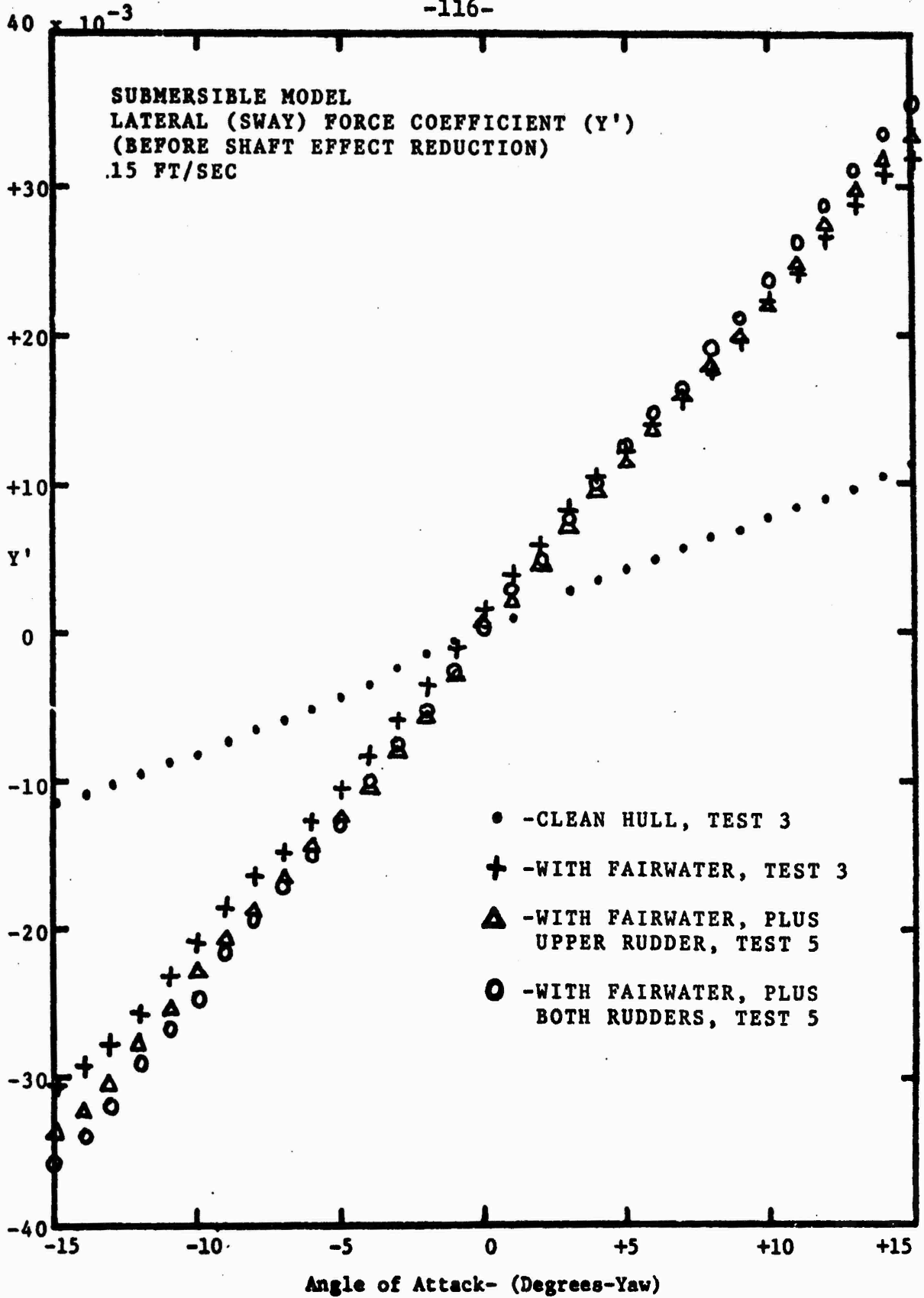


Figure 66



40 x 10<sup>-3</sup>

-117-

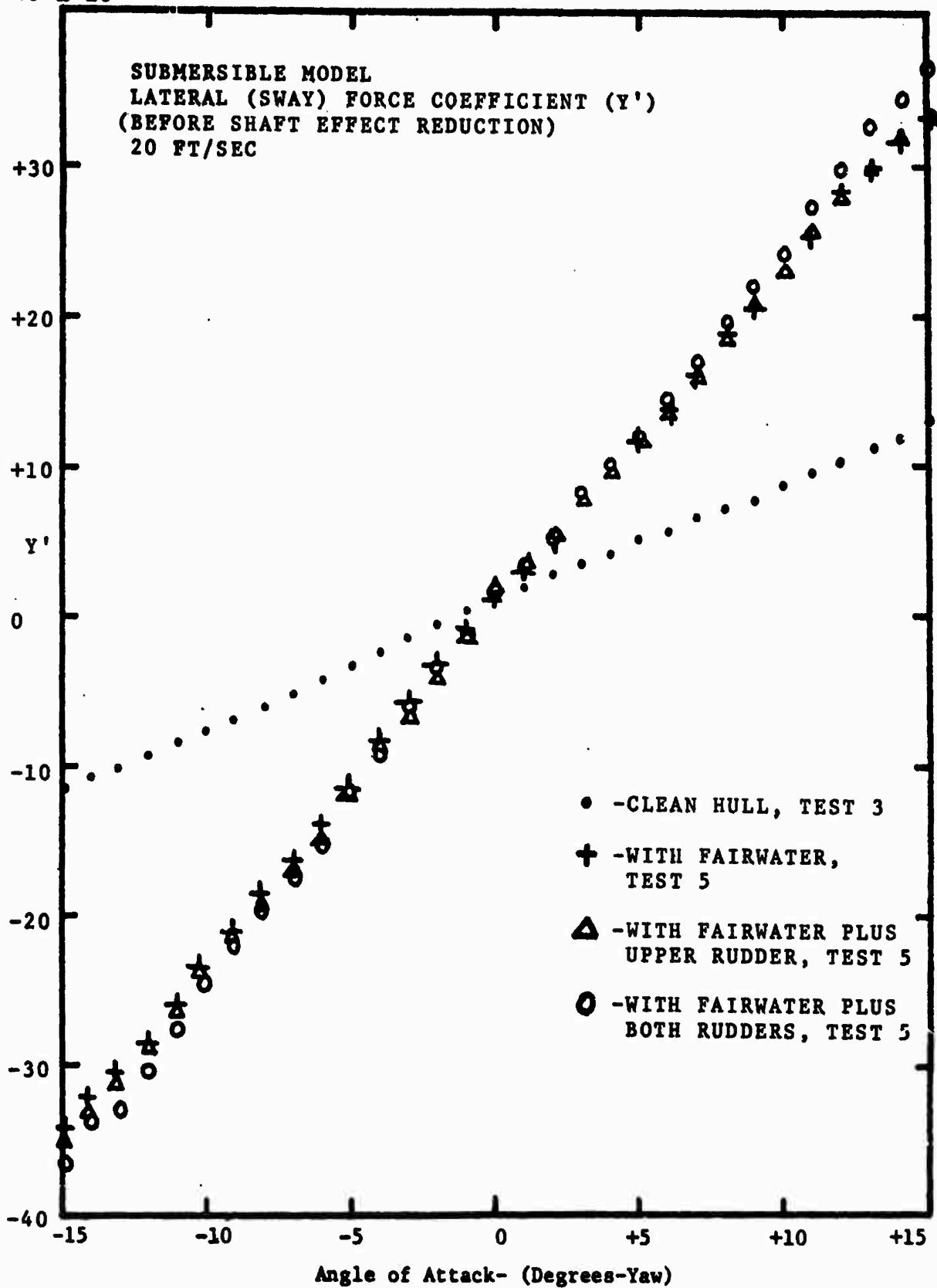


Figure 67

70 x 10<sup>-3</sup>

-118-

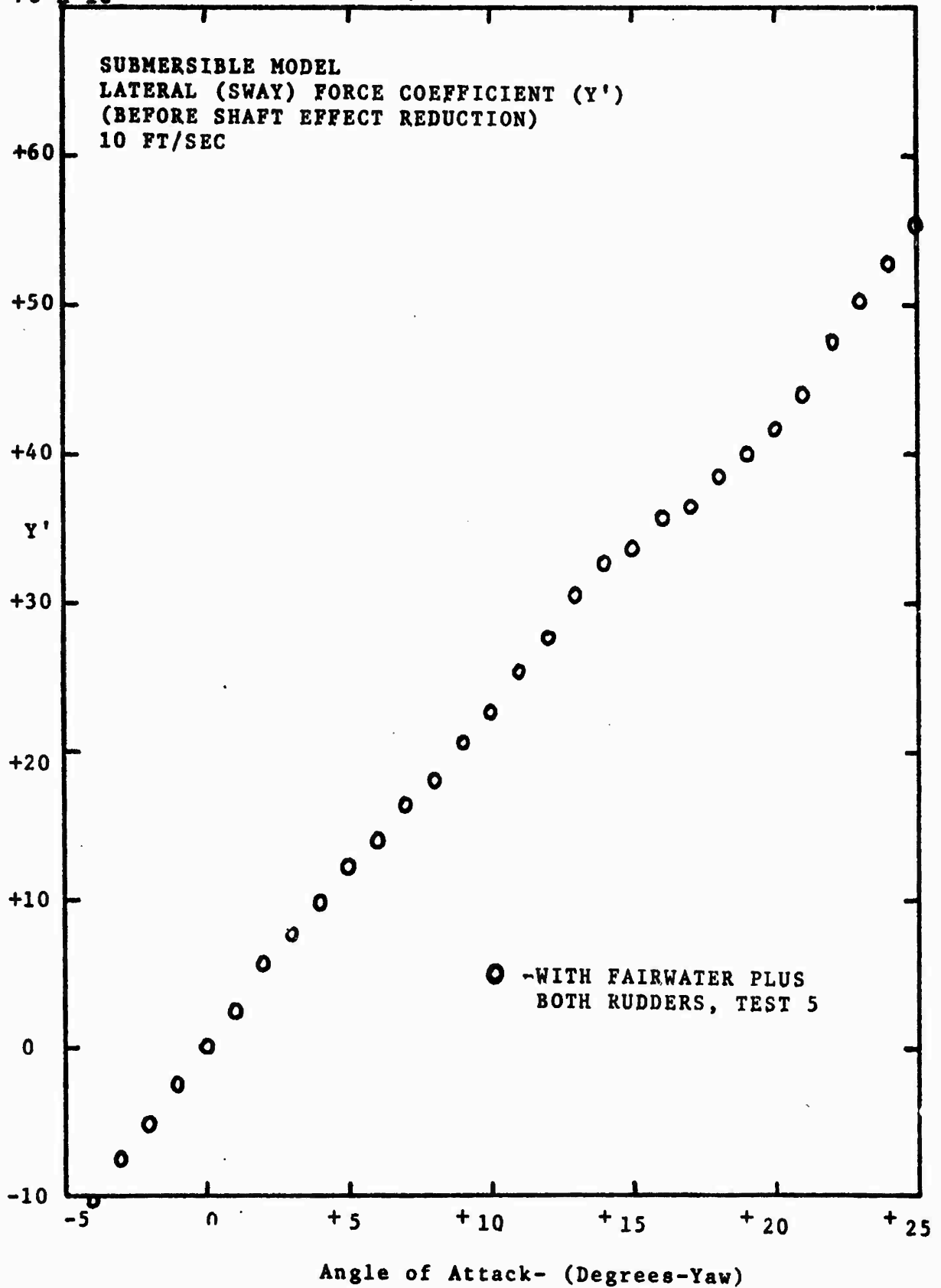


Figure 68

4 x 10<sup>-3</sup>

-119-

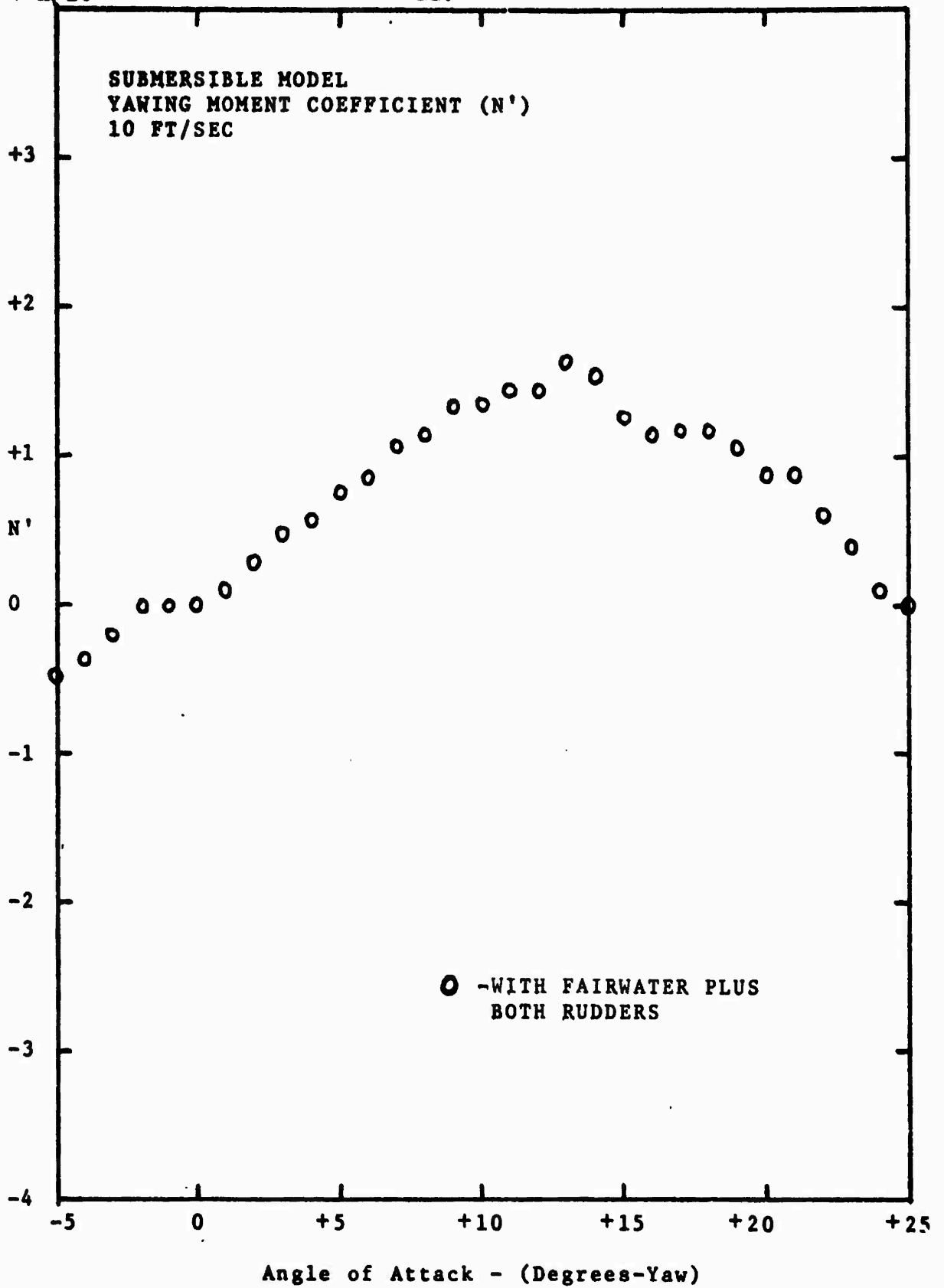


Figure 69

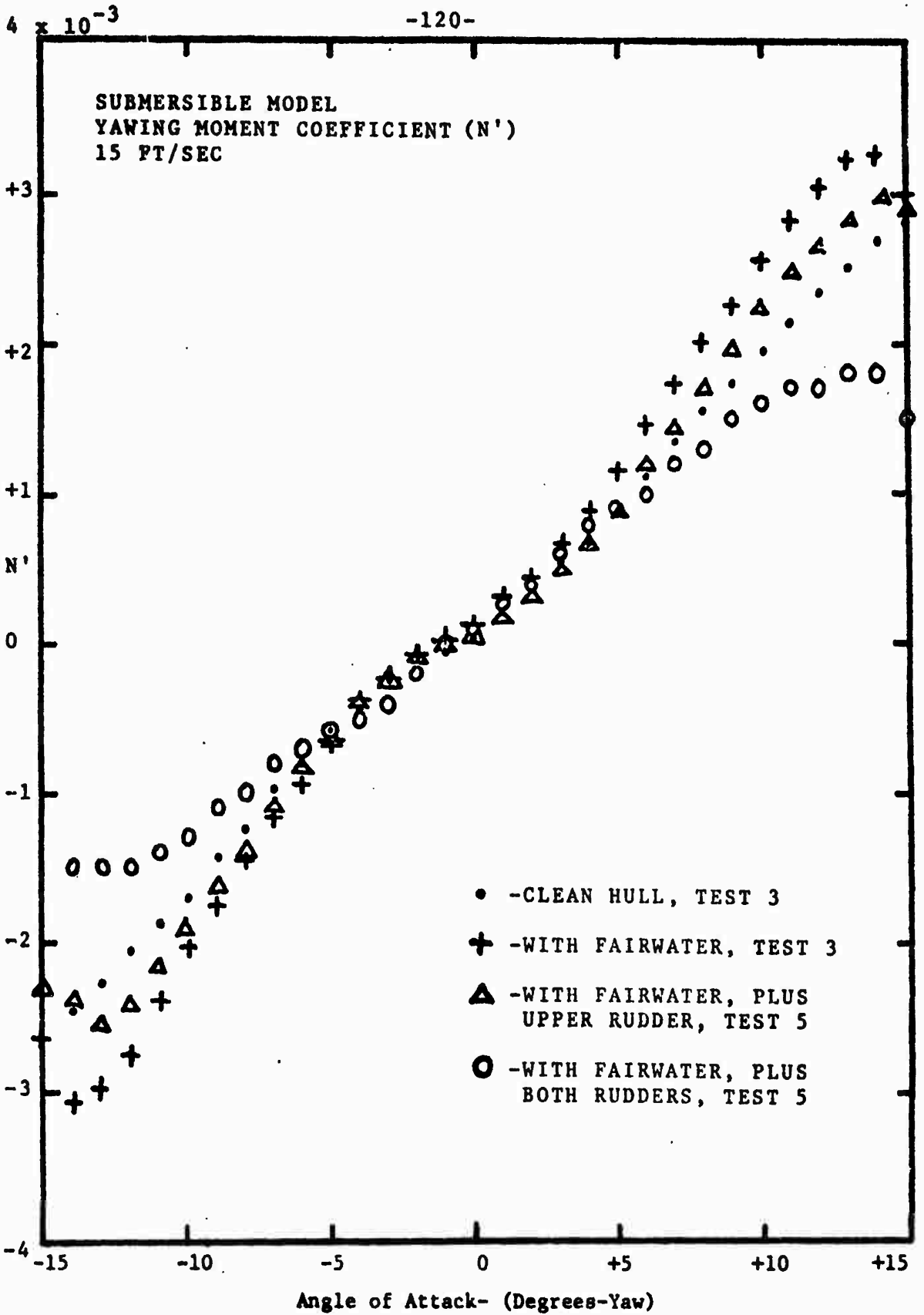


Figure 70

$4 \times 10^{-3}$

-121-

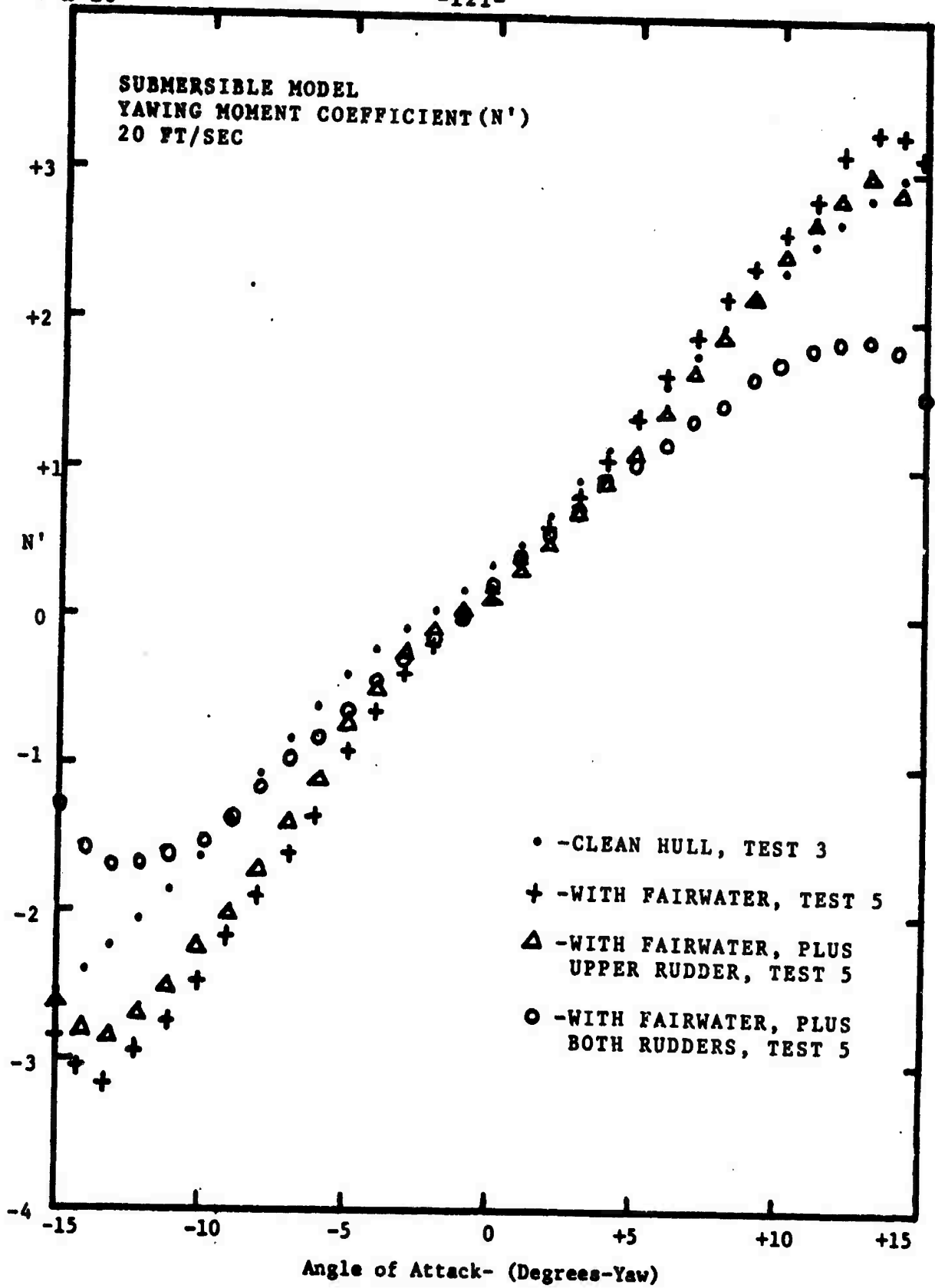


Figure 71

B. Newman-Rodriguez Results

Theoretical results obtained by Dr. J. N. Newman and Neptune Rodriguez from an investigation of a linearized low aspect ratio slender body theory are presented for comparison with experimental results, see Figures 72 and 73, taken from (13).

$$\text{Lift Coefficient} = C_L = \frac{L}{\rho b_o^2 U^2 \alpha \pi}$$

where:

L = lift force, perpendicular to flow

$\rho$  = fluid density

$b_o$  = radial distance to tip of fairwater

U = flow velocity

$\alpha$  = yaw angle.

Configuration 2 (with fairwater)

$$\frac{r_o}{b_o} = .354$$

$$\frac{b_t}{b_o} = 0$$

$C_L$  (experimental) = .433, using Figure 74

$C_L$  (Newman-Rodriguez) = .375

Configuration 3 (with fairwater and upper rudder)

$$\frac{r_o}{b_o} = .354$$

$$\frac{b_t}{b_o} = .417$$

$C_L$  (experimental) = .445, using Figure 75

$C_L$  (Newman-Rodriguez) = .270

Configuration 4 (with fairwater and both rudders)

$$\frac{r_o}{b_o} = .354$$

$$\frac{b_t}{b_o} = .417$$

$C_L$  (experimental) = .497, using Figure 76

$C_L$  (Newman-Rodriguez) = .475

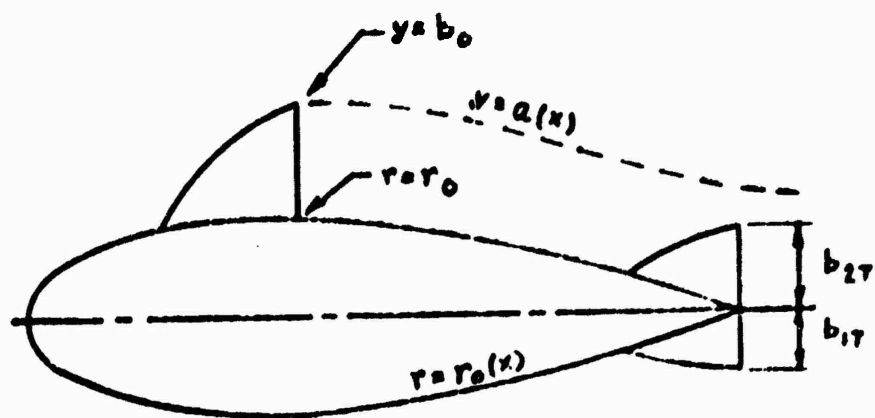
The greater difference in lift coefficients for configuration 3 results from the fact that the downwash from the fairwater, although decreasing the effective angle of attack of the rudder, does not cause the flow to become parallel to the body axis. In the linear theory, the trailing vortex sheet passes directly over the upper rudder, thereby decreasing the

rudder angle of attack. Experimentally and in the numerical model, the trailing vortex system misses the rudder.

Therefore, more lift is generated by the rudder than would appear in the linearized theory used by Newman and Rodriguez.

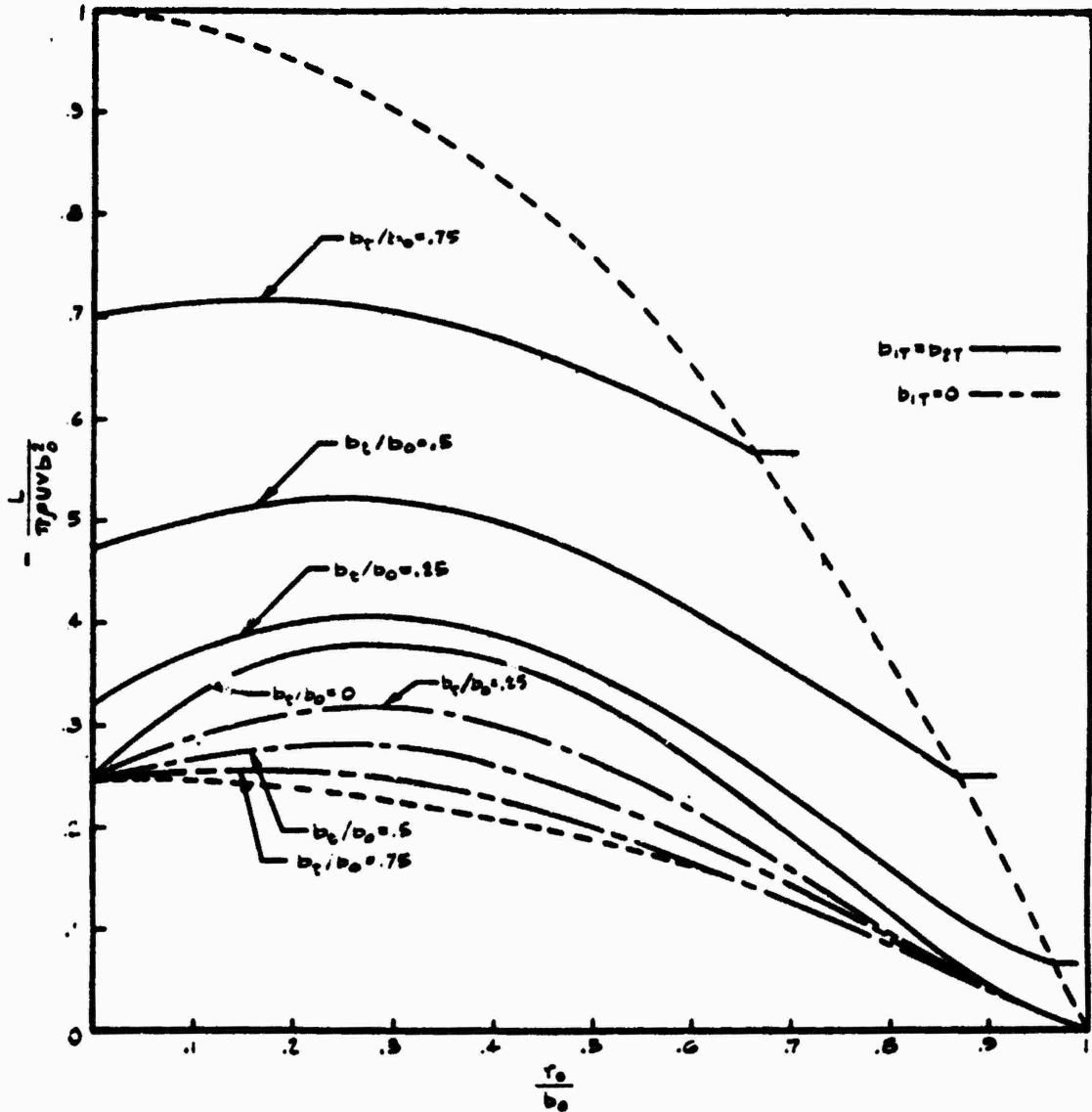
The experimental and theoretical values of  $C_L$  are actually in better agreement than presented, since the experimental lift coefficients calculated included a minor component of lift resulting from the support shaft, which was not deducted before calculation.





The axi-symmetric body with asymmetric tail fins and one upstream fin.

Figure 72



Lift coefficient of the axi-symmetric body with asymmetric fins shown in Figure 72. The upper family of curves (—) are for a symmetric tail configuration ( $b_{1T} = b_{2T}$ ), and the lower family of curves (---) are for a single upper tail fin ( $b_{1T} = 0$ ). The curve  $b_{2T}/b_0 = 0$  is for a body without tail fins. Note that the symmetric tail fin carries a positive lift force, whereas the upper tail fin experiences a negative lift force due to the effects of downwash.

Figure 73

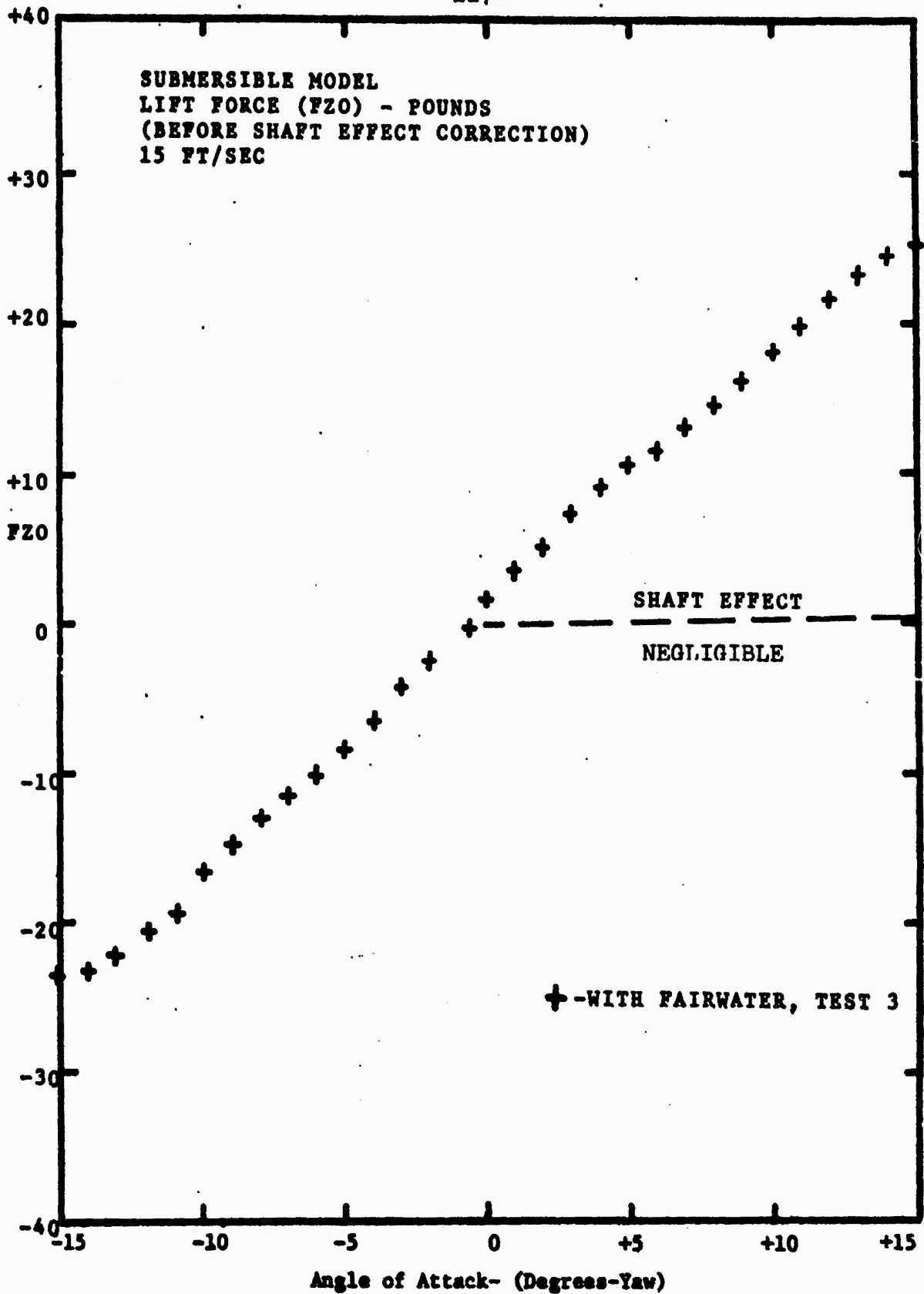


Figure 74

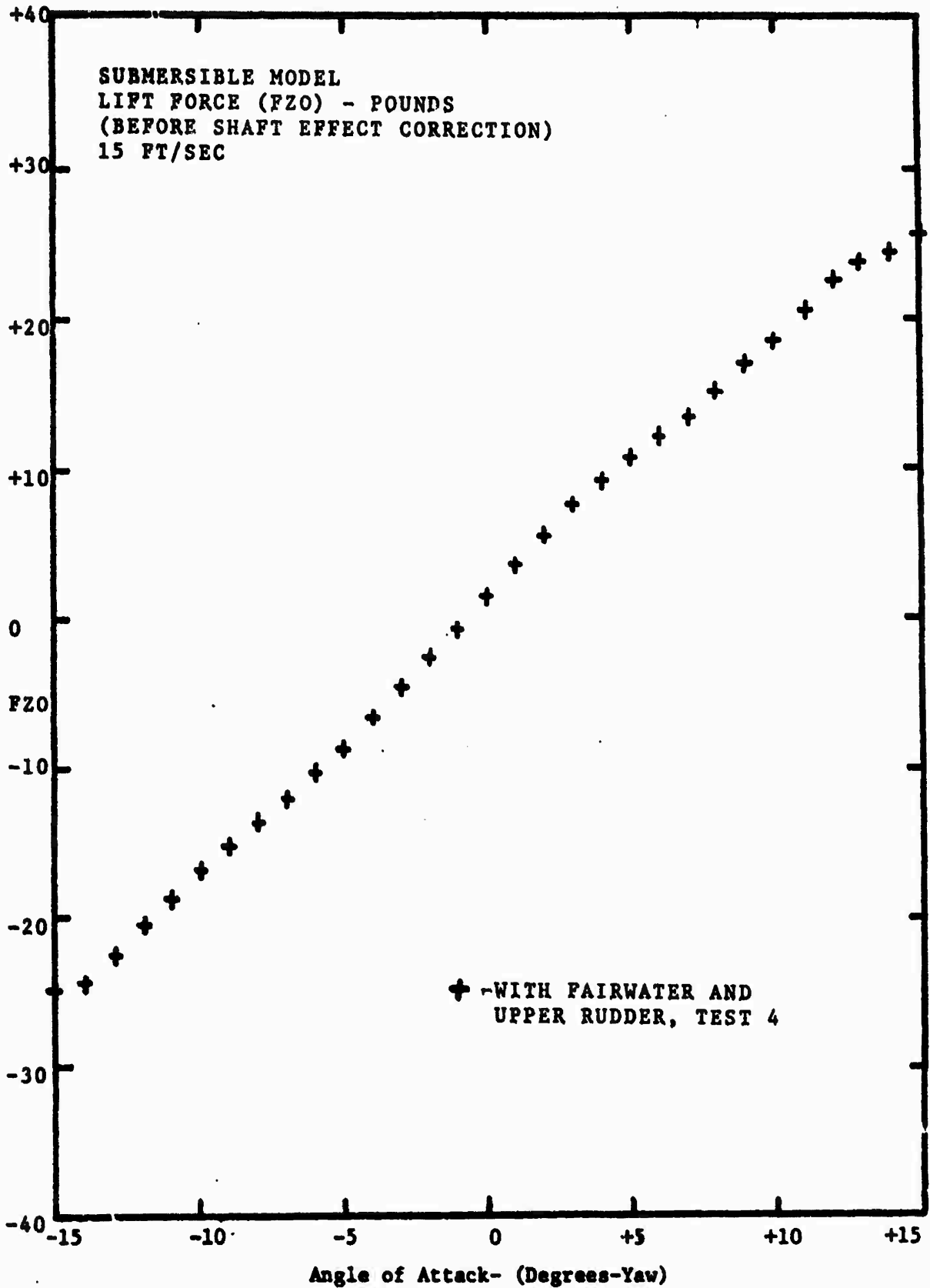


Figure 75

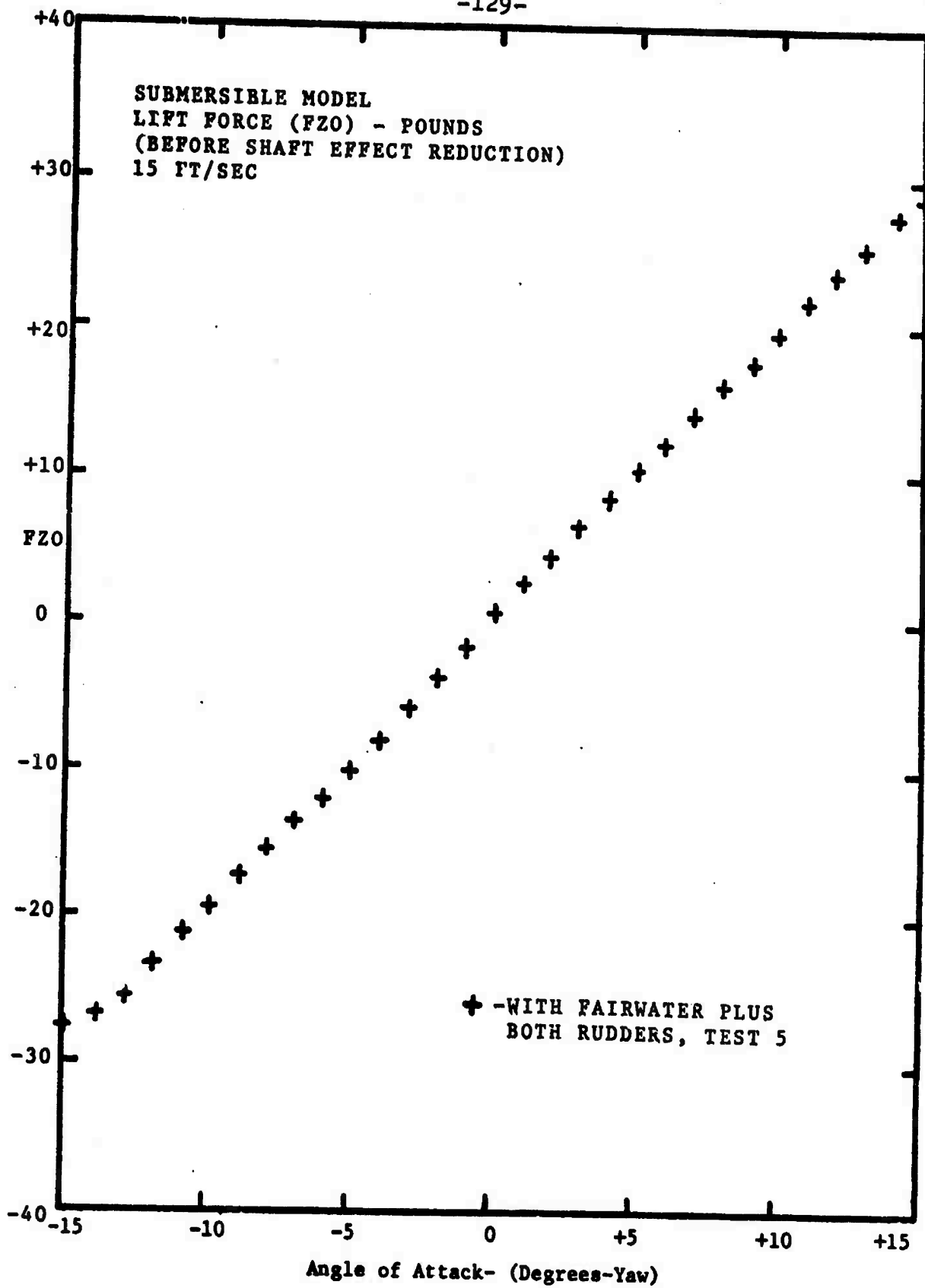


Figure 76

C. Numerical Prediction

Numerical procedure results for a submersible

with:

1. fairwater and upper rudder
2. Angle of yaw = 10 degrees
3. flow velocity = 15 ft/sec; therefore, free stream velocity = 14.77 ft/sec, side velocity = 2.6 ft/sec
4. wake angle = 10 degrees (free stream)

were:

Rudder side force	= 1.025 lb
Fairwater side force	= 11.754 lb
<u>Source side force</u>	<u>= 1.394 lb</u>
Total side force	= 14.173 lb
Rudder yaw moment	= 1.0947 ft·lb
Fairwater yaw moment	= -0.8960 ft·lb
Source yaw moment	= 7.2101 ft·lb
<u>Doublet yaw moment</u>	<u>= -9.0152 ft·lb</u>
Total yaw moment	= -1.064 ft·lb
Heave force on body	= -5.0780 lb
Pitch moment on body	= 3.5585 ft·lb

Comparable averaged experimental results were:

<u>Test 4 results</u>	<u>Test 5 results</u>	
18.0	19.0	Side force (FZ) lb
-3.75	-4.0	Yaw moment (MYO) ft·lb
-1.7	-2.7	Heave force (FYO) ft
3.0	7.0	Pitch moment (MZ) ft·lb

Numerical results were also compared with preliminary results from NSRDC for the base hull configurations. Bare hull configuration for the numerical program was accomplished by reducing the span length of the fairwater and rudder, measured from the body axis of symmetry to the radius of the hull surface at the appropriate points on the hull. The results were:

Rudder side force	= 0.012 lb
Fairwater side force	= 0.003 lb
<u>Source side force</u>	<u>= 2.990 lb</u>
Total side force (FZ)	= 3.004 lb

No side force should result from fairwater or rudder; therefore,

Total side force (FZ)	= 2.99 lb
-----------------------	-----------

Rudder yaw moment	= 0.0134
Fairwater yaw moment	= 0.0000
Source yaw moment	= 8.5134
<u>Doublet yaw moment</u>	<u>= -9.7262</u>
Total yaw moment	= -1.1994

No moment should result from fairwater or rudder; therefore,

Total yaw moment (MYO)	= -1.2128 ft lb
------------------------	-----------------



Since

$$Y' = \frac{-FZ}{\frac{1}{2} \rho U^2 L^2} = \text{Lateral Force Coefficient}$$

$$N' = \frac{MYO}{\frac{1}{2} \rho U^2 L^3} = \text{Yaw Moment Coefficient}$$

where  $\rho$  = fluid density

$U$  = free stream velocity

$L$  = model length

$$Y'(\text{numerical}) = -3.41 \times 10^{-3}$$

$$N'(\text{numerical}) = -.679 \times 10^{-3} \quad (\text{needs a greater doublet strength correction aft of the fairwater})$$

Comparable results for NSRDC and this investigation were:

NSRDC

Experimental

$$Y' = -3.5 \times 10^{-3}$$

$$Y' = -5.92 \times 10^{-3}$$

$$N' = -1.9 \times 10^{-3}$$

$$N' = -1.8 \times 10^{-3}$$

### VIII. CONCLUSION

The purpose of this project was to investigate hull-control surface interactions on submerged bodies, to include the effects imposed on the body by the fairwater and rudders, when the body is at a constant yaw angle.

It has been shown through experimental and numerical models, and flow visualization, that the addition of a non-symmetric appendage (fairwater) on a symmetrical body of revolution has a significant effect on the hull and the control surfaces (rudders) located downstream.

The fairwater, besides being a lifting surface and generating a side (sway) force when at an angle of yaw, also induces a circulation around the hull of a submersible. When this circulation and a sway velocity are combined, a lift is generated on the hull. These asymmetric forces then produce moments around each of the three coordinate axes and cross-coupling moments. The fairwater was also instrumental in decreasing the effective angle of attack of the upper rudder, located on the same side and downstream of it. The trailing vortex sheet, shed from the fairwater, induced velocities on this rudder and effectively changed the direction of fluid flow meeting the rudder. This change in flow direction was readily seen during the flow visualization experiments.

The upper and lower rudders produced relatively minor

effects on the forces and moments at small angles of yaw. Only at high angles of yaw, when the fairwater and support-shaft downwashes were least effective on the rudders, did the side (sway) force of the rudders combine with the extended moment arm to produce a major effect. Investigation of the effects of the rudders on the body of revolution, without the fairwater, is needed for a more complete analysis.

The numerical model considered the effects of the fairwater and although requiring refinement, the initial results are comparable with experimental results obtained during this investigation.

LIST OF REFERENCES

1. Department of Naval Architecture and Marine Engineering, Massachusetts Institute of Technology, Technical Proposal to The General Hydrodynamics Research Program, NSRDC; "Hull-Control Surface Interactions on Submerged Bodies," Submitted March 1971.
2. E. S. Arentzen, Capt. USN and Philip Mandel, "Naval Architectural Aspects of Submarine Design," paper presented at Annual Meeting, SNAME, New York, New York, November 17 - 18, 1960.
3. L. M. Milne-Thomson, Theoretical Hydrodynamics, Fourth Edition, the Macmillan Company, New York, New York, 1960.
4. V. M. Falkner, "The Calculation of Aerodynamic Loading on Surfaces of Any Shape," Aeronautical Research Committee R & M No. 1910, 1943.
5. V. M. Falkner, "The Solution of Lifting-Plane Problems by Vortex Lattice Theory," Aeronautical Research Council, R & M No. 2591, 1947.
6. V. M. Falkner, "The Scope and Accuracy of Vortex Lattice Theory," Aeronautical Research Council, R & M No. 2740, 1952.
7. J. E. Kerwin, "The Solution of Propeller Lifting Surface Problems by Vortex Lattice Methods," Report, Department of Naval Architecture and Marine Engineering, M.I.T., Cambridge, Mass., June 1961.
8. D. E. Cummings, "Vortex Interaction in a Propeller Wake," Report No. 68-12, Department of Naval Architecture and Marine Engineering, M.I.T., Cambridge, Mass., June 1968.
9. J. E. Kerwin and R. Leopold, "A Design Theory for Sub-cavitating Propellers," paper presented at Annual Meeting, SNAME, New York, New York, November 12 - 13, 1964.
10. F. B. Hildebrand, Advanced Calculus for Applications, Prentice-Hall, Inc., Englewood Cliffs, New Jersey, 1962.
11. W. R. McCreight, "Force and Moment on a Slender Body of Revolution Moving in Water of Finite Depth," M. S. Thesis, M.I.T., Cambridge, Mass., June 1970.

12. W. R. McCreight, "Heave Force and Pitching Moment on a Submerged Body of Revolution in Finite Depth," Report No. 70-7, Department of Naval Architecture and Marine Engineering, M.I.T., Cambridge, Mass., June 1970.
13. J. N. Newman and T. Y. Wu, "A Generalized Slender-Body Theory For Fish-Like Forms," Journal of Fluid Mechanics, Volume 57, pp. 673-693, 1973.
14. C. O. Horton, "Design and Construction of a System for Measurement of Unsteady Propeller Forces," Naval Engineer Thesis, Department of Naval Architecture and Marine Engineering, M.I.T., Cambridge, Mass, June 1970.
15. T. Brockett, "Minimum Pressure Envelopes for Modified NACA - 66 Sections With NACA a = 0.8 Camber and BuShips Type I and Type II Sections," Report 1780, DTMB, Washington, D. C., February 1966.

OTHER REFERENCES CONSULTED

J. P. Comstock (editor), Principles of Naval Architecture, Society of Naval Architects and Marine Engineers, New York, New York, 1967.

R. F. Elliott, "Experiments on a Slender Body of Revolution Moving Near a Wall," M. S. Thesis, Department of Naval Architecture and Marine Engineering, M.I.T., Cambridge, Mass., 1969.

J. N. Newman, Marine Hydrodynamics, (Lecture Notes), Revised Edition, Department of Naval Architecture and Marine Engineering, M.I.T., Cambridge, Mass. 1971.

B. Thwaites (editor), Incompressible Aerodynamics, Oxford University Press, Oxford, England, 1960.

-138-

APPENDIX A

THE M.I.T.

VARIABLE PRESSURE WATER TUNNEL

## APPENDIX A

### THE M.I.T. VARIABLE PRESSURE WATER TUNNEL (14)

The M.I.T. Variable Pressure Water Tunnel was built in 1938 - 39, and provided a significant advance in propeller and model test facilities at that time. Since then, several modifications have been made to the tunnel to extend its useful life, to make it more convenient to use, and to give it additional capabilities in keeping with current research needs.

#### General Features

The tunnel is a closed-return type and is approximately a 24-foot diameter square in shape. See Figure A-1. It occupies parts of the first and second floors of Building 3 on the M.I.T. campus. The smallest internal diameter is approximately 30 inches, but this gradually widens to a 60-inch maximum before narrowing again to enter the test section. The tunnel cross-section is circular except at the test section and in the tapered transition section. The transition section narrows the 60-inch circular cross-section to the 20-inch square test section.

#### Testing Facilities

The tunnel can provide water velocities in the test

section up to 33 ft/sec and maintain any selected internal pressure from atmospheric (760mm Hg) down to approximately 140 mm Hg.

The test section is accessible via any of four identical removable plexiglas windows. The windows are 2.0 inches thick by 13 7/16 in. by 41 15/16 in. high and cover access holes measuring 41 15/16 by 13 7/16 in. The windows are readily cut or drilled and are thus ideal for mounting experiments. The dynamometer apparatus used allows measuring six-degrees-of-freedom forces on lifting surfaces, such as rudders or hydrofoils. Fittings are installed in the windows to accept Pitot tubes at several locations.

The tunnel may also be operated with a free surface to test-surface piercing hydrofoils or to simulate a miniature towing tank for small ship model testing.

#### Impeller Drive Systems

A 100 HP motor drives three DC generators. One of these, a 60 KW shunt-wound generator, provides power for the 75 HP DC impeller drive motor. The second, a 30 KW shunt-wound DC generator, provides power for the 40 HP propeller drive motor. The third is a 3 KW compound-wound DC generator and provides excitation for the other two DC generators.

A variable resistance vernier control system provides close control of impeller RPM.



A device attached to the impeller drive shaft provides a 60 pulse per revolution output. The signal is fed to a Hewlett-Packard 5212A electronic counter. By using 60 pulses per revolution, the counter reads directly in RPM instead of RPS.

### Water Flow

A four-bladed bronze impeller is used to provide water flow. It is located in the lower level horizontal run in the 30-inch diameter section. It is immediately followed by straightening vanes to remove rotation from the water.

Each 90° bend has several thin stainless steel turning vanes with a non-symmetrical cross-section developed from airfoil theory. The vanes have a low power loss and the resolving turbulence generated by rounding the corners is fine-patterned and on the order of the turning vane spacing.

The 30-inch diameter widens out to 60 inches to slow the water velocity and further reduce turbulence. After rounding a 90° bend, the water is passed through a honeycomb of one-inch diameter plastic tubes and 2 sections of metal screens.

The 60-inch diameter is then smoothly constricted to flow through the 20-inch square test section. The section area reduction is 7.07. The constriction speeds up the flow velocity and at the same time stretches out any remaining turbulence. A smooth flow pattern results.

### The Variable Pressure System

Any pressure in the range of atmospheric to 140 mm Hg can be maintained by the vacuum pump. The lower limit is dictated by the vapor pressure of water and small air leaks in the tunnel. Water vapor pressure at 60° F is 135 mm Hg.

Suction from the vacuum pump is taken at three points on the tunnel: (1) from the vacuum dome; (2) from the manhole cover over the 60-inch horizontal section; and (3), at the last 90° bend before entering the honeycomb.

If the tunnel is completely filled with water, some water may be sucked into the vacuum line to the pump. This is trapped in a receiver tank. Suction by the pump is taken from the top of the tank, while a drain line is provided at the bottom of the tank. The drain line drops 35 feet and is kept below water level in the building basement.

The vacuum system is the primary means of removing dissolved gases from the tunnel water. Dissolved oxygen is chemically removed for corrosion protection of the mild steel walls, and other gases are removed by keeping the tunnel at reduced pressure for several hours. If this is not done, dissolved gases form bubbles at reduced pressure and obscure the viewing of experiments in the test section.

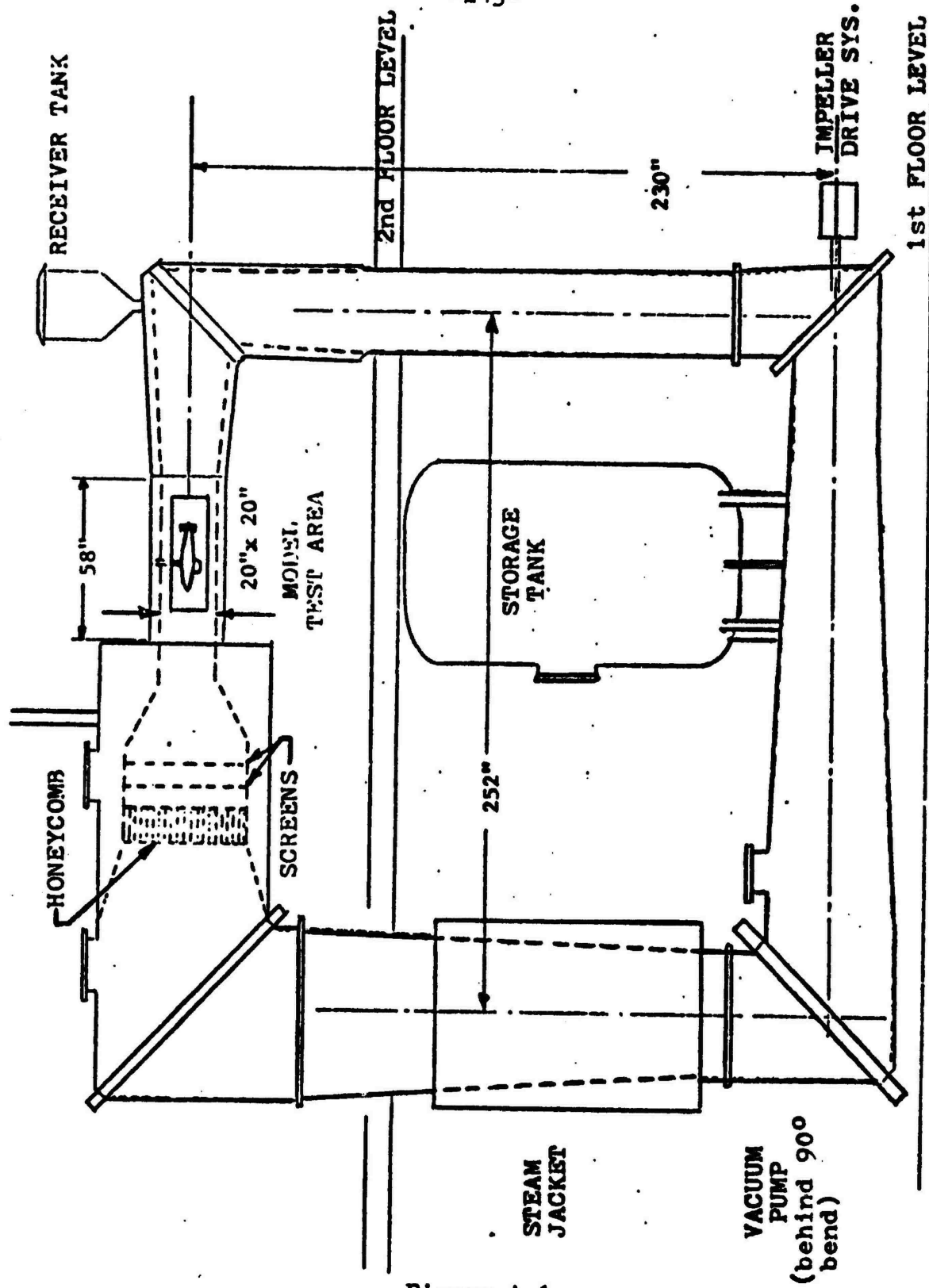


Figure A-1

M.I.T. VARIABLE PRESSURE WATER TUNNEL

-144-

APPENDIX B

DYNAMOMETER PROGRAM USED  
FOR  
EXPERIMENTAL MODEL TESTS

```

C DYNAMCLTER PROGRAM USED TO EVALUATE THE FORCES AND MUMENT UN THE
C SUBMERSIBLE ANU FAIRWATER MODELS (EXPERIMENTAL)
C MK4 RUDDER DYNAMMETER DATA REDUCTION PROGRAM KERWIN/LEWIS MAY 72
INTEGER KS,S,BLANK
REAL MX,MYU,MZ,MZL,MFLAP
DIMENSION IDENI(16),ZM(2),ZI(6,2,2),ZF(2),NTAP(32),NFLD(32),ANUM(3
12),ANGL(32),S(32,6),R(32,7),DZI(6,2),CL(32),CM(32),CPL(32),
ZCY(32),CMF(32),VC(5),VE(5),FM(2),C(C),CLU(32),CLSQ(32),KN(32),SI(3
22),CU(32)
DATA VC/4.11447,2.60068,C.9J16,0.6214,4.7381/,VE/.49353,.05,.4724,0
1.00038,.5/,KS/'K'/,BLANK/' '/
READ(5,104)C(N),N=1,6),TWIST,SHAFT
FORMAT(6F10.5)
104 READ(5,103)(IDLNI(N),N=1,18)
103 FORMAT(16A4)
READ(5,100) DF,NKI,NTI,AREA,SPAN,AC,XAC,ZAC,FMC
FORMAT(5F10.2,F9.1,F9.3,F9.3,F10.2,F9.5)
100 IF(AREA.LE.0) GO TO 99
KHJ=1.9274-0.00028*NTI
SCALL=1.000552-13.3E-6*NKI
FM(1)=1.4073-0.00071*NKI
FM(2)=24.5234-0.00256*NKI
WRITE(6,200)(IDENT(N),N=1,16)
200 FORMAT(1',1X,'FLAPPED RUDDER INPUT DATA',1X,16A4/3X,'DF',3X,'TR'
1,4X,'11',3X,'AREA',6X,'SPAN',4X,'C-MAC',4X,'X-MAC',14X,'ZAC',6X,'F
ZMC')
WRITE(6,100) DF,NKI,NTI,AREA,SPAN,AC,XAC,ZAC,FMC
READ(5,101)(ZM(K),(ZI(M,L,K),L=1,2),N=1,6),ZF(K),K=1,2)
101 FORMAT(5F10.2,12X,F5.0,F4.0,F5.0,F4.0,F5.0,F4.0,F5.0,F4.0,F5.0,F4.0)
1F5.0,F4.0,F9.0)
WRITE(6,201)
201 FORMAT(0 ZERO READINGS BEFORE AND AFTER',0 ANOM 1-N 1-R 2-N
1 2-K 3-N 3-K 4-N 4-K 5-N 5-K 6-N 6-K FLAP')
WRITE(6,204)(ZM(K),(ZI(M,L,K),L=1,2),N=1,6),ZF(K),K=1,2)
204 FORMAT(2(F4.0,4(2X,F4.0),2(1X,F4.0),6(2X,F4.0),1X,F6.0/))
WRITE(6,212)(C(N),N=1,6),TWIST,SHAFT

```



```

102 FORMAT(0) CELL LBS/COUNT 1=,F7.5, 2=,F7.5, 3=,F7.5, 4=,F
17.5, 5=,F7.5, 6=,F7.5, 7= TWIST=,F7.1, SHAFT DIA.=,F7.2
2, IN. )
WRITE(6,202)
202 FORMAT( / )
      1 5 2 S INPUT DATA AS RECORDED, TF ANUM ANGLE S 1
      UU 2 J=1,32 FLAP)
      JI=J-1
      READ(5,102) NTAP(J),NFLD(J),ANOM(J),ANGL(J),(S(J,M),K(J,M),M=1,6),
1(KJ,7)
102 FORMAT(14,I1,F5.0,F6.1,3X,A1,F8.2,A1,F8.2,A1,F8.2,A1,F8.2,A1,F8.2,
1A1,F6.2,F7.0)
      IF(ANOM(J).LE.0.0) GO TO 3
4 WRITE(6,203) NTAP(J),NFLD(J),ANUM(J),ANGL(J),(S(J,M),K(J,M),M=1,6)
1, N(J,7)
203 FORMAT(13,I1,F6.0,F6.1,3),6(A1,F6.0,2X),F7.0)
      UU 10 99
      BUU=1.0/(JI-1)
      UZ1=(ZM(2)-ZM(1))*BUG
      UU 4 M=1,6
      UU 4 L=1,2
      UZ1(M,L)=(Z1(M,L,2)-Z1(M,L,1))*BUG
      UZ1=(Z1(2)-Z1(1))*BUG
      UU 5 J=1,JI
      IF(J.EQ.1) GO TO 6
      IF(NTAP(J).EQ.0) NTAP(J)=NTAP(J-1)
      IF(NFLD(J).EQ.0) NFLD(J)=NFLD(J-1)
      BUU=J-1
6 ANUM(J)=ANUM(J)-ZM(1)-BUU*UZM
      KAT=(ANGL(J)-100.0)*0.0174532
      S1(J)=SIN(KAT)
      CU(J)=COS(KAT)
      ANGL(J)=ANGL(J)-ZAC
      UU 7 M=1,6
      IF(S(J,M).EQ.0LANK) S(J,M)=S(J-1,M)
      IF(S(J,M).EQ.0RS) GO TO 8

```

PGM1J037  
 PGM1J038  
 PGM1J039  
 PGM1J040  
 PGM1J041  
 PGM1J042  
 PGM1J043  
 PGM1J044  
 PGM1J045  
 PGM1J046  
 PGM1J047  
 PGM1J048  
 PGM1J049  
 PGM1J050  
 PGM1J051  
 PGM1J052  
 PGM1J053  
 PGM1J054  
 PGM1J055  
 PGM1J056  
 PGM1J057  
 PGM1J058  
 PGM1J059  
 PGM1J060  
 PGM1J061  
 PGM1J062  
 PGM1J063  
 PGM1J064  
 PGM1J065  
 PGM1J066  
 PGM1J067  
 PGM1J068  
 PGM1J069  
 PGM1J070  
 PGM1J071  
 PGM1J072

```

K(J,M)=K(J,M)-ZI(M,1,1)-EUG*DZI(M,1)
6  GO TO 7
K(J,M)=-K(J,M)+ZI(M,2,1)+BUG*DCZI(M,2)
7  CONTINUE
5  K(J,7)=K(J,7)-ZF(1)-BUG*CFZ
WRITE(6,205)(INTAP(J),NFLD(J),ANUM(J),ANGL(J),(K(J,M),M=1,6),R(J,7)
1,J=1,7)
205  FURMAT(// ' INPUT DATA CORRECTED FOR ZERO READINGS AND SIGNS'/(I
13,I1,F6.0,F7.2,2X,CF9.2,F7.0))
*KITL(6,207)(IDENT(N),N=1,18)
207  FURMAT(// ' *FLAPPED RUGGER DATA REDUCTION**'//IX,18A4//3X, ' ALP
IHA FX-LB FZ-LB FX-INLB MZ-INLB FYU-LB FZU-LB
2 MAU-INLB MYU-INLB MZU-INLB MYGLAP-INLB VEL-FPS')
BEAK=AL/(12*3.9739*EXP(67.6032/NTT))
30 9 J=1,7
I=INTAP(J)
IF(I.LT.1.OR.I.GT.5) GO TO 99
K=NFLD(J)
IF(K.LT.1.OR.K.GT.2) GO TO 99
300=VE(I)
V=(ANCH(J)*FM(K)*SCALE/(VC(I)*RHO))*RUG
FYHAFI=0.00327*SHAFT**2*V**2
FBOX1=C(1)*K(J,1)
FBOX2=C(2)*K(J,2)
FBOX3=C(3)*K(J,3)
FBOX4=C(4)*K(J,4)+FYHAFI*0.41477
FBOX5=C(5)*K(J,5)+FYHAFI*0.41477
FBOX6=C(6)*K(J,6)+FYHAFI*0.17045
FA=-FBOX5
FY=-FBOX4-FBOX5-FBOX6
FZ=-FBOX1-FBOX2
MA=14.725*(FBOX1+FBOX2)+6.002*(FBOX5-FBOX4)
MY=-18.002*FBOX2
MZ=17.034*FBOX6-14.725*FBOX3-3.5*(FBOX4+FBOX5)
FAU=FX*CC(J)+FZ*SI(J)
FYU=FY

```

PGMJ073  
PGMJ074  
PGMJ075  
PGMJ076  
PGMJ077  
PGMJ078  
PGMJ079  
PGMJ080  
PGMJ081  
PGMJ082  
PGMJ083  
PGMJ084  
PGMJ085  
PGMJ086  
PGMJ087  
PGMJ088  
PGMJ089  
PGMJ090  
PGMJ091  
PGMJ092  
PGMJ093  
PGMJ094  
PGMJ095  
PGMJ096  
PGMJ097  
PGMJ098  
PGMJ099  
PGMJ100  
PGMJ101  
PGMJ102  
PGMJ103  
PGMJ104  
PGMJ105  
PGMJ106  
PGMJ107  
PGMJ108

```

FZU=FZ*CU(J)-FX*SI(J)
MXU=MX*CU(J)+MZ*SI(J)
MYU=MY
MZU=MZ*CU(J)-MX*SI(J)
MFLAP=K(J,7)*FMC
ANGL(J)=ANGL(J)+MYG/TWIST
*RITE(6,206) ANGL(J),FX,FZ,MX,MZ,FXL,FYU,FZU,MXU,MYU,MZU,MFLAP,V
*FORMAT(11F9.2,F15.2,F8.2)
KVS=U.0*RHCH*AKEA*V**2/144.0
CL(J)=FZU/KVS
CLSQ(J)=CL(J)**2
CU(J)=FAU/KVS
CLU(J)=CL(J)/CU(J)
CM(J)=(MYU+FL*XC)/KVS/AC
CPL(J)=(MXU/FZU)/SPAN
CY(J)=FYU/KVS
KN(J)=V*BLAK
CMF(J)=MFLAP/KVS/AC
*RITE(6,208) IDENT(N),N=1,18)
*FORMAT(11) **FLAPPED RUDDER DATA IN NON-DIMENSIONAL FORM**//3X18A
14// ALPHA CL CE CM CPL CY L/U CMF C
2LSJ KN*10**6)
*RITE(6,209) ANGL(J),CL(J),CU(J),CM(J),CPL(J),CY(J),CLU(J),CMF(J),
1CLSQ(J),KN(J),J=1,JT)
209 *FORMAT(13.2,F7.3,F8.4,F8.3,F8.3)
DU 15 J=1,JT
ANGL(J)=ANGL(J)+.01562*AREA#CL(J)
CU(J)=CU(J)+.0005425*AREA#CL(J)**2
CLU(J)=CL(J)/CU(J)
*RITE(6,211)
*FORMAT(//) ABOVE DATA CORRECTED FOR TUNNEL INTERFERENCE
1// ALPHA CL CC CM CFL CY L/D CMF C
2LSJ KN*10**6)
*RITE(6,209) ANGL(J),CL(J),CU(J),CM(J),CPL(J),CY(J),CLU(J),CMF(J),
1CLSQ(J),KN(J),J=1,JT)
209 TU 1

```

PGMJ109  
PGMJ110  
PGMJ111  
PGMJ112  
PGMJ113  
PGMJ114  
PGMJ115  
PGMJ116  
PGMJ117  
PGMJ118  
PGMJ119  
PGMJ120  
PGMJ121  
PGMJ122  
PGMJ123  
PGMJ124  
PGMJ125  
PGMJ126  
PGMJ127  
PGMJ128  
PGMJ129  
PGMJ130  
PGMJ131  
PGMJ132  
PGMJ133  
PGMJ134  
PGMJ135  
PGMJ136  
PGMJ137  
PGMJ138  
PGMJ139  
PGMJ140  
PGMJ141  
PGMJ142  
PGMJ143  
PGMJ144



99 STJP  
ENJ

PGMLU145  
PGMLU146

-149-

PAGE 5

IBM

FORTRAN Coding Form

NAME: \_\_\_\_\_

PROJECT: \_\_\_\_\_

DATE: \_\_\_\_\_

FORTRAN STATEMENT

Flap angle Deg	TR P	TT P	Rud. Area in. <sup>2</sup>	Rud. span in.	Rud. MAC in.	Axis Shift to Qtr. Chord of MAC in. (+ downstream)	Flap Nom Cal Inlb./C.		
Zeros Before	Zeros After	Zeros Before	Zeros After	Zeros Before	Zeros After	Zeros Before	Zeros After		
Tap/Pld	Manom	Angle	1	2	3	4	5	6	Flap Nom.
			sign	sign	sign	sign	sign	sign	

Tap Code: 7/4-1 6/5-2 7/6-3 5/4-4 Pitot Static - 5 Fluid Code: 1 Blue; 2 Mercury  
Sign Code: N Normal; R Reverse

Figure B-1 Sample Data Sheet

```

C   SAMPLE DATA DECK FOR SUBMERSIBLE MODEL
    SUB WITH FAINWATER, UPPER & LOWER RUDDERS 10 FT/SEC
    O.U  75  62.06  100 100 50 50 3.5 24.600 0.0 100 100 50 50 97.60  .0
    UU   81  100 100 50 50 50 50 50 50 100 100 50 50 50 50
    JJ   81  100 100 50 50 50 50 50 50 100 100 50 50 50 50
    11   81  110 N 100 100 50 50 50 50 77 N 150 R 45 64
        96.6 121 130 142 153 162 169 75
        95.6 130 142 153 162 169 75
        94.6 142 153 162 169 75
        93.6 153 162 169 75
        92.6 162 169 75
        91.6 169 75
        90.6 169 75
    PGM1JU01
    PGM1JU02
    PGM1JU03
    PGM1JU04
    PGM1JU05
    PGM1JU06
    PGM1JU07
    PGM1JU08
    PGM1JU09
    PGM1JU10
    PGM1JU11
    PGM1JU12

```

Sample Results

FLAPPED RUDDER INPUT DATA  
 SUR WITH FAIRWATER, UPPER & LOWER RUDDERS 10 FT/SEC  
 DF TR TY AFPA SPAN C-MAC X-MAC ZAC FMC  
 0.0 75 81 62.06 3.5 24.600 0.0 97.63 0.0  
 ZERO READINGS BEFORE AND AFTER  
 ANGLE 1-N 1-R 2-N 7-R 3-N 3-B 4-N 4-R 5-N 5-R 6-N 6-R FLAP  
 0. 100. 100. 50. 50. 50. 50. 100. 100. 50. 50. 50. 50. 0.  
 0. 100. 100. 50. 50. 50. 50. 100. 100. 50. 50. 50. 50. 0.

CELL LWS/COUNT 1=0.79926 2=0.75030 3=7.20030 4=0.10050 5=0.48970 6=0.20490  
 THRST= 323.7 SWAFT DIA.= 0.75 IN.

INPUT DATA AS RECORDED

TF	ANG	ANGLE	S	1	S	2	S	3	S	4	S	5	S	6	FLAP
11	676.	96.6	N	117.	N	50.	R	77.	N	136.	R	49.	R	64.	0.
00	675.	95.6		121.		51.		77.		148.		52.		63.	0.
00	674.	94.6		130.		53.		77.		160.		55.		63.	0.
07	674.	91.6		142.		55.		76.		175.		58.		62.	0.
00	627.	92.6		153.		56.		76.		185.		60.		62.	0.
00	626.	91.6		162.		56.		76.		203.		63.		62.	0.
00	627.	90.6		169.		58.		75.		210.		66.		61.	0.

INPUT DATA CORRECTED FOR ZERO READINGS AND SIGNS

11	626.	-1.00		10.00		0.00		-27.00		36.00		1.00		-14.00	0.
11	625.	-2.70		21.70		1.00		-26.83		49.70		-2.70		-13.00	0.
11	624.	-3.00		30.00		3.00		-26.67		60.00		-5.00		-13.00	0.
11	624.	-4.00		42.00		5.00		-25.50		75.00		-8.70		-12.00	0.
11	627.	-5.00		53.00		6.00		-25.33		85.00		-10.00		-12.00	0.
11	626.	-6.00		62.00		6.00		-25.17		100.00		-13.00		-12.00	0.
11	627.	-7.00		69.70		8.70		-24.00		110.77		-16.70		-11.70	0.

COOLAPPED RUDDER DATA REDUCTIONS

SUR WITH FAIRWATER, UPPER & LOWER RUDDERS 10 FT/SEC

ALPHA	FX-LB	FZ-LB	MX-IMLR	MZ-IMLB	FHO-LB	FVO-LB	FZO-LB	MID-IMLR	MY-IMLR	MZO-IMLR	MYFLAP-IMLR	VFL-FPS
-1.00	5.61	-0.99	-4.35	16.39	5.46	-1.43	-0.47	-5.31	0.0	16.11	3.7	10.30
-2.50	5.37	-2.13	-3.75	20.31	5.52	-1.38	-1.72	-5.30	0.0	19.97	0.0	10.29
-3.01	5.34	-3.13	-5.34	20.74	5.61	-1.11	-2.61	-7.27	-7.00	20.15	0.0	10.29
-4.71	5.11	-4.42	-6.37	20.66	5.57	-1.36	-3.82	-6.65	-4.77	20.06	0.0	10.30
-5.02	5.07	-5.56	0.41	20.08	5.75	-1.38	-4.06	-2.19	-5.00	19.94	0.0	10.31
-6.02	5.04	-6.45	-4.48	19.45	5.91	-1.42	-5.45	-7.27	-5.00	19.59	1.7	10.30
-7.02	4.81	-7.25	-7.77	21.12	5.93	-1.16	-6.37	-11.12	-7.00	19.57	0.0	10.31

REFLAPPEL BURDEP DATA IN NON-DIMENSIONAL FORMS

SUB WITH FAIRWATER, UPPER & LOWER BUNDERS 10 FT/SEC

ALPHA	CL	CD	CM	CPL	CY	L/D	CMF	CLSQ	EM1700-0
-1.00	-0.015	0.1734	0.0	2.265	-0.032	-0.123	0.0	0.0002	2.304
-2.00	-0.039	0.1251	0.0	0.882	-0.031	-0.311	0.0	0.0015	2.302
-3.11	-0.259	0.1273	-0.002	2.795	-0.025	-0.465	0.0	0.0035	2.300
-4.01	-0.084	0.1259	-0.004	0.497	-0.031	-0.636	0.0	0.0075	2.304
-5.07	-0.110	0.1298	-0.005	0.128	-0.031	-0.846	0.0	0.0120	2.306
-6.07	-0.124	0.1341	-0.005	0.162	-0.032	-0.953	0.0	0.0163	2.304
-7.07	-0.144	0.1338	-0.006	0.449	-0.026	-1.074	0.0	0.0207	2.306

AP7VF DATA CORRECTED FOR TUNNEL INTERFERENCE

ALPHA	CL	CD	CM	CPL	CY	L/D	CMF	CLSQ	EM1000-0
-1.02	-7.315	0.1234	0.0	2.265	-0.032	-0.123	0.0	0.7002	2.374
-2.05	-0.039	0.1751	0.0	0.882	-0.031	-0.311	0.0	0.0015	2.302
-3.08	-0.059	0.1774	-0.002	0.795	-0.025	-0.465	0.0	0.0035	2.303
-4.12	-0.086	0.1261	-0.004	0.497	-0.031	-0.636	0.0	0.0075	2.304
-5.15	-0.110	0.1300	-0.005	0.128	-0.031	-0.846	0.0	0.0120	2.306
-6.17	-0.124	0.1344	-0.005	0.162	-0.032	-0.953	0.0	0.0163	2.304
-7.20	-0.144	0.1347	-0.006	0.449	-0.026	-1.071	0.0	0.0207	2.306

-155-

APPENDIX C  
NUMERICAL PROGRAM TO GENERATE OFFSETS  
FOR  
CONSTRUCTION OF FOIL SHAPES

C MILLING GEOMETRY FOR DEVELOPING LIFTING SURFACES FOR EXP. MODELS

C GEOMETRY POINT, DRILL DIAMETER, SPACING IN X, SPACING IN Y,

C DIMENSION XCIN(27), YCIN(27)

READ(5,100) A,R,C,D,F,G,H

WRITE(6,100) A,R,C,D,F,G,H

READ(5,101) (XCIN(I),I=1,27)

WRITE(6,101) (XCIN(I),I=1,27)

READ(5,101) (YCIN(I),I=1,27)

WRITE(6,101) (YCIN(I),I=1,27)

K=1

100 FORMAT(2F10.5)

101 FORMAT(2E10.5)

C LEADING ZEROS

XCEN=EF/2.0

YCEN=0.0-F/2.0

XCUTE=XCEN+EF/2.0

YCUTE=YCEN-F/2.0

C OFFSET AT XCUT & YCUT

SPEA=XCUT

CHED=C\*XCUT

TKED=FYCUT

YTR=XCUT-C

YTRID=EXTD/2.0

IF(XTRIDND .GT. 0.0 .OR. YTRIDND .GT. 1.0) GO TO 4

C DEVELOPING SURFACES (XTRIDND, XCIN, YCIN, Z)

NEZCF=0.0

NEZ=0.0

WRITE(6,102) YCF, YCFM, YCUT, YCUT, OF

FORMAT(5E10.3)

XCEN=XCEN+C

IF(YCF .GT. 4.5) GO TO 3

GO TO 1

CONTINUE

XCEN=0.0-F/2.0

DO BACK HALF

C

102

4

3



```
2 IF (K .EQ. 2) STOP
   K=2
   YCEN=F/2.0
   YCFM=0.0+F/2.0
   WRITE(6,103)
103 FORMAT(//.0 BACK HALF.)
   GO TO 1
   END
C ** FILL IN ** PARABOLIC INTERPOLATION
C STOPS Y(X) FROM TABLE OF
C AB(N) AND CD(N) CONTAINING NO POINTS.
C FUNCTION FILLI(X,CH,0,NO)
C DIMENSION AR(2),CD(2)
C ANTPA(X1,X2,X3,X,Y1,Y2,Y3)=Y1*(X-X2)*(X-X3)/((X1-X2)*(X1-X3))+
1 Y2*(X-X1)*(X-X3)/((X2-X1)*(X2-X3))+Y3*(X-X1)*(X-X2)/((X3-X1)*
2 (X2-X2))
3 IF (X-AR(1)) 1,3,2
   Y=CD(1)
   GO TO 00
1 Y=ANTPA(AR(1),AR(2),AR(3),X,CD(1),CD(2),CD(3))
   GO TO 00
2 IF (X-AR(2)) 1,6,5
   Y=CD(2)
   GO TO 00
3 DO 7 I=3,NO
   *M1
4 IF (X-AR(I)) 8,9,7
   Y=CD(I)
   GO TO 00
7 CONTINUE
8 Y=ANTPA(AR(N-2),AR(N-1),AR(N),X,CD(N-2),CD(N-1),CD(N))
9 FILLI=Y
   RETURN
   END
```

C	SAMPLE DATA	DECH FOR	NACA	GA (MOD)	A = R	CAMPER		
.0000	4.45	.0000	1.0000	.0000	.0000	.2500	.1	.2907
0.0	.005	.0075	.0125	.025	.025	.05	.075	.4962
.15	.2	.25	.3	.35	.35	.4	.45	
.55	.6	.65	.7	.75	.75	.4	.85	
.95	.975	1.0						
0.0	.0465	.0412	.1044	.1466	.1466	.2066	.2525	.2907
.3521	.4000	.4363	.4537	.4832	.4832	.4952	.5	.4962
.4846	.4653	.4343	.4135	.3612	.3612	.3110	.2532	.1877
.1143	.0744	.0333						

APPENDIX D  
NUMERICAL MODEL OF A SUBMERSIBLE  
BODY OF REVOLUTION  
WITH  
LIFTING SURFACE APPENDAGES

```

C NUMERICAL MODEL OF A SUBMERSIBLE BODY OF REVOLUTION WITH LIFTING
C SURFACE APPENDAGES, TO DETERMINE THE HYDRODYNAMIC FORCES AND
C MOMENTS AND THEIR INTERACTIONS.
COMMON ALPHA,ALR,AUX(12),AK(5),AUX2(6),L,CHOR(20),CSA,CMSSI(7),CHO
IKKI(30),CMSKI(7)
COMMON DELX,DELTA(4),DBT1,DELCL,DBCPC,CCX,DBTKI
COMMON GS(30,8),G1,G2,GWKS(31),GTR(31),GTF(51),GBVSI(31,20,3,2),G
IK(30,8),GBVKI(30,20,3,2)
COMMON I,IPIV(6),IPI(3),IHOL,J,JM,L(6),IEK,EPS,ISPI(35)
COMMON NSTA,NIS,MHSC,NCPS,NCPC,NBS,NHS,NHLFT,NMIN,PI,PIINV,UPIINV,
14
COMMON KHU,KIN(21),KSL(2),KKUD(2),KHS,MW1,RHR,KHS2,KHR2,KWIR,RF,R
IT,KHSSI(32),RILHS(32,7),RFK,KTK,KIRHS(32)
COMMON SINV(21),SPNS,SPNR,SLEF,STEF,SCC,SA,SY,SZ,S32,SIA,SILHS(32,
17),SPRH(21),SLEK,SLTEK
COMMON IMETA,TVSSI(31,20,3,2),IEN(32,4),TVSK1(31,20,3,2)
COMMON UO,VZB(8,4,3,2),VZT(8,4,3,2),VZK(8,4,3,2),VZBR1(8,4,3,2),VZ
1TKI(8,4,3,2),VZWK1(8,4,3,2),VZ
COMMON WFS,WBSSI(8,4),WBSIRI(31),WDSKI(8,4),WTSK1(31,21),
16
16IK(31,21),W(21)
COMMON XIN(21),XLET(2),XLEP(2),XLET(2),XILB(2),XLEIR(2),XLEDR(2),X
17ILIN(2),XLESK(2),XBVSI(20),XLE,XTE,XCPSI(8,4),XB,XBVKI(20),XCPRI(8
2,4)
COMMON YTKSI(31),YBSSI(30),YCPSI(8),Y,YWKS1(31,21),YDUMK(31),YTKKI(
131),YBRI(30),YCPRI(6),ZBKS1
REAL LENGTH
FORMAT(14,5X,3F10.4)
FORMAT(1,10,5)
FORMAT(5F10.5)
FORMAT(6F10.3)
FORMAT(2F10.4)
FORMAT(4F5)
C INPUT HULL AND FLWG PROPERTIES
NSM=2
KLEAD(5,100)NSTA,UO,WFS,RHO
KLEAD(5,101)(XIN(J),J=1,NSTA)

```

```

PGM30001
PGM30002
PGM30003
PGM30004
PGM30005
PGM30006
PGM30007
PGM30008
PGM30009
PGM30010
PGM30011
PGM30012
PGM30013
PGM30014
PGM30015
PGM30016
PGM30017
PGM30018
PGM30019
PGM30020
PGM30021
PGM30022
PGM30023
PGM30024
PGM30025
PGM30026
PGM30027
PGM30028
PGM30029
PGM30030
PGM30031
PGM30032
PGM30033
PGM30034
PGM30035
PGM30036

```

```

1      READ (5,101)(RIN(J),J=1,NSTA)
      DELX=XIN(1)-XIN(2)
      PI=3.14159
      PIINV=1.0/PI
      GPIINV=0.25*PIINV
      DO 1 J=1,NSTA
      SINV(J)=PI*KIN(J)**2
      INPUT FIN PROPERTIES
      DO 2 J=1,2
      READ (5,102) RSL(J),XLET(J),XLEB(J),XTET(J),XTEB(J)
      INPUT KUDDER PROPERTIES
      DO 3 J=1,2
      READ (5,103) RNOD(J),XLETP(J),XLEBR(J),XTETR(J),XTEBR(J),DELTA(J)
      INPUT MAKE SCHEDULING ANGLES
      READ (5,104) ALPHA,ALR
      IF (ALPHA.LT.0.9999) ALPHA=MFS/UO
      IF (ALR.LT.0.9999) ALR=MFS/UO
      INPUT GRID SIZES
      READ (5,105) NTS,NBSC,NCPS,NCPC
      CALCULATE SPAN OF FIN
      DUMX=C.5*(XLEU(1)+XTEB(1))
      KMS=FILLI (DUMX,XIN,RIN,NSTA)
      KMS2=:HMS*KMS
      KMS=KMS2/KSL(1)
      SPNS=KSL(1)-KMS
      CALCULATE KUDDER SPAN
      DUMX=C.5*(XLEBR(1)+XTEBR(1))
      KMR=FILLI (DUMX,XIN,KIN,NSTA)
      KMR2=KMR*KMR
      KMR=KMR2/RRUD(1)
      SPNR=KRU(1)-KMR
      TRAILING VORTEX RADII ON FIN 1
      UBTL=SPNS/FLUAT(NTS-1)
      YTKS1(1)=KMS
      DO 4 N=2,NTS
      YTKS1(N)=YTKS1(N-1)+DBTL

```

PGM3J037  
 PGM3J038  
 PGM3J039  
 PGM3J040  
 PGM3J041  
 PGM3J042  
 PGM3J043  
 PGM3J044  
 PGM3J045  
 PGM3J046  
 PGM3J047  
 PGM3J048  
 PGM3J049  
 PGM3J050  
 PGM3J051  
 PGM3J052  
 PGM3J053  
 PGM3J054  
 PGM3J055  
 PGM3J056  
 PGM3J057  
 PGM3J058  
 PGM3J059  
 PGM3J060  
 PGM3J061  
 PGM3J062  
 PGM3J063  
 PGM3J064  
 PGM3J065  
 PGM3J066  
 PGM3J067  
 PGM3J068  
 PGM3J069  
 PGM3J070  
 PGM3J071  
 PGM3J072

PGM3J073  
 PGM3J074  
 PGM3J075  
 PGM3J076  
 PGM3J077  
 PGM3J078  
 PGM3J079  
 PGM3J080  
 PGM3J081  
 PGM3J082  
 PGM3J083  
 PGM3J084  
 PGM3J085  
 PGM3J086  
 PGM3J087  
 PGM3J088  
 PGM3J089  
 PGM3J090  
 PGM3J091  
 PGM3J092  
 PGM3J093  
 PGM3J094  
 PGM3J095  
 PGM3J096  
 PGM3J097  
 PGM3J098  
 PGM3J099  
 PGM3J100  
 PGM3J101  
 PGM3J102  
 PGM3J103  
 PGM3J104  
 PGM3J105  
 PGM3J106  
 PGM3J107  
 PGM3J108

```

WRITE(6,120)(YTRSI(N),N=1,NTS)
FUKMAT( TRAILER RADII ON SAIL',/(,16F7.3))
CALCULATE MIDPOINT RADII ON SAIL 1
YBSI(1)=YTRSI(1)+DBTI*0.5
NDJ=NTS-1
DO 2 N=2,NBS
  YBSI(N)=YBSI(N-1)+DBTI
CALCULATE X VALUE OF BOUND VORTEX LINES ON SAIL 1
XVSI(1)=XLEB(1)
NHS=NBS-1
ULLCI=(XLEB(1)-XTIB(1))/FLOAT(NHS)
DO 3 M=2,NBSC
  XVSI(M)=XVSI(M-1)-ULLCI
WRITE(6,121)(XVSI(M),M=1,NBSC)
FUKMAT(' X LOCATION OF BOUND VORTEX LINES ON SAIL',/(,16F7.2))
LOCATE SAIL 1 CONTROL POINTS SPANWISE
DBCP=(RSL(1)-RHS)/FLOAT(NCPS+1)
YCPSI(1)=RHS+DBCP
DO 7 N=1,NBS
  N=1
  IF(YCPSI(1).GT.YBSI(N).AND.YCPSI(1).LE.YBSI(N+1)) GO TO 8
  CONTINUE
  YCPSI(1)=YBSI(N)
  NMLFT=NBS-N
  IHUL=FLOAT(NMLFT)/FLOAT(NCPS)
  DO 9 N=2,NCPS
    YCPSI(N)=YCPSI(N-1)+IHUL*DBTI
  CONTROL POINT SPACING CHORDWISE
  KF=FILLI (XLEB(1),XIN,KIN,NSTA)
  KT=FILLI (XTIB(1),XIN,KIN,NSTA)
  SLEF=(XLLB(1)-XLET(1))/(RSL(1)-RF)
  ST'F=(XLEB(1)-XTET(1))/(RSL(1)-RT)
  DO 10 N=1,NCPS
    Y=YCPSI(N)
    XLL=XLEB(1)-SLEF*(Y-RF)
    XTL=XTIB(1)-STEF*(Y-RT)

```

120  
 C  
 5  
 C  
 6  
 121  
 C  
 7  
 8  
 9  
 C

```

C=XLE-XTE
DCX=C/FLUAT(NCPC+1)
XCPS1(N,1)=XTE+DCX
DU 11 M=1,NHS
M=M
IF(XCPS1(N,1).LT.XBVS1(M).AND.XCPS1(N,1).GE.XBVS1(M+1))GO TO 12
CONTINUE
11 XCPS1(N,1)=XBVS1(M)-0.5*DELCL
DU 13 M=2,NCPC
XCPS1(N,M)=XCPS1(N,M-1)+CCX
DU 15 J=1,NHS
JM=JM
IF(XCPS1(N,M).LT.XBVS1(JM).AND.XCPS1(N,M).GE.XBVS1(JM+1))XCPS1(N,M
1)=XBVS1(JM)-0.5*DELCL
CONTINUE
12 CONTINUE
DU 125 N=1,NCPS
WRITE(6,122)(YCPS1(N),(XCPS1(N,M),M=1,NCPC))
122 FORMAT(' YCP=',F10.3,' XCP=',4F7.3)
C SUMU VURTEX STRENGTHS FOR SAIL 1 UNIT MUJES
DU 14 N=1,NBS
XLE=XLE+(1-SLEF*(YBS1(N)-RF)
IF(XLE.GT.XLEB(1)) XLE=XLEB(1)
XFL=XTEB(1)-SLEF*(YBS1(N)-RT)
IF(XTE.LT.XTEB(1)) XTE=XTEB(1)
CHJR(N)=XLE-XTE
W=(YBS1(N)-RHS)/(RSL(1)-RHS)
SWW=(1.0-W**4)**0.5
DU 15 NSP=1,NSM
S(N,NSP)=SWW**2*(2*NSP-2)
GSUM1=0.0
GSUM2=0.0
G1=J.0
G2=0.0
DU 14 M=1,NBSC
AD=XLE+.5*DELCL

```

```

IF(XBVS1(M) .GT. XD) GO TO 16
XI=XTE-.5*DELCL
IF( XBVS1(M).LT. XT ) GO TO 16
XI=XTE+.5*DELCL
IF( XBVS1(M) .LT. XI) GO TO 951
GO TO 952
951 THETA=PI
GO TO 955
952 CONTINUE
GO TO 17
16 G1=J.C
G2=J.C
GO TO 16
17 LUSX= (1.-2.*(XLE-XBVS1(M)+DELCL*.5)/CHUK(N))
THETA=AKCOS(CUSX)
FORMAT(0, CCX=0, F20.8, THETA=0, F20.5)
J1=(THETA+SIN(THETA))*PIINV -GSUM1
G2=2.*PIINV*(THETA*.5-SIN(2.*THETA)*.25)-GSUM2
GSUM1=GSUM1+G1
GSUM2=GSUM2+G2
DO 14 NSP=1,NSM
GBVS1(N,M,NSP,1)=G1*GS(N,NSP)
GBVS1(N,M,NSP,2)=G2*GS(N,NSP)
DO 124 NSP=1,NSM
WRITE(6,125) NSP, (GS(N,NSP),N=1,N6S)
FORMAT(0, MDEL, I2, (16F7.3))
NUNJ=IFIX(FLOAT(NTS)/2.)
WRITE(6,120) NOUT, (GBVS1(NCUT,M,1,1),M=1,N6SC)
FORMAT(0, N=0, I2, CIRC MODE 1, I, (12F7.5))
CALCULATE TRAILER STRENGTH UN SAIL 1
NMIN=NTS-1
DO 19 NSP=1,NSM
DO 19 MCR=1,2
IVSS1(1,1,NSP,MCR)=GBVS1(1,1,NSP,MCR)
DO 20 M=2,N6SC
IVJS1(1,M,NSP,MCK)=GBVS1(1,M,NSP,MCF)+TVSS1(1,M-1,NSP,MCR)

```

PGMJ143  
PGMJ140  
PGMJ147  
PGMJ148  
PGMJ149  
PGMJ150  
PGMJ151  
PGMJ152  
PGMJ153  
PGMJ154  
PGMJ155  
PGMJ150  
PGMJ157  
PGMJ158  
PGMJ159  
PGMJ160  
PGMJ161  
PGMJ162  
PGMJ163  
PGMJ164  
PGMJ165  
PGMJ166  
PGMJ167  
PGMJ168  
PGMJ169  
PGMJ170  
PGMJ171  
PGMJ172  
PGMJ173  
PGMJ174  
PGMJ175  
PGMJ176  
PGMJ177  
PGMJ178  
PGMJ179  
PGMJ180



```

20 CONTINUE
   DO 21 N=2,NMIN
   TVSSI(N,1,NSP,MCR)=GBVSI(N,1,NSP,MCR)-GBVSI(N-1,1,NSP,MCR)
   DO 21 M=2,NBSC
   TVSSI(N,M,NSP,MCR)=TVSSI(N,M-1,NSP,MCR)+GBVSI(N,M,NSP,MCR)-GBVSI(N
1-1,M,NSP,MCR)
21 CONTINUE
   TVSSI(NTS,1,NSP,MCR)=-GBVSI(NBS,1,NSP,MCR)
   DO 19 N=2,NBSC
   TVSSI(NTS,M,NSP,MCR)=TVSSI(NTS,M-1,NSP,MCR)-GBVSI(NBS,M,NSP,MCR)
   WRITE(6,128) TVSSI(1,1,1),TVSSI(1,NBSC,1,1),TVSSI(NTS,1,1,1),I
1VSSI(NTS,NBSC,1,1)
128 FORMAT('  TRAILERS FOR UNIT MODE(1,1) AT BASE(LE,TE) AND TIP(LE,TE)
1,4F10.4)
C VELOCITY ON SI DUE TO SI BCUNE VCKTEX SYSTEM
   DO 22 MCP=1,NCPS
   DO 22 MCP=1,NCPC
   DO 22 NSP=1,NSM
   DO 22 MCK=1,2
   VZB(NCP,MCP,NSP,MCR)=0.0
   VZT(NCP,MCP,NSP,MCR)=0.0
   VZM(NCP,MCP,NSP,MCR)=0.0
   VZUKI(NCP,MCP,NSP,MCR)=0.0
   VZTKI(NCP,MCP,NSP,MCR)=0.0
   VZWKI(NCP,MCP,NSP,MCR)=0.0
   DO 23 NCP=1,NCPS
   DO 23 MCP=1,NCPC
   DO 23 N=1,NBS
   DO 23 M=1,NBSC
   SX=XBVS1(M)-XCPS1(NCP,MCP)
   SY=YBVS1(N)-YCPS1(NCP)
   S2=SUKI(SX*SY+SY*SY)**3
   VZ=QPITGV/S32*(DBTI*SX)
   DO 23 NSP=1,NSM
   DO 23 MCK=1,2
   VZB(NCP,MCP,NSP,MCR)=VZB(NCP,MCP,NSP,MCR)+VZ*GBVSI(N,M,NSP,MCR)

```

```

PGM3J181
PGM3J182
PGM3J183
PGM3J184
PGM3J185
PGM3J186
PGM3J187
PGM3J188
PGM3J189
PGM3J190
PGM3J191
PGM3J192
PGM3J193
PGM3J194
PGM3J195
PGM3J196
PGM3J197
PGM3J198 165
PGM3J199 165
PGM3J200
PGM3J201
PGM3J202
PGM3J203
PGM3J204
PGM3J205
PGM3J206
PGM3J207
PGM3J208
PGM3J209
PGM3J210
PGM3J211
PGM3J212
PGM3J213
PGM3J214
PGM3J215
PGM3J216

```

```

129 1000 VERTICES.)
      NMID=FIX(FLOAT(NCPS)/2.)
      WKITE(6,129)XCPSI(NMID,NCPC),YCPSI(NMID),VZB(NMID,NCPC,1,1)
      FURMAT(' VEL AT CP X=',F7.3,' Y=',F7.3,F20.4,' DUE TO MODE 1,1 BU
C      VELUCITY UN SAIL 1 DUE TO SAIL 1 TRAILERS
      UU 24 MCK=1,NCPS
      UU 24 MCK=1,NCPC
      UU 24 N=1,NTS
      SY=YTRSI(N)-YCPSI(NCP)
      UU 24 M=1,NHS
      SA=0.5*(XBVSI(M)+XBVSI(M+1))-XCPSI(NCP,MCP)
      SS2=SQRT(SX*SX+SY*SY)**3
      VZ=QPIIKV/S32*SY*(XBVSI(M+1)-XBVSI(M))
      UU 24 NSP=1,NSM
      UU 24 MCK=1,2
      VZ1(NCP,MCP,NSP,MCR)=VZ1(NCP,MCP,NSP,MCR)+VZ*TVSSI(N,M,NSP,MCR)
C      VLLUCITY UN SAIL 1 DUE TO SAIL 1 WAKE
      SIA=SIN(ALPHA)
      CSA=CCS(ALPHA)
      X0=AD VSI(NUSC)
      UU 25 MCK=1,NCPS
      UU 25 MCK=1,NCPC
      UU 25 N=1,NTS
      KS=1(XCPSI(NCP,MCP)-XB)*SIA)**2+(YTRSI(N)-YCPSI(NCP))**2
      K=SQRT(KS)
      QS=(XCPSI(NCP,MCP)-XB)**2+(YTRSI(N)-YCPSI(NCP))**2
      W=SQRT(QS)
      QV=QPIINV/R*((XB-XCPSI(NCP,MCP))/Q*CSA+1.0)
      IF(YTRSI(N).GT.YCPSI(NCP)) QV=-QV
      VZ=QV*CSA
      UU 25 NSP=1,NSM
      UU 25 MCK=1,2
      VZ0(NCP,MCP,NSP,MCR)=VZ0(NCP,MCP,NSP,MCR)+VZ*TVSSI(N,NBSC,NSP,MCR)
      WKITE(6,130)VZT(NMID,NCPC,1,1),VZW(NMID,NCPC,1,1)
      FURMAT(' VEL AT SAME POINT DUE TO TRAILERS ON BLADE=',F15.4,' AND
130 WAKE=',F15.4,' DUE TO UNIT MODE 1,1')

```

```

PGMJ0217
PGMJ0218
PGMJ0219
PGMJ0220
PGMJ0221
PGMJ0222
PGMJ0223
PGMJ0224
PGMJ0225
PGMJ0226
PGMJ0227
PGMJ0228
PGMJ0229
PGMJ0230
PGMJ0231
PGMJ0232
PGMJ0233
PGMJ0234
PGMJ0235
PGMJ0236
PGMJ0237
PGMJ0238
PGMJ0239
PGMJ0240
PGMJ0241
PGMJ0242
PGMJ0243
PGMJ0244
PGMJ0245
PGMJ0246
PGMJ0247
PGMJ0248
PGMJ0249
PGMJ0250
PGMJ0251
PGMJ0252

```

```

C      VELOCITY UN SAIL 1 DUE TO HULL
      UU 26 NCP=1,NCPS
      UU 26 MCP=1,NCPC
      K=FILLI(XCPSI(NCP,MCP),XIN,RIN,NSTA)
      WDSI(NCP,MCP)=WFS*K*R/(YCPSI(NCP)**2)
      WRITE(6,131)WDSI(NMID,NCPC)
      FUKMAT(0) VELOCITY AT SAME POINT DUE TO HULL=0,F15.5)
      GET KFS FOR EACH CP
      I=1
      UU 27 NCP=1,NCPS
      UU 27 MCP=1,NCPC
      RHSSI(I)=-WFS-WDSI(NCP,MCP)
      WRITE(6,JUL) I,RHSSI(I)
      FUKMAT(14,F40.10)
      I=I+1
      IMAX=NCPS*NCPC
      GET LEFT HAND SIDE FUK EACH CP
      I=1
      UU 28 NCP=1,NCPS
      UU 28 MCP=1,NCPC
      J=1
      UU 89 MCR=1,2
      UU 99 NSP=1,NSM
      SILHS(I,J)=VZM(NCP,MCP,NSP,MCR)+VZT(NCF,MCP,NSP,MCR)+VZB(NCP,MCP,N
      ISF,MCR)
      WRITE(6,802) I,J,SILHS(I,J)
      FUKMAT(214,F40.10)
      J=J+1
      I=I+1
      UU 90U K=1,IMAX
      SILHS(K,5)=RHSSI(K)
      EPS=.0001
      CALL GLSQ(SILHS,CMSSI,ISP,IMAX,4,BUG,EPS,EPS)
      C
      WRITE(6,132) (CMSSI(J),J=1,4)
      FUKMAT(0) MODE STRENGTHS ON SAIL=0,6F10.5)
      132

```

PGM3J253  
 PGM3J254  
 PGM3J255  
 PGM3J256  
 PGM3J257  
 PGM3J258  
 PGM3J259  
 PGM3J260  
 PGM3J261  
 PGM3J262  
 PGM3J263  
 PGM3J264  
 PGM3J265  
 PGM3J266  
 PGM3J267  
 PGM3J268  
 PGM3J269  
 PGM3J270  
 PGM3J271  
 PGM3J272  
 PGM3J273  
 PGM3J274  
 PGM3J275  
 PGM3J276  
 PGM3J277  
 PGM3J278  
 PGM3J279  
 PGM3J280  
 PGM3J281  
 PGM3J282  
 PGM3J283  
 PGM3J284  
 PGM3J285  
 PGM3J286  
 PGM3J287  
 PGM3J288

```

C      VELOCITY AT RI DUE TO S1 WAKE
      UU 29 MS=1,NSTA
      MS=MS
      IF(XIN(MS).LT.XTEB(1)) GC TO 30
      CONTINUE
      NSTS=MS
      UU 31 MS=NSTS,NSTA
      MS=MS
      IF(XIN(MS).LT.XLEBR(1)) GO TO 32
      CONTINUE
      NSTE=MS
      UU 33 N=1,NTS
      YWKS1(N,NSTS)=YTRS1(N)
      NSTE=NSTE-1
      UU 34 MS=NSTS,NSTEM
      CONST=-.5*PIINV*(SINV(MS)-SINV(MS+1))
      UU 34 N=1,NTS
      YWKS1(N,MS+1)=YWKS1(N,MS)+CONST/YWKS1(N,MS)
      IF(YWKS1(N,MS+1).LT.RIN(MS+1)) YWKS1(N,MS+1)=RIN(MS+1)*YTKS1(N)/RHS
      CONTINUE
      WRITE(6,133)(YWKS1(NOUT,MS),MS=NSTS,NSTEM)
      FORMAT(' TYPICAL TRAILER CONTRACTION TRAJECTORY ',12F7.3)
      ZWKS1=ALPHA*(XTEB(1)-XLEER(1))
      UU 35 N=1,NTS
      YWKS1(N)=U.0
      J=1
      UU 35 MCK=1,2
      UU 35 NSP=1,NSM
      YWKS1(N)=YWKS1(N)+CMSSI(J)*IVSSI(N,NBSC,NSP,MCR)
      J=J+1
      WRITE(6,134)(GWKS1(N),N=1,NTS)
      FORMAT(' KEAL WAKE TRAILER STRENGTHS FROM SAIL 1',/,1X,16F7.3)
      UU 36 N=1,NBS
      YUWKS(N)=.5*(YWKS1(N,NSTE)+YWKS1(N+1,NSTE))
      YWSIK1(N)=U.0
      UU 36 NV=1,NTS

```

PGM30289  
 PGM30290  
 PGM30291  
 PGM30292  
 PGM30293  
 PGM30294  
 PGM30295  
 PGM30296  
 PGM30297  
 PGM30298  
 PGM30299  
 PGM30300  
 PGM30301  
 PGM30302  
 PGM30303  
 PGM30304  
 PGM30305  
 PGM30306  
 PGM30307  
 PGM30308  
 PGM30309  
 PGM30310  
 PGM30311  
 PGM30312  
 PGM30313  
 PGM30314  
 PGM30315  
 PGM30316  
 PGM30317  
 PGM30318  
 PGM30319  
 PGM30320  
 PGM30321  
 PGM30322  
 PGM30323  
 PGM30324

PGM30325  
 PGM30326  
 PGM30327  
 PGM30328  
 PGM30329  
 PGM30330  
 PGM30331  
 PGM30332  
 PGM30333  
 PGM30334  
 PGM30335  
 PGM30336  
 PGM30337  
 PGM30338  
 PGM30339  
 PGM30340  
 PGM30341  
 PGM30342  
 PGM30343  
 PGM30344  
 PGM30345  
 PGM30346  
 PGM30347  
 PGM30348  
 PGM30349  
 PGM30350  
 PGM30351  
 PGM30352  
 PGM30353  
 PGM30354  
 PGM30355  
 PGM30356  
 PGM30357  
 PGM30358  
 PGM30359  
 PGM30360

```

K=SJRT(ZWKSI**2+(YDUHR(N)-YKSI(NV,ASTE))**2)
V=L*G*WKSI(NV)*.5*PI*INV/R
MWSIKI(N)=MWSIKI(N)+VEL*(YDUHR(N)-YKSI(NV,ASTE))/R
WRITE(6,135)(MWSIKI(N),N=1,NBS)
FUKMAT(' KAW VELOCITY ON RUDDER DUE TO SAIL',/(IX,16F7.3))
FIT WITH POLYNOMIAL
KMIN=FULLI(XLEBK(1),XIN,KIN,NSTA)
DU 028 N=1,NBS
NU=N
IF(YULMK(N).GT.KMIN) GC TO 629
CONTINUE
NKN=NBS-NU+1
DU 37 N=1,NKN
TEN(N,1)=1.0
TEN(N,2)=YDUHR(N+NO-1)
TEN(N,4)=MWSIKI(N+NU-1)
TEN(N,5)=TEN(N,2)**2
L2=1
EPS=.0001
CALL GL5J(TEN,AK,ISP,NKN,3,BUG,.0001,.0001)
WRITE(6,136)(AK(J),J=1,3)
130 FUKMAT(' POLYNOMIAL COEFFICIENTS FOR RUDDER VEL DUE TO SAIL',3F10.
13)
C GRID SETUP ON R1
DBTRI=SPWR/FLOAT(NBS)
YIKI(1)=KWIR
DU 38 N=2,NTS
YIKI(N)=YIKI(N-1)+DBTRI
WRITE(6,140)(YIKI(N),N=1,NTS)
FUKMAT(' TRAILER RADII CN KL',/(16F7.3))
YUKI(1)=YIKI(1)+0.5*DBTRI
DU 39 N=2,NBS
YUKI(N)=YUKI(N-1)+DBTRI
XBVKI(1)=XLEBK(1)
DELCKI=(XLEBK(1)-XTEBK(1))/FLOAT(NHS)
DU 40 M=2,NU5C
  
```

30  
 135  
 C  
 629  
 629  
 37  
 130  
 C  
 38  
 140  
 39

```

40 XBVR1(M)=XBVR1(M-1)-DELCR1
WRITE(0,141)(XBVR1(M),M=1,NBSC)
141 FORMAT(' X LUCATION CF BCUND VORTEX LINES UN R1',/, (16F7.2))
DUCPSH=(KRUD(1)-KHR)/FLOAT(NCPS+1)
YCPRI(1)=KHR+DUCPSK
DU 41 N=1,NBS
N=N
IF(YCPRI(1).GT.YBRI(N).AND.YCPRI(1).LE.YBRI(N+1)) GO TO 42
CONTINUE
YCPRI(1)=YBRI(N)
NHLFT=NDS-N
IHUL=FLOAT(NHLFT)/FLOAT(NCPS)
DU 43 N=2,NCPS
YCPRI(N)=YCPRI(N-1)+IHUL*DBTRI
KFR=FILLI(XLEBK(1),XIN,KIN,NSTA)
KTR=FILLI(XTEBK(1),XIN,KIN,NSTA)
SLEN=(XLEBK(1)-XLETR(1))/(KRUD(1)-KFR)
SLTER=(XTEBK(1)-XTETR(1))/(KRUD(1)-KTR)
DU 44 N=1,NCPS
Y=YCPRI(N)
XLLK=XLEBK(1)-SLTER*(Y-KFR)
XTEK=XTEBK(1)-SLTER*(Y-KTR)
CK=XLLK-XTEK
DUAR=CK/FLOAT(NCPC+1)
ACPRI(N,1)=XTEK+UCXR
DU 45 MC=1,NHS
MC=MC
IF(XCPRI(N,1).LT.XBVR1(MC).AND.XCPRI(N,1).GE.XBVR1(MC+1))GO TO 46
CONTINUE
46 ACPRI(N,1)=(XBVR1(MC)+XBVR1(MC+1))*0.5
DU 44 M=2,NCPC
XCPRI(N,M)=XCPRI(N,M-1)+CCXR
DU 47 MC=1,NHS
MC=MC
IF(XCPRI(N,M).LT.XBVR1(MC).AND.XCPRI(N,M).GE.XBVR1(MC+1))GO TO 44
CONTINUE
47

```

PGM30361  
 PGM30362  
 PGM30363  
 PGM30364  
 PGM30365  
 PGM30366  
 PGM30367  
 PGM30368  
 PGM30369  
 PGM30370  
 PGM30371  
 PGM30372  
 PGM30373  
 PGM30374  
 PGM30375  
 PGM30376  
 PGM30377  
 PGM30378  
 PGM30379  
 PGM30380  
 PGM30381  
 PGM30382  
 PGM30383  
 PGM30384  
 PGM30385  
 PGM30386  
 PGM30387  
 PGM30388  
 PGM30389  
 PGM30390  
 PGM30391  
 PGM30392  
 PGM30393  
 PGM30394  
 PGM30395  
 PGM30396

```

44  XCPK1(N,M)=0.5*(XBVR1(MC)+XBVR1(MC+1))
    UJ 143 N=1,NCPS
143  WRITE(6,142)(YCPK1(N),(XCPRI(N,M),M=1,NCPC))
142  FORMAT(1, YCP=1, F10.3,1 XCP=1,4F7.2)
C    BUJND VUKTEX STRENGTHS CN KI FUK UNIT MODES
    DU 48 N=1,NBS
    XLER=XLEBR(1)-SLLEK*(YBR1(N)-RFK)
    IF(XLER.GT.XLEBR(1)) XLER=XLEBR(1)
    XTER=XTEBR(1)-SLTER*(YBR1(N)-RTR)
    IF(XTER.LT.XTEBR(1)) XTER=XTEBR(1)
    CHUNK1(N)=XLER-XTER
    W=(YBR1(N)-RHR)/(RKUD(1)-RHR)
    SUQ=SQRT(1.0-Q*Q)
    DU 49 NSP=1,NSM
49  GK(N,NSP)=SUQ*W*(2*NSP-2)
    G1=0.0
    G2=J.0
    GSUM1=0.0
    GSUM2=0.0
    JU 40 M=1,NBSC
    XU=XLER+.5*DELCK1
    IF(XBVK1(M).GT.XC) GO TO 50
    XI=XTER-.5*DELCK1
    IF(XBVK1(M).LT.XT) GO TO 50
    XI=XTER+.5*DELCK1
    IF(XBVK1(M).LT.XT) GO TO 953
    GU TO 954
953  THEFA=PI
    GU TO 950
954  CUMLINE
    GU TO 51
50  G1=J.0
    G2=0.0
    GU TO 52
51  CUSX= (1.0-2.0)*(XLER-XBVK1(M)+.5*DELCK1)/CHORR1(N)
    THEFA=AKCOS(CUSX)

```

```

PGM30397
PGM30398
PGM30399
PGM30400
PGM30401
PGM30402
PGM30403
PGM30404
PGM30405
PGM30406
PGM30407
PGM30408
PGM30409
PGM30410
PGM30411
PGM30412
PGM30413
PGM30414
PGM30415
PGM30416
PGM30417
PGM30418
PGM30419
PGM30420
PGM30421
PGM30422
PGM30423
PGM30424
PGM30425
PGM30426
PGM30427
PGM30428
PGM30429
PGM30430
PGM30431
PGM30432

```

```

550 G1=(THETA+SIN(THETA))*PI INV -GSUM1
G2=2.0*PI INV*(THETA*0.5-SIN(2.0*THETA)*0.25) -GSUM2
GSUM1=GSUM1+G1
GSUM2=GSUM2+G2
UU 48 NSP=1,NSM
G2VRI(N,M,NSP,1)=G1*GR(N,NSP)
G2VRI(N,M,NSP,2)=G2*GR(N,NSP)
DU 144 NSP=1,NSM
WRITE(6,145) NSP,(GK(N,NSP),N=1,NBS)
144 FURMAT(6,MUDE',12,(16F7.3))
145 WRITE(6,146) NUUT,(GBVRI(NCUI,M,1,1),M=1,NBSC)
146 FURMAT(6,N=0,12,' CIKC MCDE 1,1',(12F7.5))
UU 55 NSP=1,NSM
UU 55 MCR=1,2
TVSRI(1,1,NSP,MCR)=GBVRI(1,1,NSP,MCR)
UU 54 M=2,NBSC
TVSRI(1,M,NSP,MCR)=TVSRI(1,M-1,NSP,MCR)+GBVRI(1,M,NSP,MCR)
UU 55 N=2,NMIN
TVSRI(N,1,NSP,MCR)=GBVRI(N,1,NSP,MCR)-CBVRI(N-1,1,NSP,MCR)
UU 55 M=2,NBSC
TVSRI(N,M,NSP,MCR)=TVSRI(N,M-1,NSP,MCR)+GBVRI(N,M,NSP,MCR)-GBVRI(N
1-1,M,NSP,MCR)
TVSRI(NIS,1,NSP,MCR)=-GEVRI(NBS,1,NSP,MCR)
UU 53 M=2,NBSC
TVSRI(NIS,M,NSP,MCR)=TVSRI(NIS,M-1,NSP,MCR)-GBVRI(NBS,M,NSP,MCR)
WRITE(6,148) TVSK1(1,1,1,1),TVSK1(1,NBSC,1,1),TVSRI(NIS,1,1,1),TVS
IRI(NIS,NBSC,1,1)
148 FURMAT(6,TRAILERS FOR UNIT MUDE(1,1) AT BASE(LE,TE) AND TIP(LE,TE)
1,1,4F10.4)
C
VELOCITIES ON RI
UU 56 MCP=1,NCPS
UU 56 MCP=1,NCPC
UU 56 N=1,NBS
UU 56 M=1,NBSC
SX=XBARI(M)-XCPRI(NCP,MCP)
SY=YBARI(1)-YCPRI(NCP)

```

```

PGM30433
PGM30434
PGM30435
PGM30436
PGM30437
PGM30438
PGM30439
PGM30440
PGM30441
PGM30442
PGM30443
PGM30444
PGM30445
PGM30446
PGM30447
PGM30448
PGM30449
PGM30450
PGM30451
PGM30452
PGM30453
PGM30454
PGM30455
PGM30456
PGM30457
PGM30458
PGM30459
PGM30460
PGM30461
PGM30462
PGM30463
PGM30464
PGM30465
PGM30466
PGM30467
PGM30468

```



PGM3J469  
 PGM3J470  
 PGM3J471  
 PGM3J472  
 PGM3J473  
 PGM3J474  
 PGM3J475  
 PGM3J476  
 PGM3J477  
 PGM3J478  
 PGM3J479  
 PGM3J480  
 PGM3J481  
 PGM3J482  
 PGM3J483  
 PGM3J484  
 PGM3J485  
 PGM3J486  
 PGM3J487  
 PGM3J488  
 PGM3J489  
 PGM3J490  
 PGM3J491  
 PGM3J492  
 PGM3J493  
 PGM3J494  
 PGM3J495  
 PGM3J496  
 PGM3J497  
 PGM3J498  
 PGM3J499  
 PGM3J500  
 PGM3J501  
 PGM3J502  
 PGM3J503  
 PGM3J504

```

S32=SQRT(SX*SX+SY*SY)**3
VZ=QPIINV/S32*(DGTKI*SX)
UU 56 NSP=1,NSM
UU 56 MCR=1,2
VZUKI(NCP,MCP,NSP,MCR)=VZBRI(NCP,MCF,NSP,MCR)+VZ*GBVKI(N,M,NSP,MCR
1)
WRITE(6,145)XCPRI(NMID,NCPC),YCPRI(NMIC),VZBRI(NMID,NCPC,1,1)
149 . FURMAT(0 VEL AT CP X=,F7.2, Y=,F7.3,F20.4, DUE TO MUDE 1,1 BOU
1ND VORTICES)
UU 57 NCP=1,NCPS
UU 57 MCP=1,NCPC
UU 57 N=1,NIS
SY=YTRRI(N)-YCPRI(NCP)
UU 57 M=1,NHS
SX=U.5*(XBVKI(M)+XBVKI(M+1))-XCPRI(NCP,MCP)
S32=SQRT(SX*SX+SY*SY)**3
VZ=QPIINV/S32*SY*(XBVKI(M+1)-XBVKI(M))
UU 57 NSP=1,NSM
UU 57 MCR=1,2
VZIRI(NCP,MCP,NSP,MCR)=VZTRI(NCP,MCF,NSP,MCR)+VZ*TVSKI(N,M,NSP,MCR
1)
SIAR=SIN(ALK)
CSAR=UJS(ALK)
ABK=XBVKI(NBSC)
UU 56 NCP=1,NCPS
UU 58 MCP=1,NCPC
UU 58 N=1,NTS
KSR=((XCPRI(NCP,MCP)-XBK)*SIAR)**2+(YTRKI(N)-YCPRI(NCP))**2
RR=SQRT(KSR)
WSK=(XCPRI(NCP,MCP)-XBR)**2+(YTRKI(N)-YCPKI(NCP))**2
QR=SQRT(QSR)
WVR=QPIINV/RR*((XBR-XCPRI(NCP,MCP))/CR*CSAR+1.0)
IF(YTRKI(N).GT.YCPRI(NCP))QVR=-QVK
VZ=WVR*LSAR
UU 58 NSP=1,NSM
UU 58 MCR=1,2

```

173

```

50  VZWR1(NCP,MCP,NSP,MCR)=VZWR1(NCP,MCP,NSP,MCR)+VZ*TVSKI(N,NBSC,NSP,
    1,MCR)
    WRITE(6,150)VZTR1(NMID,NCPC,1,1),VZ*RI(NMID,NCPC,1,1)
150  FORMAT(' VEL AT SAME POINT DUE TO TRAILERS ON BLADE=',F15.4,' AND
    1 WAKE=',F15.4,' DUE TO UNIT MODE 1,1')
    VLLUCITY ON RI DUE TO HULL
    DO 59 MCP=1,NCPS
    DO 59 MCR=1,NCPC
    K=VZTR1(NCP,MCP,NSP,MCR),XIN,KIN,NSTA)
    WDSRI(NCP,MCP)=WFS*RR*(YCPRI(NCP)**2)
59  WRITE(6,151)WDSRI(NMID,NCPC)
151  FORMAT(' VELOCITY AT SAME POINT DUE TO HULL=',F15.5)
    VELOCITY AT RI DUE TO SI AT CONTROL POINTS
    DO 60 MCP=1,NCPS
    K=YCPRI(NCP)
    U=W*(1)+AK(2)*K+AK(3)*R*R
    DO 60 MCR=1,NCPC
    WSKI(NCP,MCP)=U
60  CALCULATE LHS FOR RUDDER
    I=1
    DO 61 MCP=1,NCPS
    DO 61 MCR=1,NCPC
    J=1
    DO 62 MCR=1,2
    DO 62 NSP=1,NSM
    KILHS(I,J)=VZWR1(NCP,MCP,NSP,MCR)+VZTR1(NCP,MCP,NSP,MCR)+VZBRI(NCP
    1,MCP,NSP,MCR)
    WRITE(6,602) I,J,RILHS(I,J)
62  J=J+1
61  I=I+1
    CALCULATE RHS FOR RUDDER
    I=1
    DO 63 MCP=1,NCPS
    DO 63 MCR=1,NCPC
    KRHS(I)=DELTA(I)*U-WFS-WDSRI(NCP,MCP)-WDSRI(NCP,MCP)
    WRITE(6,601) I,RIRHS(I)

```

PGM3J0505  
PGM3J0506  
PGM3J0507  
PGM3J0508  
PGM3J0509  
PGM3J0510  
PGM3J0511  
PGM3J0512  
PGM3J0513  
PGM3J0514  
PGM3J0515  
PGM3J0516  
PGM3J0517  
PGM3J0518  
PGM3J0519  
PGM3J0520  
PGM3J0521  
PGM3J0522  
PGM3J0523  
PGM3J0524  
PGM3J0525  
PGM3J0526  
PGM3J0527  
PGM3J0528  
PGM3J0529  
PGM3J0530  
PGM3J0531  
PGM3J0532  
PGM3J0533  
PGM3J0534  
PGM3J0535  
PGM3J0536  
PGM3J0537  
PGM3J0538  
PGM3J0539  
PGM3J0540

```

63 I=I+1
EPS=.0001
DU 901 K=1, IMAX
901 KILHS(K,5)=KILHS(K)
CALL GLSQ(RILHS, CMSKI, ISP, IMAX, 4, BUG, EFS, LPS)
152 WRITE(6,152)(CMSRI(J), J=1,4)
C FORMAT(0, NUDE STRENGTHS CN R1 =', DF1J.5)
GET TOTAL WAKE TRAILER STRENGTHS
DU 66 N=1, NTS
GT(N)=0.0
GTF(N)=0.0
J=1
DU 66 MCR=1,2
DU 66 NSP=1, NSM
GT(N)=GTR(N)+TVSP1(N, NBSC, NSP, MCR)*CMSKI(J)
GTF(N)=GTF(N)+TVSSI(N, NBSC, NSP, MCR)*CMSKI(J)
66 J=J+1
C VELOCITY ON CL DUE TO FIN WAKE
DU 64 N=1, NTS
N=N
IF(YTKSI(N)-GT.RHS)GO TO 64
CONTINUE
64 NUOT=N
NIN=N-1
DU 65 N=NUOT, NTS
Y=YTKSI(N)
YD=Y*Y
DU 65 M=1, NSTA
CPI=XIN(M)-XB
CPI=CPI /SQRT(YSQ+(XIN(M)-XB)**2)
65 WTF(N, M)=(CPI-1.0)*QPIINV/Y*GTF(N)
C VELOCITY ON CL DUE TO RUDDER WAKE
DU 67 N=1, NTS
N=N
IF(YTKRI(N)-GT.RHS) GO TO 68
CONTINUE
67

```

```

PGM3J541
PGM3J542
PGM3J543
PGM3J544
PGM3J545
PGM3J546
PGM3J547
PGM3J548
PGM3J549
PGM3J550
PGM3J551
PGM3J552
PGM3J553
PGM3J554
PGM3J555
PGM3J556
PGM3J557
PGM3J558
PGM3J559
PGM3J560
PGM3J561
PGM3J562
PGM3J563
PGM3J564
PGM3J565
PGM3J566
PGM3J567
PGM3J568
PGM3J569
PGM3J570
PGM3J571
PGM3J572
PGM3J573
PGM3J574
PGM3J575
PGM3J576

```

```

68 NUUTR=N
   N1NK=N-1
   UU 69 N=NUUTR,NIS
   Y=YTRK1(N)
   Y2=Y*Y
   UU 69 M=1,NSTA
   CPI=XIN(M)-XBR
   CPI=CPI /SQRT(Y2+(XIN(M)-XBR)**2)
69 WTK(N,M)=(CPI-1.0)*UPIINV/Y*GTR(N)
   C TOTAL VELOCITY AT STATION M UN CL
   UU 70 M=1,NSTA
   W(M)=WFS
   UU 71 N=NUUT,NIS
   W(M)=W(M)+WTF(N,M)
   UU 70 N=NUUTR,NIS
   W(M)=W(M)+WTK(N,M)
   W(L(0,153))=W(M),M=1,NSTA)
71 FORMAT(0,153) (W(M),M=1,NSTA)
   C FURMAT(0 VELOCITY CN CL DUE TO FIN, RUDDER, FREE SIR',/, (12F7.3))
   W1 SLOPE AT INPUT POINTS
   UU 72 M=1,NSTA
   SPM(M)=SFIL(XIN(M),XIN,SINV,NSTA)
   WTL(6,154)(SPM(M),M=1,NSTA)
72 FURMAT(0 SLOPE AT INPUT POINTS',/, (12F7.2))
   C FORCES + MOMENTS DUE TO CIRC AROUND HULL DUE TO FIN
   NSUM=NSTA-1
   NTS=NUT-1
   GAMMA=0.0
   UU 81 N=1,NTSH
   GAMMA=GAMMA+GTF(N)
   SY=0.0
   SIN=0.0
   UU 82 M=1,NSDUM
   IF(XIN(M).GE.XTEB(1)) GO TO 82
   SY=SY+RHU*W(M)*GAMMA*DELX
   SIN=SIN+RHU*W(M)*GAMMA*DELX*XIN(M)
82 CONTINUE

```

PGM3J0613  
 PGM3J0614  
 PGM3J0615  
 PGM3J0616  
 PGM3J0617  
 PGM3J0618  
 PGM3J0619  
 PGM3J0620  
 PGM3J0621  
 PGM3J0622  
 PGM3J0623  
 PGM3J0624  
 PGM3J0625  
 PGM3J0626  
 PGM3J0627  
 PGM3J0628  
 PGM3J0629  
 PGM3J0630  
 PGM3J0631  
 PGM3J0632  
 PGM3J0633  
 PGM3J0634  
 PGM3J0635  
 PGM3J0636  
 PGM3J0637  
 PGM3J0638  
 PGM3J0639  
 PGM3J0640  
 PGM3J0641  
 PGM3J0642  
 PGM3J0643  
 PGM3J0644  
 PGM3J0645  
 PGM3J0646  
 PGM3J0647  
 PGM3J0648

```

C
SIY=SIY+0.5*RRHO*W(NSTA)*GAPMA*DELX
SIN= SIN+0.5*RHU*W(NSTA)*GAMMA*DELX*XIN(NSTA)
GET FORCES + MOMENTS DUE TO SOURCES ON CL
SOURZ=J.5*DELX*W(1)*RHO*LO*SPRM(1)
SOURM=-SOURZ*XIN(1)
SOURZ=SOURZ+0.5*DELX*W(NSTA)*RHO*UC*SPRM(NSTA)*2
SOURM=SOURM-0.5*DELX*W(NSTA)*RHO*UU*SPRM(NSTA)*XIN(NSTA)*2
LENGTH=XIN(1)-XIN(NSTA)
DO 73 M=2, NSJUM
  IF(XIN(M).GE.0.0) FAC=1.0
  IF(XIN(M).LT.0.0) FAC=1.0-2.*(XIN(M)/LENGTH)
  SOURZ=SOURZ+DELX*W(M)*RHC*LU*SPRM(M)*FAC
  SOURM=SOURM-DELX*W(M)*RHO*UC*SPRM(M)*XIN(M)*FAC
  MOMENT DUE TO DOUBLETS
  DUUM=-DELX*W(1)*RHO*UU*SINV(1)
  DUUM=DUUM-DELX*W(NSTA)*RFO*UU*SINV(NSTA)*.5
  DO 74 M=2, NSJUM
    IF(XIN(M).GE.0.0) FAC=1.0
    IF(XIN(M).LT.0.0) FAC=1.0+2.*(XIN(M)/LENGTH)
    DUUM=DUUM-2.0*DELX*W(M)*RHC*UU*SINV(M)*FAC
  FORCE AND MOMENT ON FIN
  SIZ=0.0
  SIM=0.0
  DO 77 N=1, NBS
    SIZ=SIZ+RHC*UU*DBT1*(GS(N,1)*(CMSSI(1)+CMSSI(3))+GS(N,2)*(CMSSI(2)
    +CMSSI(4)))
    XLE=XLEB(1)-SLEF*(YBSI(N)-RF)
    IF(XLE.GT.XLEB(1)) XLE=XLEB(1)
    XCP1=XLL-.25*CHUK(N)
    XCP2=XLL-.50*CHUK(N)
    SIM=SIM+RHC*UU*DBT1*(CMSSI(1)*XCP1*GS(N,1)+CMSSI(3)*XCP2*GS(N,1)+C
    MSSI(2)*XCP1*GS(N,2)+CMSSI(4)*XCP2*GS(N,2))
  FORCE AND MOMENT ON RUDDER
  RIZ=0.0
  RIM=0.0
  DO 80 N=1, NBS
  
```



```

R1Z=K1Z+KMG*UO*DBTRI*(GR(N,1))*(CMSK1(1)+CMSK1(3))+GR(N,2)*(CMSR1(2
1)+CMSR1(4)))
XLE=XLEBK(1)-SLLEK*(YBRI(N)-RFR)
IF(XLE.GT.XLEB(1)) XLE=XLEB(1)
XCPI=XLE-0.25*CHORK1(N)
XCP2=XLE-0.50*CHURKI(N)
80 K1M=K1M+KHC*UO*DBTRI*(CMSK1(1)*XCPI*GR(N,1)+CMSK1(3)*XCP2*GR(N,1)+
1 CMSK1(2)*XCPI*GR(N,2)+CMSK1(4)*XCP2*GR(N,2))
C TOTAL FORCE AND MOMENT
K1Z=-R1Z
S1Z=-S1Z
FZJK=R1Z+S1Z+SUURZ
ZUJK=K1M+SIM+SUURM+DOUM
WRITE(6,106) NSTA,LU,WFS,RHO
106 FURMAT('1 NO. OF STATIONS ',I4,' FREE STREAM FORWARD SPEED ',F8.3,
1' SWAY VELOCITY ',F8.3,' WATER DENSITY ',F8.4)
WRITE(6,250) (XIN(J),J=1,NSTA)
250 FURMAT(' XIN ',(6F10.5))
251 FURMAT(' RIN ',(6F10.5))
252 FURMAT(' WAKE AND RUDDER ANGLES ',3F20.5)
253 FURMAT(' KSL(1),RNUD(1)
107 FURMAT(' SAIL AND RUDDER TIP RADII ',2F20.5)
WRITE(6,107) R1Z,S1Z,SOURZ,FZDK
FURMAT(' RUDDER SIDE FORCE ',F10.3,' FIN SIDE FORCE ',F10.3,' SOUR
ICE SIDE FORCE ',F10.3,' TOTAL SIDE FORCE ',F10.3)
WRITE(6,108)K1M,SIM,SOURM,DOUM,ZDIRM
108 FURMAT(' RI MMENT',F11.4,' FIN MMENT',F11.4,' SOURCE MMENT',
1F11.4,' DOUBLET MMENT',F11.4,' TOTAL MMENT',F11.4)
WRITE(6,109)S1Y,SIN
109 FURMAT(' HEAVE FORCE ON HULL',F11.4,' PITCH MMENT',F11.4)
STOP
END

```

```

PGM3J049
PGM3J050
PGM3J051
PGM3J052
PGM3J053
PGM3J054
PGM3J055
PGM3J056
PGM3J057
PGM3J058
PGM3J059
PGM3J060
PGM3J061
PGM3J062
PGM3J063
PGM3J064
PGM3J065
PGM3J066
PGM3J067
PGM3J068
PGM3J069
PGM3J070
PGM3J071
PGM3J072
PGM3J073
PGM3J074
PGM3J075
PGM3J076
PGM3J077
PGM3J078
PGM3J079
PGM3J080
PGM3J081
PGM3J082

```

```

C      FUNCTION SFIL(X,XI,YI,NO)
      THIS WORKS ONLY FOR DECREASING VALUES OF X WITH INDEX
      DIMENSION XI(2),YI(2)
      YU(XI,X1,X2,X3,Y1,Y2,Y3)=Y1*(2.*X-(X2+X3))/((X1-X2)*(X1-X3))+Y2*(
      12.*X-(X1+X3))/((X2-X1)*(X2-X3))+Y3*(2.*X-(X1+X2))/((X3-X1)*(X3-X2)
      2)
      IF(X.GT.XI(3)) GO TO 1
      IF(X.LT.XI(NO-2)) GO TO 2
      GO TO 3
      Y=JYUX(X,XI(2),XI(1),YI(3),YI(2),YI(1))
      GO TO 99
      Y=UYUX(X,XI(NO),XI(NO-1),XI(NO-2),YI(NO),YI(NO-1),YI(NO-2))
      GO TO 99
      DO 4 I=3,NO
      I=I
      IF(X.LE.XI(I).AND.X.GT.XI(I+1)) GO TO 5
      CONTINUE
      Y=UYUX(X,XI(I+1),XI(I),XI(I-1),YI(I+1),YI(I),YI(I-1))
      SFIL=Y
      RETURN
      END

```

PGM3J001  
 PGM3J002  
 PGM3J003  
 PGM3J004  
 PGM3J005  
 PGM3J006  
 PGM3J007  
 PGM3J008  
 PGM3J009  
 PGM3J010  
 PGM3J011  
 PGM3J012  
 PGM3J013  
 PGM3J014  
 PGM3J015  
 PGM3J016  
 PGM3J017  
 PGM3J018  
 PGM3J019  
 PGM3J020  
 PGM3J021

```

C
FUNCTION FILLI(X,XI,YI,NC)
  FITS ONLY FOR DECREASING VALUES OF X
  DIMENSION XI(2),YI(2)
  A(A1,X2,X3,X,Y1,Y2,Y3)=Y1*(X-X2)*(X-X3)/((X1-X2)*(X1-X3))+Y2*(X-X1
  1)*(X-X3)/((X2-X1)*(X2-X3))+Y3*(X-X1)*(X-X2)/((X3-X1)*(X3-X2))
  IF(X-XI(1))2,3,1
  Y=YI(1)
  GO TO 99
  1 Y=A(XI(3),XI(2),XI(1),X,YI(3),YI(2),YI(1))
  GO TO 99
  2 IF(X-XI(2))5,6,1
  Y=YI(2)
  GO TO 99
  3 DO 7 I=3,NC
  M=I
  IF(X-XI(I))7,9,8
  Y=YI(I)
  GO TO 99
  4 CONTINUE
  5 Y=A(XI(M-2),XI(M-1),XI(M),X,YI(M-2),YI(M-1),YI(M))
  FILLI=Y
  RETURN
  END

```

```

PGM30001
PGM30002
PGM30003
PGM30004
PGM30005
PGM30006
PGM30007
PGM30008
PGM30009
PGM30010
PGM30011
PGM30012
PGM30013
PGM30014
PGM30015
PGM30016
PGM30017
PGM30018
PGM30019
PGM30020
PGM30021
PGM30022
PGM30023

```



```

SUBROUTINE GLSQ(A,X,IL,N,M,ALPHA,E1,E2)
GLSQ SUBROUTINE *****
DIMENSION A( 32, 21),X(1),IL(1)
MM=M+1
LL=1
DO 60 J=1,MM
  IL(J)=0
  I=1
  DO J K=1,MM
    II=I+1
    DO 4 J=II,N
      IF(AUSIA(J,K))-E1)4,4,6
    II=SQRT((A(J,K))**2+(A(I,K))**2)
    S=A(J,K)/II
    C=A(I,K)/II
    DO 5 L=K,MM
      T2=C*A(I,L)+S*A(J,L)
      A(J,L)=-S*A(I,L)+C*A(J,L)
      A(I,L)=T2
      LL=LL+1
    CONTINUE
    IF(ABS(A(I,K))-E2)3,3,8
    IL(K)=I
    I=I+1
  CONTINUE
  X(M)=-1.0
  II=M
  DO 35 I=1,M
    X(I)=0.0
  DO 30 J=1,M
    IF(IL(II))50,30,31
  S=J.0
  LL=II+1
  I=IL(II)
  DO 32 K=LL,MM
    S=S+A(I,K)*X(K)

```

```

0454 PGM3J001
0453 PGM3J002
0455 PGM3J003
0456 PGM3J004
0457 PGM3J005
0458 PGM3J006
0459 PGM3J007
0460 PGM3J008
0461 PGM3J009
0462 PGM3J010
0463 PGM3J011
0464 PGM3J012
0465 PGM3J013
0466 PGM3J014
0467 PGM3J015
0468 PGM3J016
0469 PGM3J017
0470 PGM3J018
0471 PGM3J019
0472 PGM3J020
0473 PGM3J021
0474 PGM3J022
0475 PGM3J023
0476 PGM3J024
0477 PGM3J025
0478 PGM3J026
0479 PGM3J027
0480 PGM3J028
0481 PGM3J029
0482 PGM3J030
0483 PGM3J031
0484 PGM3J032
0485 PGM3J033
0486 PGM3J034
0487 PGM3J035
0488 PGM3J036
PAGE 22

```

```

30 X(I,I)=-S/A(I,I)
31 I=I-1
32 IF(I(L(MM))50,51,50
    ALPHA=0.0
    GO TO 52
33 I=I(MM)
34 ALPHA=A(I,MM)
35 RETURN
36 ENU

```

```

0489 PGM3J0037
0490 PGM3J0038
0491 PGM3J0039
0492 PGM3J0040
0493 PGM3J0041
0494 PGM3J0042
0495 PGM3J0043
0496 PGM3J0044
0497 PGM3J0045

```

SAMPLE DATA DECK FOR NUMERICAL PREDICTION OF FORCES AND MOMENTS										
C	13	14.772	2.606	2.0						PGM3J001
	.833	.666	.500	.333	.166	.000	-.166			PGM3J002
	-.500	-.006	-.833	-1.000	-1.166	.000				PGM3J003
	.000	.077	.110	.133	.143	.147	.143			PGM3J004
	.120	.100	.086	.059	.023					PGM3J005
	.414	.115	.141	-.153	-.242					PGM3J006
	.172	-1.051	-1.051	-1.150	-1.150	0.0				PGM3J007
	.1740	.1740								PGM3J008
	24	12	4	4						PGM3J009
										PGM3J010
										PGM3J011
										PGM3J012
										PGM3J013



1 -0.215182074  
 2 0.122493937  
 3 -0.410597601  
 4 0.023616011  
 5 -0.112909787  
 6 -0.1448735106  
 7 -0.155145943  
 8 2.57711601  
 9 2.52520952  
 10 2.45953759  
 11 2.471249574  
 12 2.35587253  
 13 2.252353965  
 14 1.91722775  
 15 0.255408601  
 16 2.14077620  
 17 2.451306771  
 18 2.021310267  
 19 2.057440026  
 20 1.05042545  
 21 0.443062773  
 22 -0.645037143  
 23 -0.141053511  
 24 0.06262675  
 25 1.49455997  
 26 2.02746024  
 27 1.21167708  
 28 2.44221306  
 29 1.74054660  
 30 1.50070380  
 31 1.01500345  
 32 2.14022645  
 33 1.50512123  
 34 2.44734311  
 35 2.46000353  
 36 1.57851844  
 37 1.00000017  
 38 -0.00000017  
 39 -0.1300002776  
 40 0.52597  
 41 0.44123  
 42 -0.25194  
 43 0.225  
 44 0.210  
 45 0.199  
 46 0.190  
 47 0.000  
 48 0.000  
 49 0.000  
 50 0.000  
 51 0.000  
 52 0.000  
 53 0.000  
 54 0.000  
 55 0.000  
 56 0.000  
 57 0.000  
 58 0.000  
 59 0.000  
 60 0.000  
 61 0.000  
 62 0.000  
 63 0.000  
 64 0.000  
 65 0.000  
 66 0.000  
 67 0.000  
 68 0.000  
 69 0.000  
 70 0.000  
 71 0.000  
 72 0.000  
 73 0.000  
 74 0.000  
 75 0.000  
 76 0.000  
 77 0.000  
 78 0.000  
 79 0.000  
 80 0.000  
 81 0.000  
 82 0.000  
 83 0.000  
 84 0.000  
 85 0.000  
 86 0.000  
 87 0.000  
 88 0.000  
 89 0.000  
 90 0.000  
 91 0.000  
 92 0.000  
 93 0.000  
 94 0.000  
 95 0.000  
 96 0.000  
 97 0.000  
 98 0.000  
 99 0.000  
 100 0.000

REPRODUCED FROM  
 BEST AVAILABLE COPY.

0.324 0.356 0.376 0.385 0.375 0.331 0.217  
 N-12 C14C MUD 1.14322000.14940.14140.087440.070720.058510.048750.040340.032600.025110.016720.00580  
 TRAILERS FOR UNIT NUMBERS AT BRATTLE, TEL AND TIPILLITEJ U.2042 0.9806 -0.0617 -0.229J  
 VEL AT CP 10 -1.07 V= J.08J  
 VEL AT SARE PLAIN, WA TO TRAILERS UN ELAGE= J.042Z DUE TO MUD 1.1 BOUND VORTICES  
 VELOCITY AT SARE POINT DUE TO MUD= J.73504 1.0761 AND BARK= 0.5501 DUE TO UNIT MAKE 1.1

1	1	0.9726000
1	2	-0.555501944
1	3	0.04307384
1	4	-0.828054007
2	1	0.66171474
2	2	-0.055978212
2	3	0.10459709
2	4	-0.70105447
3	1	0.33108010
3	2	-0.754185106
3	3	1.54876519
3	4	-0.558740543
4	1	3.0232322
4	2	-0.250592756
4	3	-1.35074405
4	4	-0.43174712E
5	1	0.55776615
5	2	-0.126690262
5	3	0.20440380
5	4	-0.01426000E3
6	1	0.1141425
6	2	-0.0776201627
6	3	3.7066552
6	4	-0.153452654
7	1	2.01735134
7	2	-0.0025540701
7	3	1.11475707
7	4	-0.251757414
8	1	2.474850E
8	2	-0.104218304
8	3	-1.40513024
8	4	-0.421190520
9	1	0.50100421
9	2	1.37440521
9	3	2.07609304
9	4	1.05507334
10	1	2.0747114
10	2	1.32410021
10	3	2.07001171
10	4	0.003512752
11	1	2.43067414
11	2	1.20601873
11	3	1.04602030
11	4	0.23495310
12	1	2.04200308
12	2	1.40525306
12	3	-1.36080510
12	4	-0.324190000
13	1	2.03113240
13	2	3.4740041
13	3	2.44050672
13	4	3.250000430
14	1	2.30217008
14	2	3.20605508

10 4 3.29458237  
11 4 2.15019761  
12 1 5.06952285  
13 2 2.95771934  
14 3 1.07602692  
15 4 1.02057034  
16 1 4.07154681  
17 2 2.06621333  
18 3 -1.12378604  
19 4 -0.008602621  
20 1 -2.0045486  
21 2 -2.23243713  
22 3 -2.44154505  
23 4 -2.06618347  
24 5 -1.00593200  
25 6 -1.77160108  
26 7 -1.00725550  
27 8 -2.01146493  
28 9 -1.4022401  
29 10 -1.94972555  
30 11 -1.62362085  
31 12 -1.70108472  
32 13 -1.38254368  
33 14 -1.03190342  
34 15 -1.48245521  
35 16 -1.53075276  
36 17 -0.37483 0.10165 0.11383 -0.14011  
MODE STRENGTHS US AT 2 -0.37483 0.10165 0.11383 -0.14011  
VELOCITY (M CL LUL IN FIN. ANNUAL RATE SIX  
2.591 2.585 2.577 2.564 2.553 2.544 2.556 2.191 2.076 2.022 1.992 1.963  
1.933  
SCALE AT INPUT POINTS  
-0.11 -0.11 -0.11 -0.08 -0.04 0.0 0.03 0.05 0.06 0.08 0.06 0.06  
0.05

NO. OF STATIONS 13 FINE STREAM FORWARD SPEED 14.772 SWAY VELOCITY 2.000 WATER DENSITY 6.0000  
FIN 0.03300 0.00000 0.00000 0.03300 0.10000 0.0 0.00000 0.0  
-0.03300 -0.00000 -0.00000 -0.03300 -0.10000 -0.03300  
FIN 0.0 0.07700 0.10000 0.13300 0.16300 0.19700 0.19300 0.19000  
0.12000 0.10000 0.00000 0.00000 0.00000 0.00000 0.00000 0.00000  
WAVE ARC BUOYER ANGLE 0.17400 0.17400 0.0  
SAIL AND BUOYER TIP ANGLE 0.01400 0.17400  
RUDDER SILL FORCE 1.025 FIN SIDE FORCE 11.754 SCURCE SILE FORCE 1.596 TOTAL SIDE FORCE 19.173  
RI MOMENT 1.0007 FIN MOMENT -0.0000 SCURCE MOMENT 7.0101 DOUBLET MOMENT -9.0152 TOTAL MOMENT -1.0004  
WEAVE FORCE ON WALL -0.0700 PITCH MOMENT 0.5500